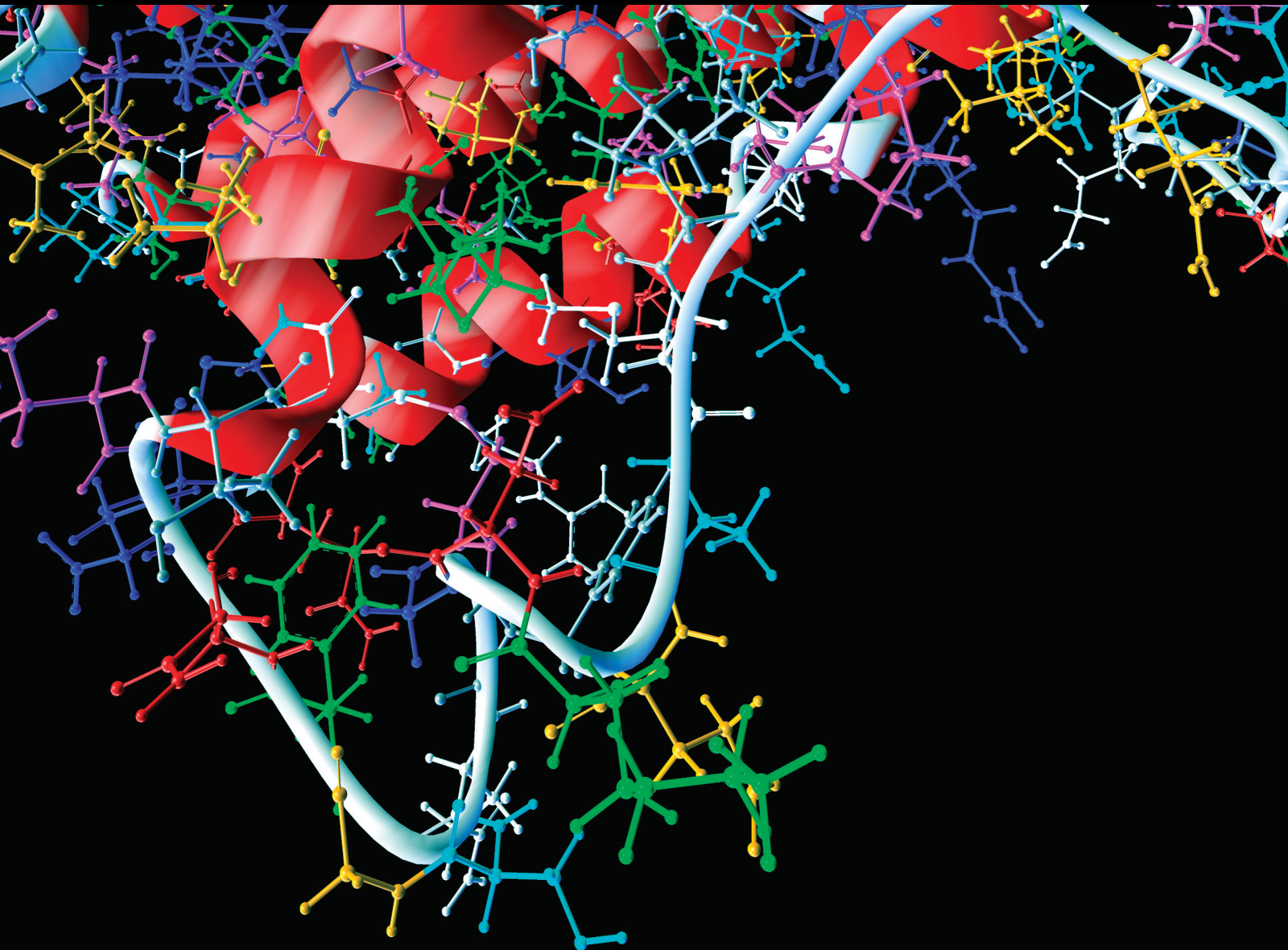


Innovation in Deep Learning Approaches for Medical Data/Big Data Analysis

Lead Guest Editor: Sujatha Krishnamoorthy

Guest Editors: Shohel Sayeed and Vijiyalakshmi Saravanan



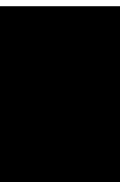


Innovation in Deep Learning Approaches for Medical Data/Big Data Analysis

Computational and Mathematical Methods in Medicine

**Innovation in Deep Learning
Approaches for Medical Data/Big Data
Analysis**




Lead Guest Editor: Sujatha Krishnamoorthy
Guest Editors: Shohel Sayeed and Vijiyalakshmi
Saravanan



Copyright © 2023 Hindawi Limited. All rights reserved.

This is a special issue published in “Computational and Mathematical Methods in Medicine.” All articles are open access articles distributed under the Creative Commons Attribution License, which permits unrestricted use, distribution, and reproduction in any medium, provided the original work is properly cited.

Associate Editors

Ahmed Albahri, Iraq
Konstantin Blyuss , United Kingdom
Chuangyin Dang, Hong Kong
Farai Nyabadza , South Africa
Kathiravan Srinivasan , India

Academic Editors

Laith Abualigah , Jordan
Yaser Ahangari Nanekaran , China
Mubashir Ahmad, Pakistan
Sultan Ahmad , Saudi Arabia
Akif Akgul , Turkey
Karthick Alagar, India
Shadab Alam, Saudi Arabia
Raul Alcaraz , Spain
Emil Alexov, USA
Enrique Baca-Garcia , Spain
Sweta Bhattacharya , India
Junguo Bian, USA
Elia Biganzoli , Italy
Antonio Boccaccio, Italy
Hans A. Braun , Germany
Zhicheng Cao, China
Guy Carrault, France
Sadaruddin Chachar , Pakistan
Prem Chapagain , USA
Huiling Chen , China
Mengxin Chen , China
Haruna Chiroma, Saudi Arabia
Watcharaporn Cholamjiak , Thailand
Maria N. D.S. Cordeiro , Portugal
Cristiana Corsi , Italy
Qi Dai , China
Nagarajan Deivanayagam Pillai, India
Didier Delignières , France
Thomas Desaive , Belgium
David Diller , USA
Qamar Din, Pakistan
Irina Doytchinova, Bulgaria
Sheng Du , China
D. Easwaramoorthy , India



Esmaeil Ebrahimie , Australia
Issam El Naqa , USA
Ilias Elmouki , Morocco
Angelo Facchiano , Italy
Luca Faes , Italy
Maria E. Fantacci , Italy
Giancarlo Ferrigno , Italy
Marc Thilo Figge , Germany
Giulia Fiscon , Italy
Bapan Ghosh , India
Igor I. Goryanin, Japan
Marko Gosak , Slovenia
Damien Hall, Australia
Abdulsattar Hamad, Iraq
Khalid Hattaf , Morocco
Tingjun Hou , China
Seiya Imoto , Japan
Martti Juhola , Finland
Rajesh Kaluri , India
Karthick Kanagarathinam, India
Rafik Karaman , Palestinian Authority
Chandan Karmakar , Australia
Kwang Gi Kim , Republic of Korea
Andrzej Kloczkowski, USA
Andrei Korobeinikov , China
Sakthidasan Sankaran Krishnan, India
Rajesh Kumar, India
Kuruva Lakshmana , India
Peng Li , USA
Chung-Min Liao , Taiwan
Pinyi Lu , USA
Reinoud Maex, United Kingdom
Valeri Makarov , Spain
Juan Pablo Martínez , Spain
Richard J. Maude, Thailand
Zahid Mehmood , Pakistan
John Mitchell , United Kingdom
Fazal Ijaz Muhammad , Republic of Korea
Vishal Nayak , USA
Tongguang Ni, China
Michele Nichelatti, Italy
Kazuhisa Nishizawa , Japan
Bing Niu , China

Hyuntae Park , Japan
Jovana Paunovic , Serbia
Manuel F. G. Penedo , Spain
Riccardo Pernice , Italy
Kemal Polat , Turkey
Alberto Policriti, Italy
Giuseppe Pontrelli , Italy
Jesús Poza , Spain
Maciej Przybyłek , Poland
Bhanwar Lal Puniya , USA
Mihai V. Putz , Romania
Suresh Rasappan, Oman
Jose Joaquin Rieta , Spain
Fathalla Rihan , United Arab Emirates
Sidheswar Routray, India
Sudipta Roy , India
Jan Rychtar , USA
Mario Sansone , Italy
Murat Sari , Turkey
Shahzad Sarwar, Saudi Arabia
Kamal Shah, Saudi Arabia
Bhisham Sharma , India
Simon A. Sherman, USA
Mingsong Shi, China
Mohammed Shuaib , Malaysia
Prabhishek Singh , India
Neelakandan Subramani, India
Junwei Sun, China
Yung-Shin Sun , Taiwan
Min Tang , China
Hongxun Tao, China
Alireza Tavakkoli , USA
João M. Tavares , Portugal
Jlenia Toppi , Italy
Anna Tsantili-Kakoulidou , Greece
Markos G. Tsiouras, North Macedonia
Po-Hsiang Tsui , Taiwan
Sathishkumar V E , Republic of Korea
Durai Raj Vincent P M , India
Gajendra Kumar Vishwakarma, India
Liangjiang Wang, USA
Ruisheng Wang , USA
Zhouchao Wei, China
Gabriel Wittum, Germany
Xiang Wu, China







KI Yanover , Israel
Xiaojun Yao , China
Kaan Yetilmezsoy, Turkey
Hiro Yoshida, USA
Yuhai Zhao , China

Contents


Sleep Deprivation and Heart Rate Variability in Healthy Volunteers: Effects of REM and SWS Sleep Deprivation

YaHui Xu, BinBin Qu, FengJuan Liu, ZhiHua Gong, Yi Zhang , and DeXiang Xu 
Research Article (5 pages), Article ID 7121295, Volume 2023 (2023)

MSeg-Net: A Melanoma Mole Segmentation Network Using CornerNet and Fuzzy K -Means Clustering

Marriam Nawaz , Tahira Nazir , Muhammad Attique Khan , Majed Alhaisoni , Jung-Yeon Kim , and Yunyoung Nam 
Research Article (16 pages), Article ID 7502504, Volume 2022 (2022)


Analysis of the Influence of Midwife Led Antenatal Clinic on the Delivery Outcomes of Primipara under the Evaluation of Medical Data

Wei Fan, Ling Wang, Lili Zhang, Xiaoling Liu, and Zhaoyan Meng 
Research Article (6 pages), Article ID 7454258, Volume 2022 (2022)



Research on CT Lung Segmentation Method of Preschool Children based on Traditional Image Processing and ResUnet

Zheming Li , Li Yang, Liqi Shu, Zhuo Yu, Jian Huang , Jing Li , Lingdong Chen, Shasha Hu, Ting Shu , and Gang Yu 
Review Article (10 pages), Article ID 7321330, Volume 2022 (2022)

Recognition of Handwritten Medical Prescription Using Signature Verification Techniques

Seerat Rani, Abd Ur Rehman , Beenish Yousaf , Hafiz Tayyab Rauf , Emad Abouel Nasr , and Seifedine Kadry 
Research Article (14 pages), Article ID 9297548, Volume 2022 (2022)

Effect of Gender on Serum Leptin in Type 2 Diabetes Mellitus: A System Review and Meta-Analysis

Yushan Li , Xiao Chen, Xingji Gong, Jian Yao, Dongyong He, and Wenjie Du 
Research Article (8 pages), Article ID 4875799, Volume 2022 (2022)










Effect of Ultrasonic Osteotome on Therapeutic Efficacy and Safety of Spinal Surgery: A System Review and Meta-Analysis

Leilei Wu  and Sheng Wang 
Research Article (8 pages), Article ID 9548142, Volume 2022 (2022)

A Rule-Based Inference Framework to Explore and Explain the Biological Related Mechanisms of Potential Drug-Drug Interactions

Adeeb Noor  and Abdullah Assiri 
Research Article (9 pages), Article ID 9093262, Volume 2022 (2022)

Predicting Breast Cancer Leveraging Supervised Machine Learning Techniques

Sanam Aamir , Aqsa Rahim , Zain Aamir , Saadullah Farooq Abbasi , Muhammad Shahbaz Khan , Majed Alhaisoni , Muhammad Attique Khan , Khyber Khan , and Jawad Ahmad 
Research Article (13 pages), Article ID 5869529, Volume 2022 (2022)

Research Article

Sleep Deprivation and Heart Rate Variability in Healthy Volunteers: Effects of REM and SWS Sleep Deprivation

YaHui Xu,¹ BinBin Qu,¹ FengJuan Liu,² ZhiHua Gong,³ Yi Zhang^{ID},⁴ and DeXiang Xu^{ID}¹

¹Department of Respiratory and Critical Care Medicine, The Affiliated Central Hospital of Qingdao University, Qingdao, Shandong, China

²Clinical Trial Research Center, The Affiliated Central Hospital of Qingdao University, Qingdao, Shandong, China

³Electrocardiogram Department, The Affiliated Central Hospital of Qingdao University, Qingdao, Shandong, China

⁴Department of Respiratory and Critical Care Medicine, Beijing China-Japan Friendship Hospital, China

Correspondence should be addressed to Yi Zhang; czzhangyi1985@126.com and DeXiang Xu; dexiangxu2008@126.com

Received 15 July 2022; Revised 15 August 2022; Accepted 22 August 2022; Published 11 July 2023

Academic Editor: Sujatha Krishnamoorthy

Copyright © 2023 YaHui Xu et al. This is an open access article distributed under the Creative Commons Attribution License, which permits unrestricted use, distribution, and reproduction in any medium, provided the original work is properly cited.

Objective. Using PSG-guided acute selective REM/SWS sleep deprivation in volunteers, this study examined the effects of sleep deprivation on the cardiovascular and autonomic nervous systems, as well as the relationship between cardiac neuromodulation homeostasis and cardiovascular disease. **Methods.** An experiment was conducted using 30 healthy volunteers (male : female = 1 : 1, aged 26.33 ± 4.5 years) divided into groups for sleep deprivation of SWS and REM sleep, and then, each group was crossed over for normal sleep (2 days) and repeated sleep deprivation (1 day, 3 times). During the study period, PSG and ELECTRO ECG monitoring were conducted, and five-minute frequency domain parameters and blood pressure values were measured before and after sleep deprivation. **Results.** Changes in VLF, LFnu, LF/HF, HF, and HFnu after SWS sleep deprivation were statistically significant ($P < 0.05$), but not LF ($P = 0.063$). Changes in VLF, LF, HF, LF/HF, LFnu, and HFnu after REM sleep deprivation were not statistically significant ($P > 0.05$). **Conclusions.** An increase in sympathetic nerve activity results from sleep deprivation and sudden awakening from SWS sleep is associated with a greater risk of cardiovascular disease.

1. Introduction

In addition to changes in awareness, sleep is characterized by a relatively inhibited sensory activity, decreased muscular activity, and inhibition of practically all voluntary muscles during fast eye movements, as well as decreased interaction with the surrounding environment [1]. It differs from wakefulness in that it is less responsive to stimuli, yet it is more reactive than comas or disturbing states of consciousness. As a result of sleep, the brain exhibits a different pattern of active activity [2]. A good night's sleep enhances the human body's energy and resistance, supports proper human growth and development, and ensures that the human body receives sufficient rest. It is impossible to overestimate the importance of sleep in maintaining mental activity and protecting mental health [3, 4]. Getting enough sleep and maintaining good sleep quality can help maintain a normal metabolism and reduce the occurrence and mortality of

certain diseases. It has become increasingly evident that sleep deprivation (SD) is a serious public health issue [5]. Aging, lifestyle, time stress, shift work, insomnia, and sleep disorders are all factors that contribute to insufficient sleep, microawakening, and fragmented sleep [5, 6]. In addition to cardiovascular disease, obesity, and diabetes, SD can also increase the risk of depression. Clinical trials have shown that SD can weaken the autonomic nervous system and change the stability of the cardiovascular system [7]. Heart rate changes and the maintenance of cardiac sinus rhythm are primarily regulated by sympathetic and parasympathetic nerves. In terms of cardiac autonomic nerve regulation analysis, heart rate variability (HRV) is the best noninvasive monitoring method [8]. Studies examining cardiovascular neuromodulation during sleep have been widely evaluated using 5-minute frequency domain analysis [9]. According to the literature, the sympathetic nervous system is enhanced after acute sleep deprivation, and the vagal nerve is

decreased after acute sleep deprivation [5]. However, there is a significant difference between the activity of sympathetic and parasympathetic nerves during different sleep stages, and the effects of sleep deprivation on the autonomic nervous system in different sleep stages have not been reported. By analyzing heart rate variability 5 minutes before and after selective sleep deprivation (frequency domain analysis), this study investigated the relationship between acute selective sleep deprivation HRV and cardiovascular disease.

2. Methods

2.1. Samples and Standards. This study has been approved by the Medical Ethics Committee of Qingdao Central Hospital (Ethics Review Approval No. Ky-p201807501), and the clinical trial has been registered online (registration number ChiCTR1900020622). Prior to explaining the purpose and procedure of the study to the healthy subjects, healthy volunteers were recruited, and the study was conducted between February 2019 and December 2020. During the clinical screening process, patients undergo a detailed history and physical examination in addition to basic examinations (heart function, blood pressure, electrocardiogram, lung function, etc.) and evaluation questionnaires.

2.2. Criteria for Inclusion and Exclusion. Criteria for inclusion are as follows: between 20 and 39 years of age, one week of stable sleep prior to the experiment, no shift work during the preceding three months, and one week of stable daily activities and work prior to the experiment. Criteria for exclusion are as follows: a BMI of more than 30 kg/m^2 , acute or chronic cardiopulmonary diseases, smoking more than ten cigarettes per day, alcoholism, consuming more than 100 g of alcohol per week, recent negative life events, physical and neurological examinations that are abnormal, mothers who are pregnant or nursing, and any sleep-related breathing disorder. The study protocols for the examinations were conducted in accordance with the Helsinki Declaration (2000), and the participants were compensated monetarily upon completion of the tests.

2.3. Sleep Intervention. 30 volunteers (male: female ratio of 1:1, mean age of 26.3 ± 4.5 years) who met the inclusion and exclusion criteria were randomly assigned to either the REM sleep deprivation or SWS sleep deprivation group. Prior to the trial, all subjects were instructed to maintain a regular sleep schedule between 10:00 p.m. and 7:00 a.m. Trials were conducted for three days: normal sleep on day one (excluding the effects of first night sleep and screening for exclusion criteria during sleep), selective sleep deprivation on day two, and normal sleep after sleep deprivation on day three. In the event of sleep restriction and normal sleep, PSG monitoring was performed in order to determine sleep stages, and a dynamic electrocardiogram was worn in order to evaluate autonomic nervous system indicators. Monitoring took place from 21:00 to 7:00 the following morning. During the night of sleep deprivation, volunteers woke up after entering SWS sleep or REM sleep. Sensei's methods were to turn on the light, and by playing a specific

TABLE 1: Baseline characteristics of healthy volunteers.

| Factor | Mean ($\bar{X} \pm S$) |
|-------------------------|--------------------------|
| Age (y) | 26.27 ± 4.479 |
| Height (cm) | 168.93 ± 7.803 |
| Weight (kg) | 65.53 ± 13.568 |
| BMI (kg/m^2) | 22.76 ± 3.283 |
| HR (bpm) | 72.53 ± 8.561 |
| SBP (mmHg) | 114.80 ± 12.344 |
| DBP (mmHg) | 70.73 ± 9.381 |

decibel of ringtones and vibration signals, wake up the loser for three minutes of artificial intervention, let it stay awake for five minutes, and then, turn off the light into the next round of sleep. Three times a night, they were deprived of sleep. Blood pressure monitoring: during sleep and after waking, the blood pressure is monitored in terms of systolic and diastolic values.

2.4. Data Collection. Data from polysomnography (PSG) was recorded simultaneously in order to assess sleep phases. A dynamic ECG recorder (CT-086, CT-082, and CT-083s) was developed by Hangzhou Baihui Medical Equipment Co., Ltd. The data was analyzed using the company's most recent software (V1.0.0), and the recording period was from 21:00 to 07:00 in the evening. An analysis of the frequency domain of the dynamic ECG was performed in order to determine the HRV. During and after sleep deprivation, continuous 5-minute HRV frequency domain data was analyzed without interruption. In addition to the VLF (very low frequency), LF (low frequency), HF (high frequency), and LF/HF (low frequency/high frequency) ratios, the LFnu (standardized low-frequency component) and HFnu (standardized high-frequency component) represent sympathetic tone. HF is a marker of cardiac vagal tone, and the LF/HF ratio is a more sensitive indicator of sympathetic nerves.

2.5. Statistical Analysis. For the statistical analysis, SPSS24.0 statistical software was used. In this study, the measurement data of normal distributions were expressed as $X \pm S$. A paired *T*-test was used to compare quantitative data with a normal distribution before and after treatment, and $P < 0.05$ was considered statistically significant.

3. Results

3.1. Analysis of Patient Data Using Statistical Methods. The study recruited 30 qualified participants from a pool of fifty healthy participants. In the SWS sleep deprivation group, one individual was eliminated from the study due to a lack of slow-wave sleep on the night of sleep deprivation, resulting in a total of 29 subjects being included in the analysis. As shown in Table 1, healthy individuals have the following baseline characteristics.

3.2. An Analysis of the HRV Frequency Domain for Five Minutes. As compared with before deprivation, VLF, LFnu, and LF/HF increased after sleep deprivation, whereas HF

TABLE 2: Analyses of 5-minute HRV frequency domains before and after selective sleep deprivation in volunteers ($\bar{X} \pm S$).

| Project | REM deprivation (before) | REM deprivation (after) | P | SWS deprivation (before) | SWS deprivation (after) | P |
|---------|--------------------------|-------------------------|-------|--------------------------|-------------------------|-------|
| VLF | 2925 \pm 2724 | 3524 \pm 2425 | 0.403 | 808 \pm 665 | 2299 \pm 1745 | 0.003 |
| LF | 974 \pm 612 | 1005 \pm 603 | 0.867 | 608 \pm 433 | 1048 \pm 854 | 0.063 |
| HF | 1273 \pm 670 | 916 \pm 676 | 0.387 | 1169 \pm 571 | 548 \pm 214 | 0.001 |
| LF/HF | 1.42 \pm 1.01 | 1.65 \pm 2.09 | 0.665 | 0.58 \pm 0.49 | 2.05 \pm 1.43 | 0.005 |
| LFNU | 52.50 \pm 16.70 | 52.87 \pm 14.92 | 0.94 | 33.20 \pm 3.61 | 59.63 \pm 19.23 | 0.002 |
| HFNU | 47.50 \pm 16.70 | 46.93 \pm 14.85 | 0.909 | 66.80 \pm 13.50 | 40.37 \pm 19.23 | 0.002 |

and HFnu decreased, and the difference was statistically significant ($P < 0.05$). There was a significant difference between the LF/HF before SWS deprivation and the LF/HF before REM deprivation. In contrast, the LF/HF after SWS deprivation was significantly higher than the LF/HF after REM deprivation, as shown in Table 2. Table 2 shows that there was no statistical significance between before and after REM sleep deprivation in VLF, LF, HF, LF/HF, LFnu, or HFnu in the REM sleep deprivation group ($P > 0.05$).

Heart rate variability is measured through HRV (heart rate variability), VLF (extremely low frequency), LF (low frequency), HF (high frequency), LF/HF (low-frequency to high-frequency ratio), LFnu (normalized low-frequency component), and HFnu (normalized high-frequency component).

3.3. The Results of Changes in Blood Pressure. A significant difference ($P < 0.05$) was found between the diastolic blood pressure after waking after SWS and REM sleep deprivation, as shown in Table 3.

4. Discussion

An adult experiences four to six cycles of REM and non-REM sleep during the night, and increased dopamine (DA) secretion in the basolateral amygdala (BLA) terminates SWS sleep and initiates REM sleep [9]. The sympathetic nervous system is primarily responsible for regulating REM sleep, and sympathetic activity may result in dramatic fluctuations in cardiopulmonary function [10, 11]. Consequently, sleep deprivation has been linked to cardiovascular disease in epidemiological studies, but the extent of the association is unclear [12].

There have been several studies suggesting that sleep deprivation may increase blood pressure, regardless of whether the deprivation is complete or partial [13, 14]. Five healthy adults were subjected to partial sleep deprivation (4.2 hours of nighttime sleep) by Meier-Ewert et al. [15]. It was found that the systolic blood pressure and heart rate increased as well as the high-sensitivity C-reactive protein (CRP) level during sleep deprivation. There is evidence to suggest that sleep deprivation may activate inflammatory processes and therefore result in an increase in cardiovascular disease incidence.

According to our findings, SWS sleep deprivation decreases vagal innervation activity and increases sympathetic activity, such as decreased HF, increased LF to HF ratio, and decreased LFNU and HFNU, reflecting sleep

deprivation's subtle effects on cardiovascular health that are difficult to capture through clinical assessments. The HRV-related indicators (VLF, LF, HF, LF/HF, LFnu, and HFnu) did not differ statistically significantly after REM sleep deprivation, which may be explained by the dominance of sympathetic activity during REM sleep deprivation. A study by Scholz et al. [16] found that LF/HF began to increase even 15 minutes before REM sleep, suggesting that the risk of cardiovascular disease may be associated with REM sleep, which may also explain the higher rate of cardiovascular events in the morning [17]. A typical eight-hour sleep cycle includes 90 to 120 minutes of REM sleep, which means that there is a higher risk of sudden death, up to 1.2 times that of awakened sleep [18]. It is assumed that sympathetic innervation is enhanced during REM sleep than during SWS sleep due to the body's physiological waking activity, since LF/HF values decrease after SWS sleep deprivation but remain higher than those after REM sleep deprivation. According to current theories, the body's physiological regulation of waking activity enables it to avoid a surge in sympathetic activity levels during sudden awakening as a result of increased sympathetic innervation during REM sleep compared to SWS sleep. Sudden awakening from slow-wave sleep causes greater fluctuations in autonomic activity, and an increased cardiovascular risk is associated with sudden awakening from slow-wave sleep in vulnerable individuals. It is consistent with the experimental results of Goff et al. [19] who found that waking from slow-wave sleep was associated with more dramatic fluctuations in blood pressure in the morning than waking from rapid eye movement sleep. Consequently, a sudden change in autonomic nervous system innervation during transitions between deep sleep and light sleep or awakening may result in adverse cardiac events in patients with severe impaired autonomic nervous system function [20].

Pure diastolic hypertension has been reported, especially in the early stages of sleep-disordered breathing, as a specific pattern of hypertension associated with the disease [21], and DBP may be an early indicator of cardiovascular outcomes in OSA patients. Elevated DBP is generally associated with increased peripheral resistance, which is primarily determined by the arterial vessels, whereas elevated SBP is primarily determined by the large and medium vessels [22, 23]. In the absence of elevated SBP, DBP increases suggest that repeated sleep deprivation has a greater impact on the peripheral vasculature than the large to medium vessels. In this study, blood pressure studies after selective sleep

TABLE 3: The effects of selective sleep deprivation on blood pressure in 30 healthy volunteers ($\bar{X} \pm S$).

| Project | REM deprivation | | SWS deprivation | |
|--------------------|--------------------|------------------|--------------------|------------------|
| | SBP (mmHg) | DBP (mmHg) | SBP (mmHg) | DBP (mmHg) |
| BP before sleeping | 106.07 \pm 11.32 | 62.13 \pm 5.25 | 105.00 \pm 11.09 | 62.40 \pm 5.22 |
| BP after waking | 108.87 \pm 11.29 | 67.80 \pm 8.03 | 108.67 \pm 11.70 | 66.27 \pm 1.71 |
| <i>P</i> | 0.134 | 0.038 | 0.117 | 0.019 |

deprivation indicated that following repeated deprivation of SWS and REM sleep for three times, postwake DBP was higher than prewake DBP, while changes in SBP were not statistically significant, which suggests that peripheral resistance and fluctuation in blood pressure are caused by sympathetic activation [24]. Nevertheless, changes in sympathetic nerve activity are not always accompanied by changes in blood pressure, and more research is necessary to determine the exact mechanisms behind these changes.

Several health risks are associated with sleep deprivation, including cardiovascular, respiratory, neurological, gastrointestinal, immune, cutaneous, endocrine, and reproductive health [25]. As the number of indicators for analysis in our study was limited, we intend to expand the cohort to include more indicators in our next study in order to obtain clinical data.

5. Conclusions

As a result of REM/SWS sleep deprivation, diastolic blood pressure increased. Various HRV parameters are associated with different sleep stages after sleep deprivation. For example, the REM period is not significantly affected by sleep-related parameters of HRV after sleep deprivation of the SWS period. People with a healthy autonomic nervous system are better able to tolerate this fluctuation, whereas people with a vulnerable autonomic nervous system are at a higher risk of cardiovascular events as a result of slow-wave sleep. Due to the increased sympathetic activity of REM sleep compared to NREM sleep, the impact of REM sleep on patients at high risk of cardiovascular disease cannot be overlooked. Therefore, cardiac monitoring and advance intervention are important in high-risk patients during different sleep periods at night in order to reduce the occurrence of adverse events. In addition, we will further investigate the changes in hemodynamics and related factors during different sleep periods and the specific mechanisms of cardiovascular events during different sleep periods.

Data Availability

Datasets used in the current study may be obtained from the corresponding author upon request.

Conflicts of Interest

It is claimed that none of the researchers have any conflicts of interest.

Acknowledgments

Using the program number 2019YFC2003705, research has been conducted on closed-loop breathing airflow intervention.

References

- [1] D. R. Hillman and L. C. Lack, "Public health implications of sleep loss: the community burden," *The Medical Journal of Australia*, vol. 199, no. 8, pp. S7–10, 2013.
- [2] C. A. Palmer and C. A. Alfano, "Sleep and emotion regulation: an organizing, integrative review," *Sleep Medicine Reviews*, vol. 31, pp. 6–16, 2017.
- [3] M. Brianza-Padilla, H. Bonilla-Jaime, J. C. Almanza-Pérez, A. L. López-López, F. Sánchez-Muñoz, and G. Vázquez-Palacios, "Effects of different periods of paradoxical sleep deprivation and sleep recovery on lipid and glucose metabolism and appetite hormones in rats," *Applied Physiology, Nutrition, and Metabolism*, vol. 41, no. 3, pp. 235–243, 2016.
- [4] S. Periasamy, D. Z. Hsu, Y. H. Fu, and M. Y. Liu, "Sleep deprivation-induced multi-organ injury: role of oxidative stress and inflammation," *EXCLI Journal*, vol. 14, pp. 672–683, 2015.
- [5] E. Tobaldini, G. Costantino, M. Solbiati et al., "Sleep, sleep deprivation, autonomic nervous system and cardiovascular diseases," *Neuroscience and Biobehavioral Reviews*, vol. 74, pp. 321–329, 2017.
- [6] K. Ackermann, R. Plomp, O. Lao et al., "Effect of sleep deprivation on rhythms of clock gene expression and melatonin in humans," *Chronobiology International*, vol. 30, no. 7, pp. 901–909, 2013.
- [7] A. Cincin, I. Sari, M. Oğuz et al., "Effect of acute sleep deprivation on heart rate recovery in healthy young adults," *Sleep & Breathing*, vol. 19, no. 2, pp. 631–636, 2015.
- [8] G. A. Reyes del Paso, W. Langewitz, L. J. M. Mulder, A. van Roon, and S. Duschek, "The utility of low frequency heart rate variability as an index of sympathetic cardiac tone: a review with emphasis on a reanalysis of previous studies," *Psychophysiology*, vol. 50, no. 5, pp. 477–487, 2013.
- [9] E. Hasegawa, A. Miyasaka, K. Sakurai, Y. Cherasse, Y. Li, and T. Sakurai, "Rapid eye movement sleep is initiated by basolateral amygdala dopamine signaling in mice," *Science*, vol. 375, no. 6584, pp. 994–1000, 2022.
- [10] E. Tobaldini, M. Pecis, and N. Montano, "Effects of acute and chronic sleep deprivation on cardiovascular regulation," *Archives Italiennes de Biologie*, vol. 152, no. 2-3, pp. 103–110, 2014.
- [11] S. Javaheri and S. Redline, "Sleep, slow-wave sleep, and blood pressure," *Current Hypertension Reports*, vol. 14, no. 5, pp. 442–448, 2012.
- [12] J. L. Dettoni, F. M. Consolim-Colombo, L. F. Drager et al., "Cardiovascular effects of partial sleep deprivation in healthy

- volunteers,” *Journal of Applied Physiology*, vol. 113, no. 2, pp. 232–236, 2012.
- [13] S. K. Davies, J. E. Ang, V. L. Revell et al., “Effect of sleep deprivation on the human metabolome,” *Proceedings of the National Academy of Sciences of the United States of America*, vol. 111, no. 29, pp. 10761–10766, 2014.
- [14] J. M. Mullington, M. Haack, M. Toth, J. M. Serrador, and H. K. Meier-Ewert, “Cardiovascular, inflammatory, and metabolic consequences of sleep deprivation,” *Progress in Cardiovascular Diseases*, vol. 51, no. 4, pp. 294–302, 2009.
- [15] H. K. Meier-Ewert, P. M. Ridker, N. Rifai et al., “Effect of sleep loss on C-reactive protein, an inflammatory marker of cardiovascular risk,” *Journal of the American College of Cardiology*, vol. 43, no. 4, pp. 678–683, 2004.
- [16] U. J. Scholz, A. M. Bianchi, S. Cerutti, and S. Kubicki, “Vegetative background of sleep: spectral analysis of the heart rate variability,” *Physiology & Behavior*, vol. 62, no. 5, pp. 1037–1043, 1997.
- [17] S. M. Oh, S. H. Choi, H. J. Kim, K. S. Park, and Y. J. Lee, “The association between obstructive sleep apnea during REM sleep and autonomic dysfunction as measured by heart rate variability,” *Sleep & Breathing*, vol. 23, no. 3, pp. 865–871, 2019.
- [18] R. L. Verrier, J. E. Muller, and J. A. Hobson, “Sleep, dreams, and sudden death: the case for sleep as an autonomic stress test for the heart,” *Cardiovascular Research*, vol. 31, no. 2, pp. 181–211, 1996.
- [19] E. A. Goff, C. L. Nicholas, A. K. Simonds, J. Trinder, and M. J. Morrell, “Differential effects of waking from non-rapid eye movement versus rapid eye movement sleep on cardiovascular activity,” *Journal of Sleep Research*, vol. 19, no. 1p2, pp. 201–206, 2010.
- [20] A. U. Viola, C. Simon, J. Ehrhart et al., “Sleep processes exert a predominant influence on the 24-h profile of heart rate variability,” *Journal of Biological Rhythms*, vol. 17, no. 6, pp. 539–547, 2002.
- [21] Y. Wu, R. Huang, X. Zhong, and Y. Xiao, “Cardiovascular consequences of repetitive arousals over the entire sleep duration,” *BioMed Research International*, vol. 2017, Article ID 4213861, 8 pages, 2017.
- [22] G. Beevers, G. Y. Lip, and E. O’Brien, “ABC of hypertension: the pathophysiology of hypertension,” *BMJ*, vol. 322, no. 7291, pp. 912–916, 2001.
- [23] G. de Simone and F. Pasanisi, “Systolic, diastolic and pulse pressure: pathophysiology,” *Italian Heart Journal Supplement*, vol. 2, no. 4, pp. 359–362, 2001.
- [24] M. J. Carrington and J. Trinder, “Blood pressure and heart rate during continuous experimental sleep fragmentation in healthy adults,” *Sleep*, vol. 31, no. 12, pp. 1701–1712, 2008.
- [25] S. C. Liew and T. Aung, “Sleep deprivation and its association with diseases- a review,” *Sleep Medicine*, vol. 77, pp. 192–204, 2021.

Research Article

MSeg-Net: A Melanoma Mole Segmentation Network Using CornerNet and Fuzzy K -Means Clustering

Marriam Nawaz ^{1,2}, Tahira Nazir ³, Muhammad Attique Khan ⁴, Majed Alhaisoni ⁵,
Jung-Yeon Kim ⁶ and Yunyoung Nam ⁶

¹Department of Software Engineering, University of Engineering and Technology Taxila, 47050, Pakistan

²Department of Computer Science, University of Engineering and Technology Taxila, 47050, Pakistan

³Department of Computing, Riphah International University, Islamabad, Pakistan

⁴Department of Computer Science, HITEC University, Taxila, Pakistan

⁵Computer Sciences Department, College of Computer and Information Sciences, Princess Nourah Bint Abdulrahman University, Riyadh 11671, Saudi Arabia

⁶Department of ICT Convergence, Soonchunhyang University, Asan 31538, Republic of Korea

Correspondence should be addressed to Yunyoung Nam; ynam@sch.ac.kr

Received 18 August 2022; Accepted 17 September 2022; Published 14 October 2022

Academic Editor: Sujatha Krishnamoorthy

Copyright © 2022 Marriam Nawaz et al. This is an open access article distributed under the Creative Commons Attribution License, which permits unrestricted use, distribution, and reproduction in any medium, provided the original work is properly cited.

Melanoma is a dangerous form of skin cancer that results in the demise of patients at the developed stage. Researchers have attempted to develop automated systems for the timely recognition of this deadly disease. However, reliable and precise identification of melanoma moles is a tedious and complex activity as there exist huge differences in the mass, structure, and color of the skin lesions. Additionally, the incidence of noise, blurring, and chrominance changes in the suspected images further enhance the complexity of the detection procedure. In the proposed work, we try to overcome the limitations of the existing work by presenting a deep learning (DL) model. Descriptively, after accomplishing the preprocessing task, we have utilized an object detection approach named CornerNet model to detect melanoma lesions. Then the localized moles are passed as input to the fuzzy K -means (FLM) clustering approach to perform the segmentation task. To assess the segmentation power of the proposed approach, two standard databases named ISIC-2017 and ISIC-2018 are employed. Extensive experimentation has been conducted to demonstrate the robustness of the proposed approach through both numeric and pictorial results. The proposed approach is capable of detecting and segmenting the moles of arbitrary shapes and orientations. Furthermore, the presented work can tackle the presence of noise, blurring, and brightness variations as well. We have attained the segmentation accuracy values of 99.32% and 99.63% over the ISIC-2017 and ISIC-2018 databases correspondingly which clearly depicts the effectiveness of our model for the melanoma mole segmentation.

1. Introduction

The abnormal growth of the skin cells results in cancer inside the human body which is broadly categorized into three types namely squamous cell carcinoma, melanoma, and basal, respectively [1]. Among all three types, melanoma is designated as the most fatal type of skin cancer that develops inside the skin cells namely melanocytes. In a recent study published in [2], it is found that only in the US, approximately 10 thousand victims are dying annually

due to this dangerous disease. The unnecessary expansion of the skin cells generates lesions in the human body that differ in structure, appearance, and mass. The irregular lesion is about 6 mm in size and contains a rare appearance usually in red, brown, pink, or black color which requires an urgent inspection by the dermatologist. Melanoma is further distributed into two categories named benign and malignant. The first category of melanoma known as benign is the less fatal type of skin cancer and is easily curable, whereas malignant is the advanced stage of skin cancer that

may cause the victim death if not detected timely. Mainly, experts execute physical checkups of skin lesions by examining their appearance, structure, and size. However, such an examination process is a time-consuming activity because of the shortage of dermatologists. The timely detection of melanoma lesions is vital as it can control the mortality rate of victims and also protect them from painful surgical processes. Now, computer vision (CV) and artificial intelligence (AI) approaches have assisted the research community to design valued and computer-aided melanoma diagnostic techniques.

Research areas of AI which are working in the medical area are widely distributed into two types namely the machine learning (ML) and DL frameworks. For the ML techniques, the researchers employ pattern-based methods to extract the feature vector from the input samples which are later classified into respective classes with the help of some classifiers like KNN, SVM, and decision tree (DT). However, due to the complex structural properties of melanoma lesions, the conventional ML approaches are not found much proficient as the extensive changes in the color, size, and shape of lesions decrease the recognition ability of these methods. To enhance the effectiveness of the melanoma recognition systems, classification is performed after segmenting the diseased area of skin from the healthy region. Hence, the segmentation of diseased portions is mandatory for the reliable detection of melanoma lesions. Some works like those performed in [3, 4] have tried to better elaborate the significance of the segmentation procedure. However, the segmentation accuracy of existing approaches have been dropped significantly for images with intense changes in light, brightness, and sample distortions, whereas for practical cases, it is impossible to obtain samples with unchanged characteristics. Therefore, there exists a demand for a more accurate melanoma moles recognition system.

Recently, the robustness and better recall ability of the DL frameworks have encouraged scientists to test them in the area of medical image analysis. These systems have exhibited tremendous performance in several areas of the medical including eye abnormalities recognition [5], brain cancer identification [6], heart diseases [7], and skin cancer classification [8]. The ability of DL methods to better compute ambiguity in health-related systems has empowered them to effectively identify and locate the unhealthy regions of the human body [9–16]. The DL approaches highly rely on the selected convolutional neural network (CNN) that is responsible for extracting useful information from the input images and assisting to locate the diseased portion like melanoma moles from human skin. Several methods have used the CNN frameworks for the timely recognition of the melanoma moles from the dermoscopic images and showed impressive results which clearly depict the better adaptability of these methods toward skin cancer recognition. However, most of these methods accomplished some preprocessing steps to tackle the problem of keypoints maps saturation [17]. To avoid such issues, many works have utilized sample mapping along with pixel-wise labels [18, 19]. However, there is a demand for a more reliable model that can better tackle the issues of existing methods.

Reliable and timely detection of skin cancers from images with intense distortion like the incidence of noise, blurring, and brightness variations is still a complex procedure. Besides, the complex properties of skin moles containing alterations in the size, architecture, and color further enhance the difficulty of the recognition method. Moreover, the presence of hair and small blood vessels also hinders the accurate localization of the diseased region. In this work, we attempted to deal with the problems of existing works by proposing a more robust framework. We have used the CornerNet model along with the FKM approach to detect and segment the skin lesions from the dermoscopic images. The presented work provides the following main contributions:

- (i) Employed CornerNet model with the FKM approach for calculating a reliable set of features, which resulted to improve segmentation ability by locating the moles of varying sizes
- (ii) Present a more robust framework that reduces the model train and test time complexity due to its power to tackle the framework overfitted data
- (iii) The presented framework is capable of identifying the abnormal skin moles for samples with intense chrominance, brightness, changes, and suffering from noise and blurring attacks
- (iv) Enhanced skin lesion segmentation ability of the presented work because of the ability of the CornerNet model to nominate a more representative set of features
- (v) A huge evaluation has been carried out on two standard databases named ISIC-2017 and ISIC-2018 and confirmed the robustness of the introduced work for the melanoma lesions segmentation

We have followed the following structural scheme for the rest of the article: Section 2 explains the work from history that is already performed for skin cancer moles recognition. The presented framework is explained in detail under Section 3 while the model evaluation results are presented in Section 4. Finally, the work is concluded under Section 5.

2. Related Work

In this section, an in-depth analysis of already performed work for moles melanoma detection is performed, and the results of all related works are discussed. Extensive work accompanying conventional ML approaches has been carried out by scientists for the automated recognition of skin cancers from dermoscopic samples. One such work was presented in [20] where a segmentation step was performed to locate the area of interest. Secondly, the features from the processed samples were computed by employing the ABCD rule along with the cooccurrence matrix [21]. Finally, the SVM approach was applied to perform the skin moles categorization task. The work proposed in [20] has attained an average accuracy value of 92.10%. Codella et al. [22]

introduced a framework by employing the ensembling technique for skin cancer identification. Initially, the U-Net model was used to segment the moles from the input images, after which the features were computed from the segmented areas via using a sparse coding approach and pattern-based methods. Finally, the SVM model was trained on the computed feature to compute the classification score. In the last step, results are averaged to determine the final class label associated with each image. The work discussed in [22] acquired a classification accuracy of 76% and needs results enhancement. Dagherir et al. [23] proposed a hybrid method to classify the skin moles from dermoscopic images. In the first step, the Otsu method along with the Gaussian approach was used to accomplish the preprocessing step over the input images. Then, the features from the processed samples were extracted by using the scale-invariant feature transform (SIFT) and the histogram of oriented gradients methods, while for the classification of the samples, two renowned ML classifiers named SVM and KNN were used. Besides, the work also proposed a CNN model to compute the deep features as well. The final class associated with each sample is determined by employing a majority vote method. This framework [23] presents improved melanoma lesion identification and categorization results; however, the model requires a huge set of samples for efficient training.

Another framework was presented in [24] that accomplished the melanoma lesion segmentation task by employing the superpixel area growth approach. The approach inherited the idea of the Gaussian mixture model (GMM) which effectively distributed the suspected sample into equal-sized portions. The skin moles were then presented by assigning colored labels to all superpixels extracted with the delta metric approach, which are capable of differentiating the various color shades that are difficult to recognize by the naked eye. The method discussed in [24] attained the segmentation results of 86.83%; however, the segmentation accuracy needs more enhancement. Moreover in [25], another conventional ML approach was introduced that employed the concept of the codeword that used the keypoints similarity computation to accomplish the classification task of melanoma moles. In the first step, a highly correlated set of sample keypoints was computed by employing the linear prediction method, after which the SIFT method along with the RGB color spaces was utilized to compute the feature vector. The acquired feature vectors were employed for the SVM training to accomplish the melanoma moles classification job. The work [25] robustly utilizes processing resources; however, the classification results have highly relied on the selected codebook size.

Now, the efficiency of the CNN and DL approaches has gained much popularity which insisted scientists to test them in the area of health and care as well. Several approaches have been presented by the researcher to provide automated solutions for several medical-related applications like assisting the practitioner in radiology or automatically recognizing several types of syndromes including skin cancers. One such technique was proposed in [26], where the author presented a lightweight framework for recognizing melanoma moles that could be deployed on smartphones.

This work utilized a DL method named the AlexNet model and trained it over the HAM10000 dataset to classify the melanoma moles. The work discussed in [26] attained the classification accuracy of 84%; however, unable to perform well for lesions of very small sizes. Acosta et al. [27] introduced a DL framework to locate and categorize skin moles into various classes. Initially, the Mask-RCNN model was employed to identify the diseased area from the input image. Next, a CNN framework namely the ResNet152 was applied over the segmented region to compute the features and specify the class associated with the detected part. The samples were recognized as benign or malignant. Zhang et al. [28] also employed a DL approach where the fully convolution network (FCN) technique was employed to segment the diseased areas from the dermoscopic samples. The used model named the FCN employed the VGG model as its base network for calculating the nominative feature set from the input images. Moreover, a small framework was employed to fuse the texton pattern-based pixel keypoints with the deep features. This work [28] shows better melanoma moles classification performance; however, the detection results reduce on images containing moles with arbitrary shapes and similar looks. Another approach was proposed in [29] where a DL model namely FC-DPN was introduced to enhance the melanoma lesions segmentation results. The FC-DPN model employed the FCN approach by replacing the dense blocks with the dual-path network (DPN) blocks to better extract the sample features. The DPNs were then distributed into two subregions namely the DPN-projection and processing units, respectively. The major reason for this distribution was to successfully reemploy the computed keypoints. The work discussed in [29] attains the classification accuracy of 95.14% over the ISBI 2017 dataset,4 however, at the charge of increased model computational complexity. Lei et al. [30] proposed a work to perform the automated detection and classification of skin cancers. The approach utilized the residual framework with the FCN method to differentiate the healthy and diseased areas from dermoscopic samples. After this, the employed framework was utilized to calculate the estimation of all pixels combined iteratively to produce the resultant segmentation mask of the skin moles. The methodology elaborated in [30] has shown an average segmentation accuracy value of 95.78% over the ISBI 2016 repository; however, this approach is computationally expensive. A similar method was introduced in [31] that employed the pixel-wise contribution of samples to locate the melanoma moles from the input samples. Initially, a step was performed to improve the visual appearance of the dermoscopic images. Then, an encoder-decoder framework was used to process the improved images to accomplish the classification task as normal or melanoma-affected. The framework discussed in [31] is efficient to locate the skin moles from the dermoscopic images; however, the model is suffering from an overfitting problem. An object detection-based approach was proposed in [32] to present an automated system for skin mole detection and segmentation. First, annotations were developed to exactly identify the diseased portion from the training samples, on which a DL approach namely the

Faster-RCNN was trained. At the test stage, the trained model locates the melanoma-affected region that was further segmented by the fuzzy K -means algorithm. The work was capable of locating the small lesions and acquired the average segmentation accuracy of 95.60% over the PH2 repository. Similarly, many other segmentation approaches [33, 34] have shown robust performance for clustering the diseased areas from the input images.

Nawaz et al. [35] presented another framework for the automated identification and classification of the skin model via employing the Faster-RCNN model together with the SVM approach. The work elaborated in [35] is robust to melanoma classification because of its empowerment to tackle the model overfitting data. However, the works discussed in [32, 35] have highly relied on the selection of hyperparameters in the model training phase. Banerjee et al. [36] also presented a framework for melanoma lesion segmentation. The work utilized an object detection model named the YOLO that extracted a feature vector from the dermoscopic images to locate the position of the affected region. After this, the L-type fuzzy approach was employed to accomplish the segmentation task. The work proposed in [36] performs well for the skin cancer moles segmentation task; however, the detection performance degrades for the lesions of very small sizes. Another DL work was elaborated in [37] where a CNN model was designed to accomplish the skin moles classification task. The CNN model consisted of 68 layers along with the classification unit. The model [37] provides a lightweight solution to melanoma classification; however, results are reported for a small database. Khan et al. [38] proposed a computer-aided framework to locate and classify melanoma moles from the input images. The method initially employed an object detection approach named the Mask-RCNN model to locate and segment the skin moles via computing the deep features with the ResNet50 base network. The detected regions were passed to the DenseNet-201 model to understand the structural description of moles which were later categorized by employing the SVM algorithm. The method elaborated in [38] attained the clustering and categorization results of 93.60% and 96.30%, correspondingly, however, at the expense of increased model complexity. Many other researchers have attempted to classify and segment the skin cancer moles [39–45]; however, there is a demand for performance enhancement. Besides, the expense of processing power for such methods is a substantial barrier in medical applications. An analysis of existing work is presented in Table 1.

3. Methodology

In the presented work, we have introduced a DL approach namely the CornerNet model along with the FKM method to detect and segment melanoma lesions from dermoscopic images. In the first step, a preprocessing step is executed on the input images to eradicate the unwanted objects from the images under analysis. That is, hair or tiny blood vessels can hinder the recognition ability of the CornerNet model. After this, the processed images are used as input to train

the CornerNet model for computing the deep features set and detecting melanoma lesions. Once the moles are detected by the CornerNet model, next the FKM clustering approach is applied to exactly segment the moles. The entire flow of the proposed approach is explained in Figure 1. We have confirmed through analysis that the employment of the CornerNet model with the FKM clustering approach is proficient for locating and segmenting skin lesions of varying masses, shapes, and colors. A detailed description of all steps is given in the proceeding sections.

3.1. Preprocessing. The advancement of DL approaches has presented several automated systems for recognizing different medical diseases via employing image modalities. However, the incidence of noise, blurring, and light variation in samples during the capturing process are unavoidable. The major cause of the occurrence of these transformation changes is the quick variations in the lighting conditions and shadows reflected from the human bodies. The presence of such artifacts in samples can reason for performance degradation for any detection model. Furthermore, in the dermoscopic samples of skin cancers, the occurrence of hair and minute blood vessels further increases the complexity of melanoma mole detection and segmentation. To tackle the above-elaborated issues, a preprocessing step is accomplished on the input images by considering several morphological closing operations to remove the unrequired details from images. Besides, an unsharp filter [47] is also applied to enrich the graphic details of the skin cancer samples which contributes to effectively recognizing the melanoma lesions from the dermoscopic images. We have mentioned the mathematical description of the employed preprocessing operation in the following.

$$S_x(u, v) = (S(u, v) \oplus W) \ominus W. \quad (1)$$

In Equation (1), $S(u, v)$ is presenting the input sample with u and v depicting the pixel location. Moreover, W presents the structuring kernel with a squared shape along with the size of 10 and angles 90° and 180° for all image values, respectively, while $S_x(u, v)$ denotes processed samples free from artifacts. During the artifacts removal process, some other effects like smoothness and blurring are added to samples, so we have applied an unsharp filter to improve the visual appearance of images. The mathematical construction of the unsharp filter is discussed in the following:

$$S_p(u, v) = S_x(u, v) \times \omega(u, v), \quad (2)$$

$$\omega(u, v) = -\frac{1}{\pi\sigma^4} \left[1 - \frac{u^2 + v^2}{2\sigma^2} \right] e^{-(u^2+v^2)/2\sigma^2}.$$

Finally, the resultant image $S_o(u, v)$ is attained by employing Equation (3) free from all unnecessary details. After this, the processed images are passed to the CornerNet model for its training to detect the skin moles.

$$S_o(u, v) = S(u, v) - S_p(u, v). \quad (3)$$

TABLE 1: Relative investigation of existing approaches for recognizing melanoma moles.

| Author | Year | Approach | Task | Database | Accuracy |
|----------------------|------|---------------------------------|----------------|----------------------------|----------|
| <i>ML techniques</i> | | | | | |
| Alquran et al. [20] | 2017 | Pattern features + SVM | Categorization | Custom database | 92.10% |
| Codella et al. [22] | 2017 | U-Net + SVM | Categorization | ISIC-2016 | 76% |
| Daghrir et al. [23] | 2020 | SIFT + SVM and KNN | Categorization | ISIC-2017 | 88.40% |
| Bama et al. [24] | 2021 | GMM model | Segmentation | PH2 | 86.83% |
| Hu et al. [25] | 2019 | SIFT + SVM | Categorization | PH2 | 82% |
| Durgarao et al. [44] | 2021 | LVP, and LBP + C-means | Segmentation | PH2 | 79.44% |
| <i>DL techniques</i> | | | | | |
| Ameri et al. [26] | 2020 | AlexNet | Categorization | HAM10000 | 84% |
| Acosta et al. [27] | 2021 | ResNet-152 | Categorization | ISIC-2017 | 90.40% |
| Zhang et al. [28] | 2019 | VGG-16 | Categorization | ISIC-2017 | 92.72% |
| Shan et al. [29] | 2020 | FC-DPN | Segmentation | ISIC-2017 | 95.14% |
| Bi et al. [30] | 2019 | Res-FCN | Segmentation | ISIC-2016 | 95.78% |
| Adegun et al. [31] | 2019 | Encoder-decoder | Categorization | ISIC-2017 | 95% |
| Nawaz et al. [32] | 2021 | Faster-RCNN + FKM | Segmentation | PH2 | 95.6% |
| Nawaz et al. [35] | 2021 | Faster-RCNN + SVM | Categorization | ISIC-2016 | 89.10% |
| Banerjee et al. [36] | 2020 | YOLO + L-type fuzzy clustering | Segmentation | ISIC-2017 | 97.33% |
| Iqbal et al. [37] | 2021 | CNN | Categorization | ISIC-2019 | 88.75% |
| Khan et al. [38] | 2021 | Mask-RCNN, DenseNet201 + SVM | Segmentation | ISIC-2016 | 93.6% |
| Mohakud et al. [39] | 2022 | Encoder-decoder | Segmentation | ISIC-2016 | 98.32% |
| Abdar et al. [40] | 2021 | Bayesian model | Categorization | Kaggle skin cancer dataset | 88.95% |
| Pacheco et al. [41] | 2021 | Metadata and block-based method | Categorization | ISIC-2019 | 74.90% |
| Wang et al. [42] | 2022 | U-Net | Segmentation | ISIC-2017 | 94.67% |
| Zhao et al. [43] | 2022 | U-Net++ | Segmentation | ISIC-2018 | 95.30% |
| Ali et al. [46] | 2021 | DCNN | Categorization | HAM10000 | 91.93% |

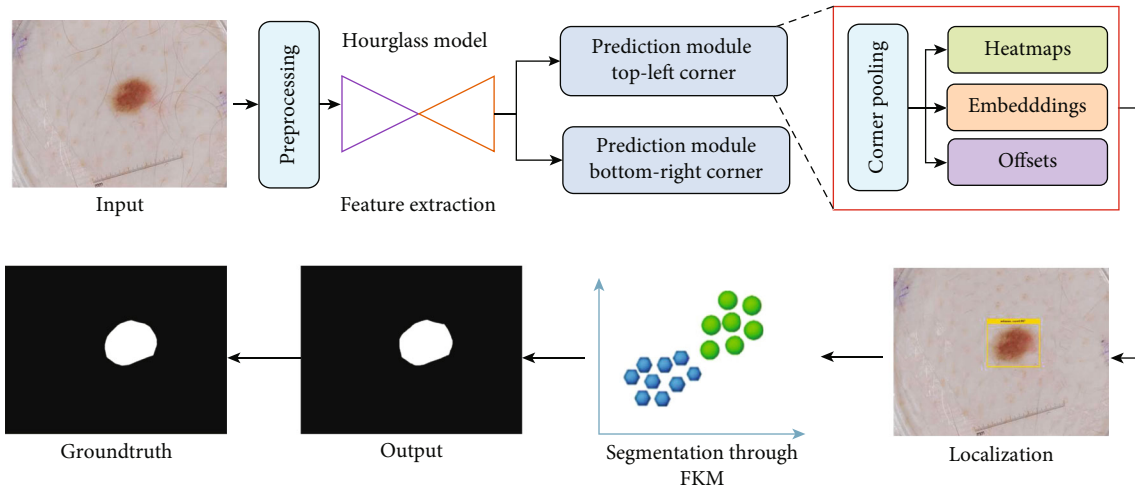


FIGURE 1: Proposed method diagram.

3.2. *CornerNet*. The CornerNet [48] is a well-known one-stage object detection model that recognizes the region of interest (RoIs) like the diseased region (skin moles) from the input samples through keypoint calculation. The CornerNet model is concerned to estimate the top-left (TL) and bottom-right (BR) corners to draw the box with more accurateness in comparison to other object detection models

[49, 50]. The CornerNet framework is comprised of two basic units which are the feature computation backbone and the prediction module (Figure 1). At the start, a keypoint extractor unit is used which extracts the reliable feature vector that is employed to estimate the heatmaps (Hms), embeddings, offset, and class (C). The Hms is concerned to give the approximation if a specific location in a

sample is a TL/BR corner associated with a particular category [51], while the embeddings are used to discriminate the detected pairs of corners and offsets to fine-tune the box position. The corners with high-scored TL and BR coordinates are employed to regulate the exact position of the box, whereas the associated category for each detected diseased region is specified by using the embedding distances on the computed feature vector.

The CornerNet framework shows robust performance in detecting and classifying several types of objects [49, 52–54]. The abnormalities of melanoma lesions have some distinct characteristics, like moles of different shapes and sizes and high color resemblance in the affected and healthy regions of skin areas which complicates the detection procedure. Moreover, the existence of several image distortions like the alterations found in the light, color, and brightness of the samples and the incidence of noise and blurring effect further increase the complexity of the skin lesions detection. Therefore, to better tackle the complexities of samples, we have used the CornerNet model with an Hourglass framework as its base network. The introduced base network is capable of locating and extracting the more relevant sample attributes which assists the CornerNet approach to enhance its recall ability in comparison to the conventional model.

The inspiration for nominating the CornerNet approach for deep features computation and detection of melanoma moles is due to its capability to effectually detect objects by utilizing keypoint approximation in comparison to earlier approaches [49, 50, 55–57]. The framework utilizes detailed keypoints and identifies the object by employing a one-stage detector, so it eliminates the need of using huge anchor boxes for diverse target dimensions than the other one-stage object recognition models, i.e., SSD [55] and YOLO (v2, v3) [56]. Moreover, the CornerNet model is more computationally robust than the other anchor-based two-stage approaches, i.e., RCNN [57], Fast-RCNN [49, 58], and Faster-RCNN [50, 59]) as these techniques employ two phases to accomplish the object localization and categorization job. Consequently, the CornerNet model efficiently tackles the problems of existing works by presenting a more proficient network that extracts more nominative sample features and reduces the computational cost as well.

3.2.1. Hourglass Network. The hourglass network [28] is employed as a backbone to obtain relevant features from the input image. It is a fully convolutional network consisting of one or more hourglass modules. Initially, the model accepts the image with dimensions of 256×256 . In an hourglass module, input features are first downsampled by using a series of max-pooling layers and convolutions. After that, the features are upsampled back to their original resolution by using a series of convolutional and upsampling layers. As details of the feature are lost during the operation of max-pooling layers, details in the upsampled features are brought back by introducing skip layers. Both global and local features are captured by the hourglass network in one uniform structure. When the network stacks multiple hourglass modules, it can reprocess the features for capturing higher-level information. Due to these properties, the hour-

glass network becomes a more suitable choice for brain tumor detection.

3.2.2. Corner Detection. After the hourglass network, there are two modules for the prediction of corners, i.e., top-left and bottom-right corners. Each corner has one positive ground-truth position location, and all other locations are set as negative. This is done this way because, for a close pair of false corner detections, a box can still be produced which overlaps the ground-truth box. The radius is determined by analyzing the size of an object, which is done by making sure that a bounding box corresponding to at least an IoU with ground-truth annotations would be generated by a pair of points residing within the radius. The parameter t is set to 0.7 in each experiment. When the radius is given, an unnormalized 2D Gaussian is used to determine the amount of penalty reduction. The 2D Gaussian, g is determined by $e^{-(a^2+b^2)/2\sigma^2}$, which has a center at locations and has σ as one-third portion of the radius.

The detection loss function is defined as

$$L_{detect} = \frac{-1}{M} \sum_{n=1}^N \sum_{j=1}^H \sum_{k=1}^W \begin{cases} (1 - p_{nj k})^\varphi \log(p_{nj k}) & \text{if } g_{nj k} = 1 \\ (1 - g_{nj k})^\omega (g_{nj k})^\varphi \log(1 - p_{nj k}) & \text{otherwise,} \end{cases} \quad (4)$$

where M represents the total number of objects in the image. For a certain location (j, k) , $p_{nj k}$ is the score for a certain class C in the set of predicted heatmaps, and $g_{nj k}$ is the heatmap labeled as “ground-truth” which is generated with the Gaussians. φ and ω are hyperparameters that are responsible for controlling the contribution of each point. In our implementation, we have set the values of φ and ω , as 3 and 5, respectively. The Gaussian bumps are encoded with $g_{nj k}$, and the term $(1 - g_{nj k})$ guarantees the reduction of the penalty around the locations which are set as ground-truth.

The downsampling layers are employed to reduce memory usage and gather global information [15, 28]. Every location denoted by a, b in the input image is mapped to another location $(a/d, b/d)$ in the heatmaps, where d is the factor to which downsampling is performed. Remapping locations from the heatmaps to the input image may result in some precision loss, which can affect the quality of the IoU of smaller bounding boxes. The CornerNet resolves this issue by predicting location offsets for adjusting the corner locations before their mapping to the input resolution and given by

$$Z_i = \left(\frac{a_i}{n} - \left\lfloor \frac{a_i}{n} \right\rfloor, \frac{b_i}{n} - \left\lfloor \frac{b_i}{n} \right\rfloor \right), \quad (5)$$

where Z_i denotes offset and a_i and b_i are the coordinators of a and b for corner i . Particularly, one group of offsets is predicted shared by top-left corners of all categories, and another group of offsets is shared by bottom-right corners. The smooth L1 loss [11] is applied at ground-truth corners for training purposes and is defined as

$$L_{off} = \frac{1}{M} \sum_{i=1}^M \text{SmoothL1Loss}(Z_i, Z'_i). \quad (6)$$

3.2.3. Corner Grouping. An image may contain multiple objects; thus, the algorithm may detect multiple bottom-right and top-left corners in a single image. In this step, the algorithm detects the pair of bottom-right and top-left corners belonging to the same bounding box. For each detected corner, the network predicts an embedding vector such that the distance between the embeddings for each bottom-right and top-left corners belonging to the same bounding box should not be large. The corners are then grouped based on these distances. Here, we incorporate the embeddings of only one dimension. The “pull” and “push” losses used to train the network for grouping and separation of the corners are given as below:

$$\begin{aligned} Loc_{pull} &= \frac{1}{M} \sum_{i=1}^M \left[(e_{tp_i} - e_i)^2 + (e_{bt_i} - e_i)^2 \right], \\ Loc_{push} &= \frac{1}{M(M-1)} \sum_{i=1}^M \sum_{\substack{j=1 \\ j \neq i}}^M \max \left[0, \Delta - |e_{tp_i} - e_j| \right], \end{aligned} \quad (7)$$

where e_{tp_i} represents the embeddings for the bottom-right corner and top-left corners with e_{bt_i} , where e denotes embeddings, tp denotes top-right corner, bt denotes bottom-right corner, and i denotes the skin moles. Moreover, e_i denotes the mean of e_{tp_i} and e_{bt_i} , and the value of $\Delta = 1$ is used in all our experiments. Same as the offset loss, the losses are only applied at the ground-truth corner location.

3.2.4. Prediction Module. The feature computation framework has consisted of two separate output units, which denote the TL and the BR corners estimation branches, respectively. Every branch unit comprises a corner pooling layer (CPL) positioned on the top of the backbone to pool keypoints and produces three results: Hms, embeddings, and offsets. This module is an improved residual block (RB) containing two 3×3 CnL and one 1×1 residual network followed by a CPL. The CPL assists the framework to identify the potential corners. The reduced keypoints are used as input into a 3×3 CnL-BtN layer, and then the reverse projection is performed. This improved RB is followed by a 3×3 CnL which produces Hms, embeddings, and offsets. The Hms is concerned to give the approximation if a specific location in a sample is a TL/BR corner associated with a particular category, while the embeddings are used to discriminate the detected pairs of corners and offsets to fine-tune the box position. A suspected image can contain more than one affected region; therefore, embeddings assist the model to determine if the predicted corner points belong to a single or different class.

3.3. Skin Lesion Segmentation Using FKM. Once the lesions are detected by the CornerNet model, then the FKM approach is applied to the detected moles to segment them

by separating the diseased pixels from the healthy regions. The major purpose of nominating the FKM in comparison to the K -means clustering technique is that the K -means model belongs to the hard clustering category in which one sample belongs to a single cluster. While in comparison, in the FKM approach, one sample can reside in several clusters, so it is better suited to overlapped data.

The detected lesions from the last step are passed as input to the FKM approach to accomplish the segmentation task. The FKM approach distributes the suspected sample into l segments $r_k = (k = 1, 2, 3, \dots, l)$ that are linked to the center of the cluster denoted as C_j . The FKM algorithm employs “fuzzy” or “soft” relation among ROIs and samples and minimizes distortion by utilizing the following formulation:

$$L = \sum_{u=1}^k \sum_{v=1}^N b_{u,v}^f g_{u,v}. \quad (8)$$

In Equation (3), k denotes the total clusters, whereas f represents the fuzzifier parameter that operates the keypoints and resultant clusters. Moreover, $b_{u,v} \in [0, 1]$, and $g_{u,v}$ shows the link and the computed Euclidean distance among the center of clusters and keypoints. A detailed description of the FKM approach is given in Algorithm 1.

4. Results

In this part, a detailed description of the used datasets is given. Moreover, we have defined the performance measures used to evaluate the segmentation results of the presented methodology. Furthermore, a comprehensive experimental evaluation has been carried out to explain the segmentation ability of our work in comparison to other latest frameworks. Table 2 shows the description of the trainable parameters for the proposed approach.

4.1. Datasets. To validate the model in segmenting the melanoma moles, we have considered two standard databases named ISIC-2017 and ISIC-2018. The mentioned datasets are provided by the “International Symposium on Biomedical Images (ISBI) in the Challenge of Skin Lesion Analysis toward Melanoma Detection” [60]. A detailed explanation of the employed repositories is elaborated in Figure 2. In both datasets, the ground-truths are provided which are examined and verified by a panel of experts in this domain. The major cause of nominating the ISIC repositories for evaluating the segmentation ability of the presented work is that both datasets contain samples of varying attributes like the intense changes in the size, mass, shape, and color of the moles. Moreover, images are subject to several distortions like containing blurring, noise, and intensity variations which make them challenging and close to real-world examples. We have divided the datasets into three sets where 60% of data is used for model training, 10% for validation, and 30% is employed for model testing.

We have trained the presented work with an epoch rate of 20. To show the effective learning of our work, we have reported the training accuracy and loss graphs in Figure 3

Sequence of steps performed by FKM for melanoma moles segmentation.

1. Input:
 - Clusters = C_k
 - Clusters initialization = $C_k = \mathbf{0}$
 - Keypoints = $g_{i,j}$
 - Fuzzification parameter = m
- //FKM ()
2. Compute membership for all keypoints of clusters

$$b(i, j) = ((g_{(i,j)}^{(1/m-1)} \sum_{l=1}^k (1/g_{il})^{1/m-1}))^{-1}$$
3. Change value of the cluster centers:

$$C_j(p) = \sum_{i=1}^N b_{i,j}^m X_i / \sum_{i=1}^N b_{i,j}^m.$$
4. Replicate step 2, until the convergence of the FKM technique.
5. Output: Show samples with segmented healthy and diseased areas

ALGORITHM 1

TABLE 2: Training parameters of the presented methodology.

| Model parameters | Value |
|--|--------|
| No of epochs | 20 |
| Value of learning rate | 0.0001 |
| Selected batch size | 8 |
| The threshold for the confidence score | 0.2 |
| The threshold for the unmatched region | 0.5 |

which are clearly depicting the robust performance of our approach.

4.2. Evaluation Metrics. To measure the segmentation results of the presented work, several standard measures named sensitivity [61], specificity [62], accuracy [63], dice coefficient [64], and Jaccard Index [65] are nominated. The mathematical depiction of the used measures is given in the following:

$$\begin{aligned}
 \text{Specificity} &= \frac{TP}{TP + FP}, \\
 \text{Sensitivity} &= \frac{TP}{TP + FN}, \\
 \text{Accuracy} &= \frac{TP + TN}{TP + FP + TN + FN}, \\
 \text{Dice} &= \frac{2 \times TP}{2 \times TP + FN + FP}.
 \end{aligned} \tag{9}$$

4.3. Assessment of Presented Framework. A precise skin mole detection and segmentation approach should be empowered to accurately locate the lesions of variable mass and structure. To check this, an analysis is performed in this section. For this reason, the test images from both nominated ISIC datasets are taken and evaluated on the trained framework. The test samples from both repositories contain cancer moles of arbitrary shape and size with extensive changes in the chrominance appearance. The visual results for both the detection and segmentation of melanoma moles are shown in Figure 4. The effective recognition ability of the CornerNet model empowers it correctly identify the mel-

noma lesions by altering mass and structures. To numerically determine the recognition power of the CornerNet model, we employed the mAP performance measure as it helps in understanding the capability of a framework in locating the melanoma moles. The CornerNet model identified the melanoma moles with the mAP value of 0.967, 0.988, and 0.971 over the ISCI-2017 and ISIC-2018 repositories, respectively. For segmentation results, the FKM approach grouped the skin cancer moles with white color to determine the region of interest, while the remaining information is referred to as the black area in the segmented samples. The visual results from both datasets are shown in Figure 4 from where it is quite evident that the proposed approach is proficient in recognizing the melanoma moles and vigorous to variations exist in the position, volume, and architecture of the skin moles.

To further discuss the recognition ability of our method, numerous standard performance metrics are selected to numerically show the robustness of our approach. Initially, we have discussed the sensitivity, specificity, and accuracy values attained over the ISIC-2017 and ISIC-2018 repositories, and the acquired values are shown in Figure 5. Descriptively, over the ISIC-2017 repository, the presented approach reported the sensitivity, specificity, and accuracy values of 98.76%, 99.68%, and 99.32%, respectively, whereas for the ISIC-2018 dataset, the introduced methodology has shown the values of 99.48%, 99.39%, and 99.63% for the sensitivity, specificity, and accuracy measures, respectively.

Then, we have selected the Jaccard index and dice coefficient performance metrics as these are considered the standard measures by the researchers for discussing the segmentation results of a model. These measures assist to determine how much a proposed model is capable of locating and recognizing the skin moles of varying sizes and shapes. The attained results are depicted with the help of a box plot as this graph is capable of better discussing the attained values by showing the lowest, highest, and average results (Figure 6). The values shown in Figure 6 clearly show that our work is empowered to depict better segmentation results for both nominated datasets. More clearly, in the case of ISIC-2017 respiratory, the presented technique has attained the Jaccard index and dice scores of 0.9693, and

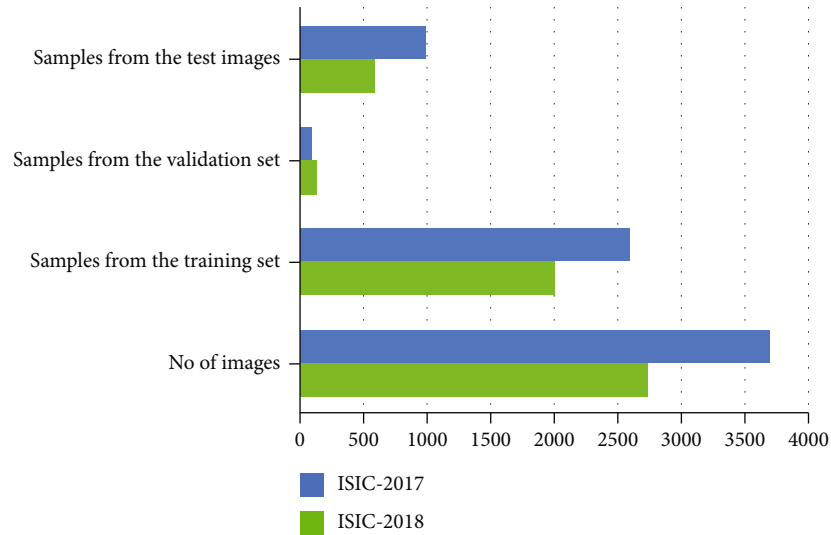


FIGURE 2: Details of samples from both employed datasets.

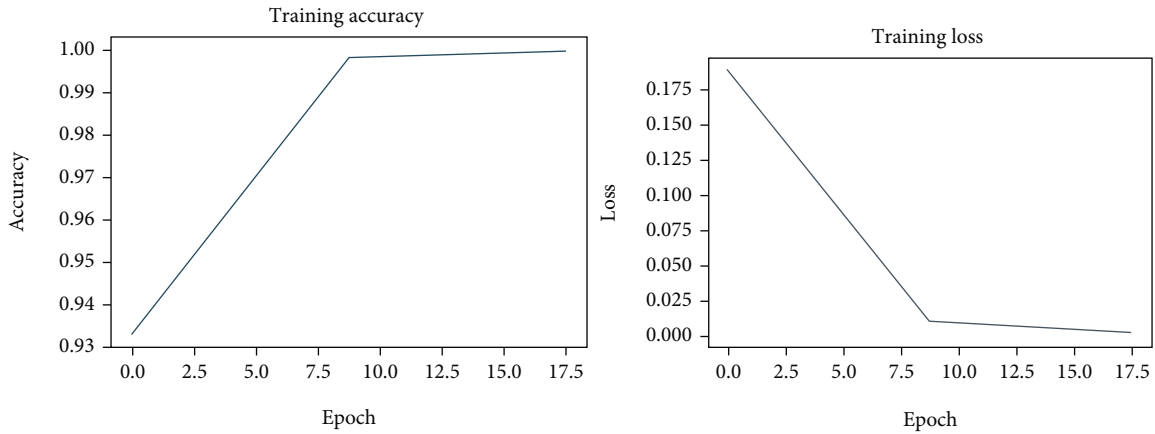


FIGURE 3: Pictorial illustration of train time accuracy and loss graphs.

0.9813, while for the ISIC-2018, the proposed approach has shown the Jaccard index and dice scores of 0.9783 and 0.9886. The values clearly show that our work is quite proficient in locating the lesions under huge changes in the shape and structure of moles.

Another important measure employed by the scantiest to elaborate on the recognition ability of any model is the confusion matrix as this plot assists to understand the ability of the model to differentiate the healthy samples from the diseased. The attained confusion matrix for both ISIC-2017 and ISIC-2018 repositories with the help of the proposed approach is shown in Figure 7. The reported values in the figure clearly show the effectiveness of our approach in accurately locating and recognizing the diseased and healthy samples.

It is quite evident from the visual and quantitative results discussed above that the proposed framework has exactly segmented the skin moles with a high recall ability and robust performance results. The model has depicted better results because of its power to nominate the representative set of key-points capable of better discussing the structural information

of suspected samples which eventually improves the segmentation results of the proposed approach.

4.4. Comparison with Challenge Teams. We performed an analysis to evaluate the segmentation results of the proposed approach for both employed results against the highest performing teams from the ISIC-2017 and ISIC-2018 competitions.

For the ISIC-2017 dataset, the obtained analysis with the challenge teams is shown in Table 3 where we have taken the five highest performing teams and compared our results with them. The stated values in Table 3 are reported from the ISIC-2017 challenge leaderboard. It is quite visible from the comparison shown in Table 3 that the proposed approach has attained the highest segmentation values for all employed evaluation metrics compared to the competitive approaches. The approaches discussed in [66–70] acquired the accuracies of 93.40%, 93.20%, 93.40%, 93.10%, and 93.0%, while comparatively, our work has shown the accuracy results of 99.32%. Similarly, for the Jaccard index, dice score, specificity, and sensitivity, the proposed approach

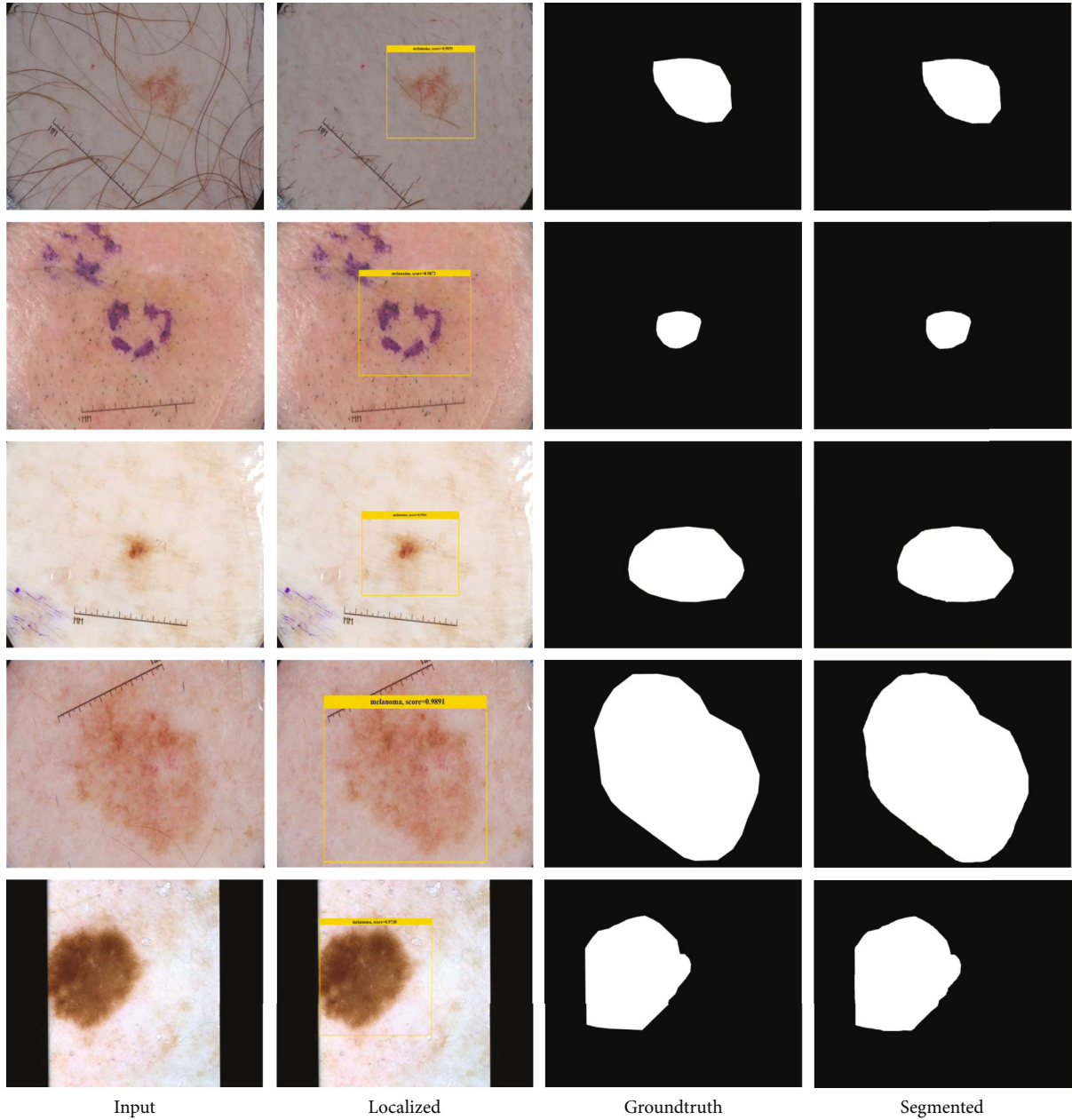


FIGURE 4: A pictorial representation of both localized and segmented images with the CornerNet model along with the FKM approach.

has shown the values of 0.9693, 0.9813, 99.68%, and 98.76%, respectively, which are higher than the values shown in [66–70]. More descriptively, for the Jaccard index metric, we have shown a performance gain of 20.91% which is 13.81% for the dice measure in comparison to the competitive method. Similarly, for the accuracy performance metric, we have attained a performance gain of 6.10%. Besides, for the specificity and sensitivity evaluation measures, we have shown a performance gain of 2.02% and 17.22%, respectively, in comparison to the selected methods. Hence, we can say that our approach is more competent than the peer approaches in segmenting skin lesions and shows the state-of-the-art performance.

Further, we have elaborated on the comparative analysis of our work with the top three teams of the ISIC-2018 chal-

lenge to conduct a performance comparison for the ISIC-2018 repository. The obtained comparison is shown in Table 4. For the ISIC-2018 dataset, the proposed approach has performed better than all the selected teams from the competition leaderboard. More clearly, for the Jaccard index, the selected models have shown the average results of 0.8363, which is 0.9783 for our work. Therefore, for the Jaccard index, the proposed work has given an average performance gain of 14.20%. Similarly, for the dice measure, the competitor methods have elaborated the average score of 0.9001, which is 0.9886 for our work. So, we have given an average performance gain of 8.79% for the dice score. Similarly, for accuracy, the peer teams have shown average results of 94.33%, while our work has gained an accuracy value of 99.63%. So, for the accuracy measure, we have

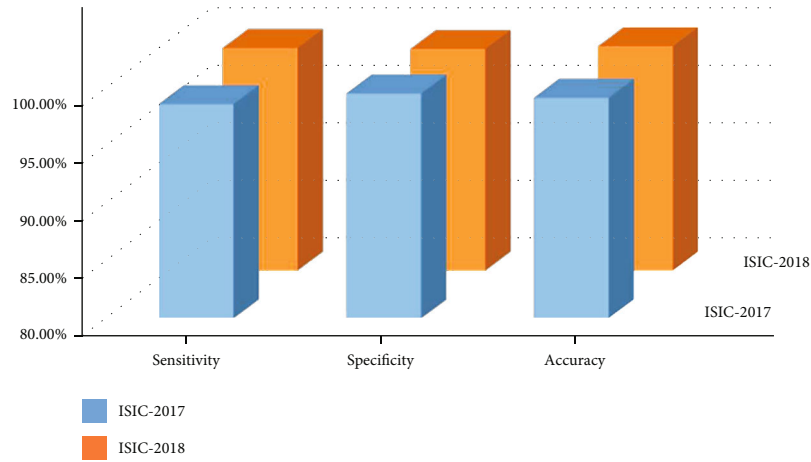


FIGURE 5: Dataset-wise attained segmentation results.

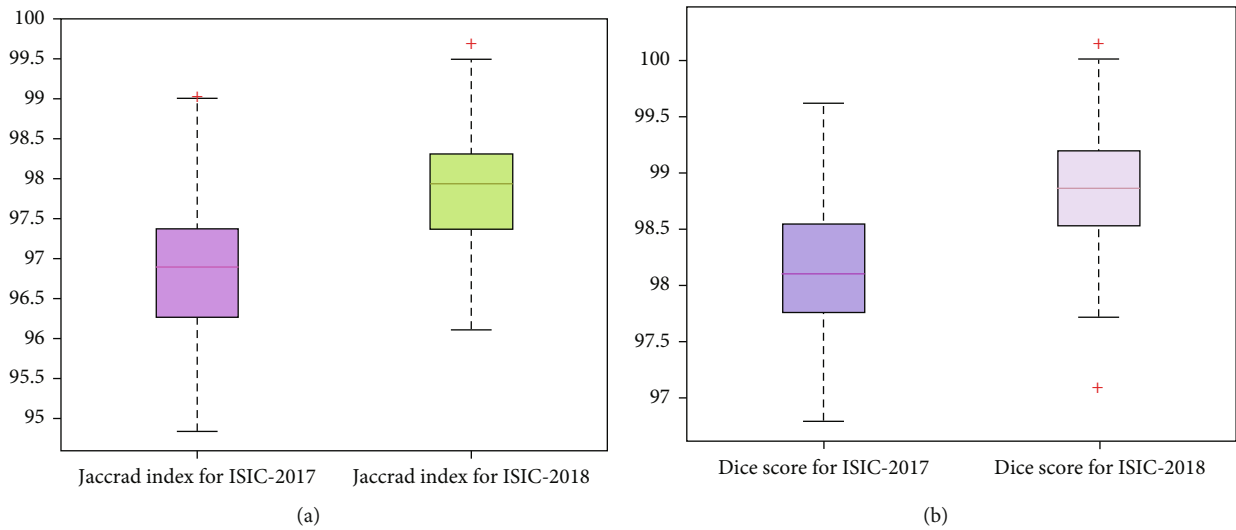


FIGURE 6: Performance measure of the presented technique in the forms of attained (a) Jaccard index and (b) dice score over the ISCI-2017 and ISIC-2018 datasets correspondingly.

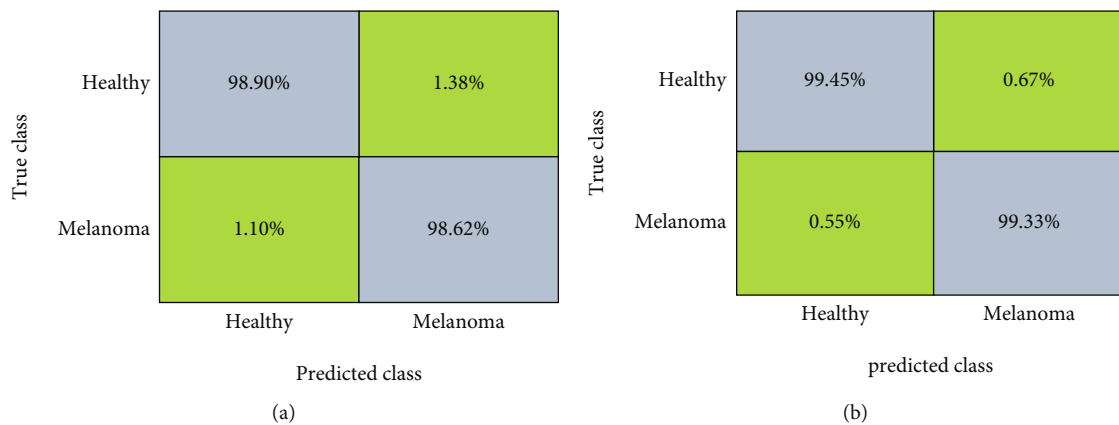


FIGURE 7: Attained confusion matrix results for the employed databases as (a) ISIC-2017 and (b) ISIC-2018 correspondingly.

attained an average performance gain of 5.30%. Moreover, for the specificity metric, the nominated teams have attained an average score of 95.96%, which is 99.39% for our method.

So, for the specificity measure, we have given a performance gain of 3.42%. Furthermore, for the sensitivity measure, the comparative approaches have given an average value of

TABLE 3: Comparative analysis of our work with performance values from the ISIC-2017 challenge leaderboard.

| Method | Jaccard index | Dice | Accuracy | Specificity | Sensitivity |
|----------------------------|---------------|--------|----------|-------------|-------------|
| CDNN [66] | 0.7650 | 0.8490 | 93.40% | 97.50% | 82.50% |
| U-Net [67] | 0.7620 | 0.8470 | 93.20% | 97.80% | 82.00% |
| Deep residual network [68] | 0.7600 | 0.8440 | 93.40% | 98.50% | 80.20% |
| U-Net [69] | 0.7540 | 0.8390 | 93.10% | 96.90% | 81.70% |
| FCNN [70] | 0.7.20 | 0.8370 | 93.00% | 97.60% | 81.30% |
| Proposed | 0.9693 | 0.9813 | 99.32% | 99.68% | 98.76% |

TABLE 4: Comparative analysis of our work with performance scores from the ISIC-2018 challenge leaderboard.

| Method | Jaccard index | Dice | Accuracy | Specificity | Sensitivity |
|-----------------------------|---------------|--------|---------------|-------------|-------------|
| Mask-RCNN2+segmentation | 0.838 | 0.898 | 94.20% | 96.30% | 90.60% |
| Ensemble with CRFv3 | 0.837 | 0.904 | 94.50% | 95.20% | 93.40% |
| Lesion segmentation by DCNN | 0.834 | 0.900 | 94.30% | 96.40% | 91.80% |
| Proposed | 0.9783 | 0.9886 | 99.63% | 99.39% | 99.48% |

91.93%, which is 99.48% for our approach. So, for the sensitivity measure, we achieved a performance gain of 7.55%. In accordance with the conducted evaluation, this analysis demonstrates that the advised method is accomplished in attaining better segmentation results as compared to top-ranked approaches on the same datasets.

4.5. Performance Analysis with the Latest Methods. In this part, we have selected numerous new techniques employing the ISIC-2017 and ISIC-2018 datasets and compared our results with them by using several standard performance metrics.

Initially, for the ISIC-2017 datasets, the approaches described in [71–78] are selected, and the attained performance comparative analysis is exhibited in Table 5. Descriptively, the work in [71] was based on a deep learning framework for accomplishing the automated segmentation of the skin moles. In the first phase, the model employed the ResNet50 network to calculate a set of feature vectors, in which later, the segmentation was applied with the decoder unit. This approach [71] exhibited segmentation accuracy, Jaccard index, and dice scores of 94.50%, 80.53%, and 87.92%. Wu et al. [72] proposed a DL framework for recognizing the skin moles and acquired the average accuracy, Jaccard index, and dice scores of 93.26%, 76.53%, and 85.00%, while the work presented in [74] represents a model namely *W-net* for segmenting the melanoma lesions and reported sensitivity, specificity, and accuracy with the values of 0.9486, 0.9889, and 97.94%. The methods discussed in [73, 75] attained the average segmentation results with accuracies of 98.67% and 86%, respectively. Moreover, the approaches in [76–78] also showed promising segmentation results with values of 94.08%, 94.30%, and 93.13%, respectively, while it is quite evident from the results reported in Table 5 that the proposed approach has shown the highest performance values for all used evaluation measures.

It is quite clear from the values shown in Table 5 that the comparative methods have shown an average sensitivity value of 0.8890, while our work has depicted a sensitivity

TABLE 5: Performance analysis of the proposed work with the new methods over the ISIC-2017 dataset.

| Reference | Sensitivity | Specificity | Accuracy (%) | Jaccard index (%) | Dice (%) |
|-----------|---------------|---------------|--------------|-------------------|--------------|
| [71] | 0.8804 | 0.9659 | 94.50 | 80.53 | 87.92 |
| [72] | 0.8392 | 0.9725 | 93.26 | 76.53 | 85.00 |
| [74] | 0.9486 | 0.9889 | 97.94 | — | 93.22 |
| [73] | 0.9695 | 0.9950 | 98.67 | 95.98 | 97.95 |
| [75] | 0.8600 | — | — | — | — |
| [76] | — | — | 94.08 | 78.55 | 86.48 |
| [77] | — | — | 94.30 | — | — |
| [78] | 0.8364 | — | 93.13 | 74.88 | 85.63 |
| Proposed | 0.9876 | 0.9968 | 99.32 | 96.93 | 98.13 |

score of 0.9876 and given a performance gain of 9.86%, while for the specificity measure, the competitive approaches have shown a value of 0.9806 which is 0.9968 for our work. So, we have shown a performance gain of 1.62% for the specificity measure. Moreover, for the accuracy, Jaccard index, and dice score, the selected methods have shown the average values of 99.13%, 81.29%, and 89.37%, which are 99.32%, 96.93%, and 98.13% for the proposed approach. Therefore, we have presented the performance gains of 4.20%, 15.64%, and 8.76% for the accuracy, Jaccard index, and dice score.

We have also performed the comparison of our approach for the ISIC-2018 dataset against the latest approaches mentioned in [72–76, 79–81], and the attained comparison is given in Table 6. In [72], a network named *FAT-Net* was proposed to perform the segmentation of skin moles from the dermoscopic images and attained sensitivity, specificity, and accuracy scores of 0.9100, 0.9699, and 95.78%, while the work in [74] also utilized a CNN model and depicted the sensitivity, specificity, and accuracy scores of 0.9554, 0.9840, and 97.39%, whereas the method described in [73] deployed a deep learning framework and attained sensitivity, specificity, and accuracy scores of 0.9910, 0.9878, and 98.86%. Araújo et al. [79] presented a

TABLE 6: Performance analysis of the proposed work with the new methods over the ISIC-2018 dataset.

| Reference | Sensitivity | Specificity | Accuracy (%) | Jaccard index (%) | Dice (%) |
|-----------|---------------|---------------|--------------|-------------------|--------------|
| [72] | 0.9100 | 0.9699 | 95.78 | 82.02 | 89.00 |
| [74] | 0.9554 | 0.9840 | 97.39 | — | 93.00 |
| [73] | 0.9910 | 0.9878 | 98.86 | 95.66 | 97.78 |
| [79] | 0.8620 | 0.9860 | 96.70 | 80.00 | 88.90 |
| [75] | 0.8600 | — | — | — | — |
| [80] | 0.8691 | 0.9809 | 97.20 | 97.57 | — |
| [76] | 0.9049 | — | 96.19 | 83.45 | 89.99 |
| [81] | 0.7890 | 0.9800 | — | 94.00 | — |
| Proposed | 0.9939 | 0.9948 | 99.63 | 97.83 | 98.86 |

method named LinkNet to locate and clustered the melanoma lesions and gained an accuracy score of 96.70%. Furthermore, the approaches elaborated in [75, 81] demonstrate sensitivity scores of 0.86 and 0.7890, respectively. Moreover, the techniques discussed in [76, 80] presented accuracy results of 97.20% and 96.19%, respectively.

The performed analysis in Table 6 clearly shows the effectiveness of our approach in comparison to the latest methods, as we have attained the highest results for all reported performance measures. In a more descriptive manner, the selected approaches have shown an average sensitivity score of 0.8927, while our work has reported a sensitivity value of 0.9939 and given a performance gain of 10.12%. For the specificity, the comparative methods have given a score of 98.14% which is 0.9914 for the proposed work. So, we have shown a performance gain of 1.34% for the specificity measure. Moreover, for the accuracy, Jaccard index, and dice score, the comparative methods have shown average values of 97.02%, 88.78%, and 91.73%, while the proposed approach has demonstrated the values of 99.63%, 97.83%, and 98.86% and presented the performance gains of 2.61%, 9.05%, and 7.13% for the accuracy, Jaccard index, and dice score, respectively.

The performance evaluations conducted in Tables 5 and 6 are clearly confirming the proficiency of our work as compared to the other latest methods. Our approach has gained the highest results due to the shallow structural description of the proposed approach that assists it to avoid the gradient vanishing problem and makes it capable of learning the complex properties of melanoma lesions. The other approaches from history are employing very deep networks with the employment of redundant information which enhances their computational complexity and causes the model overfitting problem. The proposed approach has better tackled the limitations of peer methods by proposing an efficient approach that assists to learn a more descriptive set of the features of the sample and enhances the recall ability of the model.

5. Conclusions

The adverse stage of melanoma cancer results in complicated and expensive surgical cure processes and even can cause the demise of the victim. In the presented work, we

attempted to diagnose the lesions at the earliest stage by segmenting them from the dermoscopic samples. We have used the CornerNet model along with the FKM approach to detect and segment the skin moles from the dermoscopic samples. Our work is capable of locating and segmenting skin lesions of varying mass, orientations, and colors. Moreover, the proposed approach can easily tackle the incidence of noise, blurring, and intensity changes found in the input images. We have performed a rigorous experimental evaluation over two standard repositories named the ISIC-2017 and ISIC-2018 and attained accuracy scores of 99.32% and 99.63%. Moreover, we have shown the visual samples to elaborate on the accurate segmentation performance of our approach and confirmed that the proposed solution is proficient in accurately recognizing the skin moles and assists the dermatologist in quickly detecting the lesions to understand the severity level of the disease. The proposed framework shows enhanced melanoma lesions detection and classification results; however, small performance degradation is observed for images with extensive color variations. Therefore, in the future, we plan to investigate other DL frameworks along with feature selection techniques to deal with this limitation [82]. Moreover, we planned to evaluate the presented work on other medical diseases.

Data Availability

Two publically available datasets have been utilized for the experimental process such as ISIC-2017 and ISIC-2018 (<https://challenge.isic-archive.com/challenges/>).

Conflicts of Interest

All authors declared no conflict of interest in this work.

Authors' Contributions

All authors contributed equally in this work.

Acknowledgments

This work was supported by the Korea Technology and Information Promotion Agency (TIPA) for SMEs grant funded by the Korea government (Ministry of SMEs and Startups) (No. S3271954) and the Soonchunhyang University Research Fund.

References

- [1] R. L. Siegel, K. D. Miller, S. A. Fedewa et al., "Colorectal cancer statistics, 2017," *CA: a Cancer Journal for Clinicians*, vol. 67, no. 3, pp. 177–193, 2017.
- [2] H. W. Rogers, M. A. Weinstock, S. R. Feldman, and B. M. Colcleron, "Incidence estimate of nonmelanoma skin cancer (keratinocyte carcinomas) in the US population, 2012," *JAMA Dermatology*, vol. 151, no. 10, pp. 1081–1086, 2015.
- [3] L. Ballerini, R. B. Fisher, B. Aldridge, and J. Rees, "A color and texture based hierarchical K-NN approach to the classification of non-melanoma skin lesions," in *Color Medical Image Analysis*, pp. 63–86, Springer, 2013.

- [4] Y. Cheng, R. Swamisai, S. E. Umbaugh et al., "Skin lesion classification using relative color features," *Skin Research Technology*, vol. 14, no. 1, pp. 53–64, 2008.
- [5] T. Nazir, M. Nawaz, J. Rashid et al., "Detection of diabetic eye disease from retinal images using a deep learning based CenterNet model," *Sensors*, vol. 21, no. 16, p. 5283, 2021.
- [6] M. Masood, T. Nazir, M. Nawaz, A. Javed, M. Iqbal, and A. Mehmood, *Brain Tumor Localization and Segmentation Using Mask RCNN*, 2021.
- [7] B. Pellini and A. A. Chaudhuri, "Circulating tumor DNA minimal residual disease detection of non-small-cell lung cancer treated with curative intent," *Journal of Clinical Oncology*, vol. 20, no. 6, 2022.
- [8] A. A. Ewees, R. M. Ghoniem, L. Abualigah, and F. A. Hashim, "Boosting chameleon swarm algorithm with consumption AEO operator for global optimization and feature selection," *Knowledge-Based Systems*, vol. 246, article 108743, 2022.
- [9] M. Abdar, F. Pourpanah, S. Hussain et al., "A review of uncertainty quantification in deep learning: techniques, applications and challenges," *Information Fusion*, vol. 76, pp. 243–297, 2021.
- [10] G. K. Nilsen, A. Z. Munthe-Kaas, H. J. Skaug, and M. Brun, "Epistemic uncertainty quantification in deep learning classification by the Delta method," *Neural Networks*, vol. 145, pp. 164–176, 2022.
- [11] M. A. Khan, K. Muhammad, M. Sharif, T. Akram, and S. Kadry, "Intelligent fusion-assisted skin lesion localization and classification for smart healthcare," *Neural Computing and Applications*, pp. 1–16, 2021.
- [12] Y. Qin, Z. Liu, C. Liu, Y. Li, X. Zeng, and C. Ye, "Super-resolved q-space deep learning with uncertainty quantification," *Medical Image Analysis*, vol. 67, article 101885, 2021.
- [13] R. Rahaman, "Uncertainty quantification and deep ensembles," *Advances in Neural Information Processing Systems*, vol. 34, 2021.
- [14] M. Abdar, M. A. Fahami, S. Chakrabarti et al., "BARF: a new direct and cross-based binary residual feature fusion with uncertainty-aware module for medical image classification," *Information Sciences*, vol. 577, pp. 353–378, 2021.
- [15] Z. Senousy, M. M. Abdelsamea, M. M. Gaber et al., "Mcu: multi-level context and uncertainty aware dynamic deep ensemble for breast cancer histology image classification," *IEEE Transactions on Biomedical Engineering*, vol. 69, pp. 818–829, 2022.
- [16] M. Abdar, S. Salari, S. Qahremani et al., "UncertaintyFuseNet: robust uncertainty-aware hierarchical feature fusion model with ensemble Monte Carlo dropout for COVID-19 detection," 2022, arXiv preprint arXiv:08590.
- [17] C. Barata, M. E. Celebi, and J. S. Marques, "Development of a clinically oriented system for melanoma diagnosis," *Pattern Recognition*, vol. 69, pp. 270–285, 2017.
- [18] V. Badrinarayanan, A. Handa, and R. Cipolla, "Segnet: a deep convolutional encoder-decoder architecture for robust semantic pixel-wise labelling," 2015, arXiv preprint arXiv:07293.
- [19] L. Bi, J. Kim, E. Ahn, D. Feng, and M. Fulham, "Semi-automatic skin lesion segmentation via fully convolutional networks," in *2017 IEEE 14th International Symposium on Biomedical Imaging (ISBI)*, pp. 561–564, Melbourne, VIC, Australia, 2017.
- [20] H. Alquran, I. A. Qasmieh, A. M. Alqudah et al., "The melanoma skin cancer detection and classification using support vector machine," in *2017 IEEE Jordan Conference on Applied Electrical Engineering and Computing Technologies (AEECT)*, pp. 1–5, Aqaba, Jordan, 2017.
- [21] M. A. Khan, M. A. Khan, F. Ahmed et al., "Gastrointestinal diseases segmentation and classification based on duo-deep architectures," *Pattern Recognition Letters*, vol. 131, pp. 193–204, 2020.
- [22] N. C. Codella, Q. B. Nguyen, S. Pankanti et al., "Deep learning ensembles for melanoma recognition in dermoscopy images," *IBM Journal of Research Development*, vol. 61, pp. 1–5, 2017.
- [23] J. Daghrir, L. Tlig, M. Bouchouicha, and M. Sayadi, "Melanoma skin cancer detection using deep learning and classical machine learning techniques: a hybrid approach," in *2020 5th International Conference on Advanced Technologies for Signal and Image Processing (ATSIP)*, pp. 1–5, Sousse, Tunisia, 2020.
- [24] S. Bama, R. Velumani, N. Prakash, G. Hemalakhshmi, and A. Mohanarathinam, "Automatic segmentation of melanoma using superpixel region growing technique," *Materials Today: Proceedings*, vol. 45, pp. 1726–1732, 2021.
- [25] K. Hu, X. Niu, S. Liu et al., "Classification of melanoma based on feature similarity measurement for codebook learning in the bag-of-features model," *Biomedical Signal Processing Control*, vol. 51, pp. 200–209, 2019.
- [26] A. Ameri, "A deep learning approach to skin cancer detection in dermoscopy images," *Journal of Biomedical Physics Engineering*, vol. 10, no. 6, p. 801, 2020.
- [27] M. F. Jojoa Acosta, L. Y. Caballero Tovar, M. B. Garcia-Zapirain, and W. S. Percybrooks, "Melanoma diagnosis using deep learning techniques on dermatoscopic images," *BMC Medical Imaging*, vol. 21, no. 1, pp. 1–11, 2021.
- [28] L. Zhang, G. Yang, and X. Ye, "Automatic skin lesion segmentation by coupling deep fully convolutional networks and shallow network with textons," *Journal of Medical Imaging*, vol. 6, no. 2, article 024001, 2019.
- [29] P. Shan, Y. Wang, C. Fu, W. Song, and J. Chen, "Automatic skin lesion segmentation based on FC-DPN," *Computers in Biology Medicine*, vol. 123, article 103762, 2020.
- [30] L. Bi, J. Kim, E. Ahn, A. Kumar, D. Feng, and M. Fulham, "Step-wise integration of deep class-specific learning for dermoscopic image segmentation," *Pattern Recognition*, vol. 85, pp. 78–89, 2019.
- [31] A. A. Adegun and S. Viriri, "Deep learning-based system for automatic melanoma detection," *IEEE Access*, vol. 8, pp. 7160–7172, 2019.
- [32] M. Nawaz, Z. Mehmood, T. Nazir et al., "Skin cancer detection from dermoscopic images using deep learning and fuzzy K-means clustering," *Microscopy Research Technique*, vol. 85, p. 339, 2022.
- [33] X. Zhao, F. Nie, R. Wang, and X. Li, "Improving projected fuzzy K-means clustering via robust learning," *Neurocomputing*, vol. 491, pp. 34–43, 2022.
- [34] S. Kanniappan, D. Samiayya, D. R. Vincent P M et al., "An efficient hybrid fuzzy-clustering driven 3D-modeling of magnetic resonance imagery for enhanced brain tumor diagnosis," *Electronics*, vol. 9, no. 3, p. 475, 2020.
- [35] M. Nawaz, M. Masood, A. Javed et al., "Melanoma localization and classification through faster region-based convolutional neural network and SVM," *Multimedia Tools Applications*, vol. 80, no. 19, pp. 28953–28974, 2021.

- [36] S. Banerjee, S. K. Singh, A. Chakraborty, A. Das, and R. Bag, "Melanoma diagnosis using deep learning and fuzzy logic," *Diagnostics*, vol. 10, no. 8, p. 577, 2020.
- [37] I. Iqbal, M. Younus, K. Walayat, M. U. Kakar, and J. Ma, "Automated multi-class classification of skin lesions through deep convolutional neural network with dermoscopic images," *Computerized Medical Imaging Graphics*, vol. 88, article 101843, 2021.
- [38] M. A. Khan, T. Akram, Y.-D. Zhang, and M. Sharif, "Attributes based skin lesion detection and recognition: a mask RCNN and transfer learning-based deep learning framework," *Pattern Recognition Letters*, vol. 143, pp. 58–66, 2021.
- [39] R. Mohakud and R. Dash, "Skin cancer image segmentation utilizing a novel EN-GWO based hyper-parameter optimized FCEDN," *Journal of King Saud University-Computer Information Sciences*, 2022.
- [40] M. Abdar, M. Samami, S. D. Mahmoodabad et al., "Uncertainty quantification in skin cancer classification using three-way decision-based Bayesian deep learning," *Computers In Biology Medicine*, vol. 135, article 104418, 2021.
- [41] A. G. Pacheco and R. A. Krohling, "An attention-based mechanism to combine images and metadata in deep learning models applied to skin cancer classification," *Ieee Journal Of Biomedical Health Informatics*, vol. 25, no. 9, pp. 3554–3563, 2021.
- [42] Y. Wang and S. Wang, "Skin lesion segmentation with attention-based SC-Conv U-Net and feature map distortion," *Signal, Image Video Processing*, vol. 16, no. 6, pp. 1471–1479, 2022.
- [43] C. Zhao, R. Shuai, L. Ma, W. Liu, and M. Wu, "Segmentation of skin lesions image based on U-Net++," *Multimedia Tools Applications*, vol. 81, no. 6, pp. 8691–8717, 2022.
- [44] N. Durgarao and G. Sudhavani, "Diagnosing skin cancer via C-means segmentation with enhanced fuzzy optimization," *IET Image Processing*, vol. 15, no. 10, pp. 2266–2280, 2021.
- [45] S. Haggemüller, R. C. Maron, A. Hekler et al., "Skin cancer classification via convolutional neural networks: systematic review of studies involving human experts," *European Journal of Cancer*, vol. 156, pp. 202–216, 2021.
- [46] M. S. Ali, M. S. Miah, J. Haque, M. M. Rahman, and M. K. Islam, "An enhanced technique of skin cancer classification using deep convolutional neural network with transfer learning models," *Machine Learning with Applications*, vol. 5, article 100036, 2021.
- [47] A. Polesel, G. Ramponi, and V. J. Mathews, "Image enhancement via adaptive unsharp masking," *IEEE Transactions on Image Processing*, vol. 9, no. 3, pp. 505–510, 2000.
- [48] H. Law and J. Deng, "CornerNet: detecting objects as paired keypoints," *International Journal of Computer Vision*, vol. 128, pp. 642–656, 2019.
- [49] R. Girshick, "Fast r-CNN," in *Proceedings of the IEEE international conference on computer vision*, pp. 1440–1448, Santiago, Chile, 2015.
- [50] S. Ren, K. He, R. Girshick, and J. Sun, "Faster R-CNN: towards real-time object detection with region proposal networks," *IEEE transactions on pattern analysis machine intelligence*, vol. 39, no. 6, pp. 1137–1149, 2017.
- [51] M. Nawaz, T. Nazir, M. Masood et al., "Analysis of brain MRI images using improved cornernet approach," *Diagnostics*, vol. 11, no. 10, p. 1856, 2021.
- [52] A. Raj, V. P. Namboodiri, and T. Tuytelaars, "Subspace alignment based domain adaptation for rcnn detector," 2015, arXiv preprint arXiv:05578.
- [53] X. Zhao, W. Li, Y. Zhang, T. A. Gulliver, S. Chang, and Z. Feng, "A faster RCNN-based pedestrian detection system," in *2016 IEEE 84th Vehicular Technology Conference (VTC-Fall)*, pp. 1–5, Montreal, QC, Canada, 2016.
- [54] J. Redmon, S. Divvala, R. Girshick, and A. Farhadi, "You only look once: unified, real-time object detection," in *Proceedings of the IEEE conference on computer vision and pattern recognition*, pp. 779–788, Las Vegas, NV, USA, 2016.
- [55] W. Liu, D. Anguelov, D. Erhan et al., "SSD: single shot multi-box detector," in *European conference on computer vision*, pp. 21–37, Springer, 2016.
- [56] J. Redmon and A. Farhadi, "Yolov3: an incremental improvement," 2018, arXiv preprint arXiv:02767.
- [57] R. Girshick, J. Donahue, T. Darrell, and J. Malik, "Region-based convolutional networks for accurate object detection and segmentation," *IEEE transactions on pattern analysis machine intelligence*, vol. 38, no. 1, pp. 142–158, 2015.
- [58] T. Nazir, A. Irtaza, A. Javed, H. Malik, D. Hussain, and R. A. Naqvi, "Retinal image analysis for diabetes-based eye disease detection using deep learning," *Applied Sciences*, vol. 10, no. 18, p. 6185, 2020.
- [59] S. Albahli, M. Nawaz, A. Javed, and A. Irtaza, "An improved faster-RCNN model for handwritten character recognition," *Arabian Journal for Science Engineering*, vol. 46, no. 9, pp. 8509–8523, 2021.
- [60] C. Curiel-Lewandrowski, R. A. Novoa, E. Berry et al., "Artificial intelligence approach in melanoma," *Melanoma*, pp. 1–31, 2019.
- [61] R. Parikh, A. Mathai, S. Parikh, G. C. Sekhar, and R. Thomas, "Understanding and using sensitivity, specificity and predictive values," *Indian Journal of Ophthalmology*, vol. 56, no. 1, pp. 45–50, 2008.
- [62] A. K. Akobeng, "Understanding diagnostic tests 1: sensitivity, specificity and predictive values," *Acta Paediatrica*, vol. 96, no. 3, pp. 338–341, 2007.
- [63] A. Popovic, M. De la Fuente, M. Engelhardt, and K. Radermacher, "Statistical validation metric for accuracy assessment in medical image segmentation," *International Journal of Computer Assisted Radiology Surgery*, vol. 2, no. 3–4, pp. 169–181, 2007.
- [64] R. R. Shamir, Y. Duchin, J. Kim, G. Sapiro, and N. Harel, "Continuous dice coefficient: a method for evaluating probabilistic segmentations," 2019, arXiv preprint arXiv:11031.
- [65] L. Hamers, "Similarity measures in scientometric research: the Jaccard index versus Salton's cosine formula," *Information Processing Management*, vol. 25, no. 3, pp. 315–318, 1989.
- [66] Y. Yuan, "Automatic skin lesion segmentation with fully convolutional-deconvolutional networks," 2017, arXiv preprint arXiv:05165.
- [67] M. Berseth, "ISIC skin lesion analysis towards melanoma detection," 2017, arXiv preprint arXiv:00523.
- [68] L. Bi, J. Kim, E. Ahn, and D. Feng, "Automatic skin lesion analysis using large-scale dermoscopy images and deep residual networks," 2017, arXiv preprint arXiv:04197.
- [69] A. Menegola, J. Tavares, M. Fornaciali, L. T. Li, S. Avila, and E. Valle, "RECOD titans at ISIC challenge," 2017, arXiv preprint arXiv:04819.
- [70] J. Kawahara and G. Hamarneh, "Fully convolutional neural networks to detect clinical dermoscopic features," *IEEE Journal Of Biomedical Health Informatics*, vol. 23, no. 2, pp. 578–585, 2019.

- [71] R. Gu, L. Wang, and L. Zhang, "DE-net: a deep edge network with boundary information for automatic skin lesion segmentation," *Neurocomputing*, vol. 468, pp. 71–84, 2022.
- [72] H. Wu, S. Chen, G. Chen, W. Wang, B. Lei, and Z. Wen, "FAT-net: feature adaptive transformers for automated skin lesion segmentation," *Medical Image Analysis*, vol. 76, article 102327, 2022.
- [73] S. Banerjee, S. K. Singh, A. Chakraborty, S. Basu, A. Das, and R. Bag, "Diagnosis of melanoma lesion using neutrosophic and deep learning," *Traitement du Signal*, vol. 38, no. 5, 2021.
- [74] S. Khouloud, M. Ahlem, T. Fadel, and S. Amel, "W-net and inception residual network for skin lesion segmentation and classification," *Applied Intelligence*, pp. 1–19, 2021.
- [75] M. K. Hasan, M. T. E. Elahi, M. A. Alam, M. T. Jawad, and R. Martí, "DermoExpert: skin lesion classification using a hybrid convolutional neural network through segmentation, transfer learning, and augmentation," *Informatics in Medicine Unlocked*, vol. 28, p. 100819, 2022.
- [76] D. Dai, C. Dong, S. Xu et al., "Ms RED: a novel multi-scale residual encoding and decoding network for skin lesion segmentation," *Medical Image Analysis*, vol. 75, article 102293, 2022.
- [77] R. Kaur, H. GholamHosseini, and R. Sinha, "Skin lesion segmentation using an improved framework of encoder-decoder based convolutional neural network," *International Journal of Imaging Systems Technology*, vol. 32, no. 4, pp. 1143–1158, 2022.
- [78] R. Ramadan and S. Aly, "CU-net: a new improved multi-input color U-net model for skin lesion semantic segmentation," *IEEE Access*, vol. 10, pp. 15539–15564, 2022.
- [79] R. L. Araújo, F. H. de Araújo, and R. R. Silva, "Automatic segmentation of melanoma skin cancer using transfer learning and fine-tuning," *Multimedia Systems*, pp. 1–12, 2022.
- [80] E. S. Dos Santos, K. R. Aires, H. M. Portela, G. B. Junior, J. D. Santos, and J. M. Tavares, "Semi-automatic segmentation of skin lesions based on superpixels and hybrid texture information," *Medical Image Analysis*, vol. 77, article 102363, 2022.
- [81] N. Badshah and A. Ahmad, "ResBCU-net: deep learning approach for segmentation of skin images," *Biomedical Signal Processing Control*, vol. 71, article 103137, 2022.
- [82] A. A. Ewees, R. M. Ghoniem, and M. A. Gaheen, "Improved seagull optimization algorithm using Lévy flight and mutation operator for feature selection," *Neural Computing and Applications*, vol. 34, no. 10, pp. 7437–7472, 2022.

Research Article

Analysis of the Influence of Midwife Led Antenatal Clinic on the Delivery Outcomes of Primipara under the Evaluation of Medical Data

Wei Fan, Ling Wang, Lili Zhang, Xiaoling Liu, and Zhaoyan Meng 

Department of Obstetrics, Gansu Provincial Maternity and Child-care Hospital, Lanzhou, 730050 Gansu, China

Correspondence should be addressed to Zhaoyan Meng; b20160701129@stu.ccsu.edu.cn

Received 24 August 2022; Revised 8 September 2022; Accepted 14 September 2022; Published 11 October 2022

Academic Editor: Sujatha Krishnamoorthy

Copyright © 2022 Wei Fan et al. This is an open access article distributed under the Creative Commons Attribution License, which permits unrestricted use, distribution, and reproduction in any medium, provided the original work is properly cited.

Objective. In order to improve the comprehensive effect of primipara delivery outcomes, the midwife led prenatal clinic of data mining is analyzed to alleviate the negative emotions of patients and improve the delivery results of patients. **Methods.** A total of 86 patients who were filed in the obstetrics department of our hospital from October 2021 to May 2022 and planned to deliver in our hospital were selected as the research objects. They were divided into the reference group ($n = 43$) and the observation group ($n = 43$) according to the random number table method. Among them, the reference group received routine antenatal clinics, and the observation group received midwives' participation in antenatal clinics for intervention. The total duration of labor, the scores of various psychological states including antenatal anxiety (SAS) and antenatal depression (SDS), as well as the pregnancy outcome and delivery compliance rate of the two groups were compared. **Results.** The psychological state evaluation of delivery in the observation group, whether SAS score or SDS score, was significantly lower than that in the reference group, and the difference was statistically significant. The whole labor process time of patients in the observation group was significantly shorter than that in the reference group, and the difference was statistically significant. The delivery compliance of patients in the observation group during the whole perinatal period was also higher than that of the reference group, and the difference was statistically significant. All P values were < 0.05 . **Conclusion.** The antenatal clinic led by midwives can promote primiparas to increase the success rate of natural delivery, improve the treatment compliance of the whole perinatal period, reduce the psychological pressure of primiparas, effectively shorten the total time of production, and have a significant impact on the outcome of delivery. It should be widely used.

1. Introduction

In order to improve the informatization construction level of Obstetrics and Gynecology and the efficiency of using massive case diagnosis and treatment data, through the in-depth analysis of the general data of patients, the big data processing technology can analyze the diagnosis and treatment decisions of Obstetrics and Gynecology and the health indicators of Obstetrics and gynecology patients, and the data mining technology can use genetic algorithm to preliminarily judge the health status of primiparas and newborns from the medical database, The diagnosis results will be transmitted to the cloud database in real time, so that midwives can understand the health of pregnant women and

fetus in real time. Data mining algorithm in maternal and fetal signs information analysis, if abnormal parameter indicators occur, we can give help in time and buy valuable time for newborns. If you want to give birth smoothly, pregnant women need to master the necessary scientific knowledge during pregnancy and make full preparations before delivery. The antenatal clinic led by midwives should actively publicize the benefits of natural childbirth, establish confidence in natural childbirth and promote natural childbirth. Xiyao [1] used midwife psychological nursing intervention to significantly reduce the probability of primiparas choosing cesarean section in the whole perinatal care of primiparas. Psychological nursing intervention can improve the bad mood of primiparas, shorten the whole labor process,

and promote the newborn to be healthier [1]. Suqing et al. [2] analyzed that the role standardized progressive nursing model can alleviate primiparas' fear of delivery, improve their sense of delivery self-efficacy, and improve the outcome of delivery. Ruilan and Ruiju [3] can shorten the time of the first and second stages of labor, improve the anxiety and depression of primiparas, and promote the natural delivery rate of primiparas by implementing midwife psychological intervention on primiparas. Pei [4] pointed out that the midwife led pelvic swing intervention in the delivery process of primiparas can effectively shorten the time of each stage of labor and the total stage of labor, alleviate the degree of pain in the process of labor, improve the negative psychology of primiparas, and the application effect is obvious. Ying [5] made primiparas understand the whole process of production through the intervention of animated video of delivery education. When they rely on their mastered delivery knowledge in the process of production, they can adjust their negative emotions, reduce the pain of the whole delivery, and improve the delivery outcome of primiparas.

Suqin [6] and others discussed that clinical medical staff should pay attention to the cultivation and intervention of the positive psychological level of primiparas, which can improve the health literacy level of primiparas throughout the perinatal period, alleviate the fear of delivery, and reduce the incidence of cesarean section. Jun [7] analyzed the application of data mining technology in medical big data in terms of association rule mining, classification mining, cluster analysis, etc. through data mining technology, providing a good environmental support for data mining technology. Gang [8] analyzed that with the development of hospital informatization, medical big data has shown explosive growth. Using data mining technology, medical business information is classified and processed, and the digitalization of information management improves the overall service quality of the hospital, which can fully mine the hidden parameters in information management, so as to improve the management level of the hospital [8]. Yan [9] pointed out that the prenatal clinic led by midwives can effectively improve the negative emotions of primiparas during pregnancy and delivery, improve the natural delivery rate, and reduce the influencing factors of cesarean section.

By comparing two different groups of antenatal clinics, the antenatal clinic led by midwives can adjust the psychological state of patients, reduce the degree of depression and anxiety of patients, and relieve the negative emotions of patients. Under the data depth mining technology, through technical analysis and provide precautions corresponding to the gestational age, and carry out health education, popularize childbirth knowledge to patients, let patients know and understand, so as to improve the outcome of childbirth.

2. Data and Grouping

2.1. General Information of Patients. 86 pregnant women who were filed in the obstetrics department of our hospital from October 2021 to May 2022 and planned to deliver in our hospital were selected as the research objects. In this

study, random number table method was used to randomly divide into reference group and observation group. 43 patients in the reference group received routine antenatal clinics and 43 patients in the observation group received midwife led antenatal clinics on the basis of the reference group. The age of the reference group was 20 to 34 years old, the average age was (25.7 ± 1.8) years old, the gestational weeks were 28 to 40 weeks, the average gestational weeks were (34.3 ± 2.8) weeks, and the average weight was (69.2 ± 3.8) kg. The age of the observation group was 21 to 34 years old, the average age was (26.5 ± 2.1) years old, the gestational weeks were 29 to 41 weeks, the average gestational weeks were (35.5 ± 1.7) weeks, and the average weight was (70.9 ± 4.3) kg.

2.2. Inclusion and Exclusion Criteria

2.2.1. Inclusion Criteria

- (1) Primipara, intrauterine singleton, term pregnancy
- (2) Pelvic measurement, fetal position examination and B-ultrasound monitoring are all in the normal range
- (3) Have normal communication skills
- (4) Know and agree with this study

2.2.2. Exclusion Criteria

- (1) Severe pregnancy complications
- (2) Maternal patients older than 35 years old
- (3) Patients with contraindications
- (4) Abnormal conditions occur in the process of prenatal examination during pregnancy

2.3. Observation Indicators

- (1) The SAS scores of the two groups were observed and recorded
- (2) Observe and record the SDS scores of the two groups of patients
- (3) Observe and record the results of labor process time
- (4) Observe and record the delivery outcome of the two groups of patients
- (5) Observe and record the delivery compliance of the two groups of patients

3. Method

3.1. Routine Antenatal Clinic (Reference Group). The reference group asked the pregnant woman's medical history in detail during the antenatal examination; give routine prenatal education; regularly measure blood pressure and weight; regular monitoring of routine hematuria and blood biochemistry; conduct standard fetal heart rate monitoring; and answer the questions of pregnant women.

3.2. Antenatal Clinics Attended by Midwives (Observation Group). On the basis of routine antenatal outpatient care in the observation group, data mining technology and data analysis software are used to collect and analyze the information of past cases, so as to draw a reasonable and feasible process map of pregnancy care and provide appropriate antenatal outpatient services for primiparas. According to the nursing progress chart during pregnancy, midwives (1) record the history and requirements of pregnant women from 26 to 32 weeks of pregnancy, and establish a good doctor-patient relationship with pregnant women and their families; educate pregnant women about the importance of weight control, and formulate a personalized healthy diet plan according to the nutritional status of pregnant women; (2) from the 33rd to 35th weeks of pregnancy, explain to pregnant women when to choose hospitalization, and inform pregnant women and their families to prepare items before delivery; show pregnant women the real picture of the delivery room and relevant videos to help them understand the environment of the delivery room; (3) at the 36th week of pregnancy, according to the actual situation of pregnant women, inform pregnant women of the labor process, the selection factors of delivery methods, the process of natural delivery and cesarean section, as well as the advantages and disadvantages of various delivery methods, and guide pregnant women to exercise appropriately; guide the pregnant woman's husband's paternity work; and (4) from the 37th week of pregnancy to the time of delivery, popularize knowledge about postpartum health care and neonatal nursing skills to pregnant women and their families. During this period, big data mining technology is used to collect and count the problems that affect pregnant women's emotions. Through the analysis results, it was found that direct and effective psychological counseling and doubt elimination are implemented for pregnant women to reduce their psychological pressure.

3.3. Statistical Methods. The research conducted information grouping analysis according to statistical software, and compared the data association basis and corresponding relationship of different information of the two groups of research objects. The specific statistical methods used are measurement data: statistics are given by means of mean \pm standard deviation; counting data: percentage counting method; and the measurement data between the two groups were compared by *t*-check method, and the counting data were compared by chi square test. The correlation analysis test method of the related variables of the two groups of objects was used. $P < 0.05$, the difference was statistically significant.

4. Simulation Verification

4.1. SAS Score and SDS Score Analysis of Primiparas in the Two Groups. Most primiparas will appear varying degrees of anxiety, depression, panic, and other emotions in the perinatal period. Due to the lack of delivery experience, insufficient knowledge of delivery, and the perinatal mental state, they play a decisive role in the process of delivery. In the process of delivery, they always maintain a state of tension

and panic, which is easy to lead to uterine contraction. The antenatal clinic dominated by midwives needs to inform primiparas of the precautions to keep primiparas in a positive state. Now the scoring results of the two groups of primiparas, and the following Table 1 is obtained.

Table 1 shows the psychological state evaluation results of the two groups of primiparas. After investigating and analyzing the SAS and SDS scores of the patients, it can be seen that the anxiety and depression of the patients in the reference group are higher than those in the observation group, which indirectly shows that the prenatal clinic led by midwives can improve the psychological state and bad mood of the patients.

In order to better analyze and compare the psychological status of the two groups of primiparas, the following Figure 1 is obtained by visualizing the data in Table 2.

As shown in Figure 1, the visualization effect of the comparative data of the two groups of primiparas is shown. The psychological state of the patients in the observation group is better than that of the patients in the reference group. It can be concluded that the prenatal clinic led by midwives can help patients adjust their state.

4.2. Comparison of the First and Second Stages of Labor between the Two Groups of Primiparas. The antenatal clinic led by midwives can give patients and their families knowledge about pregnancy and childbirth, actively answer their questions and concerns, adjust and change some wrong behavior perceptions of primiparas and their families, and carry out health education for primiparas to tell the advantages and disadvantages of different delivery methods, so as to meet the knowledge needs of primiparas. Let primiparas better understand the benefits of natural childbirth for themselves and newborns, and on this basis, use data mining technology to evaluate the risk of natural childbirth of primiparas, and help them build confidence in natural childbirth. Now compare the labor process time of the two groups of primiparas, and make a chart according to the recorded results, and get the following Table 2.

Table 2 shows the time comparison results of the first stage of labor and the second stage of labor of the two groups of primiparas. From the data results, the midwife led prenatal clinic can help them understand the whole production process and effectively shorten the length of production.

In order to better compare the labor process time of the two groups of primiparas, the following Figure 2 is obtained by visualizing the data in Table 3.

As shown in Figure 2, the visualization effect of the comparison of labor process time between the two groups of primiparas is shown. The total labor process of primiparas in the observation group was significantly lower than that in the control group, which indirectly showed that the prenatal clinic dominated by midwives could shorten the labor process.

4.3. Comparison of Delivery Outcomes between the Two Groups of Primiparas. Labor is accompanied by labor pains, which will bring great pain to primiparas. Primiparas have excess nutrition in the perinatal period, and their weight

TABLE 1: Comparison of SAS and SDS scores between the two groups of primiparas.

| Grouping | SAS | SDS |
|-------------------|------------------|------------------|
| Reference group | 58.71 ± 2.19 | 59.65 ± 2.15 |
| Observation group | 45.12 ± 2.41 | 43.24 ± 2.08 |
| t | 7.416 | 7.358 |
| P | 0.042 | 0.041 |

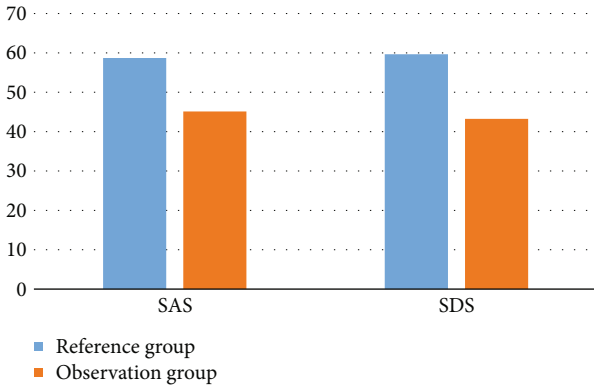


FIGURE 1: Visualization of SAS and SDS scores of primiparas in two groups.

TABLE 2: Comparison of the first and second stage of labor time of primiparas in the two groups (h).

| Grouping | Time of first stage of labor | Time of the second stage of labor |
|-------------------|------------------------------|-----------------------------------|
| Reference group | 9.11 ± 0.25 | 1.32 ± 0.23 |
| Observation group | 8.52 ± 0.29 | 1.01 ± 0.18 |

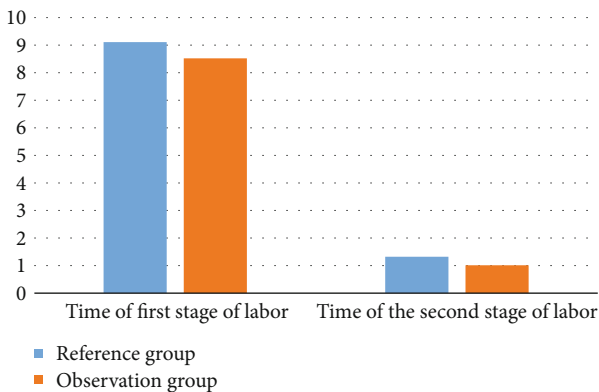


FIGURE 2: Time visualization of the first and second stages of labor of two groups of primiparas (h).

increases too fast, which will lead to macrosomia. Macrosomia is more likely to have dystocia in the process of delivery, or the method of lateral resection of delivery allows newborns to deliver smoothly. The prenatal clinic led by mid-

wives should strengthen the prenatal health education of patients, eat reasonably, and exercise to control weight, So as to reduce the birth rate of macrosomia. Among them, dystocia, emergency cesarean section and too long labor process will lead to the incidence of cesarean section. Now, the delivery outcomes of the two groups of primiparas are compared, and the chart is made according to the recorded results, and the following Table 3 is obtained.

Table 3 shows the data results of natural delivery, delivery lateral resection, involuntary cesarean section, and voluntary cesarean section of the two groups of primiparas. Prenatal clinics led by midwives have a significant impact on the delivery outcome of primiparas, which can be popularized, improve the delivery rate and the outcome of delivery.

In order to better analyze the delivery outcomes of the two groups of primiparas, the following Figure 3 is obtained by visualizing the data in Table 3:

As shown in Figure 3, it shows the visual effect of the delivery outcomes of the two groups of primiparas. From the data in the figure, the natural delivery rate of primiparas in the observation group is significantly higher than that of the reference group, which indirectly shows that the prenatal clinic led by midwives can maximize the delivery safety of patients and further improve the natural delivery rate.

4.4. Analysis of Survey Results of Production Compliance Rate of Patients. On the basis of big data analysis and in-depth mining, the prenatal clinic led by midwives can not only bring data information support to primiparas but also carry out timely health education in smart medicine. In data mining, regional population prediction and neonatal analysis can be carried out. Big data analysis provides a comprehensive knowledge explanation for primiparas, which can relieve the nervous psychological state of patients, make timely answers to the psychological questions of patients, educate the relevant health care measures of patients with appropriate gestational weeks, and improve the maternal cognition of childbirth through education, so that the maternal can realize the benefits of natural childbirth, and improve the patient's cooperation and compliance with childbirth. On the basis of data mining technology, it is safe to standardize the midwife clinic and make use of mother and baby. Now we compare the delivery compliance rate of the two groups of patients, and make a chart according to the survey results, and get the following Table 4.

Table 4 shows the comparison results of the compliance rates of the two groups of patients in the production process. From the statistical results, the cooperation and compliance of the patients in the observation group in the whole production process are obviously different from that of the reference group. Therefore, it is inferred that the midwife led prenatal clinic of data mining can improve the compliance of patients.

In order to better analyze the delivery compliance rate of the two groups of patients, the following Figure 4 is obtained by visualizing the data in Table 4:

As shown in Figure 4, the visualization effect of the delivery compliance rate of primiparas in the two groups is

TABLE 3: Comparison of delivery outcomes of primiparas between the two groups (%).

| Grouping | Natural childbirth | Parturition lateral incision | Involuntary cesarean section | Voluntary cesarean section |
|-------------------|--------------------|------------------------------|------------------------------|----------------------------|
| Observation group | 30 (69.77%) | 5 (11.63%) | 4 (9.30%) | 4 (9.30%) |
| Reference group | 18 (41.86%) | 13 (30.23%) | 5 (11.63%) | 7 (16.28%) |

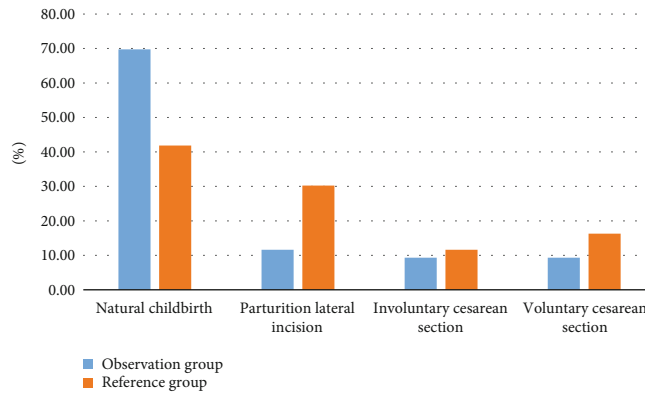


FIGURE 3: Visualization of delivery outcomes of primiparas in two groups (%).

TABLE 4: Comparison of delivery compliance rate between the two groups (%).

| Grouping | <i>n</i> | Compliance rate |
|-------------------|----------|-----------------|
| Observation group | 43 | 95.23% |
| Reference group | 43 | 78.41% |

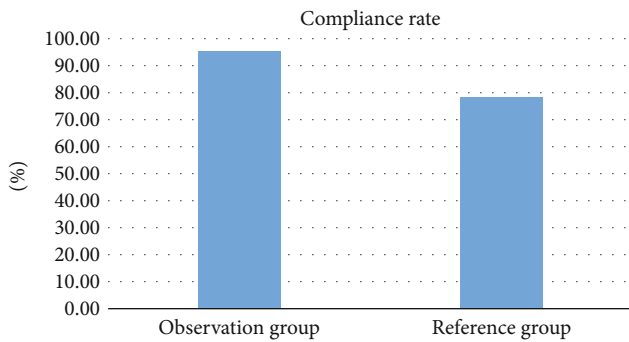


FIGURE 4: Comparison visualization of delivery compliance rate between the two groups (%).

shown. From the results in the figure, the cooperation compliance rate of primiparas in the observation group is significantly higher than that of the reference group, which indirectly shows that the prenatal clinic led by midwives can provide prenatal guidance to patients and correctly understand delivery pain.

5. Discussion

Based on data mining, the health delivery education in antenatal clinic led by midwives can improve the cooperation and compliance of primiparas. Compared with cesarean section, natural delivery is less traumatic to the maternal body,

which is conducive to the recovery speed of postpartum body. In addition, it is also beneficial to newborns, which can improve the immune ability of newborns, so as to ensure the health of newborns. Health education before delivery can relieve the panic of unknown and promote the progress of labor to a certain extent. Shaohua and Xiaohua [10] targeted to improve the professional ability of midwifery students and clinical midwives, fully integrate information technology means, and improve the professional ability and level of midwives. Lizhen and Jingdang [11] analyzed that the midwife clinic can improve the outcome of delivery by carrying out the group production education mode, which can help primiparas reduce the stress response better than pain. Improve the psychological state of primiparas and reduce the discomfort of primiparas [11]. The antenatal clinic led by midwives can reduce the occurrence of anxiety and depression of primiparas. Through the antenatal clinic, mothers can realize that their emotions will affect the fetus and help them complete self-emotion regulation. Fengling [12] discussed that the technical level of midwives directly affects the safety of pregnant women and newborns. The prenatal clinic led by midwives is conducive to building a good nurse patient relationship, effectively reducing the amount of postpartum hemorrhage, and shortening the labor process [12]. Huanyuan [13] pointed out that midwifery nursing skills can improve midwives' midwifery skills, further improve primiparas' self-efficacy and delivery control, and improve the impact of delivery outcomes [13]. Lirong et al. [14] discussed the application method and effect of simulated childbirth education combined with individualized psychological counseling in the outpatient nursing of midwives. In the vicinity of childbirth, mothers will more or less have different degrees of anxiety and depression, improve their childbirth cognitive level, and relieve the patient's mood [14]. Fengling pointed out that the level of midwives directly affects the safety of mothers and infants.

They can deal with various emergencies that may occur in the process of labor, understand the situation and reactions of mothers, and guide primiparas with midwives' prenatal clinics, which is conducive to improving the effect of labor pains and promoting the progress of labor .

In this study, under the data mining technology, the effect of midwife led antenatal clinic on the delivery outcome of primiparas was deeply discussed. The results showed that the observation group of midwife led antenatal clinic was lower than the reference group in SDS and SAS scores, which could effectively shorten the whole perinatal labor process time, and the delivery compliance was also higher than the reference group. To sum up, the midwife led antenatal clinic based on data mining has high application value.

6. Summary

This study focuses on the analysis of data mining technology in the midwife led prenatal clinic to alleviate the negative emotions of patients and improve the outcome of delivery. Through the research of statistical methods, it is found that using data mining technology to extract hidden useful information and rules can more conveniently find the rules between data, predict and evaluate the data that patients conform to the characteristics according to the rules, and there are different analysis methods for different patients, midwives can clearly grasp the nursing process, give practical measures and guidance for the stage of primiparas, directly solve the questions of primiparas, reduce the psychological pressure of primiparas, and effectively improve the outcome of delivery. After the midwife led prenatal outpatient care based on data mining, the SDS and SAS scores of primiparas are lower than those of the conventional prenatal outpatient group. At the same time, the whole labor process is shorter and the delivery compliance is higher, which proves that the midwife led prenatal outpatient care based on data mining is a more ideal method and is worthy of clinical promotion.

Data Availability

The data underlying the results presented in the study are available within the manuscript.

Disclosure

We confirm that the content of the manuscript has not been published or submitted for publication elsewhere.

Conflicts of Interest

There is no potential conflict of interest in our paper, and all authors have seen the manuscript and approved to submit to your journal.

Authors' Contributions

Wei Fan and Ling Wang are the co-first author.

Acknowledgments

This work was supported by the Lanzhou City Science and Technology Development Guidance Plan Project (2020-ZD-9).

References

- [1] L. Xiyao, "Effect of midwife psychological nursing intervention on primipara delivery mode," *Chinese Medical Guide*, vol. 20, no. 17, pp. 180–182, 2022.
- [2] L. Suqing, H. Xiaona, Y. Lizhen, and Z. Xiuying, "Effect of role standardized progressive nursing model on primipara's fear of delivery and delivery outcome," *Chinese Journal of Modern Nursing*, vol. 28, no. 17, pp. 2351–2355, 2022.
- [3] A. Ruilan and A. Ruiju, "Effect of midwife psychological intervention on primipara delivery," *Psychological Monthly*, vol. 17, no. 6, pp. 67–69, 2022.
- [4] L. Pei, "Influence of midwife led pelvic sway intervention on parturient delivery process and outcome," *Contemporary nurses (zhongxunjian)*, vol. 29, no. 3, pp. 22–25, 2022.
- [5] B. Ying, "The influence of animation video of delivery education on negative emotion, pain and outcome of primiparas," *Contemporary Nurses (zhongxunjian)*, vol. 29, no. 5, pp. 47–49, 2022.
- [6] X. Suqin, F. Yanchun, W. Jiajia, L. Fen, and L. Na, "The mediating effect of positive psychological capital between perinatal health literacy and childbirth fear of primiparas," *Nursing Research*, vol. 35, no. 13, pp. 2401–2405, 2021.
- [7] T. Jun, "Application of data mining technology in medical big data," *Electronic Technology and Software Engineering*, vol. 15, no. 12, pp. 156–157, 2021.
- [8] X. Gang, "Data mining technology and application in hospital information management system," *Digital Technology and Application*, vol. 39, no. 3, pp. 68–70, 2021.
- [9] S. Yan, "Explore the influence of midwives' antenatal clinic on primiparas' depression, anxiety and delivery mode smart," *Health*, vol. 8, no. 3, pp. 109–111, 2022.
- [10] L. Shaohua and M. Xiaohua, "Exploration on the training ways of midwife technology improvement under the background of improving quality and excellence," *Electronic Journal of Practical Gynecological Endocrinology*, vol. 7, no. 22, pp. 81–82, 2020.
- [11] H. Lizhen and H. Jingfang, "Effect of group production education mode in midwife clinic on improving delivery outcome," *Health Vocational Education*, vol. 40, no. 10, pp. 136–137, 2022.
- [12] L. Fengling, "Regulate the opening of midwife clinics to ensure the safety of mothers and infants," *Oriental Health*, vol. 10, no. 7, pp. 106–107, 2022.
- [13] C. Huanyuan, "Analysis of the influence of midwifery nursing skill guidance on primiparas' self-efficacy and delivery control," *Heilongjiang Medical Science*, vol. 45, no. 1, pp. 32–34, 2022.
- [14] Z. Lirong, W. Jieying, and L. Jinfeng, "Application of simulated delivery education combined with individualized psychological counseling in outpatient nursing of midwives," *Qilu Journal of Nursing*, vol. 27, no. 22, pp. 131–133, 2021.

Review Article

Research on CT Lung Segmentation Method of Preschool Children based on Traditional Image Processing and ResUnet

Zheming Li ^{1,2,3,4} Li Yang,^{3,5} Liqi Shu,⁶ Zhuo Yu,⁷ Jian Huang ^{1,2,3} Jing Li ^{1,2,3}
Lingdong Chen,^{1,2,3} Shasha Hu,⁸ Ting Shu ⁹ and Gang Yu ^{1,2,3,4}

¹Department of Data and Information, The Children's Hospital Zhejiang University School of Medicine, Hangzhou 310052, China

²Sino-Finland Joint AI Laboratory for Child Health of Zhejiang Province, Hangzhou 310052, China

³National Clinical Research Center for Child Health, Hangzhou 310052, China

⁴Polytechnic Institute, Zhejiang University, 866 Yuhangtang Rd, Hangzhou 310058, China

⁵Department of Radiology, Children's Hospital, Zhejiang University School of Medicine, Hangzhou 310052, China

⁶Department of Neurology, The Warren Alpert Medical School of Brown University, USA

⁷Huiying Medical Technology (Beijing), Beijing 100192, China

⁸The Children's Hospital Zhejiang University School of Medicine, Hangzhou 310052, China

⁹National Institute of Hospital Administration, NHC, Beijing 100044, China

Correspondence should be addressed to Ting Shu; nctingting@126.com and Gang Yu; yugbme@zju.edu.cn

Received 11 July 2022; Revised 13 September 2022; Accepted 21 September 2022; Published 10 October 2022

Academic Editor: Ilias Elmouki

Copyright © 2022 Zheming Li et al. This is an open access article distributed under the Creative Commons Attribution License, which permits unrestricted use, distribution, and reproduction in any medium, provided the original work is properly cited.

Lung segmentation using computed tomography (CT) images is important for diagnosing various lung diseases. Currently, no lung segmentation method has been developed for assessing the CT images of preschool children, which may differ from those of adults due to (1) presence of artifacts caused by the shaking of children, (2) loss of a localized lung area due to a failure to hold their breath, and (3) a smaller CT chest area, compared with adults. To solve these unique problems, this study developed an automatic lung segmentation method by combining traditional imaging methods with ResUnet using the CT images of 60 children, aged 0-6 years. First, the CT images were cropped and zoomed through ecological operations to concentrate the segmentation task on the chest area. Then, a ResUnet model was used to improve the loss for lung segmentation, and case-based connected domain operations were performed to filter the segmentation results and improve segmentation accuracy. The proposed method demonstrated promising segmentation results on a test set of 12 cases, with average accuracy, Dice, precision, and recall of 0.9479, 0.9678, 0.9711, and 0.9715, respectively, which achieved the best performance relative to the other six models. This study shows that the proposed method can achieve good segmentation results in CT of preschool children, laying a good foundation for the diagnosis of children's lung diseases.

1. Introduction

In recent years, the number of follow-up clinical diagnoses of respiratory diseases and the number of computed tomography (CT) lung applications has sharply increased. The proportion of CT lung examinations in children's radiological examinations has also increased, exceeding 25.12%. Lung CT is an important examination for ailments such as new coronary pneumonia, acute bronchial pneumonia, acute pneumonia, foreign bodies in the digestive tract, leukemia, sepsis, and atrial septal defect [1, 2]. However, because the

image interpretation process is quite complex, and there may be differences in image evaluation and interpretation time among radiologists, many computer technologies are used to assist in the diagnosis of these diseases [3]. Computer-aided diagnosis of childhood lung diseases relies on accurate segmentation of the lung [4, 5], such as pneumonia detection [6], tuberculosis detection [7], and pulmonary nodule detection [8]. Lung segmentation can narrow the search range of lung lesion detection and reduce the interference of others, thereby effectively improving the accuracy of the diagnosis of other lung diseases.

So far, several methods have been developed for lung segmentation. Traditional image processing methods mainly include the following [9]: (1) threshold-based segmentation [10]. This method can be used to set threshold intervals and create binary partitions. Although it is faster, it does not consider the spatial distribution of image pixels and is sensitive to noise; thus, it is not ideal for the segmentation of images with litter gray-scale differences. (2) Region-based segmentation [11]. This method is fast and has a good segmentation effect under subtle attenuation changes. However, it often has some defects and underperforms in the segmentation of pathological boundaries. (3) Clustering-based segmentation [12–14]. This method can aggregate pixels with small gray value differences into the same category and divide an image into different regions through clustering. In a study by Wu et al. [15], three different differential edge operators were utilized to preprocess the images of 80 children with RMPP. The OA, FPR, and FNR of the RO were 0.935, 0.0427, and 0.0465, respectively. However, owing to the clustering algorithm, assignment of the initial point can be quite sensitive, resulting in different segmentations depending on the initialization. Deep learning algorithms are being implemented in medical image processing. In segmentation tasks, the Unet model [16] and its improved version [17–20] are one of the most widely used. They are applied to brain tumor segmentation [21, 22], lung nodule segmentation [23, 24], lung segmentation [25–28], liver segmentation [29], heart segmentation [30], etc. In addition to the 2D segmentation model, Çiçek et al. [31] proposed a 3DUnet that replaced the 2D convolution kernel with a 3D version and could learn the 3D information of the target. 3D-based segmentation includes multiscale 3D U-Nets [32], GA-UNet [33], and V. Net [34]. However, these 3D models could be limited by their computationally intensive design and limited effects on some segmentation tasks. Among the UNet-Zoo models, ResUnet is the more common model [35]. It introduces the Res module in ResNet into the Unet model by the rich skip connections within the network to facilitate information propagation. Using ResUnet as the referential background, different improvement models have been developed for different tasks [36–38]. Besides UNet-Zoo models, transformer-based models have also achieved good results in image segmentation tasks [39–41].

Although the methods mentioned above have been implemented in the study of adults' lung segmentation, they could not be used on preschool children's CT images due to issues such as (1) presence of artifacts caused by the shaking of children, (2) loss of a local area of the lung due to failure in holding their breath, and (3) smaller CT images chest area of preschool children. These characteristics are shown in Figure 1.

Based on current clinical and literature limitations, this study was aimed at building a lung segmentation by combining traditional imaging methods with ResUnet using preschool children on CT images with the hope that it could be used for diagnosing various lung diseases in the future. First, traditional image processing techniques were used to denoise, crop, and zoom the image, reduce the amount of calculation, and improve segmentation accuracy. Then, an

optimized ResUnet model was used to segment the lungs of preschool children's CT images, whereby the unfit segmentation parts were removed through a case-based filter to improve the accuracy of the segmentation.

2. Algorithm Introduction

The proposed segmentation model consists of three parts: image preprocessing, improved ResUnet model, and case-based filtering. The method flowchart is shown in Figure 2.

2.1. Image Preprocessing. The image processing step consists of two parts. In the first part, a Gaussian filter is applied to the image to obtain a clearer CT image. In the second part, the image is cropped and resized based on the connected domain, allowing the model to learn more efficiently and quickly.

2.1.1. Gaussian Filter. Considering that CT images can be affected by machine-related issues resulting in noises and blurriness due to the body shaking of children, for improved segmentation, the CT images are preprocessed using a Gaussian filter before segmentation, yielding relatively higher image qualities.

Gaussian filters are very effective low-pass filters in the space or frequency domains and are widely used in image processing. The 2D Gaussian function has rotational symmetry, and the smoothness of the filter is the same in all directions. Thus, a 2D Gaussian filter was used in this study, based on

$$G(x, y) = \frac{1}{\sigma\sqrt{2\pi}} e^{-(x^2+y^2)/2\sigma^2}. \quad (1)$$

Here, (x, y) represents the coordinates of pixels, and σ represents the width of the Gaussian filter. The width of the Gaussian filter determines the degree of smoothing. A larger σ suggests a wider band frequency of the Gaussian filter and better smoothness. However, if σ is too large, the image features could be blurred. To maintain clarity of the lung boundaries and remove associated noises for the subsequent segmentation, a σ value of 3 was selected.

2.1.2. Image Cropping and Zooming. In the CT images of preschool children, the chest area only occupies less than 20% of the whole image. Therefore, many nontarget areas are present in the whole image, which increases the calculations and reduces the accuracy of the model. Thus, the algorithm used in this study first cuts off the original image based on the HU value of each organ in the CT image, then sets a threshold according to the gray value of the chest, performs the binarization operation on the image, forms the connected domain through the ecological opening operation, and then selects the circumscribed rectangular frame of the largest connected domain to crop the image to obtain a partial CT image containing only the chest area. Finally, all cropped CT images are zoomed to a uniform size of 256*256. Compared with the original image size of 512*512, this cropped and zoomed method reduces the model's amount of calculation and improves segmentation accuracy. The flowchart of this step is shown in Figure 3, and the corresponding effects are shown in Figure 4.

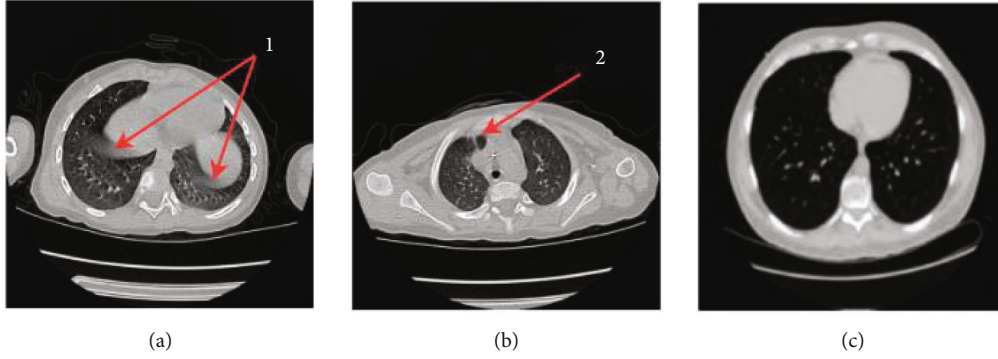


FIGURE 1: Chest CT image of a preschool child with (a) artifacts (labeled as 1), (b) loss of a local area of the lung (labeled as 2), and (c) adult lungs image which has larger lung area than children).

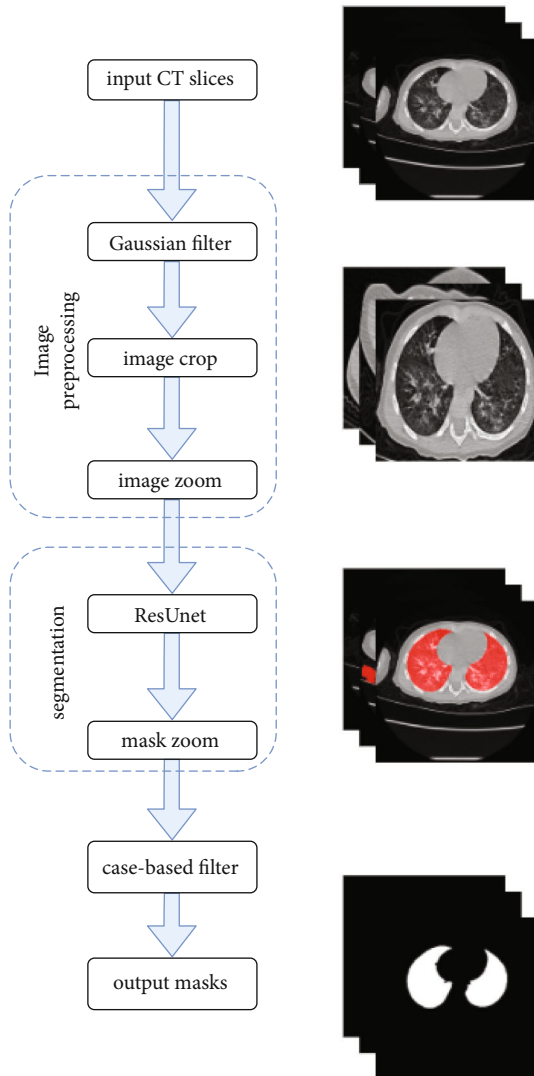


FIGURE 2: Algorithm flowchart of the proposed segmentation.

2.2. *ResUnet Module.* In this study, the ResUnet segmentation model was used as the segmentation method of preschool children's lung parenchyma. The model uses the Leaky-ReLU function, instead of the ReLU activation func-

tion, as the basic framework for the Unet network. A drop-out strategy was implemented to improve the generalization of the model. To improve the detection rate of nodules and enhance the characteristics of the edges of nodules, the Res module is added to the Unet network model to increase the learning depth of the model. The lost part is simultaneously improved, which is conducive to improving the accuracy of the model. The overall network structure of the model is shown in Figure 5.

2.2.1. *The Res Module.* To better integrate the global features of the images with their underlying features, in addition to the skip connection of the 3D Unet network in the encoding and decoding part of this study, for each convolution, the feature map before the convolution is combined with the one after the convolution. The feature maps are then connected, and the feature maps of the two parts of the concatenate are used as the output of this convolution. This operation extracts higher-dimensional features through convolutions while retaining the original dimensional features, thereby realizing an effective fusion of features at different scales and ensuring segmentation accuracy. The Res module is shown in Figure 6.

2.2.2. *Loss Improvement.* To remove the influence of artifacts, Dice loss and local loss are combined as a new loss. Dice loss has better effects on class imbalance-related issues, while local loss has better effects on boundary-related issues. Dice loss comes from the Dice coefficient, which measures the degree of overlap between two samples. The measurement range is 0 to 1, and a Dice loss of 0 suggests a complete overlap. The calculation formula is as follows:

$$L_{\text{Dice}(e,f)} = 1 - \frac{2 * |e \cap f|}{|e| + |f|}, \quad (2)$$

where e represents the ground truth and f represents the segmentation result.

Although Dice loss has better effects on class imbalance-related problems, its gradient oscillates greatly during the error backpropagation process and is unstable during the training process. The focal loss is a modification based on the cross-entropy loss function [17], which has good stability

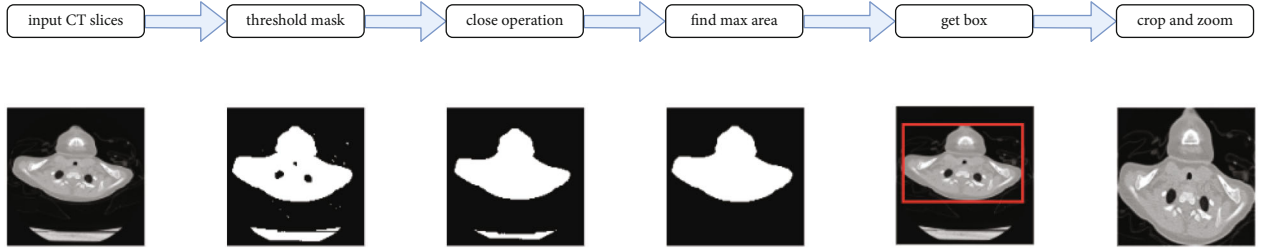


FIGURE 3: Image cropping and zooming of the model.

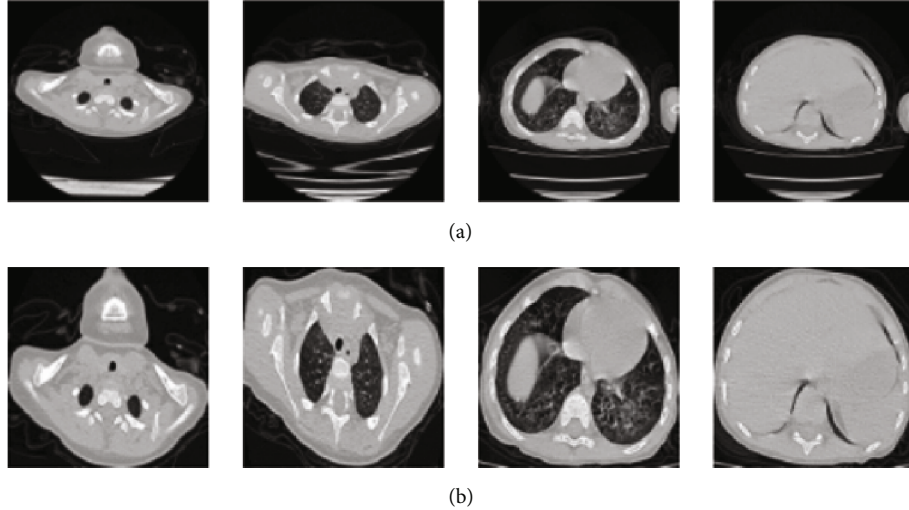


FIGURE 4: Illustration of the (a) original CT images (size, 512*512) and (b) the corresponding cropped and zoomed images (size, 256*256).

and also increases the loss value of hard negatives such as the transition area between the foreground and the background. The calculation formula is as follows:

$$L_f = \begin{cases} -\alpha(1-y')^r \log y', & y = 1, \\ (1-\alpha)y'^r \log(1-y'), & y = 0. \end{cases} \quad (3)$$

Here, r represents a reduction in the loss of easy-to-classify samples to focus more attention on difficult and misclassified samples, and α is used to balance the uneven ratio of positive and negative samples.

By combining the characteristics of focal loss and Dice loss, we hereby propose an improved focal loss based on the following formula:

$$L_{\text{all}} = \alpha \log L_{\text{Dice}} + L_f. \quad (4)$$

Here, the purpose of the logarithmic function and α is used to balance the resulting size of the two loss functions. In this paper, α is set to 0.3.

2.3. Case-Based Filter. Despite the cropping and zooming in the first step, the positioning information of the lung area is not yet completely learned by the model. At the same time, because the model is based on 2D segmentation, the 3D

information of the lungs is completely lost. Therefore, to obtain a complete case, after all the images are segmented by the model, a 3D domain connection is performed on the segmentation mask of the entire case to obtain multiple 3D volumes. Finally, according to the positioning information and the volume of the 3D body, the two larger 3D bodies, namely, the left and right pages of the lungs, are screened out. This process can effectively remove missegmentations in the pre-CT scan images and complement the loss parts of the lung due to issues such as the failure of the children to hold their breath. Segmentation after the base-cased filter is shown in Figure 7.

3. Experimental Results

3.1. Experimental Environment and Associated Parameters. The GE Optima CT660 machine was used to scan the lungs. Briefly, a child was placed in the supine position, with the head advanced, the arms held up, and the body placed in the center of the examination table. Before scanning, any metal ornaments and foreign bodies were removed to avoid artifacts. The scanning range started from the tip of the lungs to the bottom of the lungs. For children who did not cooperate with the examination procedures, a sedation was orally given using 5 mL of chloral hydrate syrup after a doctor's consultation. After the children went into a deep sleep, the CT lung examination was performed.

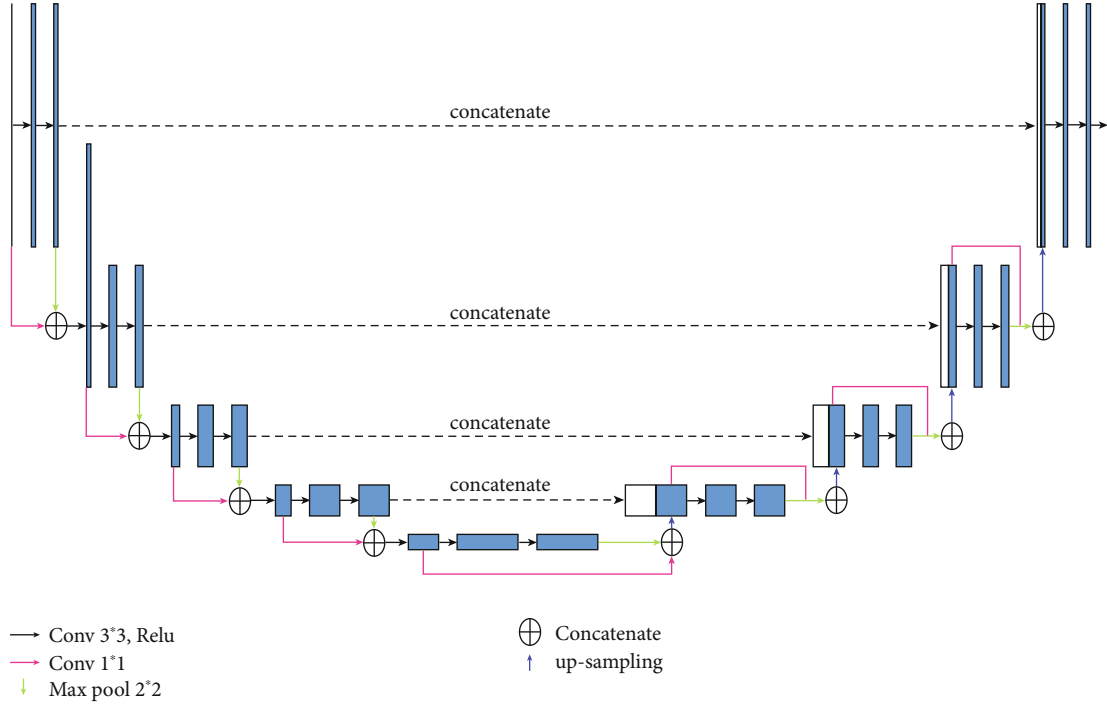


FIGURE 5: The overall structure of the ResU-net module.

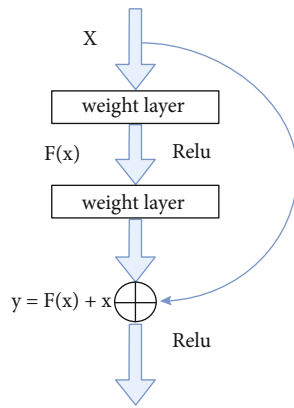


FIGURE 6: The overall layout of the Res block.

CT scanning parameters included a tube voltage of 100 kV and an automatic tube current of 30-300 mA, with a noise index of 12, pitch of 1.375 and rotation speed of 0.8 s/r. For the entire lung, the scan slice thickness and interval were both 5 mm, and the reconstruction slice thickness and interval of the lung window were both 0.625 mm.

To assess the performance of the proposed model, we conducted a method test using the chest CT images of preschool children. The LU-NA16chest CT dataset was used. We selected the thinnest CT images (0.4 mm), with each case having between 200 and 300 images after selection. All data were obtained from the Children's Hospital of Zhejiang University School of Medicine (Hangzhou, Zhejiang, China). The dataset included the CT images of 60 preschool children, of whom 33 were 0-2 years old, 23 were 3-4 years

old, and 4 were 5-6 years old. Their age distribution is shown in Table 1.

All training, testing, and verification experiments were completed using the Ubuntu 16.04 server. The basic configuration was a CPU using Intel E5-1650 3.50 GHz, a 64G DDR4 memory, and an RTX 2080Ti graphics card. All annotation work was performed in the RadCloud (Huiying Medical Technology Co., Ltd., Beijing, China).

3.2. Evaluation Standard. In this study, the intersection over union (IOU), Dice coefficient (Dice), precision, and recall [8] were used as indicators to measure the performance of the algorithm. For this purpose, the following four variables were used: true positive (TP), true negative (TN), false positive (FP), and false negative (FN). The calculation formula of each index is as follows:

$$\begin{aligned} \text{IOU} &= \frac{e \cap f}{e \cup f}, \\ \text{Dice}(e, f) &= 2 \frac{|e \cap f|}{|e| + |f|}, \\ \text{Precision} &= \frac{\text{TP}}{\text{TP} + \text{FP}}, \\ \text{Recall} &= \frac{\text{TP}}{\text{TP} + \text{FN}}, \end{aligned} \quad (5)$$

where e represents the gold standard and f represents the segmentation result.

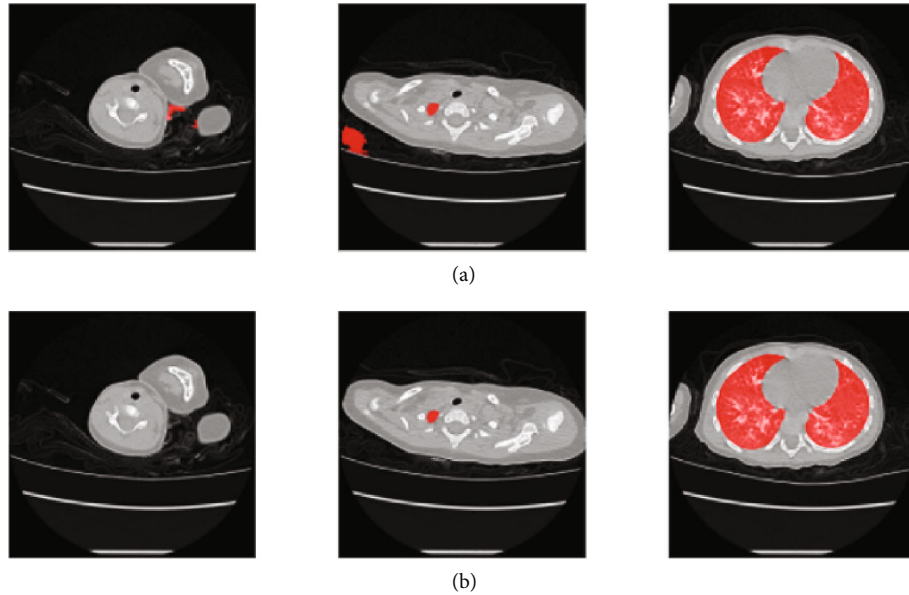


FIGURE 7: Comparisons before and after case-based filter. The red parts represent the segmentation result. (a) Segmentation results before case-based filter. (b) Segmentation results after case-based filter.

TABLE 1: Dataset.

| Ages (years) | Train set | Test set |
|--------------|-----------|----------|
| 0-2 | 28 | 5 |
| 3-4 | 17 | 6 |
| 5-6 | 3 | 1 |
| All | 48 | 12 |

3.3. Training Process. We divided the experimental data into three parts: training, validation, and test sets. In total, there were 48 cases in the training and validation sets, with 12,522 pictures, among which 11,270 pictures were for the training set and 1252 pictures for the validation set. The test set was made up of 12 cases and 3068 images. All models adopt RMSprop [42] as the optimizer with an initial learning rate of 0.001 and a training epoch of 10. All images were cross-segmented by two clinicians with at least 5 years of experience. For images with a segmentation error of less than 1% (assessed by two doctors), the gold standard was determined based on the average mask marked by the two doctors. The other images were marked as the final gold standard by the two doctors.

3.4. Result Analysis. The performance of our method based on the 12 cases of the test set is shown in Table 2.

As shown in Table 2, our method achieved an average accuracy of 0.9479, while the averages of Dice, precision, and recall on test set class are 0.9678, 0.9711, and 0.9715, respectively. We compare our method with Unet [16], Unet++ [17], Unet+++ [19], Attention-UNet [20], Swin-UNet [39], and Trans-UNet [40]. The segmentation results of different segmentation algorithms are shown in Table 3.

TABLE 2: Performance of the test set.

| Case no. | IOU | Dice | Precision | Recall |
|----------|--------|--------|-----------|--------|
| 1 | 0.9552 | 0.9754 | 0.9733 | 0.9782 |
| 2 | 0.9602 | 0.9794 | 0.9802 | 0.9789 |
| 3 | 0.9543 | 0.9746 | 0.9805 | 0.9699 |
| 4 | 0.9604 | 0.9786 | 0.9788 | 0.9791 |
| 5 | 0.9599 | 0.9783 | 0.9789 | 0.9792 |
| 6 | 0.9442 | 0.9664 | 0.9608 | 0.9809 |
| 7 | 0.9559 | 0.9753 | 0.9786 | 0.9753 |
| 8 | 0.9578 | 0.9778 | 0.9873 | 0.969 |
| 9 | 0.8874 | 0.9084 | 0.907 | 0.9481 |
| 10 | 0.9444 | 0.9647 | 0.9736 | 0.966 |
| 11 | 0.95 | 0.9717 | 0.9717 | 0.9753 |
| 12 | 0.9449 | 0.9636 | 0.9829 | 0.9587 |
| Average | 0.9479 | 0.9678 | 0.9711 | 0.9715 |

TABLE 3: Segmentation results of different segmentation algorithms.

| Method | IOU | Dice | Precision | Recall |
|-----------------|--------|--------|-----------|--------|
| Unet | 0.934 | 0.9553 | 0.9561 | 0.9625 |
| Unet++ | 0.9338 | 0.9543 | 0.9493 | 0.9699 |
| Unet+++ | 0.9359 | 0.9568 | 0.9468 | 0.9748 |
| Attention-UNet | 0.9257 | 0.9482 | 0.9424 | 0.9673 |
| Swin-UNet | 0.8738 | 0.917 | 0.8998 | 0.949 |
| Trans-UNet | 0.9364 | 0.9569 | 0.9611 | 0.9592 |
| Proposed method | 0.9479 | 0.9678 | 0.9711 | 0.9715 |
| ResUnet (adult) | 0.9163 | 0.9368 | 0.9351 | 0.9451 |

Table 3 shows that the IOU, Dice, and precision of the proposed method are higher than other algorithms by at least 1%. Unet+++ performs the best on recall, leading our method by 0.33%, but other metrics are all far from our method. For CT images of preschool children with artifacts and partial missing areas, the proposed method demonstrated good segmentation (Figure 8).

To better illustrate the value of building a preschool-specific lung segmentation model, we trained ResUnet on a publicly available adult lung database [43] containing 16,708 images and tested it on the test set used in this paper. It can be seen from the last row of Table 3 that the proposed model did not perform as well as the other models on the preschool lung segmentation task. The possible reason is that the images on the adult lung cancer dataset are relatively clear, and the lungs account for a higher proportion of the image, where these features are different from those of children. More details on the performance of the Unet model applied to adult lung segmentation on our test set are shown in Table 4.

In summary, our method achieves the best segmentation performance on CT images of preschool children.

4. Discussion

In this study, we proposed a novel model based on traditional image algorithms and ResUnet to segment lung from CT scans of preschool children. On the validation set containing 12 cases, our method achieved Dice, precision, and recall of 0.9678, 0.9711, and 0.9715.

Lung segmentation is one of the important foundations for intelligent diagnosis of many lung diseases, and accurate segmentation can effectively improve the performance of diagnostic models. In literature [44], Primakov et al. first extracted the lungs to allow the model to focus on the ROI prior to the detection and segmentation of non-small-cell carcinomas. In literature [45], the authors summarize the application of AI in the diagnostic dilemma of pulmonary nodules over the past 20 years. The first step of all methods is lung segmentation and then the detection or segmentation of pulmonary nodules. Due to the epidemic of the COVID-19, the classification and lesion detection of COVID-19 has become one of the research hotspots, and the first step in all research is also lung segmentation [6, 46–49]. However, lung segmentation studies on CT of preschool children are still relatively rare.

The first step of this paper is to collect CT images of 60 children aged 0-6 years. Compared with the adolescents and adults, preschool children have smaller lung, which brings greater challenges to lung segmentation. As shown in Tables 2–4, our experiments also demonstrate that if the model trained on the adult database is directly used to segment the lungs of CT images of preschool children, its performance is almost lower than that of all segmentation models trained on the preschool database. On the preschooler validation set, the Dice score of the ResUnet model trained on the adult database [43] is 3 percentage points lower than that of the ResUnet model trained on the preschooler database. This result suggests the necessity of designing a segmentation algorithm for preschooler lung segmentation.

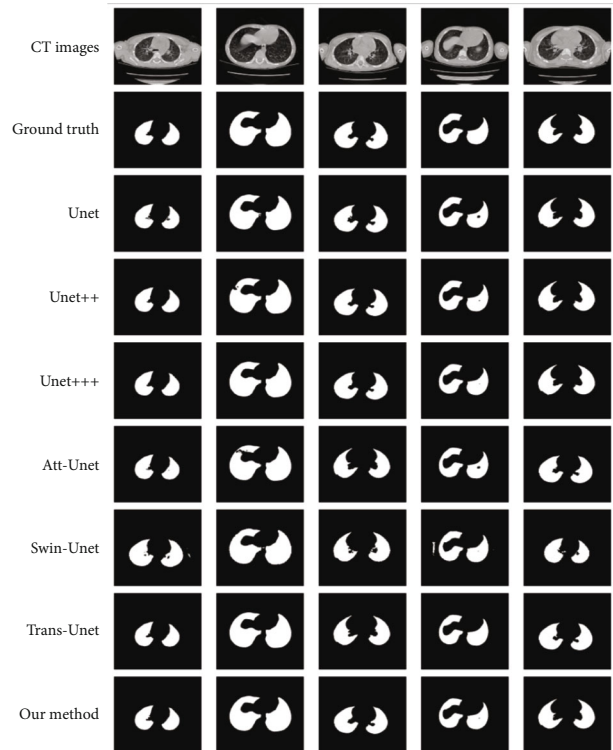


FIGURE 8: The proposed method versus gold standard method and other methods.

TABLE 4: Performance of the Unet model applied to adult lung segmentation on our test set.

| Case no. | IOU | Dice | Precision | Recall |
|----------|--------|--------|-----------|--------|
| 1 | 0.9226 | 0.9436 | 0.9357 | 0.9535 |
| 2 | 0.9305 | 0.9497 | 0.9481 | 0.9514 |
| 3 | 0.9164 | 0.9397 | 0.937 | 0.9434 |
| 4 | 0.9291 | 0.9477 | 0.9413 | 0.9558 |
| 5 | 0.9248 | 0.9441 | 0.9438 | 0.9494 |
| 6 | 0.9172 | 0.9391 | 0.9283 | 0.9562 |
| 7 | 0.9261 | 0.9459 | 0.9436 | 0.9505 |
| 8 | 0.9295 | 0.9483 | 0.9507 | 0.9476 |
| 9 | 0.8561 | 0.8766 | 0.8764 | 0.909 |
| 10 | 0.912 | 0.9333 | 0.9365 | 0.9415 |
| 11 | 0.9158 | 0.9394 | 0.9331 | 0.9497 |
| 12 | 0.9151 | 0.9345 | 0.9462 | 0.9329 |
| Average | 0.9163 | 0.9368 | 0.9351 | 0.9451 |

Second, we noticed that many literatures only use one of traditional image algorithms [10–15] or deep learning [26, 50, 51], failing to fully combine the advantages of both. For the challenges existing in the lung segmentation of preschool children, we combined traditional image algorithms and deep learning as solutions. Because preschool children’s lung is small, this paper used the traditional image algorithm based on connected domain to extract the body area first. The benefit of this step is to remove extraneous areas such

as the bed, thereby normalizing the CT images of children of different ages and concentrating the lung in the middle of the image. Then, we used a deep learning model which is good at segmentation tasks to complete the initial segmentation. Finally, we optimized the segmentation results through traditional image algorithms. Through the effective combination of different algorithms, our method achieves good performance in the lung segmentation task of preschool children.

Finally, we compared with the current mainstream methods, including models based on Unet and Transformer. The results obtained by our proposed model are superior compared to other models.

It should be noted that this study has examined only on the dataset of our hospital, and the cases included in this study are relatively small, and our model needs to be verified and optimized on other data. Secondly, on the basis of accurate lung segmentation, it is necessary to further study the intelligent diagnosis of lung diseases in preschool children.

In conclusion, this method combining traditional image algorithms and deep learning models can accurately segment the CT lung of preschool children, which provides a good foundation for subsequent studies such as classification of childhood pneumonia and detection of childhood pulmonary tuberculosis.

5. Conclusions and Prospects

Accurate lung segmentation of the CT scans of preschool children is of great significance to accurately and timely detect and analyze lung nodules and pneumonia in real-world clinical settings. This study proposes an automatic lung segmentation method that combines traditional imaging methods with ResUnet using the CT images of preschool children. First, Gaussian filtering was used to denoise the image, followed by image ecology operations to crop and zoom the CT images. Then, an optimized ResUnet model was used to segment the 2D image, and unfit segmentation parts were removed through a case-based filter to improve the accuracy of the segmentation. According to the experimental results, the proposed segmentation method could correctly segment most CT images of the investigated preschool children and extract relatively complete lungs. Compared with other deep learning models and traditional image processing methods, the proposed method could reduce the adverse effects of child hyperactivity on segmentation and improve the accuracy and speed of lung segmentation. In addition, using the proposed method, the segmentation of the lungs was closely related to specific clinical applications. Comparison with other segmentation methods showed that they could not be uniformly applied to the chest CT images of preschool children. In future studies, we will continue investigating other lung segmentation methods to achieve higher segmentation accuracy.

Data Availability

The data used to support the findings of this study are available from the corresponding author upon request.

Conflicts of Interest

The authors declare that they have no conflicts of interest.

Authors' Contributions

Zheming Li and Li Yang contributed equally to this work.

Acknowledgments

This work was partially supported by the National Key R&D Program of China (grant number 2019YFE0126200) and the National Natural Science Foundation of China (grant number 62076218).

References

- [1] M. Ma, Q. Xie, W. Wang, L. Weihua, and X. Zheng, "Comparison of the value of chest plain film, lung ultrasound, and CT plain scan in the diagnosis of pneumonia in children," *Chinese Journal of CT and MRI*, vol. 19, no. 5, pp. 30–32, 2021.
- [2] Z. Xiaojun, Z. Xinrong, B. Guo, T. Wenwei, D. Shi, and Y. Wang, "Application of lung high-resolution CT in childhood asthma," *Radiology Practice*, vol. 29, no. 11, pp. 1271–1273, 2014.
- [3] Y. Pan, H. Wang, and Y. Lu, "Application of artificial intelligence in medical imaging CAD," *International Journal of Medical Radiology*, vol. 42, no. 1, pp. 3–7, 2019.
- [4] W. Mao, R. Congyun, L. Shaozhen, Y. Wang, and J. Zhe, "The diagnostic value of artificial intelligence combined with low-dose lung CT scan in lung cancer in situ screening," *China Medical Equipment*, vol. 18, no. 12, pp. 45–48, 2021.
- [5] J. Lu, H. Wang, L. Tianzhu, and H. Donghui, "Application of intelligent recognition aids in the diagnosis of pulmonary ground glass nodules," *China Medical Equipment*, vol. 18, no. 10, pp. 19–23, 2021.
- [6] C. Zhao, Y. Xu, Z. He et al., "Lung segmentation and automatic detection of COVID-19 using radiomic features from chest CT images," *Pattern Recognition*, vol. 119, p. 108071, 2021.
- [7] Y. Gu, J. Chi, J. Liu et al., "A survey of computer-aided diagnosis of lung nodules from CT scans using deep learning," *Computers in Biology and Medicine*, vol. 137, p. 104806, 2021.
- [8] K. B. Chen, Y. Xuan, A. J. Lin, and S. H. Guo, "Lung computed tomography image segmentation based on U-Net network fused with dilated convolution," *Computer Methods and Programs in Biomedicine*, vol. 207, p. 106170, 2021.
- [9] A. Mansoor, U. Bagci, B. Foster et al., "Segmentation and image analysis of abnormal lungs at CT: current approaches, challenges, and future trends," *Radiographics*, vol. 35, no. 4, pp. 1056–1076, 2015.
- [10] S. Hu, E. A. Hoffman, and J. M. Reinhardt, "Automatic lung segmentation for accurate quantitation of volumetric X-ray CT images," *IEEE Transactions on Medical Imaging*, vol. 20, no. 6, pp. 490–498, 2001.
- [11] Y. Qian and G. Wei, "Lung nodule segmentation using EM algorithm," in *Sixth International Conference on Intelligent Human-Machine Systems and Cybernetics*, pp. 20–23, Hangzhou, 2014.
- [12] G. Xiao, X. Yun, and J. M. Wu, "A multi-cue mean-shift target tracking approach based on fuzzified region dynamic image

- fusion,” *Science China (Information Sciences)*, vol. 55, no. 3, pp. 577–589, 2012.
- [13] D. Shuangfeng, K. Lu, Z. Rui, and J. Dong, “A whole lung segmentation method based on the combination of 3D region growth method and improved convex hull algorithm,” *Journal of Electronics and Information Technology*, vol. 38, no. 9, pp. 2358–2364, 2016.
- [14] J. Hu and L. Ping, “Automatic segmentation method of lung field on chest radiograph using improved Snake model,” *Journal of Huaqiao University (Natural Science Edition)*, vol. 43, no. 3, pp. 1–10, 2022.
- [15] L. Wu, J. Ji, S. Zhao, and J. Chen, “Computed tomography image segmentation using edge correction algorithm for refractory mycoplasma pneumonia in children,” *Scientific Programming*, vol. 2021, Article ID 3578971, 8 pages, 2021.
- [16] O. Ronneberger, P. Fischer, and T. Brox, “U-Net: convolutional networks for biomedical image segmentation,” in *Proceedings of the 18th International Conference on Medical Image Computing and Computer-Assisted Intervention*, pp. 234–241, Munich, 2015.
- [17] Z. Zhou, M. M. R. Siddiquee, N. Tajbakhsh, and J. Liang, “UNet++: a nested U-Net architecture for medical image segmentation,” in *4th International Workshop on Deep Learning in Medical Image Analysis (DLMI) / 8th International Workshop on Multimodal Learning for Clinical Decision Support (ML-CDS)*, Granada, Spain, 2018.
- [18] R. Arora, I. Saini, and N. Sood, “Modified UNet++ model: a deep model for automatic segmentation of lungs from chest X-ray images,” in *2021 2nd International Conference on Secure Cyber Computing and Communications (ICSCCC)*, pp. 166–169, Jalandhar, India, 2021.
- [19] H. Huang, L. Lin, R. Tong et al., “UNet 3+: a full-scale connected UNet for medical image segmentation,” in *ICASSP 2020-2020 IEEE International Conference on Acoustics, Speech and Signal Processing (ICASSP)*, Barcelona, Spain, 2020.
- [20] O. Oktay, J. Schlemper, L. L. Folgoc et al., *Attention U-Net: Learning Where to Look for the Pancreas*, 2018.
- [21] H. Zheng, Z. Yiwen, L. Yunhui, and S. Guoli, “GCAUNet: a group cross-channel attention residual UNet for slice based brain tumor segmentation,” *Biomedical Signal Processing and Control*, vol. 70, p. 102958, 2021.
- [22] A. Motahareh, A. Ali, and E. Mehdi, “Brain tumor image segmentation via asymmetric/symmetric UNet based on two-pathway-residual blocks,” *Biomedical Signal Processing and Control*, vol. 69, p. 102841, 2021.
- [23] X. Wang, L. Mingqiu, and Y. Ji, “Segmentation of pulmonary nodules based on BBCLstm Unet,” *Journal of Physics: Conference Series*, vol. 1966, no. 1, p. 012037, 2021.
- [24] M. Muazzam, Y. Sadaf, M. Irfan, B. Maryam, and K. Muechol, “An efficient DA-Net architecture for lung nodule segmentation,” *Mathematics*, vol. 9, no. 13, p. 1457, 2021.
- [25] C. Jianning, H. Xiaoying, C. Wu, H. Wang, and J. Peng, “X-Net: multi-branch UNet-like network for liver and tumor segmentation from 3D abdominal CT scans,” *Neurocomputing*, vol. 459, pp. 81–96, 2021.
- [26] S. P. Pawar and S. N. Talbar, “LungSeg-Net: lung field segmentation using generative adversarial network,” *Biomedical Signal Processing and Control*, vol. 64, p. 102296, 2021.
- [27] K. Minki and L. B. Dai, “Automatic lung segmentation on chest X-rays using self-attention deep neural network,” *Sensors*, vol. 21, no. 2, p. 369, 2021.
- [28] Z. Wang, Y. Zou, and P. X. Liu, “Hybrid dilation and attention residual U-Net for medical image segmentation,” *Computers in Biology and Medicine*, vol. 134, p. 104449, 2021.
- [29] S. Anushikha, L. Brejesh, B. K. Panigrahi et al., “Deep LF-Net: semantic lung segmentation from Indian chest radiographs including severely unhealthy images,” *Biomedical Signal Processing and Control*, vol. 68, p. 102666, 2021.
- [30] M. Fernandes, J. Teuwen, R. Wijsman et al., “Segmentation of the heart using a residual U-net model,” *ESTRO 2020*, 2020.
- [31] Ö. Çiçek, A. Abdulkadir, S. S. Lienkamp, T. Brox, and O. Ronneberger, “3D U-Net: learning dense volumetric segmentation from sparse annotation,” in *International conference on medical image computing and computer-assisted intervention*, pp. 424–432, Cham, 2016.
- [32] S. Peng, W. Chen, J. Sun, and B. Liu, “Multi-scale 3d u-nets: an approach to automatic segmentation of brain tumor,” *International Journal of Imaging Systems and Technology*, vol. 30, no. 1, pp. 5–17, 2020.
- [33] A. Kaur, L. Kaur, and A. Singh, “GA-UNet: UNet-based framework for segmentation of 2D and 3D medical images applicable on heterogeneous datasets,” *Neural Computing and Applications*, vol. 33, no. 21, pp. 14991–15025, 2021.
- [34] K. Mohammed Kamel, H. A. Ella, and M. Afify Heba, “A 3D image segmentation for lung cancer using V. Net architecture based deep convolutional networks,” *Journal of Medical Engineering & Technology*, vol. 45, no. 5, pp. 337–343, 2021.
- [35] Z. Zhang, Q. Liu, and Y. Wang, “Road extraction by deep residual U-Net,” *IEEE Geoscience and Remote Sensing Letters*, vol. 15, no. 5, pp. 749–753, 2018.
- [36] L. Pei, A. K. Murat, and R. Colen, “Multimodal brain tumor segmentation and survival prediction using a 3D self-ensemble Res UNet,” in *International MICCAI Brainlesion Workshop*, Springer, Cham, 2021.
- [37] J. Tang, T. Li, H. Shu, and H. Zhu, “Variational-autoencoder regularized 3D MultiResUNet for the BraTS 2020 brain tumor segmentation,” in *International MICCAI Brainlesion Workshop*, pp. 431–440, Springer, Cham, 2020.
- [38] J. Liu, Y. Kang, D. Hu, and Y. Chen, “Cascade Res Unet with noise power spectrum loss for low dose CT imaging,” in *2020 13th International Congress on Image and Signal Processing, Bio Medical Engineering and Informatics (CISP-BMEI)*, Chengdu, China, 2020.
- [39] H. Cao, Y. Wang, J. Chen et al., “Swin-Unet: Unet-like pure transformer for medical image segmentation,” 2021, <https://arxiv.org/abs/2105.05537>.
- [40] Y. Sha, Y. Zhang, X. Ji, and L. Hu, “Transformer-Unet: raw image processing with Unet,” 2021, <https://arxiv.org/abs/2109.08417>.
- [41] H. Wang, S. Xie, L. Lin et al., “Mixed transformer U-Net for medical image segmentation,” in *ICASSP 2022-2022 IEEE International Conference on Acoustics, Speech and Signal Processing (ICASSP)*, Singapore, Singapore, 2021.
- [42] S. Ruder, “An overview of gradient descent optimization algorithms,” 2016, <https://arxiv.org/abs/1609.04747>.
- [43] Lung segmentation dataset by Kónya, 2020, <https://www.kaggle.com/sandorkonya/ct-lung-heart-trachea-segmentation>.
- [44] S. P. Primakov, A. Ibrahim, J. E. van Timmeren et al., “Automated detection and segmentation of non-small cell lung cancer computed tomography images,” *Nature Communications*, vol. 13, no. 1, pp. 1–12, 2022.

- [45] D. Fahmy, H. Kandil, A. Khelifi et al., "Can help in the diagnostic dilemma of pulmonary nodules," *Cancers*, vol. 1840, 2022.
- [46] J. S. Suri, S. Agarwal, R. Pathak et al., "COVLIAS 1.0: lung segmentation in COVID-19 computed tomography scans using hybrid deep learning artificial intelligence models," *Diagnostics*, vol. 11, no. 8, p. 1405, 2021.
- [47] F. Gholamiankhah, S. Mostafapour, N. A. Goushbolagh et al., "Automated lung segmentation from CT images of normal and COVID-19 pneumonia patients," 2021, <https://arxiv.org/abs/2104.02042>.
- [48] V. Bevilacqua, N. Altini, B. Prencipe et al., "Lung segmentation and characterization in COVID-19 patients for assessing pulmonary thromboembolism: an approach based on deep learning and radiomics," *Electronics*, vol. 10, no. 20, p. 2475, 2021.
- [49] A. Oulefki, S. Agaian, T. Trongtirakul, and A. Kassah Laouar, "Automatic COVID-19 lung infected region segmentation and measurement using CT-scans images," *Pattern Recognition*, vol. 114, p. 107747, 2021.
- [50] J. Tan, L. Jing, Y. Huo, L. Li, O. Akin, and Y. Tian, "LGAN: lung segmentation in CT scans using generative adversarial network," *Computerized Medical Imaging and Graphics*, vol. 87, p. 101817, 2021.
- [51] Y. Jalali, M. Fateh, M. Rezvani, V. Abolghasemi, and M. H. Anisi, "ResBCDU-Net: a deep learning framework for lung CT image segmentation," *Sensors*, vol. 21, no. 1, p. 268, 2021.

Research Article

Recognition of Handwritten Medical Prescription Using Signature Verification Techniques

Seerat Rani,¹ Abd Ur Rehman ,¹ Beenish Yousaf ,¹ Hafiz Tayyab Rauf ,² Emad Abouel Nasr ,³ and Seifedine Kadry ^{4,5}

¹Department of Computer Science, University of Gujrat, Gujrat, Pakistan

²Centre for Smart Systems, AI and Cybersecurity, Staffordshire University, Stoke-on-Trent ST4 2DE, UK

³Industrial Engineering Department, College of Engineering, King Saud University, Riyadh 11421, Saudi Arabia

⁴Department of Applied Data Science, Noroff University College, Kristiansand, Norway

⁵Department of Electrical and Computer Engineering, Lebanese American University, Byblos, Lebanon

Correspondence should be addressed to Abd Ur Rehman; a.rehman@uog.edu.pk

Received 21 June 2022; Accepted 1 September 2022; Published 17 September 2022

Academic Editor: Shohel Sayeed

Copyright © 2022 Seerat Rani et al. This is an open access article distributed under the Creative Commons Attribution License, which permits unrestricted use, distribution, and reproduction in any medium, provided the original work is properly cited.

Patient record keeping plays a vital role in diagnoses and cures. Due to a shortage of time, most doctors write prescriptions manually in Pakistan. At times, it becomes difficult for pharmacists to read prescriptions properly. As a result, they may dispense the wrong medicine. This might cause risky and deadly effects on the patient's health. This paper proposes an online handwritten medical prescription recognition system that lets doctors write prescriptions on a tablet using a stylus and automatically recognizes the medicine. We use signature verification techniques to recognize the doctor's handwriting to overcome the problem of misinterpretation of the medicine name by the pharmacist. The proposed system stores different features like the pen coordinates, time, and several pen-ups and pen-downs. Besides using features already proposed in the literature for signature verification, we propose some new features that greatly enhance recognition accuracy. We built a dataset of 24 medicine names from two users and compared results using newly proposed features. We have obtained 84%, 78%, 77.47%, 77.31%, 74.17%, 60%, 38.5%, 68%, and 61.64% accuracies for 9 users using SVM classifier.

1. Introduction

Computers are used in almost every domain of daily life, like businesses, industries, entertainment, education, personal management, and research activities. Data can be processed and reproduced in a speedy way using computers. Patient record management helps practitioners to diagnose and continue the care timely. Computerized patient record management systems are used to maintain the record of patients and employees working in the hospital [1, 2]. Health care is a broad area that deals with health care information, medical device information, pharmaceutical information, hospital management, and biological system. In the health care system, patient's precaution and patient care are the major goals [3, 4].

In developing countries like Pakistan, most hospitals, especially in the public sector, are not computerized. Due to a high patient-to-doctor ratio, doctors have a hectic schedule where they have to prescribe or take notes while standing or in walking conditions in emergency cases. Handwritten prescriptions are widely used in the tropical areas of mid-Asia. Especially in Pakistan, doctors mostly prefer to write handwritten prescriptions because they feel comfortable writing the prescription manually, even if they have enough time to access and use a computer.

Handwritten prescriptions have several potential threats associated with them. Unreadable handwriting prescription and the incapability of pharmacists to understand medicine names in medical prescriptions are causing a notable number of patients to expire [5]. Patients may get delayed or

wrong medical dosage due to wrong interpretation of hand-written prescription, which may result in further severity of disease and even patient's death.

Biometric verification is employed in several real-life business applications. It provides numerous benefits like it is difficult to be stolen, hacked, and forged. Biometrics deals with bioscience, which means the automatic identification of a human's physiological or behavioral characteristics. The biometric method is preferred over passwords and PINs for easiness of use, accuracy, and case sensitivity. There are different biometric types, such as fingerprint, iris, and face recognition [6].

Biometrics can be found in an extensive range of applications which include physical access control systems, logical access control services, consumer identification, prescription identification, and authentication. Handwritten signature verification is still widely used techniques. The biometric system performs two tasks: verification and identification [7].

The signature verification system is intended to verify the individuality of a person by recognizing their handwritten signature. Signature verification contains two types online and offline signature verification [8]. Offline techniques capture image of the signature after the person has completed writing. Online signature verification techniques capture feature which person is signing. It is done by using a tablet and stylus and recording features pen coordinates, time, pressure, etc. Signature verification includes three basic steps [9–12]. The first step is preprocessing and contains the data in raw form. After preprocessing, the features from obtained data are extracted in numeric form. In the third step, the classifier obtains results and checks whether the signatures are genuine or forged. There are many classifiers, such as neural network (NN), support vector machine (SVM), nearest neighbor, hidden Markov model (HMM), time delay neural networks, and Naive Bayes, which have been employed for signature verification [9]. Several studies in the related work are found on the optimization algorithm that can be used to solve machine learning healthcare-related optimization problems, such as the Bat algorithm [13] and particle swarm optimization [14].

For effective results, features should be dense enough and provide a better understanding of signatures because it is considered personal identification [15, 16]. In [8] offline recognition system, they used a static representation of documents to take a signature on paper which is later scanned which includes cheque, form, and documentation authentication. Offline signature verification techniques are famous for limited information [15]. Offline processing is also a difficult task due to the deficiency of dynamic characteristics [17].

On the other hand, an online recognition system uses dynamic representation, in which information can be stored at runtime. Electronic tablets [18, 19] and smartphones have on-line recognition writing interface [8, 20–22]. Most applications are based online, where a person acts and the system automatically derives data for authentication. Online verification is stronger than the other approach because it provides a higher level of security and stores dynamic features

such as pressure, coordinates, pens up, and pens down. Online signature verification can be divided into two types:

- (i) The parametric approach is used to extract the features from signals such as speed, pressure, coordinates, and the number of the pen up and pen down
- (ii) The functional approach is used for analyzing the online signatures

The representation of offline verification is shown in Figure 1.

The contribution of this work is as follows:

- (i) We propose an online medical prescription recognition system to overcome problems of unreadable handwriting prescription
- (ii) We use signature verification techniques to recognize the medicine name prescribed by a doctor
- (iii) We use tablet and stylus, like used in [23, 24], to enable doctors to prescribe in the same way they normally do

2. Literature Review

2.1. Signature Verification. Signature verification is a broad area in biometric. It has been considered an essential component of the study conducted by the researchers due to the extensively utilized signature verification techniques for experimentation.

In [25], the author proposed a secure retrieval of the classified information system using the neuro-fuzzy technique. The neuro-fuzzy technique was based on a fuzzy neural network. Dynamic signatures were tested by using Svc 2004 database. They extracted different features, including total time duration, average pen pressure, and dynamic pen pressure. The verification system was suitable; the obtained EER of the overall system was 3.952%. The proposed scheme was beneficial for the practical application of classified information.

Online signature verification uses effective and simple techniques. In their research [26], the author employed two types of features, the first was based on the histogram, and the second was based on quantized features using a model-free Manhattan distance classifier. Several tests were conducted on MCYT and SUSIG datasets. The obtained results of the proposed technique were similar to state-of-art algorithms despite their simplicity and efficiency.

The author reviewed the signature verification system, which included feature extraction algorithms [27], tablet PC, digitized pen, HMM's, modified dynamic time warping technique (DTW), and NN techniques and methodologies.

They discussed the main challenges of signature verification: signature inconsistency and intraperson variability. Different steps performed for signature verification included signature acquisition, preprocessing, feature extraction, threshold selection enrolment, and matching. The steps

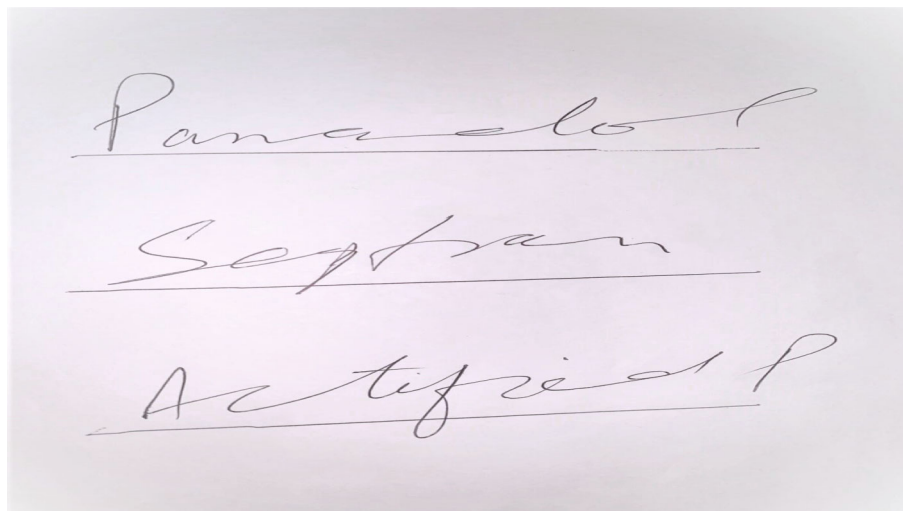


FIGURE 1: Off-line data representation.

TABLE 1: Summary table of literature review.

| Referenced paper | Features | | | | | |
|------------------|-----------------|-----------------|-----------------|-----------------|------|-----------|
| | Up _x | Up _y | Dn _x | Dn _y | Time | Midpoints |
| [38] | Yes | Yes | Yes | Yes | Yes | No |
| [39] | Yes | Yes | Yes | Yes | No | No |
| [40] | Yes | Yes | No | No | No | No |
| [41] | Yes | Yes | No | No | Yes | No |

performed in preprocessing were smoothing, normalization, and segmentation.

In the feature extraction step, performance evaluation parameters were involved, which derived false acceptance rate and false reject rate. The obtained results of the false acceptance rate (FAR) were 0.25%, and the false reject rate (FRR) was 0.5%.

In [28], the study is carried out to propose both online and offline verification approaches. The webcam was used for data collection, preprocessing, and feature extraction, including pen up and pen down, and then, classification results were obtained based on online verification. However, for offline verification, they collected data through the image, performed preprocessing and feature extraction, and in the end, obtained results from different classifiers. When those steps were completed on both online and offline approaches, then these were combined and used SVM for final verification.

Discrete cosine transformed (DCT) and sparse representation techniques [29] are used for signature verification and discussed new properties of DCT, including time-series and extracting different energy features (x, y coordinate, pressure, azimuth, and altitude). For experimental evaluation, they used SUSIG-visual and SVC2004 databases. In the end, the obtained error rate was 0.33%.

In 2016, the author [15] proposed a two-stage classification approach combining generative and discriminative modeling principles for online handwritten character recog-

inition. The first stage was based on HMM and presented a few unknown patterns in candidate characters. HMM returned the top-ranking character out of the total number of classes. In the second stage, they used SVM frequency count analysis and chose one character from the candidate character class.

The frequency count analysis was used for pairwise classifiers and same-shape characters. The two-stage approach was better than the single-stage.

In [30], they used handwritten signature verification techniques to propose hand-worn devices for genuine and forged signatures. Sixty-six applicants were included in this experiment. Data were collected in two stages; the major one was participants providing genuine signatures, and the second was forged signatures. They collected three types of datasets from accelerometer and gyroscope, which included the acceleration of accelerometer, angle of acceleration, and angle of velocity. This method provided 0.98 AUC and 0.05 EER high degree of accuracy amongst genuine and forged signatures.

In [31], the author introduced handwriting recognition techniques for Chinese characters conVent (conventional neural network) and direct Map (direction decomposition). Direct Map and conVent provided better efficiency and accuracy than the other techniques. These techniques reduced the mismatch problem between the train and tested the data. The ConVent was interesting and straightforward for the recognition system.

In [32], the authors carried out the NN model for signature verification using autoassociative memory. NN model reads the image of signature in the form of matrices. In [33], an automatic signature recognition approach was introduced. Gabor filter techniques were used for preprocessing signature images and then performed linear discriminant analysis. After that, they applied NNs used for matching the trained data. If the data matched to original data, then making a decision data is authentic or inauthentic. The obtained results from the proposed system were very

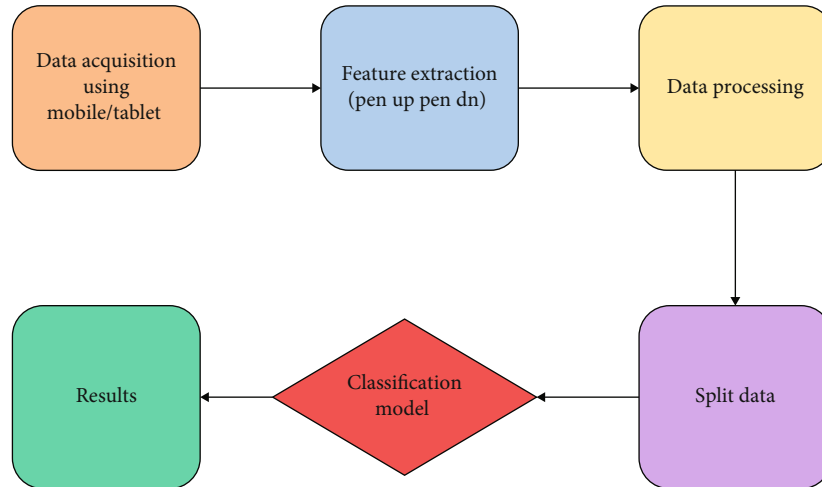


FIGURE 2: Complete research design.

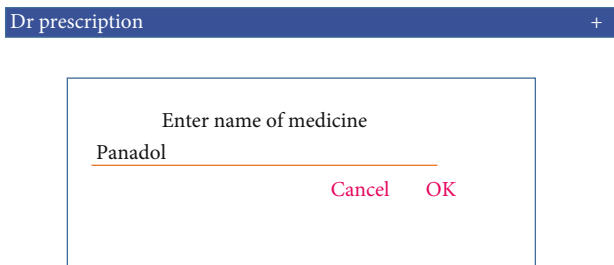


FIGURE 3: Enter medicine name.

high, 99.5%, rejection rate of 73%, and computational time of method were 0.87 s.

2.2. Prescription Recognition. The authors [5] used MediPic and Android applications to resolve the recognition problem. They used optical character recognition technology to scan the medicine name and convert it into a digital script. They used Tesseract for character recognition and an inner key algorithm to match the characters. The inner key algorithm matched the character and returned the best results in the database. The MediPic provided more efficient results and helped to decrease the misunderstanding of medicine names.

In [34], the author presented a design of printed traditional Chinese medicine (TCM) prescription and filing system based on the Microsoft office document imaging (MODI) and optical character recognition (OCR) engine.

An optical recognition engine [35] extracted complete information about the disease and stored the data in the database and made a file for further use. TCM provides information for future use. In 2017, [36] implemented a hospital information management system for medical records. Using fingerprints of patients for authentication because health is the main aim or goal of the hospital.

In addition to the health of patients in hospitals, their privacy and security are also considered. They used different technologies for biometric authentication, which included data management, system design, unified modelling lan-

guage, biometrics, and computer programming. The efficiency of the hospital was increased by using a medical record system with biometric authentication.

In [37], handwritten medical prescription systems were introduced; a prescription is written by doctors based on word spotting and uses an information retrieval approach. They proposed two approaches: the first was Tandem-HMM, used for word spotting, and the second was domain knowledge, used to reduce the text information, which increased the performance.

Different steps were involved: the first one was developing a diagnostic system. The second was information extraction, the third was wrong medication detection, and the fourth was a statistical analysis of medical prescriptions prescribed by doctors. The obtained accuracy was increased by 15.42%, which was a good achievement.

Different techniques are used for medical prescription recognition problems, but our focus is to use signature verification techniques for medical prescriptions. A summary table concerning different coordinates is presented in Table 1.

3. Methodology

Patients' death due to the wrong drug intake caused by misinterpreted prescriptions by pharmacists happens frequently. Most doctors write prescriptions manually because prescribing a stylus on a tablet is not very common or practiced regularly in Pakistan for prescription writing. Therefore, sometimes, it causes harmful effects on patients. Our work is based on handwritten medical prescriptions, but we employed signature verification techniques.

3.1. Signature Verification vs. Handwritten Medical Prescription

- (i) Through the signature verification technique, we can verify a person's identity by recognizing their handwritten signature. Signature verification uses a pattern matching technique to verify the signatures,

Dr prescription



X, Y coordinates

FIGURE 4: Write medicine name using stylus.

but most of the time, it is difficult to read the signature because there is no pen up and pen down movement. Signatures can be forged easily. Offline signature verification is only based on shapes

- (ii) Through the handwritten medical prescription, the doctor's handwriting is recognizable. The forgeries or forged signatures are automatically involved in the signature verification. Forged signatures are referenced or duplicate signatures of a person. Online handwritten medical prescription recognition is based on character recognition. Pen up and pen down are associated with handwritten medical prescriptions. There are two types of handwritten verification techniques called online and offline verification. Both techniques are linked with signature verification and handwritten medical prescription recognition

3.2. Offline and Online Handwritten Verification

- (i) The offline technique deals with the only shape of the writing and is used for limited information due to its static representation of documents to take a signature or prescription on paper. This prescription is later scanned. This approach is difficult because the segmentation is performed on scanned data. Through the offline approach, we cannot calculate the speed and pressure of a pen
- (ii) Compared to the offline technique, the online approach is more secure and accurate due to the variation of feature value each time and provides relevant results. The online approach deals with dynamic features such as speed, pen up, pen down, and pressure. A tablet or smartphone is used for an

online approach that stores the pen tip movements as well as pen up and pens down, switching

In this article, we have proposed signature verification techniques for medical prescription recognition systems to overcome the misinterpretation of medicine names. There are five steps involved in medical prescription recognition explained below:

- (i) In the phase of data acquisition, we collected data from two users and 9 users, and we used the stylus for writing a medicine's name on the tablet, which stores the movements of the stylus
- (ii) Feature extraction is the second step. We extracted different features from the original data obtained from the medical prescription system. Several extracted features involved: pen up with respect to x - y coordinates, pen down with respect to x - y coordinates, the total time between pen down to pen up, midpoints of total time with respect to x - y coordinates, quarter midpoints of total time with respect to x - y coordinates, and three-quarter of total time with respect to x , y coordinates
- (iii) Preprocessing is the third step in which the unwanted data have been removed, i.e., useless columns or extra columns and adding missing values
- (iv) We have carried out different classifiers for the experimental evaluation, which involves Naive Bayes, SVM, gradient boosted, and decision tree. Figure 2 presents a flow of the complete research activity

3.3. *Data Acquisition.* Data acquisition is a process that measures the physical condition and converts it into digital

TABLE 2: Original data obtained from medical prescription application.

| Event number | Prescription name | | Accupril | | Up | Down |
|--------------|-------------------|-------|--------------------|------------|-------|-------|
| | X | Y | Time from previous | Total time | | |
| 1 | 389.552 | 238.7 | 0 | 0 | False | True |
| 2 | 389.552 | 238.7 | 3 | 3 | False | False |
| 3 | 390.593 | 237.6 | 31 | 35 | False | False |
| 4 | 390.802 | 234.3 | 5 | 41 | False | False |
| 5 | 389.864 | 227.7 | 14 | 55 | False | False |
| 6 | 386.427 | 220.3 | 17 | 72 | False | False |
| 7 | 376.532 | 214.7 | 17 | 90 | False | False |
| 8 | 367.678 | 217.4 | 16 | 107 | False | False |
| 9 | 357.783 | 226 | 17 | 124 | False | False |
| 10 | 349.138 | 239.5 | 19 | 143 | False | False |
| 11 | 341.431 | 262.4 | 15 | 159 | False | False |
| 12 | 341.326 | 275.3 | 16 | 176 | False | False |
| 13 | 346.743 | 283.8 | 17 | 193 | False | False |
| 14 | 361.429 | 285.7 | 17 | 210 | False | False |
| 15 | 372.574 | 278.4 | 17 | 228 | False | False |
| 16 | 381.636 | 265.9 | 17 | 245 | False | False |
| 17 | 390.072 | 243.4 | 17 | 262 | False | False |
| 18 | 392.989 | 234.4 | 17 | 279 | False | False |
| 19 | 394.135 | 232.3 | 17 | 296 | False | False |
| 20 | 395.176 | 232.4 | 17 | 314 | False | False |
| 21 | 399.134 | 238 | 17 | 331 | False | False |
| 22 | 403.092 | 243.7 | 17 | 348 | False | False |
| 23 | 408.613 | 250.9 | 17 | 365 | False | False |
| 24 | 420.174 | 263.4 | 17 | 383 | False | False |
| 25 | 428.819 | 269.4 | 16 | 400 | False | False |
| 26 | 439.339 | 272.6 | 17 | 417 | False | False |
| 27 | 448.714 | 271.8 | 11 | 429 | False | False |
| 28 | 448.714 | 271.8 | 1 | 430 | True | False |
| 29 | 494.335 | 216 | 111 | 542 | False | True |

TABLE 3: Spatial feature obtained from system.

| Feature | Description |
|-----------------|----------------------------------|
| Up _x | Pen up x -coordinate |
| Up _y | Pen up y -coordinate |
| Dn _x | Pen down x -coordinate |
| Dn _y | Pen down y -coordinate |
| Time from | Start time of writing |
| Total time | Total time of complete signature |

numeric values. The doctor prescribes the tablet using a stylus. Our proposed system calculates the movement of a stylus according to x and y coordinates.

Medicine name has already been stored in the database of the proposed system. The user has to put the medicine name by using the styles into the GUI interface of the proposed system. After that, system generates values according to pen movement in the form of x and y coordinates. The

system generates an event that includes the number of x -coordinates, y -coordinates, total time, and pens up, and pens down. The real-time data experiment of the proposed system is presented in Figures 3 and 4.

Original data obtained from the proposed medical prescription application is given in Table 2.

3.4. Feature Extraction. We extracted the features from the acquired data. When the medicine name is written on the GUI of the proposed system, then the original number of strokes or movements of the stylus are recorded and accumulated in the database. We extracted two types of features called spatial and local spatial features.

3.4.1. Spatial Features. Spatial features are also called static features which are extracted from the shape of the signature or original. The extracted spatial feature is shown in Table 3.

3.4.2. Local Spatial Features. Local spatial features are extracted for signature verification which includes: x, y coordinates, total time, pen up, pen down, and angle.

Apart from the spatial features, we have extracted different features, including the following:

- (i) Pen down with respect to the X coordinate (dn_x): the system calculates values according to the x coordinate as soon as the stylus touches the screen of the tablet
- (ii) Pen down with respect to the Y coordinate (dn_y): the system calculates values according to the y coordinate as soon as the stylus touches the screen of the tablet
- (iii) Pen up with respect to X coordinate (up_x): the system calculates values according to the x coordinate when the user takes a pause or lifts the pen for the first time while writing
- (iv) Pen up with respect to the Y coordinate (up_y): the system calculates values according to the y coordinate when the user takes a pause or lifts the pen for the first time while writing
- (v) Total time of pen up (time): the total time of pen up is the total time of lifting the pen from the tablet by the user according to coordinates
 - (i) Midpoints of pen up with respect to the X coordinate (midpoints x): pen up midpoints are middle points of the total time of pen up from the tablet with respect to the x coordinate or the total time between pen up and pen down
 - (ii) Midpoints of pen up with respect to the Y coordinate (midpoints y): midpoints are middle points of the total time of pen lifting from the tablet with

TABLE 4: Extracted features from original data.

| Features | Description |
|-------------|---|
| Upx1 | First pen up with respect to x -coordinate |
| Upy1 | First pen up with respect to y -coordinate |
| Time1 | Total time of first pen up |
| Midpoints1x | Midpoint of first time pen up with respect to x -coordinate |
| Midpoints1y | Midpoint of first time pen up with respect to y -coordinate |
| Quarter1x | Quarter time of the first midpoint pen up with respect to x -coordinate |
| Quarter1y | Quarter time of first midpoint pen up with respect to y -coordinate |
| 3quarter1x | 3quarter of first midpoint pen up time with respect to x -coordinate |
| 3quarter1y | 3quarter of first midpoint pen up time with respect to y -coordinate |
| Dnx2 | Second pen down with respect to x -coordinate |
| Dny2 | Second pen down with respect to y -coordinate |
| Upx2 | Second pen up with respect to x -coordinate |
| Upy2 | Second pen up with respect to y -coordinate |
| Time2 | Total time of second pen up |
| Midpoints2x | Midpoint of second time, pen up with respect to x -coordinate |
| Midpoints2y | Midpoint of second time pen up with respect to y -coordinate |
| Quarter2x | Quarter time of second midpoint pen up with respect to x -coordinate |
| Quarter2y | Quarter time of second midpoint pen up with respect to y -coordinate |
| 3quarter2x | 3quarter of second midpoint pen up time with respect to x -coordinate |
| 3quarter2y | 3quarter of second midpoint pen up time with respect to y -coordinate |
| Dnx3 | Third pen down with respect to x -coordinate |
| Dny3 | Third pen down with respect to y -coordinate |
| Upx3 | Third pen up with respect to x -coordinate |
| Upy3 | Third pen up with respect to y -coordinate |
| Time3 | Total time of third pen up |
| Midpoints3x | Midpoint of third time pen up with respect to x -coordinate |
| Midpoints3y | Midpoint of third time pen up with respect to y -coordinate |
| Quarter3x | Quarter time of third midpoint pen up with respect to x -coordinate |
| Quarter3y | Quarter time of third midpoint pen up with respect to y -coordinate |
| 3quarter3x | 3quarter of third midpoint pen up time with respect to x -coordinate |
| 3quarter3y | 3quarter of third midpoint pen up time with respect to y -coordinate |
| Dnx4 | Fourth pen down with respect to x -coordinate |
| Dny4 | Fourth pen down with respect to y -coordinate |
| Upx4 | Fourth pen up with respect to x -coordinate |
| Upy4 | Fourth pen up with respect to y -coordinate |
| Time4 | Total time of fourth pen up |
| Midpoints4x | Midpoint of fourth time pen up with respect to x -coordinate |
| Midpoints4y | Midpoint of fourth time pen up with respect to y -coordinate |
| Quarter4x | Quarter time of fourth midpoint pen up with respect to x -coordinate |
| Quarter4y | Quarter time of fourth midpoint pen up with respect to y -coordinate |
| 3quarter4x | 3quarter of fourth midpoint pen up time with respect to x -coordinate |
| 3quarter4y | 3quarter of fourth midpoint pen up time with respect to y -coordinate |
| Dnx5 | Fifth pen down with respect to x -coordinate |
| Dny5 | Fifth pen down with respect to y -coordinate |
| Upx5 | Fifth pen up with respect to x -coordinate |
| Upy5 | Fifth pen up with respect to y -coordinate |
| Time5 | Total time of fifth pen up |
| Midpoints5x | Midpoint of fifth time pen up with respect to x -coordinate |

TABLE 4: Continued.

| Features | Description |
|-------------|--|
| Midpoints5y | Midpoint of fifth time pen up with respect to y -coordinate |
| Quarter5x | Quarter time of fifth midpoint pen up with respect to x -coordinate |
| Quarter5y | Quarter time of fifth midpoint pen up with respect to y -coordinate |
| 3quarter5x | 3quarter of fifth midpoint pen up time with respect to x -coordinate |
| 3quarter5y | 3quarter of fifth midpoint pen up time with respect to y -coordinate |
| Dnx6 | Sixth pen down with respect to x -coordinate |
| Dny6 | Sixth pen down with respect to y -coordinate |
| Upx6 | Sixth pen up with respect to x -coordinate |
| Upy6 | Sixth pen up with respect to y -coordinate |
| Time6 | Total time of sixth pen up |
| Midpoints6x | Midpoint of sixth time pen up with respect to x -coordinate |
| Midpoints6y | Midpoint of sixth time pen up with respect to y -coordinate |
| Quarter6x | Quarter time of sixth midpoint pen up with respect to x -coordinate |
| Quarter6y | Quarter time of sixth midpoint pen up with respect to y -coordinate |
| 3quarter6x | 3quarter of sixth midpoint pen up time with respect to x -coordinate |
| 3quarter6y | 3quarter of sixth midpoint pen up time with respect to y -coordinate |

TABLE 5: Sample cleaning of useless columns.

| Medicine | Dnx1 | Dny1 | Upx1 | Upy1 |
|----------|------|------|----------|----------|
| Accupril | 0 | 0 | 59.16186 | 33.01608 |
| Accupril | 0 | 0 | 67.91113 | 54.263 |
| Accupril | 0 | 0 | 67.49451 | 86.75827 |
| Accupril | 0 | 0 | 49.371 | 30.72473 |
| Accupril | 0 | 0 | -26.0396 | 66.55288 |
| Accupril | 0 | 0 | 77.80618 | 75.82236 |
| Accupril | 0 | 0 | 76.45212 | 44.68106 |
| Accupril | 0 | 0 | 41.66328 | 47.18067 |
| Accupril | 0 | 0 | 83.43072 | 56.55428 |
| Accupril | 0 | 0 | 46.45455 | 47.18066 |

TABLE 6: Sample addition of missing values.

| Medicine | Dnx6 | Dny6 |
|----------|----------|----------|
| Accupril | 502.355 | -21.4552 |
| Accupril | 521.5201 | 0 |
| Accupril | 366.2202 | -28.0168 |
| Accupril | 377.9901 | -35.3074 |
| Accupril | 0 | -50.0969 |
| Accupril | 0 | 21.24692 |
| Accupril | 386.1144 | -15.5186 |
| Accupril | 173.2151 | 0 |
| Accupril | 442.0474 | 0 |

respect to the y coordinate. Or the total time between pen up and pen down

- (iii) Quartiles of pen up with respect to X coordinate (quarter x): quartiles of pen up are the first total

time divided into four equal parts with respect to the x coordinate

- (iv) Quartiles of pen up with respect to Y coordinate (quarter y): quartiles of pen up are the total time divided into four equal parts with respect to the y coordinate
- (v) Third quartile midpoints of pen up with respect to X coordinate (3quarter x): third quartile pen up midpoints are the three equal parts out of one-quarter of total time with respect to the x coordinate
- (vi) Third quartile midpoints of pen up with respect to Y coordinate (3quarter x): third quartile pen up midpoints are the three equal parts out of one-quarter of total time with respect to the y coordinate

The accuracy obtained by using the feature includes $upx1$, $upy1$, $dnx1$, $dny1$, $time1$, $midpoints1x$, $midpoints1y$, $quarter1x$, $quarter1y$, $3quarter1x$, and $3quarter1y$ with SVM was not high enough. To boost the accuracy, we extracted some additional features, including total time, midpoints of total time, quarter time of midpoints, and 3quarter time of midpoints. We used a six-time pen up and pen down, as shown in Table 4.

3.5. Preprocessing. There exist some irrelevant data obtained from feature extraction which cannot be used in its original form. It contained useless content such as the first pen down x column, the first pen down y column, and attributes containing missing values and extra columns. This type of data has not been used in our experiments. We have cleaned up (error-free) the irrelevant data to get the best results.

3.5.1. Remove Columns. Two columns are considered useless because the first pen down concerning the x -coordinate and the first pen down concerning the y -coordinate contain "0"

TABLE 7: Sample of training data.

| Medicine | Upx1 | Upy1 | Time1 | Midpoint1x | Midpoint1y | Quarter1x | Quarter1y |
|----------|----------|----------|-------|------------|------------|-----------|-----------|
| Accupril | 59.16186 | 33.01608 | 430 | 372.5739 | 278.4178 | 389.5516 | 238.736 |
| Accupril | 67.91113 | 54.263 | 356 | 280.2897 | 240.819 | 277.165 | 214.1562 |
| Accupril | 67.49451 | 86.75827 | 302 | 378.3026 | 217.4891 | 356.3252 | 195.8256 |
| Accupril | 49.371 | 30.72473 | 409 | 352.3672 | 264.2531 | 382.2606 | 245.2976 |
| Accupril | -26.0396 | 66.55288 | 110 | 328.3066 | 249.2553 | 367.9909 | 213.6355 |
| Accupril | 77.80618 | 75.82236 | 363 | 406.3211 | 181.5568 | 373.0946 | 167.9129 |
| Accupril | 76.45212 | 44.68106 | 356 | 403.7172 | 199.9916 | 379.5525 | 204.9909 |
| Accupril | 41.66328 | 47.18067 | 281 | 280.498 | 274.9808 | 312.1621 | 189.6806 |
| Accupril | 83.43072 | 56.55428 | 341 | 372.1572 | 225.9254 | 329.2441 | 212.6981 |
| Accupril | 46.45455 | 47.18066 | 345 | 302.4754 | 211.24 | 301.2255 | 200.929 |

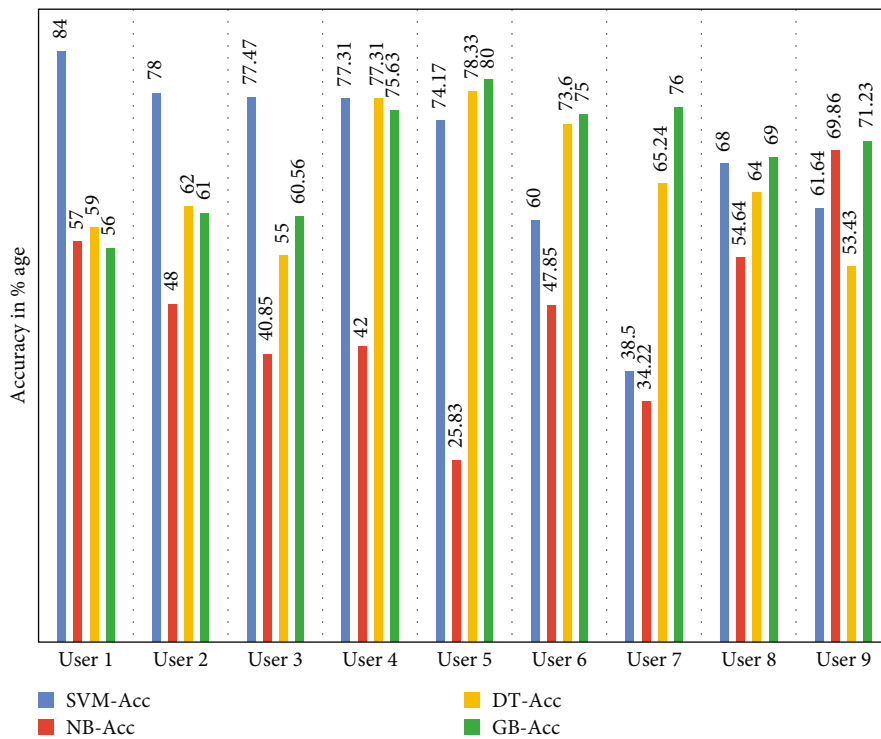


FIGURE 5: Pen up and pen down features accuracy of user 1 and user 2 data.

values. These columns have been removed. Furthermore, we took only six times to pen up and pen down, so extra columns are removed as unnecessary. This data does not affect the analysis. The description of data that is removed is given in Table 5.

3.6. *Missing Values.* Several attributes of the columns contain null values during writing medicine names. The null values affected the result analysis because the classifier does not accept these types of data and shows an error to add values containing null values. Therefore, to improve the results, we replaced “0” with the null attribute in Table 6.

3.7. *Dataset.* We collected data for 100 medicine from 2 users while data for 24 medicine from nine users. Each medicine contains at least 10 samples for the training dataset.

The total number of training data is 3000 medicine samples. Each sample is labeled with its respective medicine name. The user name is also included to train the classifier for each user separately. The sample of training data is shown in Table 7.

The classifier employed in this work is given the same features as input, the same classes of medicine, and the same number of medicines. We used the KNIME analytics platform for analysis. It is an open-source platform to verify the online signature (medicine name) of samples.

3.7.1. *F-Measures.* We have measured the performance of eleven features, including pen up x , pen up y , pen down x , pen down y , total time, midpoint x , midpoint y , quarter x , quarter y , 3quarter x , and 3quarter y , with different classifiers. Features are ranked using all the eleven feature ranking

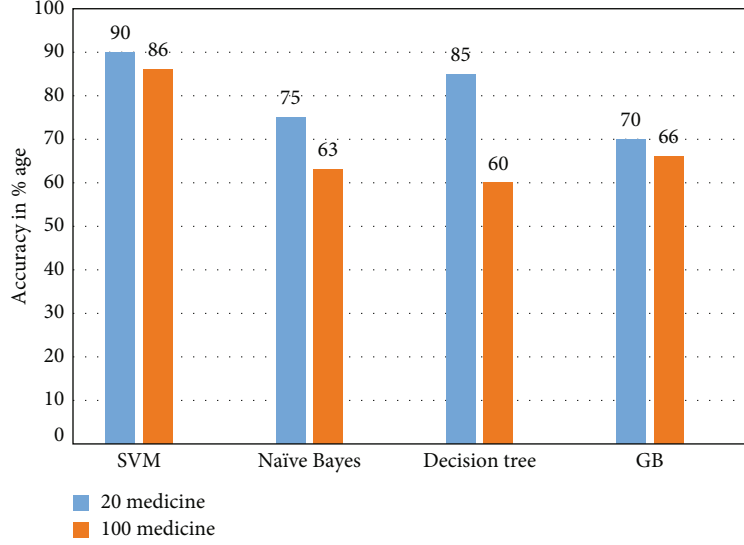


FIGURE 6: Comparison of 20 medicine with 100 medicine data.

TABLE 8: Accuracy obtained by comparing SVM, Naive Bayes, decision tree, and gradient boosted on testing data acquired from user 1 and user 2.

| Users | SVM Acc | NB-Acc | DT-Acc | GB-Acc |
|--------|---------|--------|--------|--------|
| User 1 | 84% | 57 | 59 | 56 |
| User 2 | 78 | 48 | 62 | 61 |
| User 3 | 77.47 | 40.85 | 55 | 60.56 |
| User 4 | 77.31 | 42 | 77.31 | 75.63 |
| User 5 | 74.17 | 25.83 | 78.33 | 80 |
| User 6 | 60 | 47.85 | 73.6 | 75 |
| User 7 | 38.5 | 34.22 | 65.24 | 76 |
| User 8 | 68 | 54.64 | 64 | 69 |
| User 9 | 61.61 | 69.86 | 53.43 | 71.23 |

TABLE 9: Comparison of F -measure score obtained from user 1 and user 2.

| Users | SVM-Acc | NB-Acc | DT-Acc | GB-Acc |
|--------|---------|--------|--------|--------|
| User 1 | 84% | 62 | 59 | 56 |
| User 2 | 79 | 57 | 64 | 62 |
| User 3 | 79 | 61.81 | 60.26 | 67.17 |
| User 4 | 75.75 | 56 | 76.6 | 74 |
| User 5 | 73.84 | 48.59 | 78.67 | 78 |
| User 6 | 64 | 66.7 | 71.13 | 70.5 |
| User 7 | 56 | 49.19 | 64.22 | 73.5 |
| User 8 | 75 | 60.82 | 67.48 | 70 |
| User 9 | 65.58 | 73 | 59.66 | 75.71 |

metrics. The performance of feature ranking metrics is compared with different classifiers. Macroaverage $F1$ and microaverage $F1$ are used to calculate classification performance. Precision and recall are the harmonic means of $F1$ -mea-

sure. Description of macro- $F1$ -measure is given below.

$$\text{Macro Average } F1 = \sum_{k=1}^C \frac{(2 \times P_k \times r_k) / (P_k + r_k)}{C}, \quad (1)$$

where p_k is the precision and r_k is the recall values of class k . Furthermore, it sums up the global precision and recalls for all classes of the dataset in the micro- $F1$ measure as given below.

$$\text{Micro Average } F1 = \frac{2 \times P \times r}{P + r}, \quad (2)$$

where p is the precision and r is the recall which is dependent on the overall performance of the classification decisions within the entire dataset.

$$\text{Precision} = \frac{\text{tp}}{\text{tp} + \text{fp}}, \quad (3)$$

$$\text{Recall} = \frac{\text{tp}}{\text{tp} + \text{fn}},$$

where tp is the true positive value, fp is the false positive, and fn is the false negative value, respectively.

4. Results and Discussion

The accuracy obtained using this chunk of the dataset is 90% using SVM, as compared to Naive Bayes 70%, gradient boosted 50%, and 40% from the decision tree. The experimental results reveal that SVM outperformed other states of the art algorithms for this experimentation. Empirical results of the pen up and pen down features are obtained from user 1 and user 2; data are shown in Figure 5.

The comparison evaluation on the features: upx1 , upy1 , dnx1 , dny1 , time1 , midpoints1x , midpoints1y , quarter1x , quarter1y , 3quarter1x , and 3quarter1y have been carried

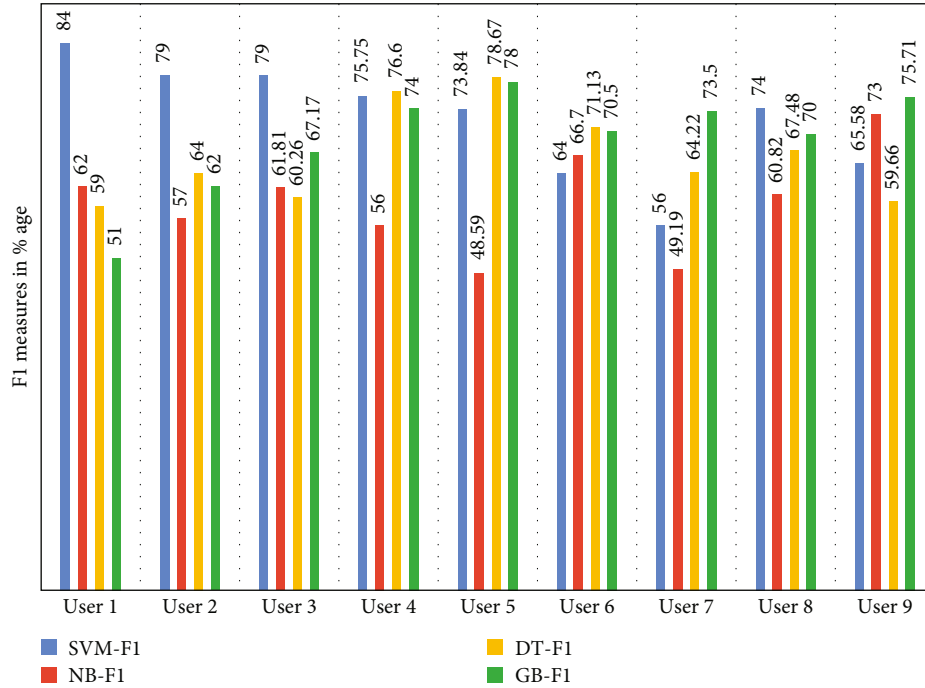


FIGURE 7: Graphical representation of F1-measure score obtained from user 1 and user 2.

TABLE 10: Descriptive states of proposed features, with user 1 data.

| Classifier name | User 1 data accuracy | User 2 data accuracy |
|------------------|----------------------|----------------------|
| SVM | 13% | 14% |
| Naive Bayes | 31% | 16% |
| Decision tree | 39% | 36% |
| Gradient boosted | 32% | 24% |

out. In this experimental setup, we used 24 medicine data and achieved 90% with SVM, 75% Naive Bayes, 70% gradient boosted, and 85% decision tree. The accuracy comparison of 20 medicine with 100 medicines for two users is shown in Figure 6. The accuracy can be enhanced if we consider more pen up and pen down features.

We observed that the sample size of the medicine is directly proportional to the accuracy. The more the sample size of medicines increases, the better the accuracy was obtained. The experimental results of classifiers obtained from user 1 and user 9 are shown in Table 8.

We can see from Table 8 that SVM performed better for every user from user 1 to user 9 with higher accuracy of 84% and 78%, 77.47%, 77.31%, 74.1%, and so on. Some users have shown low accuracy because of the slow writing of the medicine name because the time difference of the pen up and pen down was high, which is the reason for less accuracy.

We have computed the F1 score, which is the measurement of the test’s accuracy defining the weighted harmonic mean of the precision and recall of the test data of all the 9 users. Table 9 presents the performance of each classifier for F-measure obtained data from user 1 to user 9.

The first column of the table shows all the users, and the rest columns confers the F-measure of all 9 users’ data obtained according to from SVM, Naive Bayes, decision tree, and gradient boosted. The graphical representation of empirical results is shown in Figure 7.

4.1. Comparison with Other Features. Through our medical prescription features, we obtained better accuracy; however, additional features can be extracted from original data as described in [41], certain features have been extracted from the handwritten medical prescription application, and the accuracy has been calculated. The proposed features are discussed:

- (i) Pen length (PL): the path length is the total length covered by the user’s pen tip throughout the signature creation
- (ii) Pen diagonal length (DL): diagonal length is the maximum (x_{max}, y_{max}) and minimum (x_{min}, y_{min}) points in the X-Y coordinate
- (iii) Time length (TL): the total time of writing the complete signature (the time period between the first pen down and last pen up)
- (iv) Mean speed (MS): mean speed is the average speed and velocity of the user writing the signature
- (v) Covariance X-Y (CXY): covariance means to measure the scattered points on the signature path
- (vi) Vector length ratio (VLR): calculate all vector points of the signatures from the beginning to each x-y coordinate

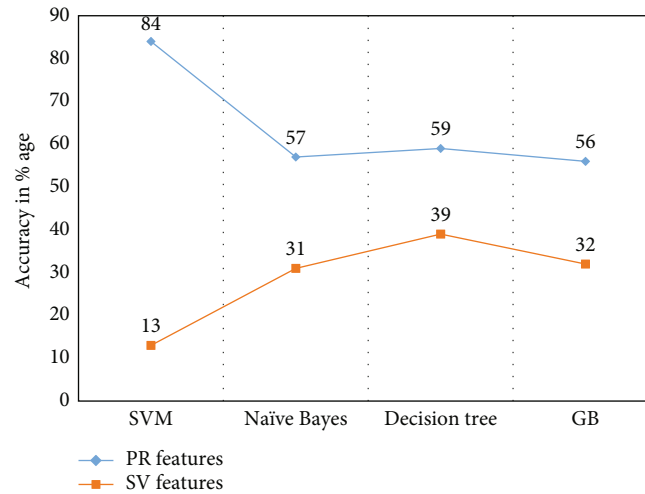


FIGURE 8: Comparison of prescription recognition system and proposed signature verification [41] feature data obtained from user 1.

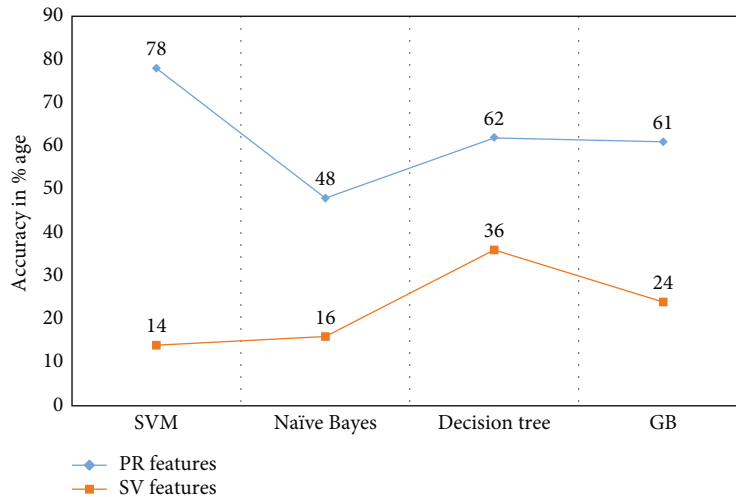


FIGURE 9: Comparison of prescription recognition system and proposed signature verification [41] feature data obtained from user 2.

We employed the same classifiers with additional features described above obtained from user 1 to user 9 for signature verification. The results of individual classifiers are shown in Table 10.

The comparison of both types of features obtained from user 1 and user 9 is shown in Figures 8 and 9, which infers that the SVM is not proven as a better choice for signature verification features [41].

Furthermore, the overall performance of each classifier is appeared as lower than the proposed prescription recognition system. Further, the observation is recorded that the proposed prescription recognition system was employing signature verification techniques performed better than the others. This confirmed that the local spatial features (extracted features) depend on spatial features (original features).

We obtained significant results from both signature verification features and handwritten prescription recognition

systems. The line curves from Figures 8 and 9 show that the overall performance of each classifier remains lower as compared to the proposed handwritten medical prescription recognition system.

5. Conclusion

Patients face difficulties when reading doctor-prescribed medication names. This research focused on the performance and analysis of various classifiers for the newly established handwritten recognition system of medical prescription. We used signature verification techniques to recognize the misinterpreted medical prescription issue better. For the performance evaluation of the proposed system, we introduced new features to increase the performance of the prescription system. We achieved 84%, 59%, 57%, and 56% with SVM, Naive Bayes, decision tree, and gradient boosted. Furthermore, the experiment is extended to determine the F -measure with 84%, 62%, 59%, and 51% from

SVM, Naive Bayes, decision tree, and gradient boosted, respectively. The experimental results revealed that the proposed system based on the handwritten medical prescription data outperformed in terms of better recognition accuracy. This research would help to recognize the prescription in a better way in the area of health care. In the future, we are intended to extract additional features based on statistics. The proposed handwritten medical prescription recognition system opens a new direction for medical prescription recognition.

Data Availability

No data were used to support this study.

Conflicts of Interest

The authors declare that they have no conflicts of interest.

Acknowledgments

This work is funded by the King Saud University from Riyadh, Saudi Arabia, Project Number (RSP-2021/164), King Saud University, Riyadh, Saudi Arabia.

References

- [1] T. B. Sheridan and J. M. Thompson, "People versus computers in medicine," in *Human Error in Medicine*, pp. 141–158, CRC Press, 2018.
- [2] A. Parziale, M. Diaz, M. A. Ferrer, and A. Marcelli, "Sm-dtw: stability modulated dynamic time warping for signature verification," *Pattern Recognition Letters*, vol. 121, pp. 113–122, 2019.
- [3] D. S. Char, N. H. Shah, and D. Magnus, "Implementing machine learning in health care—addressing ethical challenges," *The New England Journal of Medicine*, vol. 378, no. 11, pp. 981–983, 2018.
- [4] A. Banerjee, C. Chakraborty, and M. Rathi, "Medical imaging, artificial intelligence, internet of things, wearable devices in terahertz healthcare technologies," in *Terahertz Biomedical and Healthcare Technologies*, pp. 145–165, Elsevier, 2020.
- [5] R. Achkar, K. Ghayad, R. Haidar, S. Saleh, and R. Al Hajj, "Medical handwritten prescription recognition using CRNN," in *2019 International Conference on Computer, Information and Telecommunication Systems (CITS)*, pp. 1–5, Beijing, China, 2019.
- [6] Y. Jia, L. Huang, and H. Chen, "A two-stage method for online signature verification using shape contexts and function features," *Sensors*, vol. 19, no. 8, p. 1808, 2019.
- [7] M. Antal, L. Z. Szabo, and T. Tordai, "Online signature verification on mobisig finger-drawn signature corpus," *Mobile Information Systems*, vol. 2018, Article ID 3127042, 15 pages, 2018.
- [8] A. R. Ahmad, M. Khalia, C. Viard-Gaudin, and E. Poisson, "Online handwriting recognition using support vector machine," in *2004 IEEE Region 10 Conference TENCON 2004*, pp. 311–314, Chiang Mai, Thailand, 2004.
- [9] A. Nigam, P. Singh, V. K. Singh, and R. C. Tripathi, "A multiple feature-based offline handwritten signature verification system," *International Journal of Computer Applications in Technology*, vol. 59, no. 3, pp. 214–223, 2019.
- [10] S. Tanwar, M. S. Obaidat, S. Tyagi, and N. Kumar, "Online signature-based biometric recognition," in *Biometric-Based Physical and Cybersecurity Systems*, pp. 255–285, Springer, 2019.
- [11] B. Shekar, B. Pilar, and D. S. Kumar, "Offline signature verification based on partial sum of second-order Taylor series expansion," in *Data Analytics and Learning*, pp. 359–367, Springer, 2019.
- [12] R. Al-Hmouz, W. Pedrycz, K. Daqrouq, A. Morfeq, and A. Al-Hmouz, "Quantifying dynamic time warping distance using probabilistic model in verification of dynamic signatures," *Soft Computing*, vol. 23, no. 2, pp. 407–418, 2019.
- [13] H. T. Rauf, S. Malik, U. Shoaib, M. N. Irfan, and M. I. Lali, "Adaptive inertia weight Bat algorithm with Sugeno-function fuzzy search," *Applied Soft Computing*, vol. 90, p. 106159, 2020.
- [14] H. T. Rauf, U. Shoaib, M. I. Lali, M. Alhaisoni, M. N. Irfan, and M. A. Khan, "Particle swarm optimization with probability sequence for global optimization," *IEEE Access*, vol. 8, pp. 110535–110549, 2020.
- [15] S. Mandal, H. Choudhury, S. M. Prasanna, and S. Sundaram, "Frequency count based two stage classification for online handwritten character recognition," in *2016 International Conference on Signal Processing and Communications (SPCOM)*, pp. 1–5, Bangalore, India, 2016.
- [16] V. Jain, G. Chaudhary, N. Luthra, A. Rao, and S. Walia, "Dynamic handwritten signature and machine learning based identity verification for keyless cryptocurrency transactions," *Journal of Discrete Mathematical Sciences and Cryptography*, vol. 22, no. 2, pp. 191–202, 2019.
- [17] H. Saikia and K. C. Sarma, "Approaches and issues in offline signature verification system," *International Journal of Computer Applications*, vol. 42, no. 16, pp. 45–52, 2012.
- [18] J. Gao, H. Wang, and H. Shen, "Task failure prediction in cloud data centers using deep learning," *IEEE Transactions on Services Computing*, vol. 15, no. 3, pp. 1411–1422, 2022.
- [19] J. Gao, H. Wang, and H. Shen, "Smartly handling renewable energy instability in supporting a cloud datacenter," in *2020 IEEE International Parallel and Distributed Processing Symposium (IPDPS)*, IEEE, 2020.
- [20] S. D. Connell and A. K. Jain, "Template-based online character recognition," *Pattern Recognition*, vol. 34, no. 1, pp. 1–14, 2001.
- [21] J. Gao, H. Wang, and H. Shen, "Machine learning based workload prediction in cloud computing," in *2020 29th International Conference on Computer Communications and Networks (ICCCN)*, pp. 1–9, Honolulu, HI, USA, 2020.
- [22] A. Sarkar, M. Z. Khan, M. M. Singh, A. Noorwali, C. Chakraborty, and S. K. Pani, "Artificial neural synchronization using nature inspired whale optimization," *IEEE Access*, vol. 9, pp. 16435–16447, 2021.
- [23] C. M. Christensen, J. H. Grossman, and J. Hwang, *The Innovator's Prescription*, Soundview Executive Book Summaries, 2009.
- [24] B. Nassi, Y. Elovici, E. Shmueli, and A. Levy, "A method for online signature verification using wrist-worn devices," *US Patent App. 16/094, 709*, 2019.
- [25] J. Vajpai, J. Arun, and I. Vajpai, "Dynamic signature verification for secure retrieval of classified information," in *2013*

- Fourth National Conference on Computer Vision, Pattern Recognition, Image Processing and Graphics (NCVPRIPG)*, pp. 1–4, Jodhpur, India, 2013.
- [26] N. Sae-Bae and N. Memon, “A simple and effective method for online signature verification,” in *2013 International Conference of the BIOSIG Special Interest Group (BIOSIG)*, pp. 1–12, Darmstadt, Germany, 2013.
- [27] M. Prathiba and L. Basavaraj, “Online handwritten signature verification system: a review,” *International Journal of Emerging Trends & Technology in Computer Science*, vol. 3, no. 2, pp. 263–267, 2014.
- [28] K. Radhika and S. Gopika, “Online and offline signature verification: a combined approach,” *Procedia Computer Science*, vol. 46, pp. 1593–1600, 2015.
- [29] Y. Liu, Z. Yang, and L. Yang, “Online signature verification based on dct and sparse representation,” *IEEE Transactions on Cybernetics*, vol. 45, no. 11, pp. 2498–2511, 2015.
- [30] B. Nassi, A. Levy, Y. Elovici, and E. Shmueli, “Handwritten signature verification using hand-worn devices,” <https://arxiv.org/abs/1612.06305>.
- [31] X.-Y. Zhang, Y. Bengio, and C.-L. Liu, “Online and offline handwritten chinese character recognition: a comprehensive study and new benchmark,” *Pattern Recognition*, vol. 61, pp. 348–360, 2017.
- [32] A. Mukherjee, K. Priya, M. Pandit, and D. Bhattacharya, “Use of auto associative network for signature recognition,” *Journal of Current Engineering and Technology*, vol. 7, pp. 2277–4106, 2017.
- [33] S. Kedia and E. G. Monga, “Static signature matching using lda and artificial neural networks,” *International Journal of Advance Research, Ideas and Innovations in Technology*, vol. 3, 2017.
- [34] C. Zheng, W. Hong, J. Song, S. Li, J. Luan, and E. Yan, “Research and realization of printed tcm prescription recognition and filing system,” in *2015 Fifth International Conference on Instrumentation and Measurement, Computer, Communication and Control (IMCCC)*, pp. 907–910, Qinhuangdao, China, 2015.
- [35] Q.-Y. Jiang, H.-Y. Li, J.-F. Liang, Q.-X. Wang, X.-M. Luo, and H.-L. Liu, “Multi-combined features text mining of tcm medical cases with crf,” in *2016 8th International Conference on Information Technology in Medicine and Education (ITME)*, pp. 621–626, Fuzhou, China, 2016.
- [36] A. A. Azeta, D.-O. A. Iboroma, V. I. Azeta, E. O. Igbekele, D. O. Fatinikun, and E. Ekpunobi, “Implementing a medical record system with biometrics authentication in e-health,” in *2017 IEEE AFRICON*, pp. 979–983, Cape Town, South Africa, 2017.
- [37] P. P. Roy, A. K. Bhunia, A. Das, P. Dhar, and U. Pal, “Keyword spotting in doctor’s handwriting on medical prescriptions,” *Expert Systems with Applications*, vol. 76, pp. 113–128, 2017.
- [38] C. Vielhauer, R. Steinmetz, and A. Mayerhofer, “Biometric hash based on statistical features of online signatures,” in *2002 International Conference on Pattern Recognition*, pp. 123–126, Quebec City, QC, Canada, 2002.
- [39] Y.-O. Cho and J.-W. Jung, “Online signature recognition based on pseudo-inked signature image template,” *International Journal of Humanoid Robotics*, vol. 14, no. 2, p. 1750016, 2017.
- [40] D. Muramatsu and T. Matsumoto, “Effectiveness of pen pressure, azimuth, and altitude features for online signature verification,” *Advances in Biometrics*, vol. 4642, pp. 503–512, 2007.
- [41] N. Paudel, M. Querini, and G. F. Italiano, *Handwritten Signature Verification for Mobile Phones*, ICISSP, 2016.

Research Article

Effect of Gender on Serum Leptin in Type 2 Diabetes Mellitus: A System Review and Meta-Analysis

Yushan Li , Xiao Chen, Xingji Gong, Jian Yao, Dongyong He, and Wenjie Du 

Department of Emergency Internal Medicine, The Affiliated Hospital of Qingdao University, Qingdao, 266000 Shandong, China

Correspondence should be addressed to Wenjie Du; dewink@qdu.edu.cn

Received 18 July 2022; Revised 15 August 2022; Accepted 30 August 2022; Published 10 September 2022

Academic Editor: Sujatha Krishnamoorthy

Copyright © 2022 Yushan Li et al. This is an open access article distributed under the Creative Commons Attribution License, which permits unrestricted use, distribution, and reproduction in any medium, provided the original work is properly cited.

Objective. To assess the effect of gender factors on serum leptin levels in patients with diabetes mellitus. **Methods.** To remove any studies that indicated a relationship between leptin-based inflammatory variables and the prevalence of type 2 diabetes in particular patient categories, a comprehensive search of all articles published between July 2019 and June 2021 was performed on PubMed/MEDLINE, Web of Science, Scopus, and EBSCO Host, including Academic Search Premier, Africa-Wide Information, and Cumulative Index to Nursing and Allied Health Literature. A summary description of the combined analysis across multiple centers, regions, and continents will help us better understand the effect of gender on serum leptin levels in patients with diabetes. The meta-analysis was performed using RevMan 5.2 software on the literature that satisfied the inclusion and exclusion criteria. **Results.** Plasma CRP levels in women with type 2 diabetes were found to be no different from those in males with type 2 diabetes, with an OR of 0.12, 95 percent confidence interval (CI) of 0.12 to 0.12, $P = 0.01$. There was no statistically significant difference in the plasma level of interleukin-6 (IL-6) between women with type 2 diabetes and males with type 2 diabetes. However, the “inverted funnel” diagram is asymmetrical, indicating a publication bias in the included studies, despite the fact that there was no statistically significant difference in abnormal leptin levels between men with type 2 diabetes and women patients (OR = -0.69, 95 percent CI (0.88, 1.00), $P < 0.05$). **Conclusion.** Gender factors did not affect the level of inflammatory factors and leptin level in type 2 diabetes.

1. Introduction

There are 167 amino acids in leptin. Adipocytes remove the 21-amino acid N-terminal signal peptide during the secretion process of leptin to produce active leptin [1]. The omentum, mesentery, retroperitoneum, and subcutaneous adipocytes were discovered to have significant leptin quantities. Additionally, skeletal muscle, the stomach's epithelium, bone, and the heart synthesize [2]. Bursts of release punctuate the 24-hour cycle of leptin secretion. From 20:00 to 3:00 in the morning the following day, secretion is at its maximum and lowest around lunchtime [3]. An important insulin-regulatory hormone, leptin, has a role in glucose metabolism. One of leptin's primary targets in our brain and nervous system is the hypothalamic arcuate nucleus (ARC). Neuropeptide Y (NPY) neurons and pro-opiomelanocortin (POMC)/cocaine amphetamine-regulated transcription factor (CART) neurons are present in ARC.

Activating POMC/cart neurons and inhibiting AgRP/NPY neurons are only a few ways leptin works to lower blood glucose levels and boost energy expenditure while also decreasing hepatocyte glucose release [4]. Glucocorticoid and glucagon levels, insulin levels, and blood glucose stability are maintained via the hypothalamic-pituitary-adrenal axis (HPA). In the sympathetic nervous system, when hypoglycemia occurs, preinsulin mRNA and insulin gene activity may be reduced, and insulin production in the peripheral may be limited by leptin [5]. Leptin may also increase the activity of AMPK in islet B cells and activate the ATP-sensitive potassium channel (KATP), which results in potassium outflow. Leptin can also decrease insulin release after baseline and glucose stimulation and help regulate glucose homeostasis [6].

In addition to insulin resistance, hyperglycemia and hyperlipidemia are all signs of T2DM, which are all associated with obesity. Leptin levels rise in obese people due to

increased endogenous leptin resistance [7]. Long-term stimulation with high amounts of leptin reduces islet B cell responsiveness, inhibits insulin synthesis, and increases insulin release. This causes hyperinsulinemia and enhanced insulin resistance, which worsens obesity by increasing leptin secretion and exacerbating leptin resistance. Over the course of the study, leptin levels in men with type 2 diabetes mellitus (T2DM) were considerably greater than those in men without diabetes, indicating that leptin may be used to predict the development of T2DM. It has been shown that leptin levels are favorably related to blood insulin levels in obese and diabetic individuals. Some studies suggest that serum leptin may be an excellent predictor of insulin resistance in people with type 2 diabetes [8].

Prospective epidemiological studies on the association of leptin with the risk of type 2 diabetes in the last decade have shown inconclusive results, with some studies suggesting that the association between leptin and type 2 diabetes risk may be sex-specific [9, 10]. We performed a meta-analysis of prospective studies for different genders to get a more comprehensive understanding of the effect of gender on leptin levels in diabetic patients.

2. Methods

The PRISMA (Preferred Reporting Items for Systematic Reviews and Meta-Analyses) declaration was used to perform this systematic review. Because all of the analyses were based on previously published research, no ethical approval or patient permission was required to carry out the study.

2.1. Literature Search. We searched PubMed/MEDLINE, Web of Science, Scopus, and EBSCO Host (including Academic Search Premier, Africa-Wide Information, and Cumulative Index to Nursing and Allied Health Literature) for all articles published between July 2019 and June 2021. A comprehensive analysis of literature from multiple centers, regions, and continents was conducted. A manual search of pertinent references in previously published works was also carried out. There were no linguistic limitations. Keywords for search include “factor” or “cytokine” or “leptin” or “diabetes” or “leptin + diabetes.” The research methods include cohort study, prospective study, follow-up study, and case control study. This search strategy was modified to allow it to be used in more databases if required.

2.2. Study Selection. Inclusion criteria: the selected literature and research must meet all the following criteria: (1) it is a randomized controlled trial, including male group and female group, which are comparable between the two groups, (2) the subjects were type 2 diabetic patients with no definite diagnosis, and (3) published English literature with complete data. Exclusion criteria: (1) patients with type 1 diabetes and impaired fasting glucose, (2) self-controlled test, (3) animal experiments, (4) overview/meeting summary/case study, etc., (5) unable to obtain complete data, (6) republished literature, (8) summary of the meeting, and (7) documents with incomplete content and unable to extract data. Due to the separate study of leptin gender, the

number of papers is small. We also extracted and analyzed the data of other fat factors.

2.3. Data Extraction and Assessment of Quality. Endnote X7 was used to collect references (Clarivate Analytics, USA). Two distinct reviewers used search results to assess the acceptability of the papers, which a third independent reviewer subsequently evaluated. Two writers cooperated in creating a table of general research features (information on important outcome indicators and adverse events, e.g., study name, diagnosis, and participant number). Emails or phones were issued to the authors to get any missing information. When the same topic has been addressed, the data were chosen from the complete journal papers. Researchers compared two versions of the same article to identify which was the first. Blinding, sequence creation, allocation concealment, and other aspects were considered when calculating the risk of bias in each trial, which was assessed using the Cochrane Bias Scale. In addition, two reviewers independently conducted these assessments. During the previous rounds, one author was expected to arbitrate any disagreements among the reviewers. To identify the quality of the research, an in-depth methodological review was necessary; hence, unpublished articles and conference abstracts were omitted from the search.

2.4. Statistical Analysis. All statistical computations in this research were performed using RevMan 5.2. (USA). The relative risk (RR) and 95 percent confidence interval (CI) were used for binary outcomes, whereas the mean difference (MD) and confidence interval (CI) were used for continuous outcomes. Cochran’s Q test and the I^2 statistic were employed in the study to examine statistical heterogeneity, and the I^2 statistic was utilized to quantify variance. A fixed-effect model was utilized to account for the difference when I^2 was less than 50%. Aside from that, we analyzed the data using a random-effects model. Subgroup analysis means that in the study, the research objects are divided into different subgroups according to some characteristics of the research objects (such as gender and disease severity), and then, the effect values of different groups are estimated and compared among subgroups. In meta-analysis, the research can be divided into subgroups for analysis according to certain research characteristics. Its purpose is to study the interaction or effect modification, that is, whether the effect value is different in different populations or conditions. Subgroup analysis is one of the important methods to analyze heterogeneous results or to answer questions about specific patients, intervention types, or research types. A subgroup analysis was undertaken on a range of treatments in control groups. The leave-one-out strategy was employed to evaluate sensitivity. To establish whether there is evidence of publication bias, a funnel plot or a metaregression analysis may be done, depending on the number of articles. In the research, the tests Harbord’s and Egger’s were used to uncover the results for binary and continuous outcomes, respectively. A statistically significant outcome was one that had a P value of 0.05 or less.

TABLE 1: Features of each research.

| Author (year) | Participants | Outcomes |
|-----------------------------|--------------|---|
| Lilja (2012) [9] | 640 | Leptin in men and adiponectin in both sexes were independent predictors of T2DM. The association was modified by the degree of insulin sensitivity. The leptin/adiponectin ratio may add predictive information beyond the separate hormones. |
| McNeely (1999) [10] | 410 | Among Japanese Americans, increased baseline leptin levels are associated with increased risk of developing diabetes in men but not in women. |
| Sans S; Padró T (2013) [29] | 1011 | In a population with relatively high diabetes incidence, BMI and glucose were strong risk factors, while adiponectin protected against diabetes, especially in men with high glycemic level. High leptin levels, probably reflecting leptin resistance, predict an increased risk of diabetes. |
| Schmidt (2006) [13] | 10275 | Adjusting for factors purportedly related to leptin resistance unveils a protective association, independent of adiponectin and consistent with some of leptin's described protective effects against diabetes. |
| Sun (2010) [16] | 32826 | These data suggest a strong inverse association between plasma sOB-R levels and risk of type 2 diabetes, independent of BMI, leptin, and adiponectin levels. |
| Thorand (2010) [17] | 7936 | Two adipokines leptin and adiponectin interact in modulating type 2 diabetes risk, but adiponectin is more strongly associated with type 2 diabetes risk than leptin. |
| Welsh (2009) [18] | 5672 | Leptin, similar to other markers of adiposity in general, is more strongly related to risk of diabetes than CVD in the elderly. |
| Söderberg (2007) [19] | 2330 | High leptin levels are associated with the future development of diabetes, and the association is independent of other factors in men, but not in women. |
| Kouvari (2021) [20] | 2020 | Report an inverse association between Mediterranean diet and NAFLD. Mediterranean diet protected against diabetes and CVD prospectively among subjects with NAFLD. |
| Peller (2020) [21] | 273 | In type 2 DM, patients with AF have higher resistin and adiponectin concentrations than patients with no AF. None of the studied adipokines proved a predictor of future AF development. |

3. Results

3.1. Study Characteristics. This meta-analysis includes 10 articles, all of which have studied the relationship between leptin level and type 2 diabetes risk. Table 1 provides an overview of each study's characteristics. There were 31696 diabetics and 31696 nondiabetics who participated in the 10 studies, which were published between 1999 and 2021, according to the data. One study was carried out in China while the other eight were undertaken in the United States. It ranged from 3.2 years to 22 years in the follow-up period. Leptin levels and type 2 diabetes relationship have been studied in five of the ten studies using OR estimations. A radioimmunoassay or an enzyme-linked immunosorbent assay was often used to measure leptin levels, whereas self-report and blood glucose levels were frequently used to detect diabetes, as seen in Figure 1.

3.2. Quality Evaluation. 10 literatures were included, of which 10 reported the randomization method and the rest did not mention the randomization method or the method had high risk. There is no literature to implement double-blind. Only one literature used blind method for clinical evaluation and laboratory analysis report. In the outcome data report, all literatures reported preset outcome indicators, which were rated as low risk. Other biases of 10 literatures were evaluated as uncertain risk, as shown in Figure 2.

3.3. Plasma CRP Results. A total of 10 research results were included for heterogeneity test. There was heterogeneity among the groups, and the heterogeneity was large

($P < 0.00001$, $I^2 = 100\%$) using random-effects model for meta-analysis; the results showed that compared with male patients with type 2 diabetes, plasma CRP level in women with type 2 diabetes no significant difference (OR = -0.12, 95% CI (-0.13, -0.12), $P < 0.0001$); see Figure 3.

3.4. TNF- α Test Results. A total of 5 cases were included and tested for heterogeneity. The heterogeneity between each group was small ($P \leq 0.00001$, $I^2 = 100\%$); a fixed-effect model was used for meta-analysis. The results showed that plasma TNF- α level in females with type 2 diabetes has no significant difference with that in men (OR = 0.19, 95% CI (0.18, 0.19), $P < 0.00001$); see Figure 4.

3.5. Results of IL-6 Test. A total of 10 cases were included and tested for heterogeneity. There was great heterogeneity among the groups ($P < 0.00001$, $I^2 = 97\%$); a random-effects model was used to carry out the meta-analysis. The results of plasma IL-6 levels in women in type 2 diabetes areas compared with men are presented in Figure 5. The difference in plasma IL-6 levels between genders was not statistically significant (OR = -0.00, 95% CI (-0.00, -0.01), $P < 0.00001$).

3.6. Leptin Test Results. A total of 10 cases were included and tested for heterogeneity. The heterogeneity between groups was small ($P = 1.00$, $I^2 = 0\%$); a fixed-effect model was used for meta-analysis. The results showed that there was no statistically significant difference in abnormal leptin level between man patients with type 2 diabetes and woman

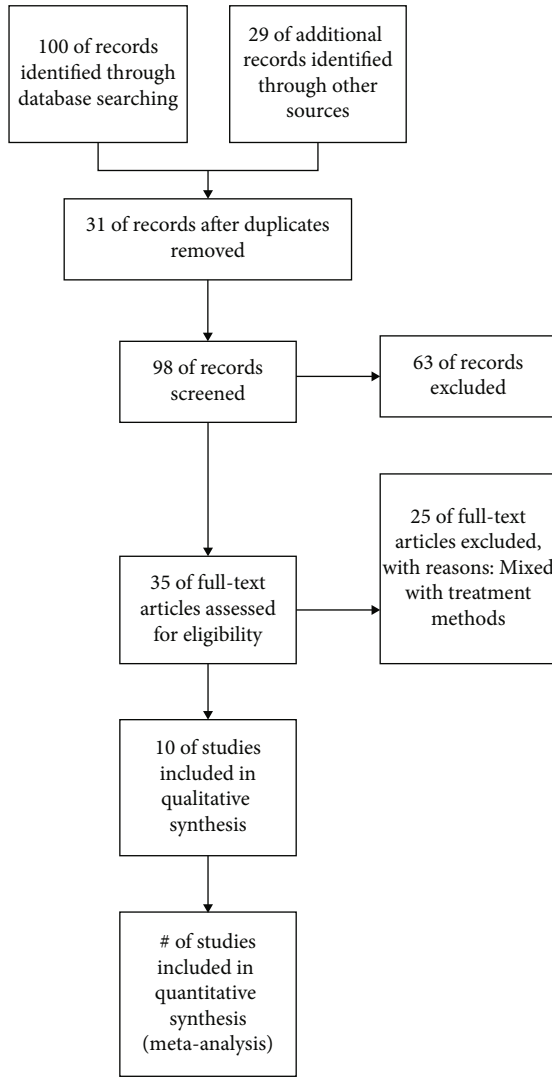


FIGURE 1: Document screening process.

patients (OR = -0.69, 95% CI (0.88, 1.00), $P < 0.05$); see Figure 6.

3.7. *Publication Bias.* A funnel chart (Figure 7) was made according to the leptin level test results, which showed that there may be publication bias.

4. Discussion

Leptin is considered to be a regulator of human food intake and energy consumption, because hypothalamic receptors easily bind to leptin, which can regulate appetite [11]. Several studies have shown that leptin decreases insulin sensitivity, which in turn decreases glucose tolerance [12]. Leptin has been shown to inhibit the expression of insulin precursor gene and finally affect the secretion of insulin. According to these results, higher leptin levels are associated with an increased risk of diabetes because of the role it plays in regulating insulin sensitivity and secretion [13]. According to the results of this prospective study, there were no gender differences in leptin levels and type 2 diabetes, which

| | Random sequence generation (selection bias) | Allocation concealment (selection bias) | Blinding of participants and personnel (performance bias) | Blinding of outcome assessment (detection bias) | Incomplete outcome data (attrition bias) | Selective reporting (reporting bias) | Other bias |
|-------------------|---|---|---|---|--|--------------------------------------|------------|
| Bartley CE, 2014 | + | + | + | + | + | | + |
| Bydon M, 2013 | + | | + | + | + | + | + |
| Hazer DB, 2016 | + | + | + | | + | + | + |
| Hu X, 2013 | + | + | + | + | + | + | + |
| Ito K, 2009 | + | + | - | + | + | | + |
| Mantovani E, 2014 | + | + | + | + | + | + | |
| Matsuoka H, 2012 | + | + | | + | + | + | + |
| Onen MR, 2015 | + | | + | + | + | + | + |
| Street JT, 2012 | + | + | + | + | - | + | + |
| Williams BJ, 2011 | - | + | + | + | | + | + |

FIGURE 2: Quality evaluation of 10 literatures.

is not consistent with the findings of Chen et al. [14]. In the present study, we also considered the obesity of the patients and found that the relationship between obese leptin levels and diabetes was not strong, which is consistent with previous studies [14, 15]. Our assessment factors were broader than previous studies (including plasma CRP results, TNF- α test results, results of IL-6 test, leptin test results, and publication bias), so the comprehensiveness of the assessment results may be higher.

Obesity and leptin have a strong correlation in humans, which may be due to a condition known as leptin resistance. So far, we have found some reasons for leptin resistance, such as the reduction of BBB transport and the lack of leptin signal transduction in neurons [16]. Chronically high levels of leptin may compromise receptor system responsiveness in insulin-producing cells, resulting in insulin resistance [17]. The inability to control insulin release is due to a reduction in the responsiveness of cells. Hyperinsulinemia may aggravate obesity by increasing leptin and gene expression in white adipose tissue (a major source of leptin production) [18]. Obesity and insulin resistance may occur from an overproduction of leptin, which in turn promotes

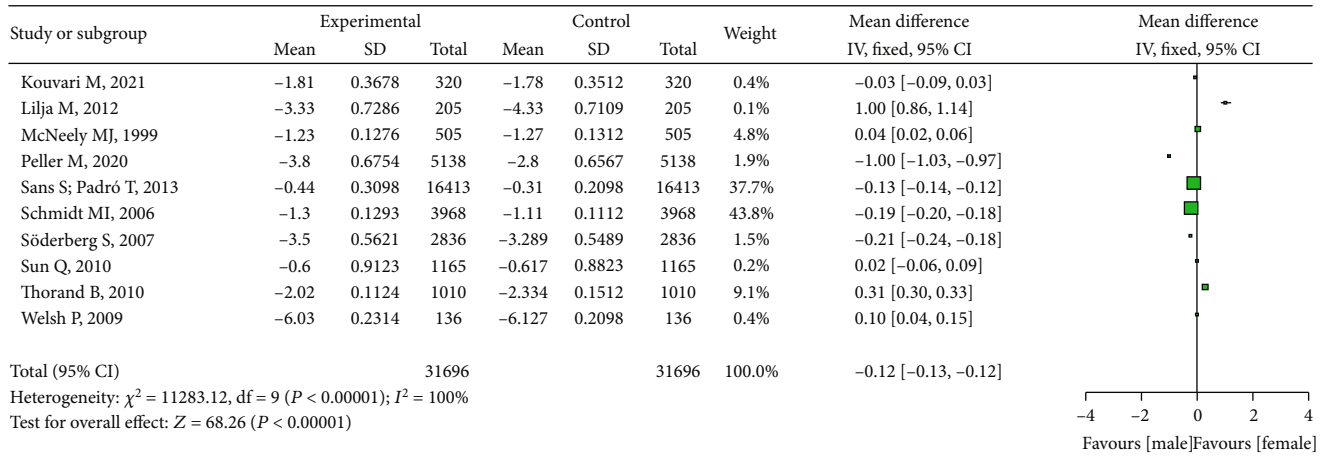


FIGURE 3: CRP level in women with type 2 diabetes with no significant difference.

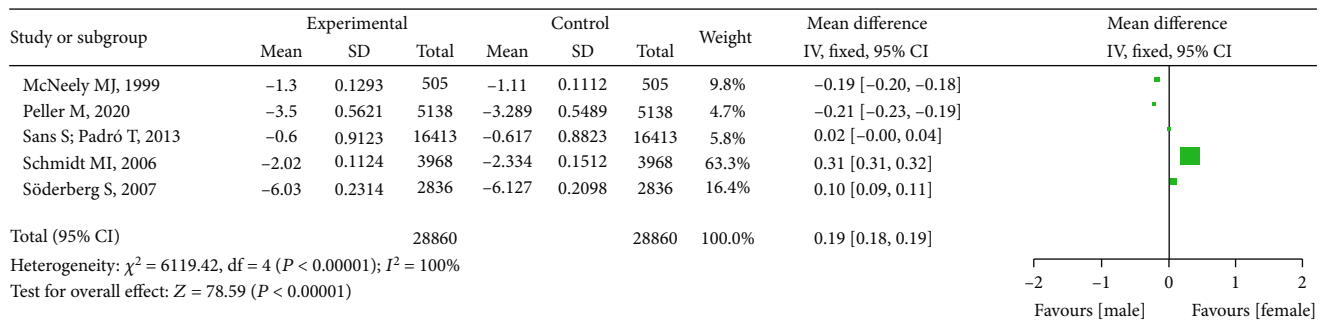


FIGURE 4: TNF- α level in females with type 2 diabetes has no significant difference with that in men.

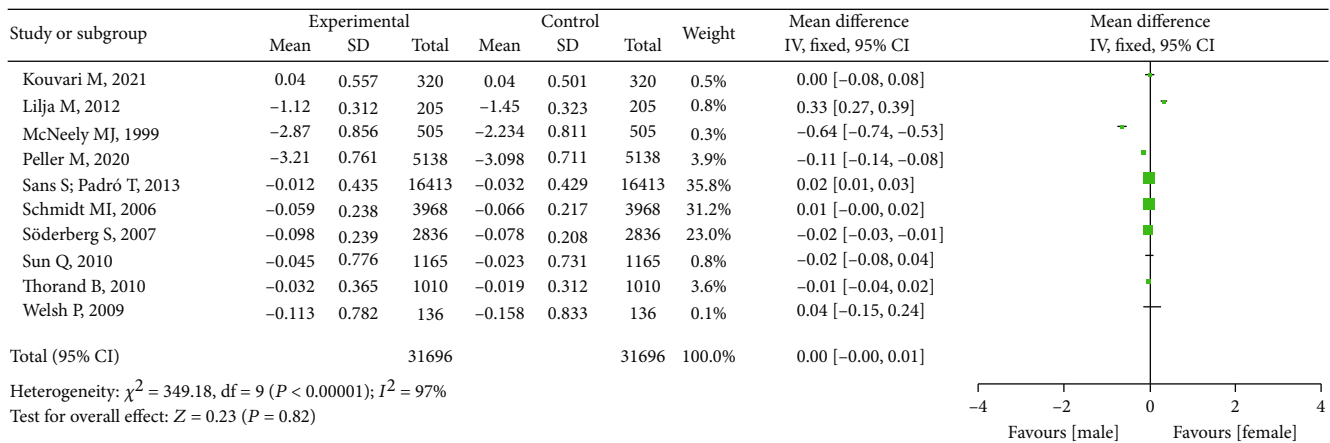


FIGURE 5: IL-6 level among women with type 2 diabetes compared with men has no significant difference.

the development of diabetes. In a prospective trial, males who were insulin sensitive had a higher risk of developing type 2 diabetes, whereas insulin resistance had a lower risk (RR = 1.03 for a 1-log ng mL⁻¹ elevation in leptin, 95% CI 0.76–1.39), according to the researchers. This study reveals that leptin and insulin sensitivity may be linked [19].

Gender differences in the association between leptin and diabetes may be caused by many different factors [11]. The

fat distributions of males and women are vastly different. Type 2 diabetes may be linked to men’s visceral fat, whereas women’s subcutaneous fat is a key source of leptin, a hormone linked to weight gain and obesity [20]. When leptin levels rise, males may have a greater chance of developing diabetes than women. Leptin has a central catabolic effect on female rats’ brains, which are more sensitive than male rats [21]. It is also possible that there are gender-specific

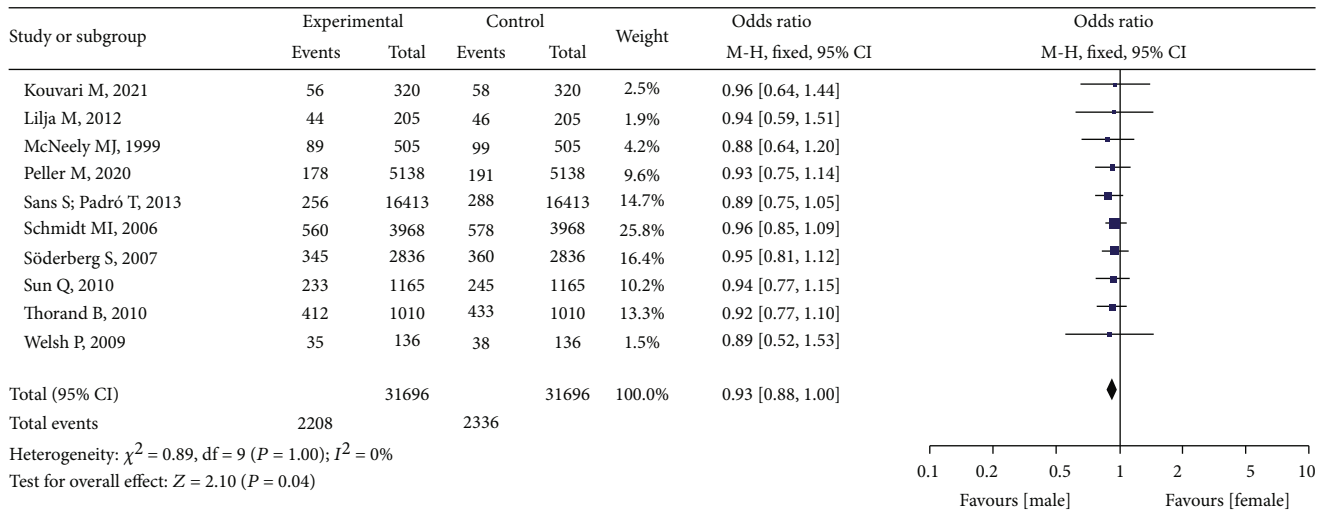


FIGURE 6: Leptin level between man patients with type 2 diabetes and woman patients has no significant difference.

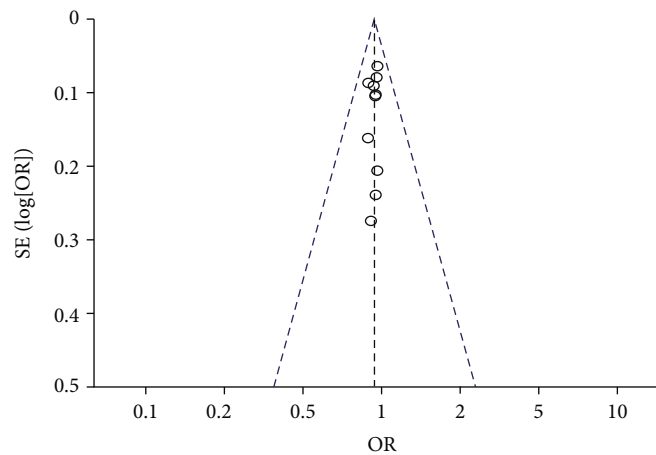


FIGURE 7: Publication bias funnel diagram.

differences in leptin transport across the BBB or in leptin intracellular signaling cascades when estrogen deficiency occurs [22]. The nonlinear leptin–diabetes association found in men may suggest that the central effect of leptin, rather than its peripheral effect, contributes to the inhibitory effect of leptin on insulin secretion because free leptin levels in cerebrospinal fluid are already saturated at low circulating levels of leptin. The results were also inconclusive when looking at the data by gender [23].

Despite variances in research design, time of follow-up, illness identification, and other technical difficulties [24], it is possible that ethnic discrepancies in the connection between leptin and diabetes led to study heterogeneity [25]. An analysis of the American Cohort Research found that blacks had greater leptin levels than whites after controlling for body mass index and other factors, according to the study [25]. In the Atherosclerosis Risk in Communities Study, it was shown that blacks had considerably higher leptin levels than whites even after controlling for age, gender, and geographic location [26]. Using a mixed ethnicity stratified research, we found that leptin had no influence

on the incidence of type 2 diabetes in males and a minor protective effect on the incidence in women (all studies within the stratum had recruited blacks) [27]. As a result, further future research is required to investigate correlations that are specific to ethnicity [28].

5. Conclusions

In summary, gender factors did not affect the level of inflammatory factor leptin in type 2 diabetes.

6. Limitation

Our research also has several limitations. (1) No consideration is given to racial characteristics. We discovered that, although there is no difference between males and women, there are disparities across races. (2) The included literature is limited and outdated. (3) There are flaws in data statistical analysis. Efforts should be taken in the future to prevent making similar mistakes in the study.

Data Availability

The datasets used during the current study are available from the corresponding author on request.

Conflicts of Interest

All the researchers claim no conflicts of interests.

References

- [1] N. Katsiki, D. P. Mikhailidis, and M. Banach, "Leptin, cardiovascular diseases and type 2 diabetes mellitus," *Acta Pharmacologica Sinica*, vol. 39, no. 7, pp. 1176–1188, 2018.
- [2] B. Wang, P. C. Chandrasekera, and J. J. Pippin, "Leptin- and leptin receptor-deficient rodent models: relevance for human type 2 diabetes," *Current Diabetes Reviews*, vol. 10, no. 2, pp. 131–145, 2014.
- [3] P. López-Jaramillo, D. Gómez-Arbeláez, J. López-López et al., "The role of leptin/adiponectin ratio in metabolic syndrome and diabetes," *Hormone Molecular Biology and Clinical Investigation*, vol. 18, no. 1, pp. 37–45, 2014.
- [4] W. Q. Xiao, J. R. He, S. Y. Shen et al., "Maternal circulating leptin profile during pregnancy and gestational diabetes mellitus," *Diabetes Research and Clinical Practice*, vol. 161, article 108041, 2020.
- [5] K. Miehle, H. Stepan, and M. Fasshauer, "Leptin, adiponectin and other adipokines in gestational diabetes mellitus and pre-eclampsia," *Clinical Endocrinology*, vol. 76, no. 1, pp. 2–11, 2012.
- [6] A. Tvarijonaviciute, C. Castillo, J. J. Ceron, S. Martinez-Subiela, F. Tecles, and P. López-Jornet, "Leptin and NGF in saliva of patients with diabetes mellitus type 2: a pilot study," *Journal of Oral Pathology & Medicine*, vol. 46, no. 9, pp. 853–855, 2017.
- [7] S. Chai, Y. Chen, S. Xin et al., "Positive association of leptin and artery calcification of lower extremity in patients with type 2 diabetes mellitus: a pilot study," *Frontiers in Endocrinology*, vol. 12, article 583575, 2021.
- [8] H. A. Al-Hussani, A. H. Alburghaif, and M. A. Najji, "Leptin hormone and its effectiveness in reproduction, metabolism, immunity, diabetes, hopes and ambitions," *Journal of Medicine and Life*, vol. 14, no. 5, pp. 600–605, 2021.
- [9] M. Lilja, O. Rolandsson, M. Norberg, and S. Söderberg, "The impact of leptin and adiponectin on incident type 2 diabetes is modified by sex and insulin resistance," *Metabolic Syndrome and Related Disorders*, vol. 10, no. 2, pp. 143–151, 2012.
- [10] M. J. McNeely, E. J. Boyko, D. S. Weigle et al., "Association between baseline plasma leptin levels and subsequent development of diabetes in Japanese Americans," *Diabetes Care*, vol. 22, no. 1, pp. 65–70, 1999.
- [11] X. Cheng, X. Guo, F. Huang, H. Lei, Q. Zhou, and C. Song, "Effect of different sweeteners on the oral microbiota and immune system of Sprague Dawley rats," *AMB Express*, vol. 11, no. 1, pp. 1–9, 2021.
- [12] M. Maffei, J. Halaas, E. Ravussin et al., "Leptin levels in human and rodent: measurement of plasma leptin and *ob* RNA in obese and weight-reduced subjects," *Nature Medicine*, vol. 1, no. 11, pp. 1155–1161, 1995.
- [13] M. I. Schmidt, B. B. Duncan, A. Vigo et al., "Leptin and incident type 2 diabetes: risk or protection," *Diabetologia*, vol. 49, no. 9, pp. 2086–2096, 2006.
- [14] G. C. Chen, L. Q. Qin, and J. K. Ye, "Leptin levels and risk of type 2 diabetes: gender-specific meta-analysis," *Obesity Reviews*, vol. 15, no. 2, pp. 134–142, 2014.
- [15] X. Cheng, F. He, M. Si, P. Sun, and Q. Chen, "Effects of antibiotic use on saliva antibody content and oral microbiota in Sprague Dawley rats," *Frontiers in Cellular and Infection Microbiology*, vol. 12, 2022.
- [16] Q. Sun, R. M. van Dam, J. B. Meigs, O. H. Franco, C. S. Mantzoros, and F. B. Hu, "Leptin and soluble leptin receptor levels in plasma and risk of type 2 diabetes in U.S. women: a prospective study," *Diabetes*, vol. 59, no. 3, pp. 611–618, 2010.
- [17] B. Thorand, A. Zierer, J. Baumert, C. Meisinger, C. Herder, and W. Koenig, "Associations between leptin and the leptin / adiponectin ratio and incident type 2 diabetes in middle-aged men and women: results from the MONICA / KORA Augsburg Study 1984–2002," *Diabetic Medicine*, vol. 27, no. 9, pp. 1004–1011, 2010.
- [18] P. Welsh, H. M. Murray, B. M. Buckley et al., "Leptin predicts diabetes but not cardiovascular disease: results from a large prospective study in an elderly population," *Diabetes Care*, vol. 32, no. 2, pp. 308–310, 2009.
- [19] S. Söderberg, P. Zimmet, J. Tuomilehto et al., "Leptin predicts the development of diabetes in Mauritian men, but not women: a population-based study," *International Journal of Obesity*, vol. 31, no. 7, pp. 1126–1133, 2007.
- [20] M. Kouvari, C. Boutari, C. Chrysohoou et al., "Mediterranean diet is inversely associated with steatosis and fibrosis and decreases ten-year diabetes and cardiovascular risk in NAFLD subjects: results from the ATTICA prospective cohort study," *Clinical Nutrition*, vol. 40, no. 5, pp. 3314–3324, 2021.
- [21] M. Peller, A. Kapłon-Cieślicka, M. Rosiak et al., "Are adipokines associated with atrial fibrillation in type 2 diabetes," *Endokrynologia Polska*, vol. 71, no. 1, pp. 34–41, 2020.
- [22] A. Khan, T. Ghaffar, A. Kainat, M. Arabdin, and S. U. Rehman Orakzai, "Correlation between serum leptin level and body mass index (BMI) in patients with type 2 diabetes mellitus," *The Journal of the Pakistan Medical Association*, vol. 70, no. 1, pp. 3–6, 2020.
- [23] K. Rehman, M. Akash, and Z. Alina, "Leptin: a new therapeutic target for treatment of diabetes mellitus," *Journal of Cellular Biochemistry*, vol. 119, no. 7, pp. 5016–5027, 2018.
- [24] M. Romanowski, V. Dziedziejko, A. Maciejewska-Karlowska et al., "Adiponectin and leptin gene polymorphisms in patients with post-transplant diabetes mellitus," *Pharmacogenomics*, vol. 16, no. 11, pp. 1243–1252, 2015.
- [25] S. Cernea, A. L. Roiban, E. Both, and A. Huțanu, "Serum leptin and leptin resistance correlations with NAFLD in patients with type 2 diabetes," *Diabetes/Metabolism Research and Reviews*, vol. 34, no. 8, article e3050, 2018.
- [26] A. P. Delitala, F. A. Sanciu, A. Errigo, G. Delitala, and G. M. Pes, "Leptin levels and insulin dependence in latent autoimmune diabetes in adults," *Journal of Interferon & Cytokine Research*, vol. 37, no. 12, pp. 550–556, 2017.
- [27] I. Dedinská, N. Máčková, D. Kantárová et al., "Leptin - a new marker for development of post-transplant diabetes mellitus?," *Journal of Diabetes and its Complications*, vol. 32, no. 9, pp. 863–869, 2018.

- [28] C. R. Ahuja, A. P. Kolte, R. A. Kolte, M. Gupta, and S. Chari, "Effect of non-surgical periodontal treatment on gingival crevicular fluid and serum leptin levels in periodontally healthy chronic periodontitis and chronic periodontitis patients with type 2 diabetes mellitus," *Journal of Investigative and Clinical Dentistry*, vol. 10, no. 3, article e12420, 2019.
- [29] S. Sans, T. Padró, J. Tuomilehto, and L. Badimon, "Incidence of diabetes and serum adipokines in Catalonian men The ADI-POCAT study," *Annals of Medicine*, vol. 45, no. 1, pp. 97–102, 2013.

Research Article

Effect of Ultrasonic Osteotome on Therapeutic Efficacy and Safety of Spinal Surgery: A System Review and Meta-Analysis

Leilei Wu  and Sheng Wang 

Spine Surgery, Affiliated Hospital of Weifang Medical University, 261031, China

Correspondence should be addressed to Sheng Wang; zbspy@163.com

Received 18 July 2022; Revised 4 August 2022; Accepted 8 August 2022; Published 29 August 2022

Academic Editor: Sujatha Krishnamoorthy

Copyright © 2022 Leilei Wu and Sheng Wang. This is an open access article distributed under the Creative Commons Attribution License, which permits unrestricted use, distribution, and reproduction in any medium, provided the original work is properly cited.

Background. A meta-analysis was performed to evaluate the effectiveness and safety of ultrasonic osteotomes in spine surgery to standard spinal surgery procedures. **Methods.** Using the search keywords “bone curette”, “cutter”, “scalpel”, “bone shaver”, “aspirator”, “osteotome”, “ultrasonic”, “piezosurgery”, and “dent **” in the databases of PubMed (1966-2021.12), Cochrane Library, Embase (1986-2018.12), Web of Science (1978-2021.12), and China Academic Journals Full-Text Database (CNKI, 1979-2021.12). Two researchers reviewed the literature, extracted and extensively assessed the data, and included information on the study quality. RevMan v5.3.5.0 was used for the meta-analysis. **Results.** A total of 10 trials with a total of 911 patients were included. The meta-analysis findings revealed that, when compared to traditional methods, ultrasonic osteotomes could save operation time (OR = -18.83, 95 percent CI (-22.76, -14.99), $P = 0.03$) and reduce intraoperative bleeding (OR = -66.73, 95 percent CI (-75.70, -57.76), $P = 0.04$) and postoperative complications (OR = 0.38, 95 percent CI (0.21, 0.69), $P = 0.001$). There was, however, no significant difference in the hospital stay (OR = -1.34, 95 percent CI (-1.90, -0.77), $P = 0.23$) and symptom improvement rate (OR = 1.03, 95 percent CI (0.73, 1.45), $P = 0.86$). **Conclusion.** There is evidence that using an ultrasonic osteotome in spine surgery is safe and effective and may minimize intraoperative bleeding and save time. However, there is no significant difference in symptom improvement rate, hospital stay length, or postoperative complications compared to standard surgical equipment. Therefore, more high-quality investigations are needed to corroborate the initial results.

1. Introduction

As the human body's second lifeline, the spine is responsible for the central axis bone and nerve conduction of the human trunk and surrounding intricate nerves and blood vessels [1]. Its clinical operation is highly complex and risky, with high demands for preoperative, midoperative, and postoperative image confirmation, surgical equipment, operator experience, and operation technology. Spinal surgery technology has advanced fast due to the advancement of surgical equipment [2]. Although high-speed drills (HSDs), osteotomes, laminectomy forceps, nucleus pulposus forceps, and other traditional surgical instruments in spinal surgery are widely used in intraoperative decompression and osteotomy [3], studies have shown that they can cause intraoperative nerve, blood vessel, spinal cord, dura mater, and other injuries. On the other hand, traditional spinal surgery relies

on physicians' clinical knowledge and intraoperative scanning pictures. It thus has several drawbacks, such as substantial trauma and long postoperative recovery [4].

Piezosurgery is a bone surgery equipment that works on the basis of high-intensity focused ultrasound (cavitation effect, thermal effect, and mechanical effect) [5]. The transducer in the knife converts electrical energy into mechanical energy by using high-intensity focused ultrasound technology [6]. After a high-frequency ultrasonic vibration, the water in the contacting tissue cells evaporates and the protein hydrogen bond is destroyed, fully damaging the bone tissue to be cut during the surgery [7]. The ultrasonic cutter head operates at a temperature of less than 38°C and a propagation distance of less than 200 microns [8]. Because high-intensity focused ultrasound can only destroy bone tissue of a certain hardness, it does not harm blood vessels or nerve tissue while also stopping bleeding at the surgical wound,

reducing the impairment of minimally invasive surgery, and significantly improving accuracy, reliability, and safety. It is currently widely used in oral and maxillofacial surgery. Hidaka employed UBC in a cervical double-door laminoplasty for the first time in 1998, indicating that it may reduce the risk of intraoperative nerve and dural injury. Since then, UBC has piqued the interest of a growing number of spine surgeons [9].

In recent years, there has been an increase in the number of reports on the use of UBC in spine surgery. However, because of the small number of cases and lack of data, there is still no consensus on UBC's effectiveness and safety [10]. As a consequence, this study collected relevant literature comparing the effectiveness and safety of UBC and traditional tools in spinal surgery in the United States and overseas for meta-analysis in order to provide evidence-based medical data supporting the use of UBC in spinal surgery.

2. Materials and Methods

2.1. Search Strategy. Search the databases of PubMed (1966-2021.12), Cochrane Library, Embase (1986-2018.12), Web of Science (1978-2021.12), China Academic Journals Full-Text Database (CNKI, 1979-2021.12), Wanfang Database (1998-2021.12), and Google Scholar (1989-2021.12), among other databases. "Bone curette", "cutter", "scalpel", "bone shaver", "aspirator", "osteotome", "ultrasonic", "piezosurgery", and "dent **" are the English search phrases. All databases have a retrieval period that runs from the moment the database was established until December 30, 2021. In addition, additional references were manually obtained in order to incorporate all of the literature.

2.2. Inclusion and Exclusion Criteria. The inclusion criteria are as follows. (1) The research was intended as a controlled clinical trial of UBC in spinal surgery, involving a randomized controlled study, a cohort study, and a case-control study. (2) The participants included patients having spinal surgery for conditions such as cervical spondylosis, ossification of the thoracic ligamentum flavum, lumbar disc herniation, and lumbar spinal stenosis; spinal trauma; spinal infection; spinal tumor; and spinal deformity; and so on. (3) The experimental group employed UBC to decompress and osteotomize the bone tissue and calcified tissue, whereas the control group used standard surgical tools such as HSD, bone biting forceps, and bone knife. (4) Outcome variables included operation duration, intraoperative bleeding, hospital stay, postoperative neurological improvement, and safety indicators, as well as postoperative sequelae. The criteria for exclusion are as follows: (1) research with less than five examples; (2) overviews, conference papers, and expert opinions; (3) non-English literature; and (4) documents unable to extract data and so on.

2.3. Study Selection and Data Extraction. According to the PRISMA flow chart, the first and second authors will undertake screening, literature quality review, and data extraction based on the inclusion and exclusion criteria before conducting the cross inspection. In the event of a dispute, they

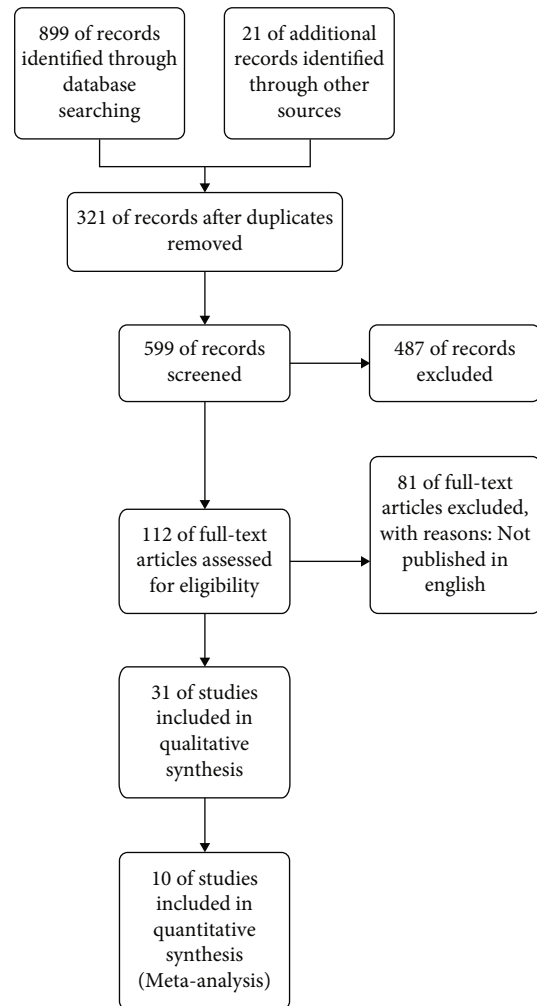


FIGURE 1: Document screening process.

will be sent to third-party arbitration, with the appropriate author appointed as the third-party arbiter. During the screening process, the authors first use the literature management software to import the title, eliminate the repetition, and then browse the label to exclude the literature not related to this study. If the information contained in the title is insufficient to exclude, the method of reading the abstract and full text shall be used to determine whether it can be included. If necessary, the authors attempt to contact the original research author through email or phone to collect data information that has not yet been identified but is critical for this investigation. A predesigned data extraction form is used for recording. The specific components are as follows: (1) the title of the article included in the study, the original author, the publication date, and the magazine in which it was published; (2) subject baseline characteristics and intervention measures for the experimental and control groups: sample size, gender, age, disease course, classification, intervention technique, length of treatment, withdrawal, follow-up, and so on; (3) relevant aspects of bias risk assessment: adherence to the randomization principle, blindness, dispersion and concealment, and so on; and (4) measurements of outcome, including main and

TABLE 1: Literature features included in the study.

| Author (year) | Participants | Outcomes |
|-------------------|--------------|---|
| Williams BJ, 2011 | 78 | Provided general benchmarks of durotomy rates and served as a basis for ongoing efforts to improve safety of care. |
| Street JT, 2012 | 942 | Identified a very high rate of previously unrecognized postoperative complications, which adversely affect LOS. Without strict adherence to a prospective data collection system, the true complexity of this surgery may be greatly underestimated. |
| Onen MR, 2015 | 46 | For patients with CSM, laminectomy using the UBS provides a safe, rapid, and effective decompression with lesser blood loss. The low rate of complications lessens the postoperative morbidity rates and shortens hospital stay. |
| Bydon M, 2014 | 30 | Decreased incidence in intraoperative durotomy and overall perioperative complication rates in the BoneScalpel cohort, although this did not reach the level of statistical significance. Nonetheless, the data demonstrate that the BoneScalpel is a safe and efficacious alternative to the high-speed drill in these challenging patients. |
| Bartley CE, 2014 | 20 | The use of an ultrasonic bone scalpel to perform the bone cuts associated with facetectomies and apical Ponte-type posterior releases resulted in significantly less bleeding compared with cuts made with standard osteotomes and rongeurs, limiting overall blood loss by 30% to 40%. |
| Bydon M, 2013 | 337 | The safety and efficacy of ultrasonic bone curettes in spine surgery has not been well established. This study shows that the ultrasonic bone curette has a similar safety profile compared with the high-speed drill, although both are capable of causing iatrogenic dural tears during spine surgery. |
| Matsuoka H, 2012 | 33 | The ultrasonic bone curette is a useful instrument for recapping hemilaminoplasty in various spinal surgeries. This method allows anatomical reconstruction of the excised bone to preserve the posterior surrounding tissues. |
| Hazer DB, 2016 | 307 | We recommend this device as an assistant tool in various spine surgeries and as a primary tool in foraminotomies. It is a safe device in spine surgery with very low complication rate. |
| Hu X, 2013 | 128 | Overall, the ultrasonic scalpel was safe and performed as desired when used as a bone cutting device to facilitate osteotomies in a variety of spine surgeries. However, caution should be taken to avoid potential thermal injury and dural tear. |
| Ito K, 2009 | 12 | The scalpel-type ultrasonic bone curette is useful for cutting bone and effective for the reconstruction of the laminae. Laminotomy with an ultrasonic bone curette is safe and minimally invasive. |

secondary: incision time, bleeding volume, postoperative JOA, complications, and so forth.

2.4. Bias Risk Assessment. The risk of bias was assessed and cross-checked by the first and second authors using the inclusion and exclusion criteria. Any issue must be resolved via arbitration with a third party. The risk of bias in RCT studies was assessed using the Cochrane Library's suggested technique, while the risk of bias in cohort studies was assessed using the NOS grading scale.

2.5. Statistical Analysis. The data in the study were meta-analyzed using RevMan software v5.3.5.0. If the information is of the counting type, the combined statistics are relative risk (RR) or odds ratio (OR); if it is of the continuous variable type, the weighted mean difference (WMD) is used for meta-analysis, and the 95 percent confidence interval (CI) is presented. In addition, use 2. Perform a heterogeneity test. If $P > 0.10$ and $I^2 > 50$, analyze heterogeneity using the fixed effect model, followed by a source of heterogeneity analysis and subgroup analysis depending on the causes for heterogeneity. If the heterogeneity cannot be decreased or the I^2 is more than 50, the random effect model is employed to analyze the data. Furthermore, if the heterogeneity is too great and lacks analytical significance, a descriptive analysis will be performed. Set the significance criterion for meta-

analysis to = 0.05. When the number of the included pieces of literature surpassed 10, an inverted funnel diagram was used to analyze the publication bias of the included research.

3. Results

3.1. Research Characteristics. In all, 920 pieces of relevant literature were gathered. Following the screening, ten studies with a total of 911 participants were chosen, including five randomized controlled trials and five cohort studies. The document screening method is shown in Figure 1. Table 1 summarizes the key elements of the included investigation.

3.2. Data Quality Assessment. The bias risk assessment found that the one randomized controlled trial had significant levels of selection bias, implementation bias, and measurement bias, as well as poor overall quality. One of the five cohort studies assessed received a NOS score of 6, two received a score of 7, and two received a score of 8. The overall quality of the cohort research was outstanding (Figure 2).

3.3. Operation Time of Patients. The operation time was recorded in ten trials. The heterogeneity test findings were $P < 0.00001$ and $I^2 = 51\%$. The random effect model was used for meta-analysis. As shown in Figure 3, the findings revealed that the mean operating time (min) of the UBC

| | Random sequence generation (Selection bias) | Allocation concealment (Selection bias) | Blinding of participants and personnel (Performance bias) | Blinding of outcome assessment (Detection bias) | Incomplete outcome data (Attrition bias) | Selective reporting (Reporting bias) | Other bias |
|-------------------|---|---|---|---|--|--------------------------------------|------------|
| Bartley CE, 2014 | + | + | + | + | + | | + |
| Bydon M, 2013 | + | | + | + | + | + | + |
| Hazer DB, 2016 | + | + | + | | + | + | + |
| Hu X, 2013 | + | + | + | + | + | + | + |
| Ito K, 2009 | + | + | ⊖ | + | + | | + |
| Mantovani E, 2014 | + | + | + | + | + | + | |
| Matsuoka H, 2012 | + | + | | + | + | + | + |
| Onen MR, 2015 | + | | + | + | + | + | + |
| Street JT, 2012 | + | + | + | + | ⊖ | + | + |
| Williams BJ, 2011 | ⊖ | + | + | + | | + | + |

FIGURE 2: Document quality evaluation.

group was shorter than that of the traditional surgical method group, and the difference was statistically significant (OR = -18.83, 95 percent CI (-22.76, -14.99), $P = 0.03$).

3.4. Intraoperative Bleeding in Patients. Five research reported on the quantity of intraoperative bleeding. The heterogeneity test findings were $P < 0.00001$ and $I^2 = 59\%$. The random effect model was used for meta-analysis. As demonstrated in Figure 4, the quantity of intraoperative bleeding in the UBC group was smaller than that in the traditional surgical method group, and the difference was statistically significant (OR = -66.73, 95 percent CI (-75.70, -57.76), $P = 0.04$).

3.5. Hospitalization Time of Patients. The duration of hospital stay was reported in six trials. The heterogeneity test findings were $P < 0.00001$ and $I^2 = 27\%$. The random effect model was used for meta-analysis. As indicated in Figure 5, there was no significant difference in the duration of hospital stay between the UBC group and the traditional surgical method group (OR = -1.34, 95 percent CI (-1.90, -0.77), $P = 0.23$).

3.6. Postoperative Symptom Improvement Rate. Eight studies found that less of the postoperative symptoms improved. The heterogeneity test findings were $P = 1.00$ and $I^2 = 0\%$. For meta-analysis, the fixed effect model was utilized. As demonstrated in Figure 6, there was no significant difference in the rate of improvement of postoperative symptoms between the UBC group and the traditional instrument group (OR = 1.03, 95 percent CI (0.73, 1.45), $P = 0.86$).

3.7. Postoperative Complications. A total of ten studies compared patients' postoperative problems. The heterogeneity test findings were $P = 0.97$ and $I^2 = 0\%$. For meta-analysis, the fixed effect model was utilized. As demonstrated in Figure 7, there was a significant difference in the incidence of postoperative problems between the UBC group and the conventional instrument group (OR = 0.38, 95 percent CI (0.21, 0.69), $P = 0.001$).

3.8. Publication Bias. A funnel chart was used to explore publication bias. In comparing the postoperative complications of patients in the UBC group and the traditional instrument group, there was no obvious asymmetry in the funnel chart, suggesting no obvious publication bias, as shown in Figure 8.

4. Discussion

Spinal disorders have risen steadily in recent years [10]. However, due to severe fatigue, the cervical and lumbar segments often produce hypertrophy and ossification of the posterior longitudinal ligament and ligamentum flavum [11]. Conventional spinal surgery, such as laminoplasty, uses the "bowstring effect" formed by the spine's physiological lordosis and kyphosis to contact the pressor of the spinal cord or open the space behind the spinal cord to keep the spinal cord from compression and achieve the effect of decompression [12]. Traditional resection primarily employs LP and HSD [13]. Although they have excellent benefits when used correctly, the average vertebral incision duration and the frequency of associated problems are considerable [14]. They have a more precise cutting ability, and the heat energy created by friction with bone tissue during osteotomy may cause hemostasis. Still, the accumulated heat is difficult to grasp, and a too-high temperature can burn the osteotomy's perimeter [15]. Hence, drip cooling is often employed in clinical settings, although studies demonstrate that it cannot diminish the heat effect created by friction. Finally, a response force is made on the handle during the high-speed rotation of the drill bit. Slippage and catastrophic accidents are easily caused by improper operation [16].

The introduction of UBS as a novel osteotomy dynamic system gives spine surgeons a new option. It may selectively cut tissue based on density and elasticity using the rupture and cavitation effects to prevent unintended harm [17]. According to Sanborn et al., the bleeding volume of UBS is smaller than that of LP. UBS is also more secure and dependable than HSD. It has two modes: "regular" and "cold cutting." The former is suitable for separating soft tissue and bone cortex, has a greater temperature, and may halt

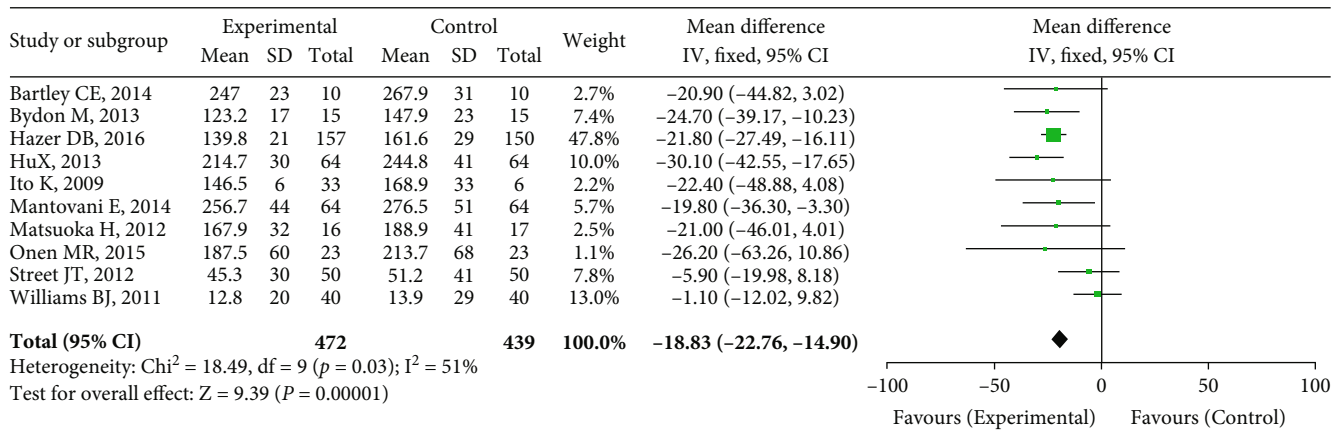


FIGURE 3: Operation time comparison.

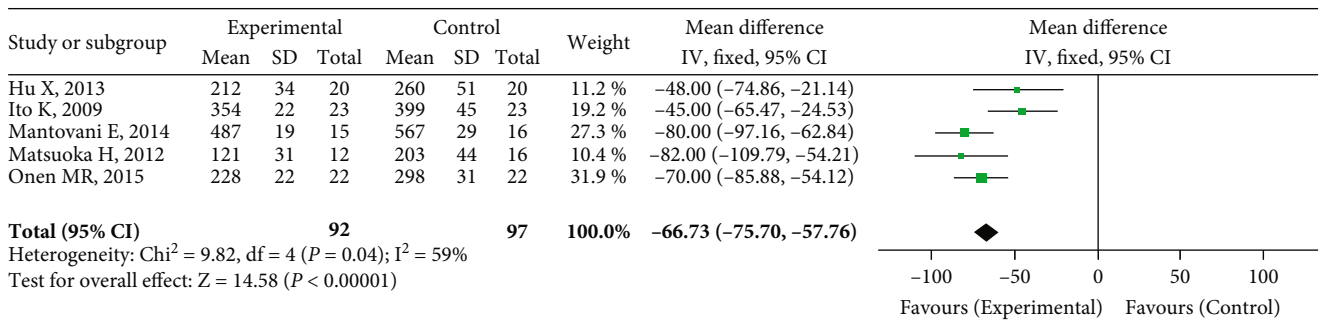


FIGURE 4: Intraoperative bleeding comparison.

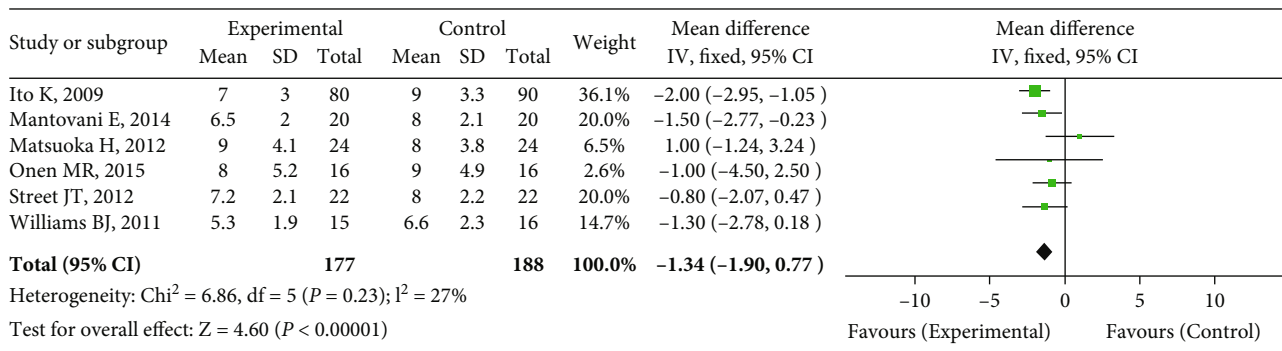


FIGURE 5: Hospitalization time comparison.

bleeding; the latter is very safe when used near the dura mater and spinal cord [18].

Furthermore, rotating the cutting section of UBS on a frequent basis, lengthening the residence time at the same place by 10s, and improving local perfusion may reduce the temperature of the cutting interface, preventing thermal injury [19]. The ability of UBC to minimize operating time has long been a subject of contention among spine surgeons. Some specialists believe that when removing a significant amount of bone or calcification, UBC is less efficient than standard instruments (such as HSD and lamina rongeur) and that the learning curve for UBC is longer. As a conse-

quence, UBC requires more time to operate than ordinary instruments. Most studies now believe that UBC may significantly reduce intraoperative bleeding when compared to typical surgical equipment [20].

However, according to a research published in 2014 by Byron, which evaluated the efficacy of UBC and HSD in decompression surgery in individuals with achondroplasia, there is no significant difference in hospital stay between the UBC and HSD groups [21]. Our research is partly in line with the results of this experiment, but there are also differences. According to the findings of this meta-analysis, there was no significant difference in hospital stay between UBC

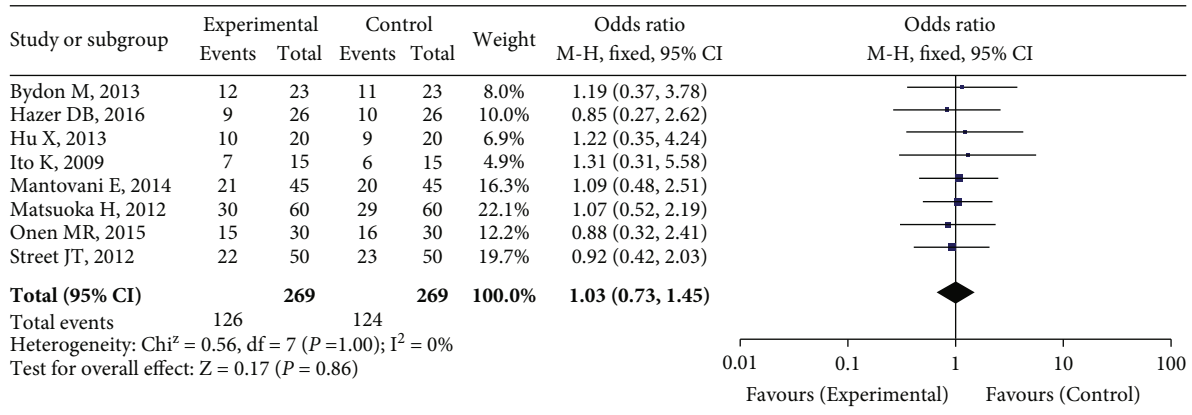


FIGURE 6: Postoperative symptom improvement comparison.

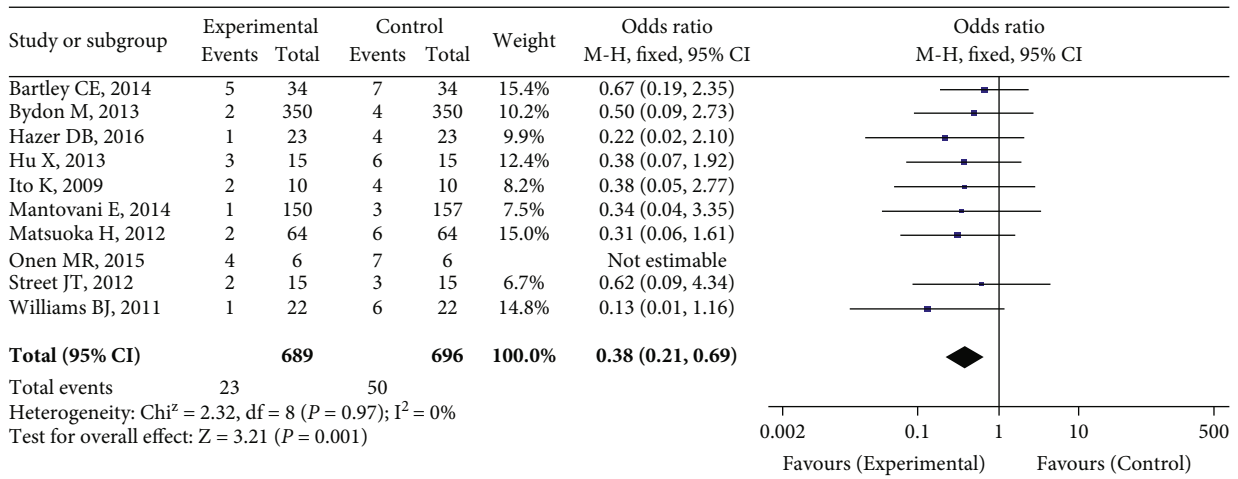


FIGURE 7: Postoperative complication comparison.

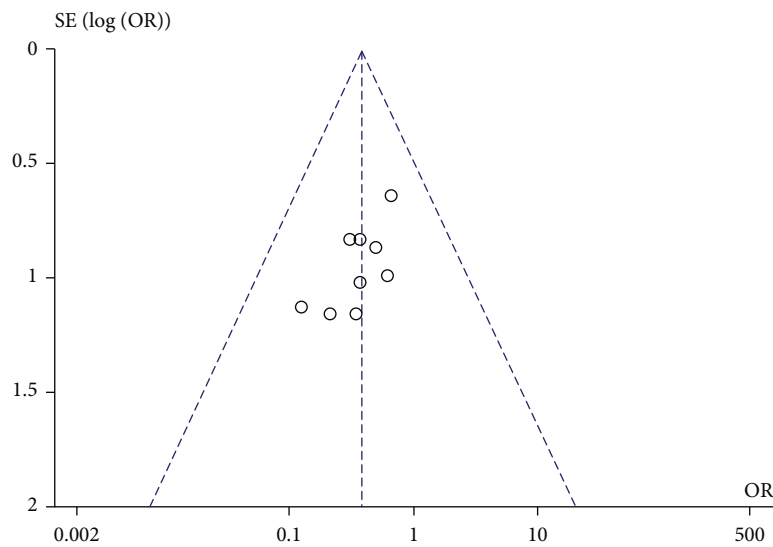


FIGURE 8: Publication bias comparison.

and conventional equipment [22]. We feel the following causes are possible. (1) The illness diagnosis of the included individuals varies and is diverse. (2) The baseline levels of patients included in relevant research vary. Most studies employ UBC in patients who have a protracted decompression or osteotomy stage, severe spinal cord compression, and a significant risk of vascular and nerve damage. (3) Each research has a modest sample size [23]. In terms of symptom improvement, two studies in this meta-analysis found no difference between the UBC group and the conventional device group. Eight research studies found that patients' symptoms in the UBC group improved considerably. We feel the following causes are possible: (1) the assessment criteria for symptom improvement in various research varied, (2) the follow-up duration was brief, and (3) the sample size is insufficient.

Bagga et al. believe that the problems in the UBC group are lower than those in the conventional instrument group based on noncontrolled trials [24]. They think this is due to UBC's selective bone cutting and slight injury to peripheral blood vessels and nerve tissue. According to this meta-analysis [25], the incidence of UBC-related complications during spinal surgery was 5.88 percent (12/204), with dural rupture being the most prevalent, accounting for 4.90 percent (10/204). According to the numerous studies, the primary causes of a dural tear include dural ossification or extreme compression, inability to absorb vibration, UBC absorption, involvement, high force, or thermal damage induced by long-term residence [26]. According to the findings of this meta-analysis, there was a statistically significant difference in the incidence of postoperative complications between UBC and conventional tools [27]. We feel the following causes are possible: (1) various physicians' competency in UBC, (2) differences in UBC of different brands, and (3) integrity and validity of medical records.

5. Limitations

The study's shortcomings are as follows. (1) There are few high-quality clinical control study papers among the 10 included studies, which include publication bias and selection bias. (2) The research solely includes 911 occurrences. However, there is a substantial gap between patients and the massive sample size and multicenter data required for statistical analysis of evidence-based treatment. (3) There are differences in the ages and diagnoses of the people included in the study, as well as variability throughout the study. (4) It is difficult to identify the details of each research execution, such as whether other traditional instruments (such as curettes) are used in combination with UBC, how skilled doctors are, and how authentic and comprehensive medical records are. As a consequence, it is hard to thoroughly examine UBC's effectiveness and safety and the meta-result analysis should be considered seriously.

6. Conclusion

In conclusion, based on the existing clinical data, using an ultrasonic osteotome in spine surgery is safe and prosperous, reducing intraoperative bleeding and shortening the opera-

tion time. However, it offers no clear benefits over standard equipment in easing patients' symptoms, shortening hospital stays, and lowering surgical complications. However, because of the low quantity and quality of the included research, the results mentioned above must be supported by more high-quality investigations.

Data Availability

The datasets used during the current study are available from the corresponding author on request.

Conflicts of Interest

All the researchers claim no conflicts of interests.

References

- [1] Y. Liao, R. Ye, Q. Tang et al., "Application of ultrasonic osteotome in the posterior lumbar interbody fusion surgery by unilateral fenestration and bilateral decompression in the treatment of degenerative lumbar spinal stenosis," *Zhongguo Xiu Fu Chong Jian Wai Ke Za Zhi*, vol. 33, no. 4, pp. 416–422, 2019.
- [2] Z. Lang, Q. Wang, X. Wu et al., "Drilling speed and bone temperature of a robot-assisted ultrasonic osteotome applied to vertebral cancellous bone," *Spine (Phila Pa 1976)*, vol. 46, pp. E760–E768, 2020.
- [3] J. Zhu, D. Hao, Y. Guo, X. Zhang, W. Gao, and X. Wang, "Safety and effectiveness of ultrasonic osteotome in posterior cervical laminectomy decompression and fusion," *Zhongguo Xiu Fu Chong Jian Wai Ke Za Zhi*, vol. 32, no. 12, pp. 1554–1559, 2018.
- [4] Z. Z. Li, Z. Cao, H. L. Zhao, W. L. Shang, and S. X. Hou, "Ultrasonic osteotome assisted full-endoscopic en block resection of thoracic ossified ligamentum flavum: technical note and 2 years follow-up," *Pain Physician*, vol. 24, no. 2, p. E239–239E248, 2021.
- [5] S. S. Sadrameli, T. M. Chan, J. J. Lee, V. R. Desai, and P. J. Holman, "Resection of spinal meningioma using ultrasonic Bone-Scalpel microshaver: cases, technique, and review of the literature," *Oper Neurosurg (Hagerstown)*, vol. 19, no. 6, pp. 715–720, 2020.
- [6] M. R. Sanborn, J. Balzer, P. C. Gerszten, P. Karausky, B. C. Cheng, and W. C. Welch, "Safety and efficacy of a novel ultrasonic osteotome device in an ovine model," *Journal of Clinical Neuroscience*, vol. 18, no. 11, pp. 1528–1533, 2011.
- [7] A. Krishnan, P. Samal, S. Mayi, S. Degulmadi, R. R. Rai, and B. Dave, "Thoracic spine stenosis: does ultrasonic osteotome improve outcome in comparison to conventional technique," *Malays Orthop J*, vol. 15, no. 2, pp. 62–69, 2021.
- [8] J. S. Yang, H. L. Gong, H. Chen et al., "Full-endoscopic decompression with the application of an endoscopic-matched ultrasonic osteotome for removal of ossification of the thoracic ligamentum flavum," *Pain Physician*, vol. 24, no. 3, pp. 275–281, 2021.
- [9] R. Gilles, T. Couvreur, and S. Dammous, "Ultrasonic orthognathic surgery: enhancements to established osteotomies," *International Journal of Oral and Maxillofacial Surgery*, vol. 42, no. 8, pp. 981–987, 2013.

- [10] X. Cheng, F. He, M. Si, P. Sun, and Q. Chen, "Effects of antibiotic use on saliva antibody content and oral microbiota in Sprague Dawley rats," *Frontiers in Cellular and Infection Microbiology*, vol. 12, 2022.
- [11] X. Cheng, X. Guo, F. Huang, H. Lei, Q. Zhou, and C. Song, "Effect of different sweeteners on the oral microbiota and immune system of Sprague Dawley rats," *AMB Express*, vol. 11, no. 1, pp. 1–9, 2021.
- [12] S. L. Parker, R. M. Kretzer, P. F. Recinos et al., "Ultrasonic BoneScalpel for osteoplastic laminoplasty in the resection of intradural spinal pathology," *Neurosurgery*, vol. 73, p. ons61, 2013.
- [13] B. J. Williams, C. A. Sansur, J. S. Smith et al., "Incidence of unintended durotomy in spine surgery based on 108, 478 cases," *Neurosurgery*, vol. 68, no. 1, pp. 117–124, 2011.
- [14] J. T. Street, B. J. Lenehan, C. P. DiPaola et al., "Morbidity and mortality of major adult spinal surgery. A prospective cohort analysis of 942 consecutive patients," *The Spine Journal*, vol. 12, no. 1, pp. 22–34, 2012.
- [15] M. R. Onen, E. Yuvruk, S. Akay, and S. Naderi, "The reliability of the ultrasonic bone scalpel in cervical spondylotic myelopathy: a comparative study of 46 patients," *World Neurosurgery*, vol. 84, no. 6, pp. 1962–1967, 2015.
- [16] M. Bydon, M. Macki, R. Xu, M. C. Ain, E. S. Ahn, and G. I. Jallo, "Spinal decompression in achondroplastic patients using high-speed drill versus ultrasonic bone curette: technical note and outcomes in 30 cases," *Journal of Pediatric Orthopedics*, vol. 34, no. 8, pp. 780–786, 2014.
- [17] C. E. Bartley, T. P. Bastrom, and P. O. Newton, "Blood loss reduction during surgical correction of adolescent idiopathic scoliosis utilizing an ultrasonic bone scalpel," *Spine Deform*, vol. 2, no. 4, pp. 285–290, 2014.
- [18] M. Bydon, R. Xu, K. Papademetriou et al., "Safety of spinal decompression using an ultrasonic bone curette compared with a high-speed drill: outcomes in 337 patients," *Journal of Neurosurgery. Spine*, vol. 18, no. 6, pp. 627–633, 2013.
- [19] H. Matsuoka, Y. Itoh, S. Numazawa et al., "Recapping hemilaminoplasty for spinal surgical disorders using ultrasonic bone curette," *Surgical Neurology International*, vol. 3, no. 1, p. 70, 2012.
- [20] D. B. Hazer, B. Yaşar, H. E. Rosberg, and A. Akbaş, "Technical aspects on the use of ultrasonic bone shaver in spine surgery: experience in 307 patients," *BioMed Research International*, vol. 2016, 8428538 pages, 2016.
- [21] X. Hu, D. D. Ohnmeiss, and I. H. Lieberman, "Use of an ultrasonic osteotome device in spine surgery: experience from the first 128 patients," *European Spine Journal*, vol. 22, no. 12, pp. 2845–2849, 2013.
- [22] K. Ito, S. Ishizaka, T. Sasaki et al., "Safe and minimally invasive laminoplastic laminotomy using an ultrasonic bone curette for spinal surgery: technical note," *Surgical Neurology*, vol. 72, no. 5, pp. 470–475, 2009, discussion 475.
- [23] B. Fiani, A. Newhouse, A. Cathel, R. Houston, and O. Hariri, "Subaxial cervical laminectomy using a Misonix BoneScalpel®: a guide to operative technique," *Surgical Technology International*, vol. 37, pp. 421–426, 2020.
- [24] R. S. Bagga, A. P. Shetty, V. K. Viswanathan, G. J. Reddy, R. M. Kanna, and S. Rajasekaran, "Thoracic myelopathy in ossified ligamentum flavum: surgical management and long-term outcome following 2 different techniques of surgical decompression," *The Spine Journal*, p. 219256822110030, 2021.
- [25] S. Garg, J. Thomas, H. Darland et al., "Ultrasonic bone scalpel (USBS) does not reduce blood loss during posterior spinal fusion (PSF) in patients with adolescent idiopathic scoliosis (AIS)," *Spine (Phila Pa 1976)*, vol. 46, pp. 845–851, 2021.
- [26] C. H. Kim, C. K. Chung, Y. Choi et al., "The efficacy of ultrasonic bone scalpel for unilateral cervical open-door laminoplasty: a randomized controlled trial," *Neurosurgery*, vol. 86, no. 6, pp. 825–834, 2020.
- [27] M. Kakiuchi, "Repair of the defect in spondylolysis. Durable fixation with pedicle screws and laminar hooks," *The Journal of Bone and Joint Surgery. American Volume*, vol. 79, no. 6, pp. 818–825, 1997.

Research Article

A Rule-Based Inference Framework to Explore and Explain the Biological Related Mechanisms of Potential Drug-Drug Interactions

Adeeb Noor ¹ and Abdullah Assiri ²

¹Department of Information Technology, Faculty of Computing and Information Technology, King Abdulaziz University, Jeddah 80221, Saudi Arabia

²Department of Clinical Pharmacy, College of Pharmacy, King Khalid University, Abha 62529, Saudi Arabia

Correspondence should be addressed to Abdullah Assiri; aalabdullah@kku.edu.sa

Received 6 July 2022; Revised 24 July 2022; Accepted 28 July 2022; Published 17 August 2022

Academic Editor: Sujatha Krishnamoorthy

Copyright © 2022 Adeeb Noor and Abdullah Assiri. This is an open access article distributed under the Creative Commons Attribution License, which permits unrestricted use, distribution, and reproduction in any medium, provided the original work is properly cited.

As more drugs are developed and the incidence of polypharmacy increases, it is becoming critically important to anticipate potential DDIs before they occur in the clinic, along with those for which effects might go unobserved. However, traditional methods for DDI identification are unable to coalesce interaction mechanisms out of vast lists of potential or known DDIs, much less study them accurately. Computational methods have great promise but have realized only limited clinical utility. This work develops a rule-based inference framework to predict DDI mechanisms and support determination of their clinical relevance. Given a drug pair, our framework interrogates and describes DDI mechanisms based on a knowledge graph that integrates extensive available biomedical resources through semantic web technologies and backward chaining inference, effectively identifying facts within the graph that prove and explain the mechanisms of the drugs' interaction. The framework was evaluated through a case study combining a chemotherapy agent, irinotecan, and a widely used antibiotic, levofloxacin. The mutual interactions identified indicate that our framework can effectively explore and explain the mechanisms of potential DDIs. This approach has the potential to improve drug discovery and design and to support rapid and cost-effective identification of DDIs along with their putative mechanisms, a key step in determining clinical relevance and supporting clinical decision-making.

1. Introduction

Drug-drug interactions (DDIs) can result in debilitating illness and sometimes death and so represent serious concerns for pharmaceutical companies, clinicians, and patients worldwide. Indeed, in the US, DDIs were recently found to be responsible for 231,000 emergency room visits [1] and 22.2% of hospital admissions [2]. These numbers illustrate the potential exponential growth of health risks that could occur due to polypharmacy [3], itself a rising concern given the high prevalence of chronic diseases, psychological disorders such as depression, and other such conditions. Interactions such as toxicity or reduced efficacy may occur when two or more agents are coadministered, necessitating dose

adjustment or switching to a different therapeutic intervention. While we may prevent additional DDIs by contraindicating drug pairs for which adverse events have been observed in clinic, it remains necessary to develop new methods to improve our understanding of known, unobserved, and potential DDIs [4].

In terms of mechanism, DDIs can be pharmacokinetic (interactions either enhance or reduce effects), pharmacodynamic (interactions occur at or close to the site of action), or both [5]. The mechanisms of most known DDIs were traditionally discovered through single-pathway studies. Examples of traditional discovery approaches include laboratory and animal model studies, as illustrated by the drug interaction guidance document published by the FDA. While this

guidance document has enabled researchers and pharmaceutical companies to gain understanding of DDIs, it has some major shortcomings [6]. First, its main limitation is that it focuses mostly on the interactions of cytochrome enzymes (CYPs), ignoring other potential mechanisms. Second, current DDI study requirements are applied during clinical trials; thus, the drugs are often tested in small numbers of patients and in the absence of many possible confounding factors [7]. As such, the slowness and limited focus of traditional approaches for discovering new and potential interactions means that the problems posed by DDIs will undoubtedly continue.

To address this issue in a cost-effective and high-throughput manner by leveraging machine learning, we proposed a rule-based inference framework to explore and explain the biological related mechanisms of potential DDI mechanisms [8]. First, we designed an extract, transform, load (ETL) method utilizing semantic web technologies to bring together extensive biomedical data, information, and knowledge from diverse resources and integrate it all into a mechanistic knowledge graph. Second, we developed a backward chaining inference rule-based framework to recognize pharmacological and other related mechanistic effects from that graph, applying a set of rules to effectively identify facts that prove and explain the mechanisms of interaction. Finally, we conducted evaluation and validation of the framework using the antineoplastic chemotherapy agent irinotecan and the quinolone antibiotic levofloxacin, whose pharmacokinetics profiles are well-documented.

2. Literature Review

Computational methods for predicting DDIs constitute an area of considerable research interest, leading to the development of diverse methods and published resources. These methods have employed a variety of algorithms and utilized many features such as biological effect interactions [9], protein similarities [10], clinical and genomic factors [11], and drug-target [12] and drug-protein [13], as well as drug information on web [14, 15], text-based data [14], protein interaction networks [16], mechanisms of toxicity [17], and enrichment analysis [18]. Among the diverse computational methods that have been used in DDI research, rule-based systems have shown especially promising results [19]. Fundamentally, these systems simulate a human expert's decision-making ability using rules (i.e., IF-THEN statements). For example, a rule-based method has been utilized to discover DDIs from numerous collections of unstructured texts [20, 21]. Others that have been used include knowledge graphs [4, 10], machine learning [22, 23], and deep learning [24].

Despite the quantity of research conducted in this area, recent efforts have realized only limited clinical utility. More specifically, study findings generally only demonstrate associations that are either pharmacokinetic or pharmacodynamic in nature; however, focusing on one level of DDIs neglects important information about other possible interactions such as multipathway interactions [10]. Furthermore, existing efforts have mostly focused on a relatively limited

scope of features and have incorporated only a small number of biomedical resources. Still, there is an enormous quantity of data, information, and knowledge available concerning DDIs and their mechanisms of interaction that could be used for exploration [25, 26]. Leveraging these large-scale resources is key to realizing the cost-effective, high-throughput prediction of DDIs that are new to clinical practice or have occult rather than overt effects, as well as diagnosing those that occur in remote treatment situations.

3. Methods

3.1. Phase 1: The Extract, Transform, Load (ETL) Methodology. In the biomedical domain, data and knowledge are often provided in an assortment of formats, in addition to being provided by a multitude of disparate, disconnected resources; this fractured availability hinders discovery and processing. In the context of DDIs, there is great variability in the reporting of interactions and associated mechanisms by the many commercial and free license resources [27, 28]. Synthesizing these resources to generate a comprehensive utility through which interactions can be discovered both handily and accurately is an ongoing challenge. To overcome these obstacles, we built an ETL method to generate a mechanistic knowledge graph for DDIs. Our ETL method represents an important development towards filling in the knowledge gaps that exist between multiple biomedical resources and ensuring the greater success of knowledge discovery.

The ETL method specifically utilized semantic web technologies for the extraction, integration, and representation of knowledge and data. We also customized it by adding a validation layer that uses reasoning capabilities to test for consistency among classes, instances, and their relationships [29], which is necessary before loading to ensure accurate reasoning. In this phase, the ETL prepares the knowledge graph that will be used later for the inferential task. This phase consists of four main steps: extracting data and knowledge from multiple resources, integrating them into a single graph, validating, and finally loading the information into a knowledge graph in a data store.

3.1.1. Extract: Collecting Information on Drug Mechanisms of Interaction. The first step was to examine data and knowledge resources and extract their relevance to our study, with a focus on information concerning DDIs and their mechanisms of interaction. We mainly examined data and knowledge that contain pharmacological, biomolecular, physiological, and genetic information. Those four groups represented the core classes of the ETL and contained subclasses that categorize the respective instances/entities, i.e., genes and drugs. For pharmacological information, we downloaded DrugBank [30] from <https://go.drugbank.com/releases/latest> in March 2022. For biomolecular information, we obtained the National Cancer Institute Thesaurus (NCI) [31] and Gene Ontology terms (GO) [32] from the Unified Medical Language System (UMLS) [33]. The National Drug File-Reference Terminology (NDF-RT) [34] for physiological information was also sourced from the UMLS, while the

Pharmacogenomics Knowledge Base (PharmGKB) [35], representing genetic information, was downloaded from <https://www.pharmgkb.org/downloads> in March 2022.

3.1.2. Transform: Building the Mechanistic Knowledge Graph. The transformation phase comprised three major steps:

Step 1: design a mapping strategy for integrating the relevant resources extracted into a single knowledge graph.

Step 2: insert and group relationships between instances and classes in the knowledge graph.

Step 3: choose the appropriate tools to describe and represent entities and relationships among DDIs and their mechanisms of interaction.

For the mapping strategy and the insertion of relationships, we used the UMLS as the backbone for our knowledge graph, as its purpose is to provide an integrated system in the biomedical domain. For semantic tools, we used Jena [36, 37] for building and storing the mechanistic knowledge graph instances and Protégé [38] for creating classes, relationships, and consistency checks.

The process of transformation relied primarily on concept unique identifiers (CUIs) from the UMLS Metathesaurus dataset, which contains more than 4,441,326 concepts and more than 200 relationships from more than 155 biomedical data and knowledge resources. We have written Javascript code using a Jena semantic tool to generate the instances and add their semantic relationships from the UMLS MySQL database into the mechanistic knowledge graph. Specifically, from the MRCONSO table, we extracted and transformed NCI, GO, and NDF-RT resources and then added semantic relationships from the MRREL table. Drug-Bank and PharmGKB are not part of the UMLS terminology system, so instances and relationships from them were added to the knowledge graph through a shared identifiers technique; for example, the genetic information (relationships) for levofloxacin in the PharmGKB dataset was added to the knowledge graph using the CUI ID link provided at <http://pharmgkb.org/chemical/PA450214/link>.

3.1.3. Validate: Using the Semantic Network. Validation is always necessary when integrating multiple resources and grouping semantic relationships between instances. Accordingly, we designed an ontology using the Protégé tool, which supports many semantic web formats such as RDF, RDFS, OWL, and XML schema. Four main classes were created to cover the pharmacological, biomolecular, physiological, and genetic levels. After that, we created subclasses as follows: (1) drugs, *rdfs:subclass* of pharmacological; (2) genes, enzymes, and biological processes, *rdfs:subclasses* of biomolecular; (3) effect and mechanism of action, *rdfs:subclasses* of physiological; and (4) SNPs, *rdfs:subclass* of genetic. To properly insert the created instances of the mechanistic knowledge graph into the classes and subclasses for each instance, we utilized corresponding semantic types from the MRSAT table, which contains more than 133 semantic types that together constitute a categorization terminology encompassing diverse biomedical domains. We asserted the semantic types as properties of each instance in the

knowledge graph; for instance, T028 represents the Gene or Genome type in UMLS, so all instances that belong to T028 were added to the genes subclass of biomolecular. After validating the knowledge graph, we next checked for consistency among classes, subclasses, and instances, a necessary step when integrating multiple data resources. We used the Pellet [39] reasoner for this task as it is compatible with Jena and wrote Javascript code to check the consistency of our ontology. The results demonstrated it to be appropriately consistent.

3.1.4. Load: Storing the Mechanistic Knowledge Graph in a Triple Store. The last step of the ETL process was to load the knowledge graph into a data store. For this, we used Jena's TDB triple store [37]. The process of creating and uploading the knowledge graph happened once and offline, which allows for fast performance as the information is stored locally with no changes [40]. Figure 1 illustrates the steps of the ETL methodology.

3.2. Phase 2: The Inference Algorithm. After creating the mechanistic knowledge graph, we developed the second part of the rule-based framework, the inference algorithm. Rule-based methods have received particular attention in DDI prediction, as they endeavor to mimic the decision-making ability of human experts and have been employed with good results [19], including when extracting information from unstructured text [20, 21]. However, existing systems are relatively limited in terms of both the knowledge resources they draw upon and the types of interactions they consider, and it remains difficult to estimate the actual clinical significance of any given computationally predicted DDI. Leveraging the full breadth of available knowledge [25, 26] and considering multiple and more complex mechanistic dimensions such as multipathway interactions [10] can allow us to not only more comprehensively identify putative DDIs but also assess their relevance to clinical practice. We aimed to do exactly this with our approach.

We used backward chaining as the inference algorithm, which starts with a hypothesis and searches a knowledge graph until that hypothesis is either accepted or rejected [41]. In our study, we hypothesized that there could be a potential interaction between two drugs that have pharmacological effects at the metabolism and transporter levels (i.e., inhibition or induction) and share some biomedical features among four main categories (pharmacological, biomolecular, physiological, and genetic). Given this hypothesis, the framework would then apply rules on a knowledge graph using the backward chaining inference algorithm to find evidence to prove the hypothesis according to a defined set of rules. More specifically, the framework takes two drugs as goals, and the inference algorithm looks for facts in the knowledge graph that return pharmacological effects and shared biomedical features.

4. Results

4.1. The Rule-Based Framework Requires Multiple Facts and Rules for DDI Exploration and Explanation. The framework

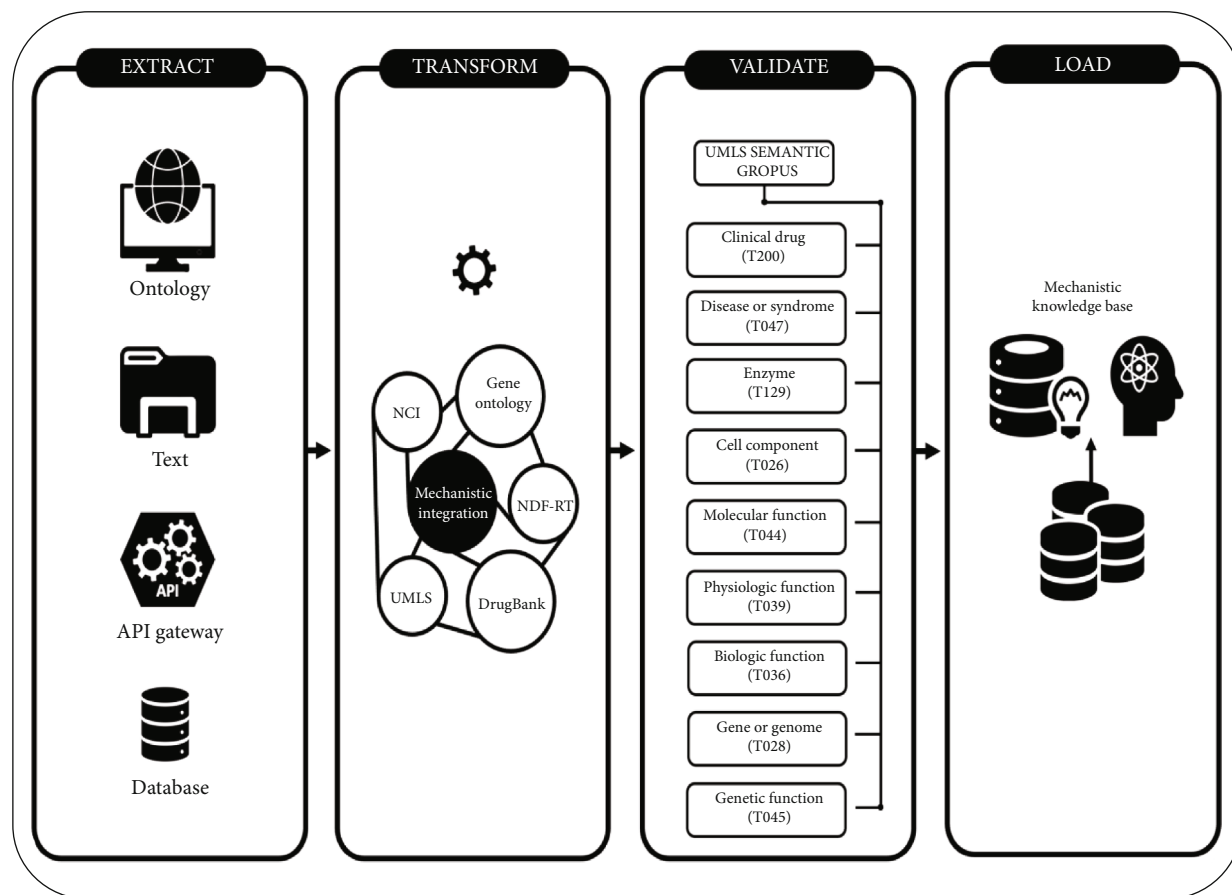


FIGURE 1: Our methodology for extracting biomedical data, information, knowledge, and features of drugs, transforming them to a knowledge graph, validating the knowledge graph, and then loading them into a comprehensive mechanistic local store.

was developed as summarized in Figure 2. In this framework, we considered a DDI as prospective if it was recognized as having pharmacological effects on the joint basis of either inhibition or induction with respect to metabolism and transport and also shared the maximum number of biomedical features among four core defined categories (pharmacological, bimolecular, physiological, and genetic). We evaluated the framework's performance on a pair of commonly co-administered drugs, the chemotherapy agent irinotecan and the antibiotic agent levofloxacin, for which a potential interaction was previously identified [42].

To explore the possibility of a DDI, we proposed a backward chaining algorithm based on a rules framework that links facts (i.e., IF parts) to conclusions (THEN parts). The developed framework is comprised of six rules, which have been validated by a clinician, to explore and explain the mechanisms of potential DDIs, which are as follows:

4.2. Integration of Mechanistic DDI Information and Pharmacological, Biomolecular, Physiological, and Genetic Effects Provide the Necessary Evidence for DDIs in the Clinical Setting. In our rule-based framework, we combined six types of biomedical data and information (genes, proteins, biological processes, molecular function, physiology, and SNPs) and achieved a high-quality knowledge representation from which to determine whether a potential DDI

may exist. A SPARQL query [40] over the mechanistic knowledge graph was generated in which all features of interactor 1, levofloxacin, were retrieved from multiple resources and incorporated in the final framework as demonstrated in Figure 3.

4.3. The Framework Proves Potential DDI through Mechanisms of Interaction. To demonstrate the reliability and effectiveness of the implemented rules, we had the framework consider two major layers of backward chaining inference in a sequence that would propose mechanisms for the possible DDI between concurrently-administered levofloxacin and irinotecan. The first layer addresses when both interactors intervene pharmacologically at the metabolism level (i.e., inhibit or induce enzymes and transporters), and the second layer when both interactors share a maximum number of features within the classes (pharmacological, bimolecular, physiological, and genetic). Through conducting backward chaining inference on the knowledge graph, our framework identified the most relevant pathways connecting the two drugs and yielded a proposed mechanism of their DDI, illustrated in Table 1. Specifically, the framework identified levofloxacin as an inhibitor for both an ABC transporter protein, ABCB1, and the CYP3A4 enzyme, while irinotecan was likewise identified as a substrate for both. In humans, CYP3A4 is the most widely

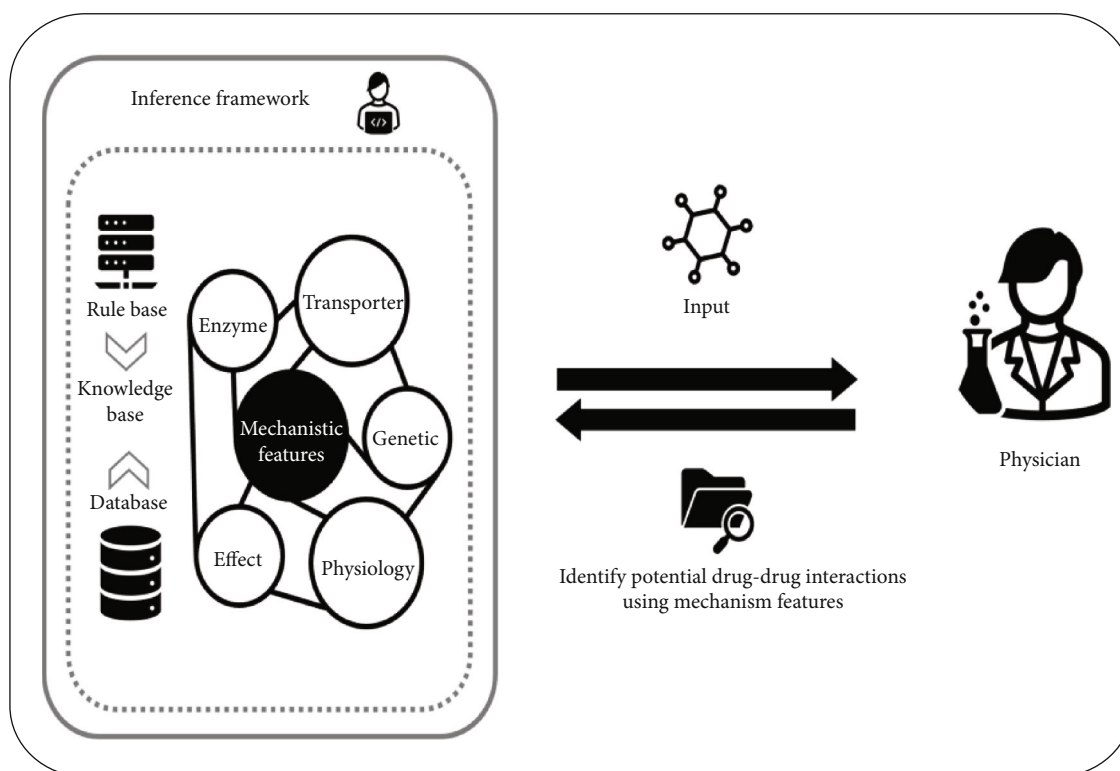


FIGURE 2: Rule-based framework for exploring and explaining the mechanisms of potential drug-drug interactions.

```

If
<one drug inhibits metabolism or transport of another >
AND<one drug induces metabolism or transport of another >
AND<two drugs share the same pharmacological target >
OR<two drugs share biomolecular features>
OR<two drugs share physiological pathways >
OR<two drugs have common genetic variations >
Then
< a DDI occurs >

```

ALGORITHM 1

expressed of CYP proteins; it constitutes as much as 70% of gastrointestinal CYP activity and mediates 40-45% of all phase 1 metabolic reactions [43–45]. In addition, similarity between the two drugs was detected at three levels, including that both agents are contraindicated when a patient is allergic to either and both decrease DNA integrity, which satisfies the backward chaining rules. Furthermore, the two drugs share substructures; that is, both contain the following: hydroxy compounds, heterocyclic compounds, aromatic compounds, phenols and derivatives, pyridines and derivatives, benzene and derivatives, carboxylic acids and derivatives, acetates, ethers, aliphatic, and aryl amines, phenyl esters, anisoles, (iso)-quinolines and derivatives, and hydroxyquinolines.

Therefore, the framework detected CYP3A4 and ABCB1 as primary candidates for the mechanism of this drug pair's interaction. Notably, CYP3A4 and ABCB1 are coexpressed in the liver and intestines, and the liver is where irinotecan

is converted to its active metabolite, SN-38, through hydrolysis by carboxylesterases (CESs) [46, 47]. In the liver, SN-38 can be glucuronized, detoxified by enzymes of the UGT1A1 family, and eliminated via release into the intestines; or it can be oxidized through the action of CYP3A proteins. Meanwhile, irinotecan can itself be oxidized by CYP3A proteins, producing either of two inactive metabolites. Ultimately, irinotecan, its elimination, and the abundance of SN-38 are regulated heavily through CYP3A4 and UGT1A1 [46, 47]. In contrast, levofloxacin metabolism in humans is limited; the drug is primarily excreted through the urine without any alteration [48, 49]. Interestingly, the findings from our computational approach suggest a potential effect of levofloxacin on CYP3A4 activity; namely, it could influence the metabolism dynamics of CYP3A4 substrates such as irinotecan. This merits further investigation to improve our understanding of levofloxacin and its DDIs.

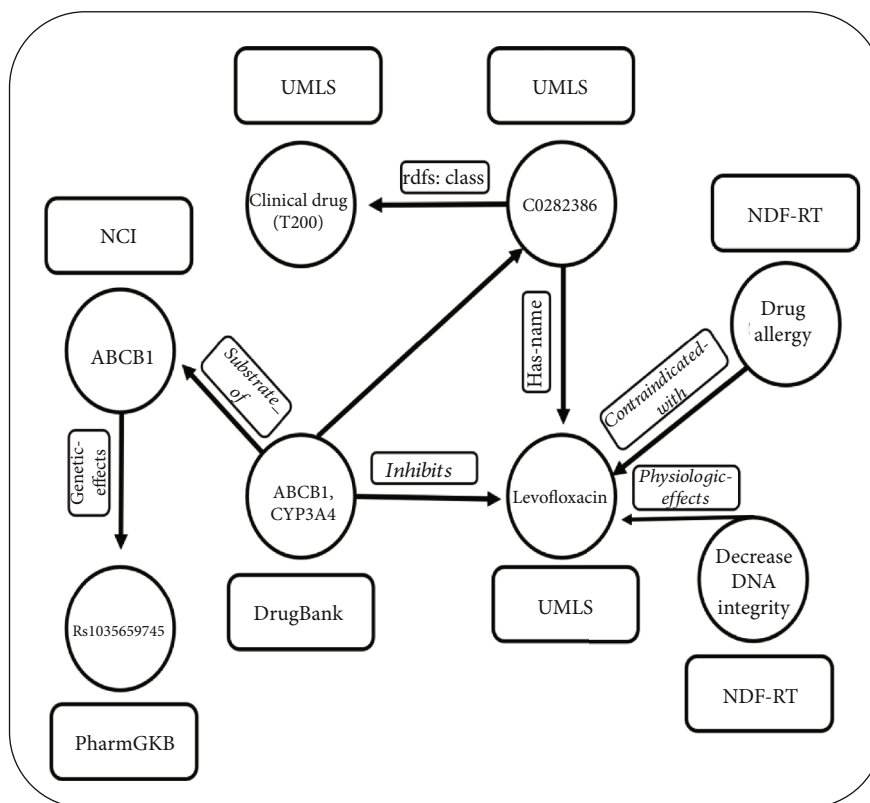


FIGURE 3: The multiple mechanistic features of levofloxacin, extracted from different biomedical resources.

TABLE 1: Summary of the potential mechanism of interaction of coadministered irinotecan and levofloxacin.

| | Irinotecan | Levofloxacin |
|--------------------------------|-------------------------|------------------|
| <i>Pharmacological effects</i> | | |
| Metabolizing enzymes | CYP3A4 substrate | CYP3A4 inhibitor |
| Transporters | ABCB1 substrate | ABCB1 inhibitor |
| <i>Biomedical features</i> | | |
| Pharmacological (MoA) | NA | NA |
| Biomolecular | NA | NA |
| Physiological | Decreased DNA integrity | |
| Genetic | NA | NA |

Another finding highlighted ATP-binding cassette transporters as a potential candidate mechanism. These transporters comprise a large superfamily of membrane proteins. ABCB1 in particular (along with its analogs) has become known for its importance in the absorption of drugs and drug candidates. Interestingly, numerous reports have found that coadministration of an ABCB1 inhibitor and substrate can greatly increase blood levels of the substrate, resulting in serious side effects [50, 51]. Accordingly, ABCB1 interactors need to be investigated in terms of both their substrate and inhibitor properties—perhaps especially the latter in the context of DDIs. Notably, the literature supports levofloxacin as an ABCB1 substrate [48], while our framework indicated a potential inhibitory effect on ABCB1 transporters; both imply

potential interaction of levofloxacin with all ABCB1 substrates, including irinotecan.

Several drugs are known to interact with irinotecan at different levels [42, 52]. Limited data suggest that oral quinolone antibiotics may have their plasma concentrations reduced upon chemotherapy with antineoplastic agents [48, 49]; however, there has not yet been any report of an interaction between irinotecan and levofloxacin. As a broad-spectrum antibiotic, levofloxacin is used extensively in cancer patients for treating infections; in addition, according to the guideline, levofloxacin is also used as a postchemotherapy course prophylactic for patients in which febrile neutropenia is a substantial risk [53]. If levofloxacin and irinotecan interact, extensive use of levofloxacin in patients receiving irinotecan would predispose them to that DDI, which may result in unwanted and potentially hazardous adverse effects.

5. Discussion

In this research, we developed a computational framework that utilized a rule-based approach to explore and explain the biological related mechanisms of potential DDIs. This present work focuses strongly on leveraging multiple large-scale biomedical resources to provide support for assessing the mechanisms of interaction at work in DDIs so as to identify potential DDIs. Further, we tested the framework by examining the putative DDI between irinotecan (an antineoplastic chemotherapy agent) and levofloxacin (a quinolone

antibiotic); the mechanisms so identified suggest directions for confirming the clinical significance of this predicted DDI.

Upon validation, our framework has the potential to add significant value to current practices surrounding DDIs. First, requirements to identify potential DDIs have been established by food and drug administrations in several countries and are mandatory for new drug approval [6, 54]. Such requirements might increase the cost of drug research and delay approval. Second, the limited knowledge available to clinicians regarding existing and unknown DDIs affects clinical decisions, especially when alternative agents are not available. The mechanism-centered approach employed in this framework allows for consideration of not only a DDI's possible occurrence but also its clinical relevance.

In having developed this framework, it has become clear that the state-of-the-art has mainly focused on a relatively limited scope of features and reasoning and has incorporated a relatively small number of knowledge resources. In existing knowledge of drug mechanisms, biomedical features are among those considered as possible causes; accordingly, if for a pair of drugs known to produce a DDI there is suspicion that a particular set of biomedical features is the cause of that DDI, then it seems reasonable to extend this concern to a hypothetical other pair of drugs sharing the same biomedical feature pattern. Our current framework uses a simplistic form of combined similarity computation that could be greatly expanded on or even replaced in further works. The present implementation considers each biomedical feature pattern to be equally important and therefore implies that the more of these patterns that are satisfied, the more likely there is a need to be concerned about a DDI. It is important to consider how "similar" two pairs need to be to raise an alarm for potential DDI. Under the current framework, the similarity does not need to be very great, and yet the number of false alarms raised seems to be reasonably low. We believe that the basic premise is sound, but enhancement/replacement of the similarity determination with more comprehensive computational methods could yield promising results; we have several thoughts in that direction. Nonetheless, this work fulfills its purpose, which is to provide a new direction as a means of differentiation from prevailing approaches and thereby invite greater attention to be given to the process of evaluation as opposed to the production and expansion of resources for use in evaluation [55].

6. Conclusion

This work introduces a rule-based framework that has utility for exploring and explaining possible DDIs, as demonstrated by our case study of the commonly coadministered chemotherapy agent irinotecan and antibiotic levofloxacin. It represents an initial step toward developing an efficient system that can be utilized by researchers and clinicians to reduce requirements for drug approval, particularly concerning DDI studies, and hence accelerate a drug's approval. In addition, such a framework would provide support that aids clinicians in making clinical decisions, especially for new drugs with limited evidence.

Data Availability

Data is available upon request.

Conflicts of Interest

The authors declare that the research was conducted in the absence of any commercial or financial relationships that could be construed as a potential conflict of interest.

Authors' Contributions

Dr. Adeeb Noor was involved in the design and execution of the project, performed the literature search, developed the data abstraction, undertook the initial data analysis, prepared tables and figures, and drafted the manuscript. Dr. Abdullah Assiri was involved in the design and execution of the project, performed the literature search, developed the data abstraction, undertook the initial data analysis, prepared tables and figures, and drafted the manuscript.

Acknowledgments

The authors extend their appreciation to the Deanship of Scientific Research at King Khalid University for funding this work through Small Groups (RGP.1-312-43).

References

- [1] D. C. Malone, D. S. Hutchins, H. Hauptert et al., "Assessment of potential drug-drug interactions with a prescription claims database," *American Journal of Health-System Pharmacy*, vol. 62, no. 19, pp. 1983-1991, 2005.
- [2] S. Dechanont, S. Maphanta, B. Butthum, and C. Kongkaew, "Hospital admissions/visits associated with drug-drug interactions: a systematic review and meta-analysis," *Pharmacoepidemiology and Drug Safety*, vol. 23, no. 5, pp. 489-497, 2014.
- [3] D. M. Qato, G. C. Alexander, R. M. Conti, M. Johnson, P. Schumm, and S. T. Lindau, "Use of prescription and over-the-counter medications and dietary supplements among older adults in the United States," *JAMA*, vol. 300, no. 24, pp. 2867-2878, 2008.
- [4] H. Hochheiser, X. Jing, E. A. Garcia et al., "A minimal information model for potential drug-drug interactions," *Frontiers in Pharmacology*, vol. 11, article 608068, 2021.
- [5] L. Z. Benet, "Pharmacokinetics: basic principles and its use as a tool in drug metabolism," in *Drug Metabolism and Drug Toxicity*, J. R. Mitchell and M. G. Horning, Eds., pp. 199-211, Raven Press, New York, 1984.
- [6] FDA Center for Drug Evaluation and Research, "Drug interactions | relevant regulatory guidance and policy documents," <https://www.fda.gov/drugs/drug-interactions-labeling/drug-interactions-relevant-regulatory-guidance-and-policy-documents>.
- [7] T. Roblek, T. Vaupotic, A. Mrhar, and M. Lainscak, "Drug-drug interaction software in clinical practice: a systematic review," *European Journal of Clinical Pharmacology*, vol. 71, no. 2, pp. 131-142, 2015.
- [8] A. Noor, "Integrating mechanistic information to predict drug-drug interactions and associated relevance for decision support," in *2022 IEEE International IOT, Electronics and*

- Mechatronics Conference (IEMTRONICS)*, pp. 1–4, Toronto, ON, Canada, 2022.
- [9] S. Vilar, R. Harpaz, E. Uriarte, L. Santana, R. Rabadan, and C. Friedman, “Drug–drug interaction through molecular structure similarity analysis,” *Journal of the American Medical Informatics Association*, vol. 19, no. 6, pp. 1066–1074, 2012.
 - [10] S. Dere and S. Ayvaz, “Prediction of drug–drug interactions by using profile fingerprint vectors and protein similarities,” *Healthc Inform Res*, vol. 26, no. 1, pp. 42–49, 2020.
 - [11] F. Cheng and Z. Zhao, “Machine learning-based prediction of drug–drug interactions by integrating drug phenotypic, therapeutic, chemical, and genomic properties,” *Journal of the American Medical Informatics Association*, vol. 21, no. e2, pp. e278–e286, 2014.
 - [12] R. Hoehndorf, T. Hiebert, N. W. Hardy, P. N. Schofield, G. V. Gkoutos, and M. Dumontier, “Mouse model phenotypes provide information about human drug targets,” *Bioinformatics*, vol. 30, no. 5, pp. 719–725, 2014.
 - [13] M. R. Kamdar and M. A. Musen, “Mechanism-based pharmacovigilance over the life sciences linked open data cloud,” *American Medical Informatics Association Annual Symposium Proceedings*, vol. 2017, pp. 1014–1023, 2017.
 - [14] I. Abdelaziz, A. Fokoue, O. Hassanzadeh, P. Zhang, and M. Sadoghi, “Large-scale structural and textual similarity-based mining of knowledge graph to predict drug–drug interactions,” *Journal of Web Semantics*, vol. 44, pp. 104–117, 2017.
 - [15] A. Noor, A. Assiri, S. Ayvaz, C. Clark, and M. Dumontier, “Drug–drug interaction discovery and demystification using semantic web technologies,” *Journal of the American Medical Informatics Association*, vol. 24, no. 3, pp. 556–564, 2017.
 - [16] K. Park, D. Kim, S. Ha, and D. Lee, “Predicting pharmacodynamic drug–drug interactions through signaling propagation interference on protein–protein interaction networks,” *PLoS One*, vol. 10, no. 10, article e0140816, 2015.
 - [17] I. J. Tripodi, T. J. Callahan, J. T. Westfall, N. S. Meitzer, R. D. Dowell, and L. E. Hunter, “Applying knowledge-driven mechanistic inference to toxicogenomics,” *Toxicology In Vitro*, vol. 66, article 104877, 2020.
 - [18] A. Noor, “A data-driven medical decision framework for associating adverse drug events with drug–drug interaction mechanisms,” *Journal of Healthcare Engineering*, vol. 2022, Article ID e9132477, 7 pages, 2022.
 - [19] B. Abu-Nasser, “Medical expert systems survey,” *International Journal of Engineering and Information Systems (IJEAIS)*, vol. 1, no. 7, pp. 218–224, 2017.
 - [20] I. Segura-Bedmar, M. Crespo, C. de Pablo, and P. Martínez, “DrugNerAR: linguistic rule-based anaphora resolver for drug–drug interaction extraction in pharmacological documents,” in *Third International Workshop on Data and Text Mining in Bioinformatics*, pp. 19–26, Association for Computing Machinery, New York, NY, USA, 2009.
 - [21] I. Segura-Bedmar, P. Martínez, and C. de Pablo-Sánchez, “A linguistic rule-based approach to extract drug–drug interactions from pharmacological documents,” *BMC Bioinformatics*, vol. 12, Suppl 2, p. S1, 2011.
 - [22] S. Liu, B. Tang, Q. Chen, and X. Wang, “Drug–drug interaction extraction via convolutional neural networks,” *Computational and Mathematical Methods in Medicine*, vol. 2016, Article ID e6918381, 8 pages, 2016.
 - [23] M. Tiftikci, A. Özgür, Y. He, and J. Hur, “Machine learning-based identification and rule-based normalization of adverse drug reactions in drug labels,” *BMC Bioinformatics*, vol. 20, no. S21, p. 707, 2019.
 - [24] X. Sun, L. Ma, X. Du, J. Feng, and K. Dong, “Deep convolution neural networks for drug–drug interaction extraction,” in *2018 IEEE International Conference on Bioinformatics and Biomedicine (BIBM)*, pp. 1662–1668, Madrid, Spain, 2018.
 - [25] R. Hoehndorf, P. N. Schofield, and G. V. Gkoutos, “The role of ontologies in biological and biomedical research: a functional perspective,” *Briefings in Bioinformatics*, vol. 16, no. 6, pp. 1069–1080, 2015.
 - [26] A. Lavertu, B. Vora, K. M. Giacomini, R. Altman, and S. Rensi, “A new era in pharmacovigilance: toward real-world data and digital monitoring,” *Clinical Pharmacology & Therapeutics*, vol. 109, no. 5, pp. 1197–1202, 2021.
 - [27] P. Vonbach, A. Dubied, S. Krähenbühl, and J. H. Beer, “Evaluation of frequently used drug interaction screening programs,” *Pharmacy World & Science*, vol. 30, no. 4, pp. 367–374, 2008.
 - [28] S. Monteith and T. Glenn, “Comparison of potential psychiatric drug interactions in six drug interaction database programs: a replication study after 2 years of updates,” *Human Psychopharmacology*, vol. 36, no. 6, article e2802, 2021.
 - [29] K. Baclawski, M. M. Kokar, R. Waldinger, and P. A. Kogut, “Consistency checking of semantic web ontologies,” in *The Semantic Web — ISWC 2002*, I. Horrocks and J. Hendler, Eds., pp. 454–459, Springer, Berlin, Germany, 2002.
 - [30] D. S. Wishart, Y. D. Feunang, A. C. Guo et al., “DrugBank 5.0: a major update to the DrugBank database for 2018,” *Nucleic Acids Research*, vol. 46, no. D1, pp. D1074–D1082, 2018.
 - [31] S. de Coronado, M. W. Haber, N. Sioutos, M. S. Tuttle, and L. W. Wright, “NCI thesaurus: using science-based terminology to integrate cancer research results,” *Studies in Health Technology and Informatics*, vol. 107, Part 1, pp. 33–37, 2004.
 - [32] M. Ashburner, C. A. Ball, J. A. Blake et al., “Gene Ontology: tool for the unification of biology,” *Nature Genetics*, vol. 25, no. 1, pp. 25–29, 2000.
 - [33] O. Bodenreider, “The Unified Medical Language System (UMLS): integrating biomedical terminology,” *Nucleic Acids Research*, vol. 32, no. 90001, pp. 267D–2270, 2004.
 - [34] S. H. Brown, P. L. Elkin, S. T. Rosenbloom et al., “VA National Drug File Reference Terminology: a cross-institutional content coverage study,” *Studies in Health Technology and Informatics*, vol. 107, Part 1, pp. 477–481, 2004.
 - [35] T. E. Klein, J. T. Chang, M. K. Cho et al., “Integrating genotype and phenotype information: an overview of the PharmGKB project,” *The Pharmacogenomics Journal*, vol. 1, no. 3, pp. 167–170, 2001.
 - [36] J. J. Carroll, I. Dickinson, C. Dollin, D. Reynolds, A. Seaborne, and K. Wilkinson, “Jena: implementing the semantic web recommendations,” in *Proceedings of the 13th international World Wide Web conference on Alternate track papers & posters*, pp. 74–83, New York, NY, USA, 2004.
 - [37] A. Owens, A. Seaborne, N. Gibbins, and M. C. Schraefel, *Clustered TDB: A Clustered Triple Store for Jena*, WWW 2009, Madrid, Spain, 2009.
 - [38] M. Horridge, H. Knublauch, A. Rector, R. Stevens, and C. Wroe, *A Practical Guide to Building OWL Ontologies Using the Protégé-OWL Plugin and CO-ODE Tools Edition 1.0*, The University of Manchester, Manchester, England, 2004.
 - [39] E. Sirin, B. Parsia, B. C. Grau, A. Kalyanpur, and Y. Katz, “Pellet: a practical OWL-DL reasoner,” *Journal of Web Semantics*, vol. 5, no. 2, pp. 51–53, 2007.

- [40] H. Shi, K. Maly, and S. Zeil, "Optimized backward chaining reasoning system for a semantic web," in *Proceedings of the 4th International Conference on Web Intelligence, Mining and Semantics (WIMS14)*, pp. 1–6, New York, NY, USA, 2014.
- [41] A. Al-Ajlan, "The comparison between forward and backward chaining," *IJMLC*, vol. 5, no. 2, pp. 106–113, 2015.
- [42] A. Assiri and A. Noor, "A computational approach to predict multi-pathway drug-drug interactions: a case study of irinotecan, a colon cancer medication," *Saudi Pharmaceutical Journal*, vol. 28, no. 12, pp. 1507–1513, 2020.
- [43] F. P. Guengerich, "Cytochromes P450, drugs, and diseases," *Molecular Interventions*, vol. 3, no. 4, pp. 194–204, 2003.
- [44] T. Lynch and A. Price, "The effect of cytochrome P450 metabolism on drug response, interactions, and adverse effects," *American Family Physician*, vol. 76, no. 3, pp. 391–396, 2007.
- [45] D. R. Nelson, "The cytochrome P450 homepage," *Human Genomics*, vol. 4, no. 1, pp. 59–65, 2009.
- [46] L. Iyer, C. D. King, P. F. Whittington et al., "Genetic predisposition to the metabolism of irinotecan (CPT-11). Role of uridine diphosphate glucuronosyltransferase isoform 1A1 in the glucuronidation of its active metabolite (SN-38) in human liver microsomes," *The Journal of Clinical Investigation*, vol. 101, no. 4, pp. 847–854, 1998.
- [47] R. H. Mathijssen, R. J. van Alphen, J. Verweij et al., "Clinical pharmacokinetics and metabolism of irinotecan (CPT-11)," *Clinical Cancer Research*, vol. 7, no. 8, pp. 2182–2194, 2001.
- [48] D. N. Fish and A. T. Chow, "The clinical pharmacokinetics of levofloxacin," *Clinical Pharmacokinetics*, vol. 32, no. 2, pp. 101–119, 1997.
- [49] T. Ito, I. Yano, K. Tanaka, and K.-I. Inui, "Transport of quinolone antibacterial drugs by human p-glycoprotein expressed in a kidney epithelial cell line, LLC-PK1," *The Journal of Pharmacology and Experimental Therapeutics*, vol. 282, no. 2, pp. 955–960, 1997.
- [50] N. Mizuno, T. Niwa, Y. Yotsumoto, and Y. Sugiyama, "Impact of drug transporter studies on drug discovery and development," *Pharmacological Reviews*, vol. 55, no. 3, pp. 425–461, 2003.
- [51] Y. Peng, Z. Cheng, and F. Xie, "Evaluation of pharmacokinetic drug–drug interactions: a review of the mechanisms, in vitro and in silico approaches," *Metabolites*, vol. 11, no. 2, p. 75, 2021.
- [52] V. Charasson, M.-C. Haaz, and J. Robert, "Determination of drug interactions occurring with the metabolic pathways of irinotecan: figure 1," *Drug Metabolism and Disposition*, vol. 30, no. 6, pp. 731–733, 2002.
- [53] A. G. Freifeld, E. J. Bow, K. A. Sepkowitz et al., "Clinical practice guideline for the use of antimicrobial agents in neutropenic patients with cancer: 2010 update by the Infectious Diseases Society of America," *Clinical Infectious Diseases*, vol. 52, no. 4, pp. e56–e93, 2011.
- [54] Ema, "Investigation of drug interactions," <https://www.ema.europa.eu/en/investigation-drug-interactions>.
- [55] A. Assiri and A. Noor, "Anti-DDI resource: a dataset for potential negative reported interaction combinations to improve medical research and decision-making," *Journal of Healthcare Engineering*, vol. 2022, Article ID e8904342, 2022.

Research Article

Predicting Breast Cancer Leveraging Supervised Machine Learning Techniques

Sanam Aamir ¹, **Aqsa Rahim** ², **Zain Aamir** ³, **Saadullah Farooq Abbasi** ⁴,
Muhammad Shahbaz Khan ⁵, **Majed Alhaisoni** ⁶, **Muhammad Attique Khan** ^{6,7},
Khyber Khan ⁸, and **Jawad Ahmad** ⁹

¹Department of Computer and Software Engineering, National University of Sciences and Technology, Islamabad 44000, Pakistan

²Faculty of Science and Technology, University of Tromsø, Tromsø, Norway

³Department of Data Science, National University of Computer and Emerging Sciences, Islamabad 44000, Pakistan

⁴Department of Electrical Engineering, National University of Technology, Islamabad 44000, Pakistan

⁵Department of Electrical Engineering, HITEC University, Taxila 47080, Pakistan

⁶Computer Sciences Department, College of Computer and Information Sciences, Princess Nourah bint Abdulrahman University, Riyadh 11671, Saudi Arabia

⁷Department of Computer Science, HITEC University, Taxila, Pakistan

⁸Department of Computer Science, Khurasan University, Jalalabad, Afghanistan

⁹School of Computing, Edinburgh Napier University, Edinburgh EH10 5DT, UK

Correspondence should be addressed to Khyber Khan; khyber.khan.khurasan@gmail.com

Received 15 June 2022; Accepted 28 July 2022; Published 16 August 2022

Academic Editor: Sujatha Krishnamoorthy

Copyright © 2022 Sanam Aamir et al. This is an open access article distributed under the Creative Commons Attribution License, which permits unrestricted use, distribution, and reproduction in any medium, provided the original work is properly cited.

Breast cancer is one of the leading causes of increasing deaths in women worldwide. The complex nature (microcalcification and masses) of breast cancer cells makes it quite difficult for radiologists to diagnose it properly. Subsequently, various computer-aided diagnosis (CAD) systems have previously been developed and are being used to aid radiologists in the diagnosis of cancer cells. However, due to intrinsic risks associated with the delayed and/or incorrect diagnosis, it is indispensable to improve the developed diagnostic systems. In this regard, machine learning has recently been playing a potential role in the early and precise detection of breast cancer. This paper presents a new machine learning-based framework that utilizes the Random Forest, Gradient Boosting, Support Vector Machine, Artificial Neural Network, and Multilayer Perception approaches to efficiently predict breast cancer from the patient data. For this purpose, the Wisconsin Diagnostic Breast Cancer (WDBC) dataset has been utilized and classified using a hybrid Multilayer Perceptron Model (MLP) and 5-fold cross-validation framework as a working prototype. For the improved classification, a connection-based feature selection technique has been used that also eliminates the recursive features. The proposed framework has been validated on two separate datasets, i.e., the Wisconsin Prognostic dataset (WPBC) and Wisconsin Original Breast Cancer (WOBC) datasets. The results demonstrate improved accuracy of 99.12% due to efficient data preprocessing and feature selection applied to the input data.

1. Introduction

In recent years, humans have become more prone to various types of cancer than they have ever been. Cancer is a leading cause of death worldwide and is considered to be responsible for one out of every six fatalities [1]. The most common type of cancer in terms of new cases is breast cancer. Breast can-

cer alone claimed the lives of around 40,920 women in 2018 [1, 2]. According to the World Health Organization (WHO), around 2.90 million women are diagnosed with breast cancer every year [3]. The term cancer refers to more than 100 diseases that affect different regions of the human body. To understand the beginning of cancer, an insight into the normal cell division is required. Cells are the fundamental

units that undergo programmed cell death (apoptosis) and proliferate (via mitosis) to regenerate. But sometimes, environmental and genetic factors interfere with the programmed process of division or death and begin to grow uncontrollably resulting in a mass of cells called a tumor. The tumor can be cancerous and has the ability to metastasize to other parts of the body and cause pathology [3]. A benign tumor, on the other hand, means that the tumor is not malignant. For the treatment of any type of cancer, early detection is an essential factor. Therefore, it is important to exploit different diagnostic methods for the automated detection of cancer. Breast cancer is caused by the rapidly proliferating cells that develop breast lumps [4, 5]. As per the reports of the World Health Organization (WHO), breast cancer is among the top-ranked reasons for fatalities in women. Hence, it is critical that in addition to the diagnosis, the treatment of breast cancer is equally important at the early stages. The diagnosis of breast cancer can be made possible because of physiological changes in the breast; therefore, monitoring and screening of breast cancer on a regular basis are important and can help in the early diagnosis of the disease.

Machine learning (ML) methods have extensively been utilized over the last few decades to develop various predictive models which are capable of effective decision making. Similarly, the use of machine learning can drastically improve the automated decision-making process and can prove to be an excellent aid to medical practitioners in the early and precise detection of breast cancer. ML techniques can effectively be utilized to identify various patterns in a dataset and, hence, can predict the type of cancer (either malignant or benign). For the automated detection of breast cancer, various important parameters, i.e., marginal adhesion, clump thickness, and uniformity of cell shape or size (bland chromatin, the normality of nuclei, single epithelial cell size, and mitosis), are extracted from breast cancer mammography (X-ray pictures). In addition to these, some other factors, such as age, number of previous biopsies, and the number of the first-degree relatives having breast cancer, can also be used to predict the occurrence and repetition of breast cancer. Furthermore, for the prediction of breast cancer using ML techniques, the utilized data may also include parameters from the blood analyses reports such as BMI, age, HOMA, glucose, and leptin. Moreover, the nonpathological data, such as ethnicity, pregnancy history, nursing history, obesity, radiation or carcinogenic chemical exposure to the face or chest in the early 30s or before, poor levels of vitamin D, sedentary lifestyle, and irregular menstrual history, can also be helpful in the prediction and diagnosis of breast cancer using ML approaches.

By carefully selecting features and manipulating data, we present a unique approach for the diagnostic prediction of breast cancer in our work. We used the WDBC dataset to diagnose features [6]. The study is aimed at predicting the tumor with high accuracy even with a reduced set of attributes. Existing research strictly focused on the use of traditional classification models in order to achieve accuracy. However, in our proposed solution, we have improved the overall classification process. This included handling data

noise, data sampling, and applying filter-based feature selection methods for determining optimal features, followed by five classification methods for comparative analysis of the performance of different classifiers. Moreover, the performance is tested multiple times over different test-train splits to determine the best split. Figure 1 shows the stages involved in the experiment that including the data preprocessing step, feature selection, data handling and application of classification models, and evaluation of their accuracy.

The subsequent part is organized as follows: Section 2 encompasses a literature review, leading datasets, and current problems, Section 3 of this paper discusses the solution proposed in this study, Section 4 explains the methods and experimentation process which have been used, Section 5 provides an analysis of the experimental results along with a comparative analysis with previous researches, Section 6 analyzes the results of our proposed approach on other datasets, and Section 7 discusses the conclusion and future works.

2. Related Work

Various researches can be found for the detection of breast cancer using different ML and neural network approaches; for example, Karabatak and Ince present a hybridized neural network-based breast cancer diagnostic system in [7]. The presented approach utilizes an association rule-based method to derive patterns from the breast cancer data. The association rules have been used to reduce the number of features, eliminating useless or less contributing features by finding relations as associations among closely related features. This technique helped in the reduction of feature space. The Wisconsin Breast Cancer dataset has been utilized for the training and testing of the presented technique. The results demonstrate the effectiveness of the presented hybridized neural network in terms of efficiency, and it also outperforms all other neural networks implemented in the study for comparison purposes [7].

Similarly, Ravdin and Clark [8] utilized a neural network to forecast a patient's chance of survival by using the prognostic data involving the time factor. A data of 1373 patients was utilized, and the neural network's prediction was also compared to that of a regression model. Moreover, Wolberg et al. [9] developed a linear diagnostic model to forecast malignant risks for nonrecurring cases and the recurring time period of diseases. This model was tested using a cross-validation approach on a dataset of 569 patients, yielding an accuracy of 97.5%. Quinlan [10] built a model for medical diagnostics and prediction by adding a Minimum Description Length (MDL) penalty to the C4.5 decision tree method, which resulted in a 94.74% accuracy. Furthermore, utilization of a large amount of data can also be found in literature; e.g., Delen et al. [11] used a big dataset of roughly 200,000 patient records. They have compared a decision tree model, i.e., C4.5, to several neural networks and linear regression models. They concluded that for large datasets, a decision tree method like C4.5 outperforms the other two, achieving an accuracy of 93.6 percent or higher.

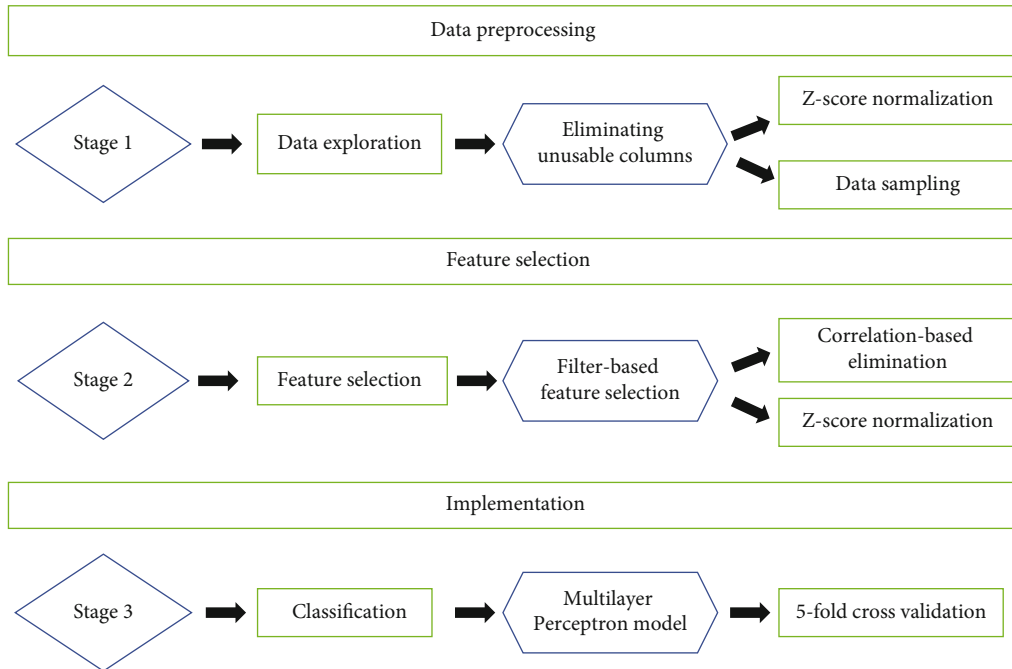


FIGURE 1: Breast Cancer Diagnostic (BCAD) framework.

Speaking of hybrid ML models, a hybrid model proposed by Ravi et al. [12] exhibits improved performance in terms of efficiency, because the model uses only critical features for its training. For this purpose, a combination of feature selection algorithms and fuzzy systems has been utilized. In this hybrid model, the number of rules used during the training process was minimized by using a modified threshold accepting algorithm. The model was trained on Wisconsin's Breast Cancer Classification (extracted from the UCI repository), and the Wine classification dataset. It was demonstrated that the model performs more efficiently when fewer but more relevant features are used. To further improve the performance of the model, another feature selection, and extraction method, i.e., the Principal Component Analysis (PCA) was also incorporated [12]. Similarly, Khan et al. [13] improved the learning performance by using various derivations of decision trees, including Fuzzy Decision Trees (FDT), Hybrid Decision Trees (HDT), and other related fuzzy rules to estimate the rate of recurrence for the breast cancer patients. The presented model has been trained and tested on the SEER dataset. The presented results demonstrate that the utilization of the Fuzzy Decision Tree model made the presented scheme more robust. Another hybrid approach for breast cancer classification has been proposed by Kaya and Uyar [14]. They combined the detection of diseases using rough sets and advanced machine learning algorithms. They used the breast cancer dataset acquired from the UCI repository and reported an accuracy of 98.6%.

Histopathological diagnosis serves as the gold standard for the diagnosis of malignant and benign breast cancer. However, mental anxiety and physical pain can come as a part of needle biopsy as it is invasive. Based on ultrasound images, medical image data mining methods are used in

order to obtain diagnostic information of malignant and benign tumors in a noninvasive manner. The authors in [15] proposed a dictionary training-based method in order to noninvasively obtain diagnostic information. They use their method to adaptively extract different texture features for selection and classification. A data of total 128 cases were used for the study, 67 of which were malignant and 61 of which were benign resulting in a classification accuracy on 0.9070. According to 2:1, the dataset was divided in a random manner into training and testing sets, including 85 training sets and 43 testing sets.

The authors in [16] performed a study to analyze the effect of ultrasound technology and deep learning technology combined on the breast-conserving surgery for breast cancer. They designed a deep LDL model and introduced two models for comparison. The first was the semiautomatic segmentation algorithm RA, and the second was the segmentation model ON. They applied their designed algorithm to the breast-conserving surgery of patients suffering from breast cancer. A total of 102 female patients with early breast cancer were divided into three groups W1, W2, and W3. The W1 group contained 34 cases (ultrasound guidance based on deep learning segmentation model), the W2 group contained 34 cases (ultrasound guidance), and the W3 group contained 34 cases (palpitation guidance). The conclusion of the study suggested that the deep LDL model improved the tumor resection very effectively.

The primary attempt at computerizing medical images happened during the 1960s, which is, until now, a significant subject of research in the field of medical imaging. Recent research in AI for the medical field has given rise to computer-aided diagnostic systems. Computer-aided detection (CAD) fills in as a symptomatic guide to help the doctor's job by using accurate and noninvasive computer

systems. In spite of these figures, automated detection software is not broadly utilized for the purpose of breast screening. In breast cancer imaging research, the focus has mainly been on ultrasound 2D/3D imaging combined with deep learning. The authors in [17] proposed a CAD framework for distinguishing the tumor grades of breast cancer by using US images. A total of 44 features were collected for the study. The viability of the proposed framework was checked in light of clinical data.

Various models found in the literature also report significantly high accuracies; for example, an LS-SVM classifier-based model by Polat and Güneş reports an accuracy of 98.53% and utilized 10-fold cross-validation. Another model based on an SVM classifier is proposed in [18] that demonstrates 99.02% classification accuracy even without using any cross-validation technique [18]. On the other hand, Akay et al. [19] presented an innovative and effective technique, by using combinations of swarm optimization statistical models for breast cancer detection and reported an accuracy of 98.71%. Another technique reporting a high model accuracy is proposed by Marcano-Cedeño et al. in [20]. This technique utilizes the AMMLP method by using an Artificial Neural Network over the biological metaplasticity property and reports an accuracy of 99.26%.

Similarly, there have been other cancerous and autoimmune diseases that have been worked upon such as multiple sclerosis (MS). It is an autoimmune disease that causes issues in the central nervous system up to a mild or severe extent. Like all such diseases, early detection and treatment are necessary in order to reduce the impact of the diseases. The authors in [21] propose a convolutional neural network-(CNN-) based framework (CNN) segmentation scheme for the extraction of MS lesion from a 2D brain MRI slice. They further implemented the VGG-UNet scheme in order to achieve a better MS detection. A pretrained VGG19 was considered as the encoder section. They performed their testing on 30 patient images. It was seen that their scheme provided a significantly better result in comparison to traditional UNet, VGG-SegNet, VGG-UNet and SegNet. Their experiment implemented on 2D slices of flair modality verified that this work provided with a better value of accuracy (>98%), dice (>92%), and Jaccard (>85%).

2.1. Limitations of Previous Frameworks. The features selected from datasets for diagnostic purposes highly impact the effectiveness and accuracy of the machine learning models [22–25]. Although various researches can be found that focus on feature selection and extraction from several popular and organized datasets, e.g., the WDBC dataset [26], it is still important to select the optimal features without changing them as it reduces the computational complexity and training time of the model and improves the accuracy to a great extent if a right subset is chosen. The typical yet significant problems like outliers, noise, unnormalized data, and high computational complexity have not been taken into consideration in previous studies. Furthermore, it is also important that the computational complexity is low. The number of features trained is linked to the computational complexity. Hence, it is important to identify the

minimum number of features that will help accurately classify the tumor. In addition to feature selection, there is a dire need for new or specifically tailored model structures to improve the diagnosis.

3. Leading Datasets

The most commonly used datasets for breast cancer prediction include the SEER Breast Cancer (SEERBCD) [27], the Coimbra Breast Cancer (CBC) dataset [28], the Wisconsin (Prognostic) Breast Cancer (WPBC) dataset [29], the Wisconsin (Diagnostic) Breast Cancer dataset [26], the Wisconsin Original Breast Cancer (WOBC) dataset [30], and the Breast Tissue Dataset (BTD) [31]. The WPBC dataset stores data based on 30 attributes that are calculated from digital photos. The WDBC dataset is comparable to the WPBC dataset. The BTD dataset is preferred due to the inclusion of the impedance measurements of newly removed breast tissues that have been acquired at various frequencies [31]. The CBC dataset [28], on the other hand, is gathered via routine blood analysis and contains anthropometric data. This dataset contains 10 predictors in total. The predictors are quantitative, and a binary-dependent variable indicates the presence or absence of breast cancer. The SEERBCD was received in November 2017 through the National Cancer Institute’s SEER program. Moreover, Dr. Wolberg’s clinical cases were used to create the WOBC dataset. It contains organized chronologically data, with eight groups containing the number of instances documented between January 1989 and November 1991.

3.1. The WDBC Dataset. The aforementioned and some other datasets have been used in a number of research studies. However, the most used and preferred dataset is the WDBC dataset which has also been used for breast cancer diagnosis in this study. This dataset has been widely utilized because it has a large number of recorded instances (699), and the data comprises medical information of real patients, hence making the dataset an important dataset used in literature. Dr. Wolberg was the contributor to this dataset. Using a graphical computer program known as Xcyt, he obtained multiple fluid samples from patients having solid breast masses. The dataset is virtually noise-free with very few missing or outlier values. Each of the features is evaluated on a scale of 1 to 10: 1 is interpreted as being closest to benign, and 10 is interpreted as a closet to malignant. Various significant studies utilizing WDBC dataset for medical diagnosis can be found in the literature; for example, Zheng et al. [32] used the WDBC dataset and applied K -means and SVM algorithms for the breast cancer diagnosis. Suryachandra and Reddy [33] also utilized the WDBC dataset and compared the performance of the Bayesian belief network, DT, and SVM.

Cherkassky [34] in his study performed the analysis of WDBC using SVM with RBF and polynomial functions as kernel functions. They achieved an accuracy of 97.1%. de Bruijne [35] used a feed-forward neural network model as well as a backpropagation learning algorithm combined with momentum and variable learning rate. The study proved

that the performance of multilayer neural networks is better than that of a one-layer neural network. This study also used the WDBC dataset [35]. In [36], Aryal and Paudel used the WDBC for Gradient Boosting and 10-fold cross-validation, resulting in the accuracy of 98.88% with a set of 30 features. Saygili [37] performed an analysis on this dataset recently. In his study, he used Random Forest for classification purposes and achieved an accuracy of 98.7%. He performed feature selection using Gain Ratio and used a set of 24 features and 10-fold cross-validation. Dubey et al. [38] performed on the WDBC dataset. They achieved an encouraging accuracy of 92.0%. Salama et al. [39] performed on the WDBC dataset with 30 features. They applied various different models. The best performance was demonstrated by Sequential Minimal Optimization (SMO) and 10-fold cross-validation. It resulted in an accuracy of 97.71%. Table 1 shows a comparison of machine learning algorithms on the WDBC dataset.

4. The Proposed BCAD Framework

This paper presents a state-of-the-art approach to breast cancer diagnosis. The objective of the paper is to identify the most accurate machine learning model which can predict the occurrence of breast cancer based on the various patients' clinical data. In order to achieve this, we propose a hybrid method for feature selection. This method includes the use of correlation-based feature selection first, followed by the recursive feature elimination method, which helps in the reduction of the feature space. The aim is to achieve encouraging classification accuracy over a reduced number of features using the original features without changing them, as opposed to the dimensionality reduction method. Feature selection is performed in order to reduce feature space and test how much influence the feature space has over classification accuracy.

Figure 1 illustrates the BCAD framework flowcharts, which elaborate the data preprocessing, attribute selection using filter-based feature selection methods, and classification using the Multilayer Perceptron Model. As previously mentioned, the dataset utilized in this study is the Wisconsin Diagnostic Breast Cancer (WDBC) dataset which contains 569 samples. The target values (labels: M (malignant)/B (benign)) indicate that the person's tumor is malignant (cancerous) or benign (noncancerous). We have used the WDBC dataset for experimentation.

4.1. Data Preprocessing. The first step of the Breast Cancer Diagnostic (BCAD) framework shown in Figure 1 is data-preprocessing. In this step, the random sampling technique (which is included in Scikit Learn) creates a unique sampling distribution that is based on real data. For data visualization, the Numpy, Pandas, and Seaborn libraries are used. Large and multidimensional matrices and arrays are supported by Numpy. It also provides a mathematical function to operate the arrays. Pandas provided data structures and operations for manipulating numerical tables. Seaborn helps with a high-level interface for drawing on statistical graphs. All these libraries are present in Scikit learn as a package.

TensorFlow is used for machine learning applications such as neural networks. Keras is a specific library designed for fast experimentation with neural networks. Normalization is then applied to normalize the distribution and increase the success rate. In this study, the standardization/z-score normalization procedure was utilized. Standardization is performed to guarantee that the features are properly normalized.

Data preprocessing is done first, then data is examined for discrepancies or missing values, and then random sampling is done. Sampling creates a one-of-a-kind sampling distribution based on actual facts. The purpose of sampling is to provide a more accurate assessment of the chosen features. After that, the data is normalized.

4.2. Feature Selection. The second step is the features selection, and it involves several filter-based methods. The analysis to identify the strongest predictors to address using correlation analysis is followed by recursive feature elimination method. For picking the strongest predictors, this approach proves better than other nonparametric approaches such as the K -Nearest Neighbors which would not be able to rank predictors according to their importance.

We advocate the use of a hybrid of correlation-based elimination strategy and recursive feature elimination because this will result in a better selection of optimal features. Even after features are eliminated by correlation, there might still be features that are not very useful; hence, a second step using recursive feature elimination will ensure the right selection of features.

4.3. Classification. The third step is classification. In this step, the selected features from the previous step are fed as input to the classification model. Fivefold cross-validation is performed; i.e., 80% percent of the whole data is used in the training phase, and 20% percent is used in the testing phase. The machine learning model then classifies this dataset to detect breast cancer. The details of the machine learning model and classification results are discussed in detail in the section.

5. Experimental Evaluation

This section explains the dataset and the tools and technologies used for the development of the EDFBC framework.

5.1. Experimental Setup

5.1.1. Dataset. In this study, the WDBC dataset has been utilized and accessed from the UCI library. The Wisconsin Diagnostic Breast Cancer (WDBC) dataset contains 569 samples in total [26]. Target values indicate that the person's tumor is malignant (cancerous) or benign (noncancerous). The WDBC includes the 569 samples distributed between malignant and benign samples. From the total 569 samples, 357 samples are benign and the rest 212 samples of malignant breast cancer cases are present.

5.1.2. Utilized Platforms. Exploratory analysis and data processing are performed in the following environment:

TABLE 1: Comparison of machine learning algorithms on the WDBC dataset.

| Author | Year | Features | Classifier | Accuracy achieved (%) |
|---------------------|------|----------|-----------------------|-----------------------|
| Aryal & Paudel [36] | 2020 | 30 | Gradient Boosting | 98.88% |
| Ahmet Saygili [37] | 2018 | 24 | Random Forest | 98.77% |
| Dubey et al. [38] | 2016 | — | K -means clustering | 92.00% |
| Salama et al. [39] | 2012 | 30 | SMO | 97.71% |

TABLE 2: Wisconsin (Diagnostic) Breast Cancer dataset.

| | |
|---------------|-----|
| Total samples | 569 |
| Malignant | 357 |
| Benign | 212 |

- (i) Python version 3.7
- (ii) Numpy (package for multidimensional array processing and indexing)
- (iii) Pandas (package for data analysis and manipulation tool, providing easy to use data structures)
- (iv) Matplotlib and Seaborn (package provides high-level interfaces for creating attractive and informative statistical graphs)
- (v) Scikit learn libraries for various classification algorithms (machine learning library that provides various algorithms)
- (vi) Keras (open-source neural network library, enabling fast experimentation with deep neural networks)
- (vii) TensorFlow (symbolic math library used for machine learning applications)

5.2. Sampling and Normalization. This section describes the data exploration and preprocessing activities and the valuable insights gathered from an exploratory analysis. The first step that is performed is data preprocessing. The process of data preprocessing including normalization, sampling, and test-train splitting is discussed below.

First, an exploratory analysis of the data was done. The data was visualized to see feature importance, correlation, and the variation in values of different features. Data visualization and exploration are important steps before we input the data into any machine learning algorithm. The WDBC constitutes nine numerical predictors and a binary dependent variable, indicative of the presence of breast cancer. Table 2 shows the distribution of the WDBC dataset.

The dataset consists of a total of 33 features, out of which there are an “unnamed 32” attribute and an ID attribute that have been removed manually. One of the features is the class tag, and the rest are used for feature selection. Further, we perform data sampling and normalization.

5.3. Attribute Selection. The attribute selection analysis is performed to identify the strongest predictors that are addressed using connected analysis followed by a repeated

feature elimination method. Other nonparametric supervised learning approaches such as K -Nearest Neighbors may not be able to rank the predictors by their importance.

Firstly, the features were eliminated on the base of correlation. The correlated attributes and the selected attributes are summarized in Table 3. The correlation among the 30 attributes is demonstrated through a heat-map analysis shown in Figure 2. The association among the multiple parameters is displayed through different colors. The lighter colors show the high correlation between the two attributes, and the white color shows the high association with a maximum value of 1. On contrary, the darker colors represent the least correlation.

This process reduced the number of features from 30 to 16. To check if the feature selection is correct, the recall value for the chosen features has been calculated. The values obtained from different algorithms were all greater than 90, with the highest recall value of 93.6% with the Random Forest algorithm, and the f -score value was 0.95. The recall was computed for the testing dataset.

The second step involved recursive feature elimination (RFE). RFE assigns weights to each feature. Those features that carry the smallest absolute weights are pruned from the present feature set [40]. This process is repeated until the required number of features is reached. 16 features were computed through RFE with an improved recall value of 93.7%. These 16 features were different from the ones computed previously. The Scikit platform provides an algorithm, i.e., the RFECV, which automatically finds the optimal number (and choice) of features required for best scoring. The RFECV algorithm is used to find the best scoring features. The optimal number of features according to the RFECV came out to be 20. However, the best 20 features included correlated features like radius_mean, perimeter_mean, and area_mean together, which did not seem to be very useful. Figure 3 shows the feature importance of features selected by recursive feature elimination.

The number of features required to optimize the algorithm after the elimination of correlated features was found to be 11. The RFE algorithm is used with fixed 11 features. The selected features were the ones that were appearing most in the solution. Table 4 shows the value of feature scores for the above 16 features.

5.4. Classification. The finalized set of 11 attributes was used for classification by the ML models including Random Forest Classifier, Gradient Boosting Classifier, Support Vector Machines (SVM), Artificial Neural Network, and Multilayer Perception model. Five classification algorithms are used in order to determine the performance of each model with a

TABLE 3: Selected attributes based on correlation.

| Correlated attributes | Selected attribute |
|--|--------------------|
| compactness_mean, concavity_mean, concave points_mean | concavity_mean |
| radius_se, perimeter_se, area_worst | area_se |
| compactness_worst, concavity_worst, concave points_worst | concavity_worst |
| compactness_se, concavity_se, concave points_se | concavity_se |
| texture_mean, texture_worst | texture_mean |
| area_worst, area_mean | area_mean |

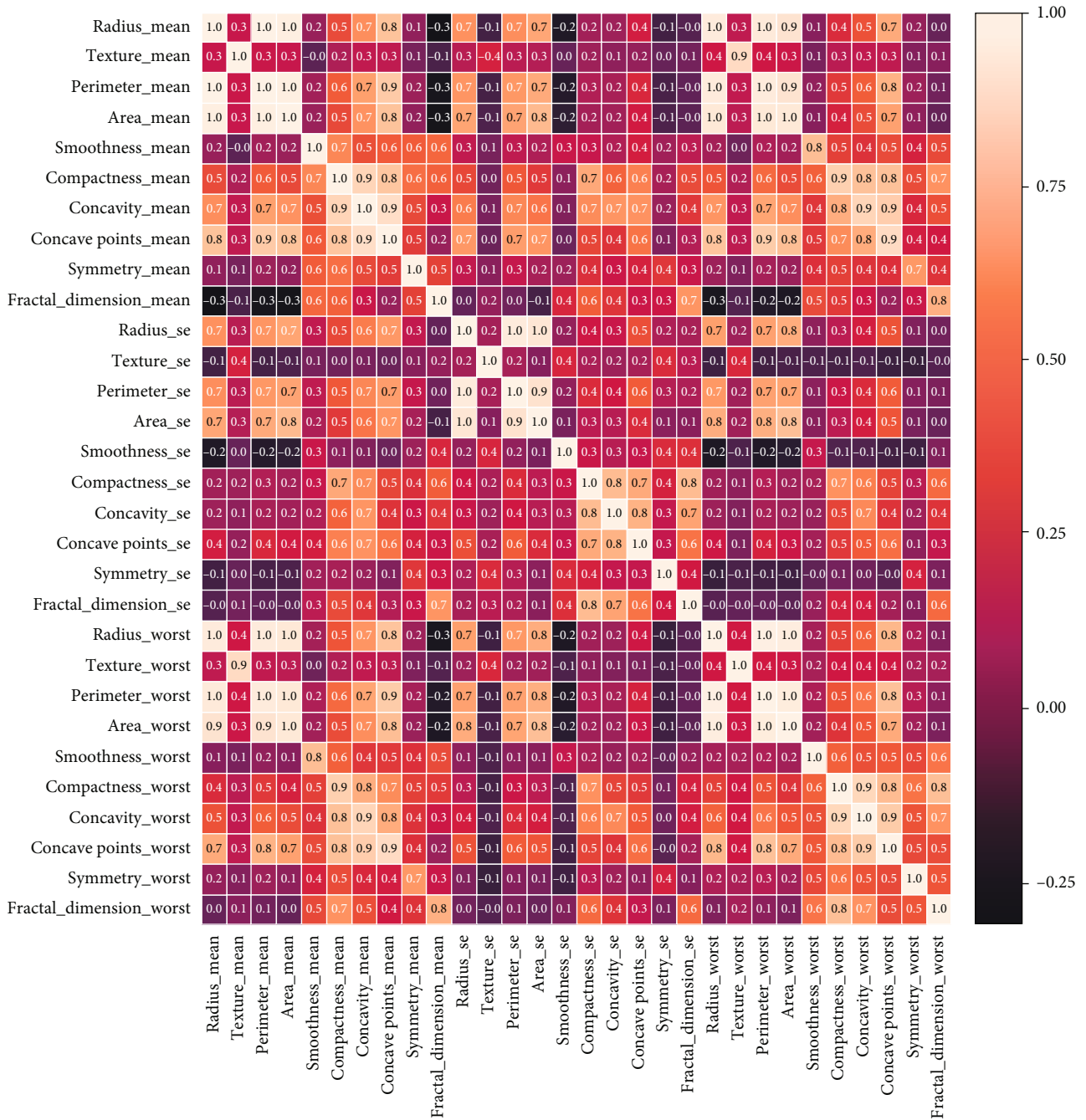


FIGURE 2: Heatmap analysis of features.

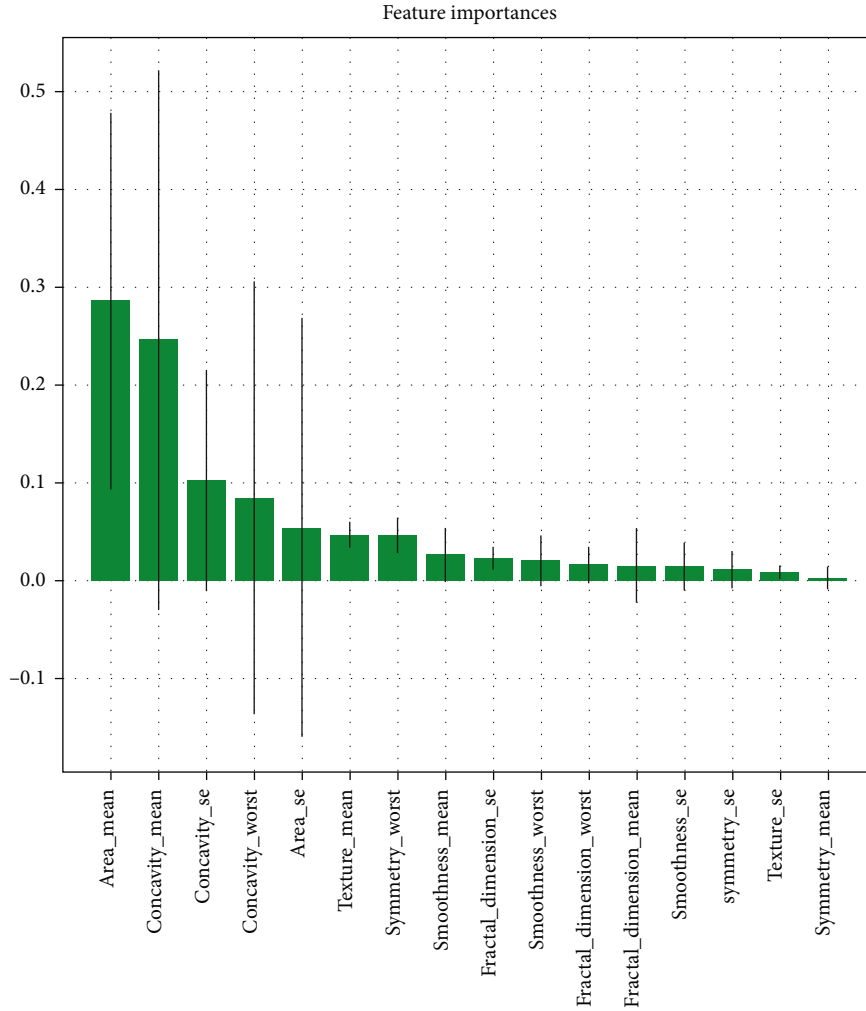


FIGURE 3: Feature importance.

TABLE 4: Feature importance scores of selected features.

| Attribute | Scores |
|-------------------------|----------|
| Area_mean | 0.213700 |
| Concavity_mean | 0.188830 |
| Area_se | 0.165063 |
| Concavity_worse | 0.143952 |
| Concavity_se | 0.058901 |
| Smoothness_worst | 0.047903 |
| Fractal_dimension_se | 0.030430 |
| Texture_mean | 0.025588 |
| Smoothness_mean | 0.025035 |
| Symmetry_worst | 0.023982 |
| Smoothness_se | 0.021418 |
| Texture_se | 0.015029 |
| Symmetry_mean | 0.014530 |
| Fractal_dimension_worst | 0.013285 |
| Fractal_dimension_mean | 0.006309 |
| Symmetry_se | 0.006046 |

reduced feature space. Their performance and accuracy are analyzed by cross-validation techniques.

Artificial Neural Networks are mainly divided into two categories based on the way to learn the data and patterns: supervised and unsupervised. In the supervised learning environment, the network is provided with both the input and correct outputs. During the training phase, the network generates its outputs, matched them with the true outputs, and then readjusted the weights to best match the true outputs in an iterative process. On the other hand, in an unsupervised environment, the neural network is provided with the inputs, but without output. The network then finds the pattern between the data and calculates acceptable weights by developing a representation of input stimuli. The input data is clustered, and features that are valuable for the solution are discovered.

Analyzing differing models in the literature, we have utilized the Multilayer Perceptron Model as it provides high generalization ability and has shown encouraging results on standard prediction and classification datasets in the medical field. Table 5 summarizes the results obtained from the finalized set of 11 attributes used for classification by machine learning models. It also displays the accuracy

TABLE 5: Classification accuracy.

| Machine learning method | Ratio (training: testing) | | |
|-------------------------|---------------------------|----------|---------|
| | 60 : 40 | 70 : 30 | 80 : 20 |
| | | Accuracy | |
| Random Forests | 95.40% | 96.67% | 98.07% |
| ANN | 93.02% | 85.53% | 97.35% |
| Gradient Boosting | 94.56% | 95.70% | 97.07% |
| SVM | 97.55% | 97.21% | 97.76% |
| MLP | 98.11% | 98.99% | 99.12% |

percentage result of each ML algorithm. The best accuracy of 99.12% is achieved by the MLP model. The best train-test split was determined to be 80-20 (5-fold cross-validation).

6. Results and Comparative Analysis

In our approach, we begin with data preprocessing. After checking for discrepancies or missing values, the data is sampled. Random sampling creates a one-of-a-kind sampling distribution based on the data. Normalization is then applied to normalize the distribution and increase the success rate. Standardization/ z -score normalization is used to ensure good normalization of the features. It is the most commonly used method in machine learning algorithms. In z -score normalization, all indicators are converted into a common scale, having a standard deviation of one and an average of zero. This method is preferred over other methods because the average of zero is used. This means that it avoids introducing aggregation distortions. Since the data has no missing value, this method will be beneficial.

As a consequence, a set of 11 characteristics is generated, which is subsequently used as input to classification models. Five classification algorithms are used in order to determine the performance of each with a reduced feature space. Their performance is analyzed, and their accuracies are analyzed. The classification was performed with different test-train splits. The best train-test split was determined to be 80-20 (5-fold cross-validation).

This allows us to select the strongest predictors from the entire feature space. Correlation-based selection and recursive feature removal approaches are then used to choose features [28]. First, the features are analyzed for correlation. The highly correlated features are set aside, and one of them is chosen, so that if three features are highly connected, one of them is chosen. The data is then subjected to recursive feature elimination (RFE) in order to extract the best features. The comparison of machine learning algorithms on Wisconsin Breast Cancer dataset is shown in Table 6.

6.1. Application of BCAD Framework on Different Datasets. Our proposed approach was targeted at improving the overall classification process by proposing a framework comprising of data handling and filter-based feature selection methods and testing the performance over different train and test splits. By reducing the number of features, the performance of the model is optimized and the overall generalizability of

the model is optimized. The overall training time is reduced and the generalizability of the model is increased. Both accuracy and generalization have been leveraged through correct and better feature selection. The computational complexity is reduced.

We advocated the use of correlation-based elimination strategy, followed by recursive feature elimination because this resulted in a better selection of optimal features. Even after features are eliminated by correlation, there might still be features that are not very useful; hence, a second step using recursive feature elimination ensures the right selection of features.

We have applied our framework to additional two datasets of breast cancer that include the Wisconsin Original Dataset for Breast Cancer (WOBC) [29] and the Wisconsin Prognostic Dataset for Breast Cancer (WPBC) [30] and recorded the results. The WPBC dataset consists of features computed from fine images of the breast mass of patients. The standard error, mean value, and largest mean (worst case-mean of the three largest values) are computed for these features, and as a result, 30 features are obtained that are listed in the dataset. The target attribute is the outcome (class label). All attributes except the attribute ID can be used as predicted variables, whose values can be used for determining the results. The WOBC dataset consists of samples collected periodically. There are a total of 10 features and one class label. The data are grouped in chronological order from groups of data recorded from January 1989 to November 1991.

We have applied our approach by selecting careful features and data handling on the WOBC and WPBC datasets. The proposed solution improves the overall classification process. The accuracy of classification is affected greatly by careful feature selection. Overall classification process, the classification accuracy, and the training time are improved by careful feature selection.

The comparison of our proposed model with various ML-based approaches developed and used by researchers on WOBC and WPBC is represented in Table 7.

Both datasets, WOBC and WPC, were subjected to our framework, and the results were recorded. First, standardization is carried out to verify that features are properly normalized, and then feature selection is carried out. Filter-based feature selection procedures like correlation analysis and recursive feature reduction are used to find the strongest predictors. Our suggested EDFBC framework clearly

TABLE 6: Comparison of machine learning algorithms on Wisconsin Breast Cancer dataset.

| Author | Year | Dataset | Imbalance handling | Feature selection | Features | Classifier | Validation type | Accuracy achieved (%) |
|---------------------|------|---------|----------------------------------|-----------------------------------|----------|----------------------------|-----------------|-----------------------|
| Aryal & Paudel [37] | 2020 | WDBC | — | — | 30 | Gradient Boosting | 10-fold | 98.88% |
| Ahmet Saygili [38] | 2018 | WDBC | — | Gain Ratio | 24 | Random Forest | 10-fold | 98.77% |
| Dubey et al. [39] | 2016 | WDBC | — | — | — | <i>K</i> -means clustering | — | 92.00% |
| Salama et al. [41] | 2016 | WDBC | — | — | 30 | SMO | 10-fold | 97.71% |
| Our approach | 2020 | WDBC | Normalization by standardization | Correlation-based selection & RFE | 11 | MLP | 5-fold | 99.12% |

TABLE 7: Comparison of machine learning algorithms on Wisconsin Breast Cancer dataset.

| Author | Year | Dataset | Imbalance handling | Feature selection | Features | Classifier | Validation type | Accuracy achieved % |
|--|------|---------|----------------------------------|-------------------------------------|----------|--------------------------|-----------------|---------------------|
| Wisconsin original breast cancer dataset (WOBC) [23] | | | | | | | | |
| Salama et al. [41] | 2012 | WOBC | — | Chi-square & PCA | 10 | J48 & MLP | 10-fold | 97.28% |
| Hamsagayathri & Sampath [42] | 2017 | WOBC | — | Feature ranking | — | Random Forest | 10-fold | 96.70% |
| Our approach | 2020 | WOBC | Normalization by standardization | Correlation based selection & RFE | 8 | MLP | 5-fold | 98.20% |
| Wisconsin Prognostic breast cancer data (WPBC) [24] | | | | | | | | |
| Tintu and Paulin [43] | 2013 | WPBC | Manual removal of instances | Feature ranking | — | Fuzzy C-means clustering | 4-fold | 97.13% |
| Khan et al. [44] | 2013 | WPBC | — | YAGGA | 19 | Linear regression | 10-fold | 84.34% |
| Our approach | 2020 | WPBC | Normalization by standardization | Correlation-based selection and RFE | 16 | MLP | 5-fold | 98.33% |

outperforms state-of-the-art techniques. Choosing the right features improves the whole classification process, increasing accuracy and minimizing the time of training data.

7. Conclusion

In this paper, a new framework has been proposed for the detection of breast cancer. The proposed framework includes three main stages, i.e., data preprocessing, feature selection, and classification. The classification experiments were performed using SVM, Random Forest, Gradient Boosting, Artificial Neural Network, and Multilayer Perceptron Model on the WDBC dataset. With a 99.12% accuracy, the Multilayer Perceptron Model outperformed all other models under investigation. In addition, the obtained results have also been compared with the experiments performed on the WPBC and WOBC datasets. The results indicate the exceptional performance of the proposed framework with the MLP model and the WDBC dataset when compared with other state-of-the-art approaches. In the future, our plan is to use a random neural network along with MLP for higher accuracy and precision. Also, we will validate the proposed model on other datasets as well.

Data Availability

The Wisconsin Diagnostic Breast Cancer dataset is available at [https://archive.ics.uci.edu/ml/datasets/breast+cancer+wisconsin+\(diagnostic%7d\)](https://archive.ics.uci.edu/ml/datasets/breast+cancer+wisconsin+(diagnostic%7d)). The SEER Breast Cancer dataset is available at <https://iee-dataport.org/open-access/seer-breast-cancer-data>.

Conflicts of Interest

The authors declare no conflict of interest.

Authors' Contributions

All authors contributed equally in this work.

References

- [1] H. You and G. Rumbe, "Comparative study of classification techniques on breast cancer FNA biopsy data," *International Journal of Artificial Intelligence and Interactive Multimedia*, vol. 1, no. 3, pp. 6–13, 2010.
- [2] World Health Organization, *WHO Position Paper on Mammography Screening*, World Health Organization, Geneva, 2014.
- [3] O. Wh, "Cancer," 2018, <http://www.who.int/en/news-room/fact-sheets/detail/cancer>.
- [4] M. Karabatak, "A new classifier for breast cancer detection based on Naïve Bayesian," *Measurement*, vol. 72, pp. 26–32, 2015.
- [5] R. Cartes-Velásquez, "Machine learning and medical diagnosis," *International Journal Of Medical And Surgical Sciences*, vol. 6, no. 4, pp. 105–106, 2019.
- [6] M. Nawaz, T. Nazir, A. Javed et al., "An efficient deep learning approach to automatic glaucoma detection using optic disc and optic cup localization," *Sensors*, vol. 22, no. 2, p. 434, 2022.
- [7] M. Karabatak and M. C. Ince, "An expert system for detection of breast cancer based on association rules and neural network," *Expert Systems with Applications*, vol. 36, no. 2, pp. 3465–3469, 2009.
- [8] P. M. Ravdin and G. M. Clark, "A practical application of neural network analysis for predicting outcome of individual breast cancer patients," *Breast Cancer Research and Treatment*, vol. 22, no. 3, pp. 285–293, 1992.
- [9] U. Zahid, I. Ashraf, M. A. Khan et al., "BrainNet: optimal deep learning feature fusion for brain tumor classification," *Computational Intelligence and Neuroscience*, vol. 2022, pp. 1–13, 2022.
- [10] J. R. Quinlan, "Improved use of continuous attributes in C4.5," *Journal of Artificial Intelligence Research*, vol. 4, pp. 77–90, 1996.
- [11] D. Delen, G. Walker, and A. Kadam, "Predicting breast cancer survivability: a comparison of three data mining methods," *Artificial Intelligence in Medicine*, vol. 34, no. 2, pp. 113–127, 2005.
- [12] M. A. Khan, M. Azhar, K. Ibrar et al., "COVID-19 classification from chest X-ray images: a framework of deep explainable artificial intelligence," *Computational Intelligence and Neuroscience*, vol. 2022, pp. 1–14, 2022.
- [13] K. Jabeen, M. A. Khan, M. Alhaisoni et al., "Breast cancer classification from ultrasound images using probability-based optimal deep learning feature fusion," *Sensors*, vol. 22, no. 3, p. 807, 2022.
- [14] Y. Kaya and M. Uyar, "A hybrid decision support system based on rough set and extreme learning machine for diagnosis of hepatitis disease," *Applied Soft Computing*, vol. 13, no. 8, pp. 3429–3438, 2013.
- [15] H. Gong, M. Qian, G. Pan, and B. Hu, "Ultrasound image texture feature learning-based breast cancer benign and malignant classification," *Computational And Mathematical Methods In Medicine*, vol. 2021, 8 pages, 2021.
- [16] H. Zhang, H. Liu, L. Ma, J. Liu, and D. Hu, "Ultrasound image features under deep learning in breast conservation surgery for breast cancer," *Journal of Healthcare Engineering*, vol. 2021, 9 pages, 2021.
- [17] D.-R. Chen, C.-L. Chien, and Y.-F. Kuo, "Computer-aided assessment of tumor grade for breast cancer in ultrasound images," *Computational and Mathematical Methods In Medicine*, vol. 2015, Article ID 914091, 2015.
- [18] K. Polat and S. Güneş, "Breast cancer diagnosis using least square support vector machine," *Digital Signal Processing*, vol. 17, no. 4, pp. 694–701, 2007.
- [19] M. F. Akay, "Support vector machines combined with feature selection for breast cancer diagnosis," *Expert Systems with Applications*, vol. 36, no. 2, pp. 3240–3247, 2009.
- [20] W. C. Yeh, W. W. Chang, and Y. Y. Chung, "A new hybrid approach for mining breast cancer pattern using discrete particle swarm optimization and statistical method," *Expert Systems with Applications*, vol. 36, no. 4, pp. 8204–8211, 2009.
- [21] S. Krishnamoorthy, Y. Zhang, S. Kadry, and W. Yu, "Framework to segment and evaluate multiple sclerosis lesion in MRI slices using VGG-UNet," *Computational Intelligence and Neuroscience*, vol. 2022, 10 pages, 2022.
- [22] A. Marcano-Cedeño, J. Quintanilla-Domínguez, and D. Andina, "WBCD breast cancer database classification applying artificial metaplasticity neural network," *Expert Systems with Applications*, vol. 38, no. 8, pp. 9573–9579, 2011.

- [23] J. Cai, J. Luo, S. Wang, and S. Yang, "Feature selection in machine learning: a new perspective," *Neurocomputing*, vol. 300, 2018.
- [24] V. Bachu and J. Anuradha, "A review of feature selection and its methods," *Cybernetics and Information Technologies*, vol. 19, p. 3, 2019.
- [25] Y. Borole, "Study on feature selection in data mining," *International Journal for Research in Applied Science and Engineering Technology*, vol. 7, no. 5, pp. 3956–3958, 2019.
- [26] M. A. Khan, S. Kadry, Y. D. Zhang et al., "Prediction of COVID-19-pneumonia based on selected deep features and one class kernel extreme learning machine," *Computers & Electrical Engineering*, vol. 90, p. 106960, 2021.
- [27] "Wisconsin diagnostic breast cancer dataset," [https://archive.ics.uci.edu/ml/datasets/breast+cancer+wisconsin+\(diagnostic\)](https://archive.ics.uci.edu/ml/datasets/breast+cancer+wisconsin+(diagnostic)).
- [28] SEER, "Breast cancer dataset," <https://ieee-dataport.org/open-access/seer-breast-cancer-data>.
- [29] "Coimbra breast cancer dataset," <https://archive.ics.uci.edu/ml/datasets/Breast+Cancer+Coimbra>.
- [30] "Wisconsin prognostic breast cancer dataset," <https://archive.ics.uci.edu/ml/datasets/Breast+Cancer+Wisconsin+%28Prognostic%29>.
- [31] "Wisconsin original breast cancer dataset," <https://archive.ics.uci.edu/ml/datasets/Breast+Cancer+Wisconsin+%28Original%29>.
- [32] <https://archive.ics.uci.edu/ml/datasets/Breast+Tissue>.
- [33] B. Zheng, S. W. Yoon, and S. S. Lam, "Breast cancer diagnosis based on feature extraction using a hybrid of K-means and support vector machine algorithms," *Expert Systems with Applications*, vol. 41, no. 4, pp. 1476–1482, 2014.
- [34] P. Suryachandra and P. V. S. Reddy, "Comparison of machine learning algorithms for breast cancer," in *IEEE International Conference on Inventive Computation Technologies (ICICT)*, pp. 1–6, Coimbatore, India, 2016.
- [35] M. Cherkassky, "Application of machine learning methods to medical diagnosis," *Chance*, vol. 22, no. 1, pp. 42–50, 2009.
- [36] M. de Bruijne, "Machine learning approaches in medical image analysis: from detection to diagnosis," *Medical Image Analysis*, vol. 33, pp. 94–97, 2016.
- [37] S. Aryal, B. Paudel, S. Aryal, and B. Paudel, "Supervised classification using gradient boosting machine: Wisconsin breast cancer dataset," *International Journal of Scientific Research and Engineering Trends*, vol. 6, no. 3, pp. 1887–1892, 2020.
- [38] A. Saygili, "Classification and diagnostic prediction of breast cancers via different classifiers," *International Scientific and Vocational Studies Journal*, vol. 2, pp. 48–56, 2018.
- [39] A. K. Dubey, U. Gupta, and S. Jain, "Analysis of k-means clustering approach on the breast cancer Wisconsin dataset," *International Journal of Computer Assisted Radiology and Surgery*, vol. 11, no. 11, pp. 2033–2047, 2016.
- [40] X.-W. Chen and J. C. Jeong, "Enhanced recursive feature elimination," in *Sixth International Conference on Machine Learning and Applications (ICMLA 2007)*, pp. 429–435, Cincinnati, OH, USA, 2008.
- [41] G. I. Salama, M. Abdelhalim, and M. A.-E. Zeid, "Breast cancer diagnosis on three different datasets using multiclassifiers," *Breast Cancer (WDBC)*, vol. 32, p. 2, 2012.
- [42] V. Ravi and H.-J. Zimmermann, "Fuzzy rule based classification with feature selector and modified threshold accept-ing," *European Journal of Operational Research*, vol. 123, no. 1, pp. 16–28, 2000.
- [43] P. B. Tintu and R. Paulin, "Detect breast cancer using fuzzy c means techniques in wisconsin prognostic breast cancer (WPBC) data sets," *International Journal of Computer Applications Technology and Research*, vol. 2, no. 5, pp. 614–617, 2013.
- [44] M. U. Khan, J. P. Choi, H. Shin, and M. Kim, "Predicting breast cancer survivability using fuzzy decision trees for personalized healthcare," in *Proceedings of the EMBS 30th Annual International Conference of the IEEE on Engineering in Medicine and Biology Society*, pp. 5148–5151, Vancouver, BC, 2008.